



**HAL**  
open science

**Design and control of a PV active generator with  
integrated energy storages : application to the  
aggregation of producers and consumers In an urban  
micro smart grid**

Di Lu

► **To cite this version:**

Di Lu. Design and control of a PV active generator with integrated energy storages : application to the aggregation of producers and consumers In an urban micro smart grid. Other. Ecole Centrale de Lille, 2010. English. NNT : 2010ECLI0021 . tel-00586393

**HAL Id: tel-00586393**

**<https://theses.hal.science/tel-00586393>**

Submitted on 15 Apr 2011

**HAL** is a multi-disciplinary open access archive for the deposit and dissemination of scientific research documents, whether they are published or not. The documents may come from teaching and research institutions in France or abroad, or from public or private research centers.

L'archive ouverte pluridisciplinaire **HAL**, est destinée au dépôt et à la diffusion de documents scientifiques de niveau recherche, publiés ou non, émanant des établissements d'enseignement et de recherche français ou étrangers, des laboratoires publics ou privés.

N° d'ordre : 147

ECOLE CENTRALE DE LILLE

## THESE

Présentée en vue  
d'obtenir le grade de

## DOCTEUR

en

**Spécialité : Génie Electrique**

par

**Di LU**

DOCTORAT DELIVRE PAR L'ECOLE CENTRALE DE LILLE

Titre de la thèse :

**Conception et contrôle d'un générateur PV actif à stockage intégré  
Application à l'agrégation de producteurs-consommateurs  
dans le cadre d'un micro réseau intelligent urbain**

Soutenue le 16 décembre 2010 devant le jury d'examen :

<b>Rapporteur</b>	<i>Hamid BEN AHMED, Dr, Maître de Conférences HDR, ENS Cachan Bretagne, SATIE</i>
<b>Rapporteur</b>	<i>Pascal MAUSSION, Professeur, INPT-ENSEEIH, LAPLACE</i>
<b>Examineur</b>	<i>Jean-Luc THOMAS, Professeur, CNAM, Equipe de recherche SUPELEC – Dpt. Energie</i>
<b>Examineur</b>	<i>Christophe FORGEZ, Professeur, Université de Technologie de Compiègne, LEC</i>
<b>Examineur</b>	<i>Antoni ARIAS PUJOL, Associate professor, Universitat Politecnica de Catalunya, Spain</i>
<b>Examineur</b>	<i>Vladimir LAZAROV, Professeur, Université Technique de Sofia, Bulgarie</i>
<b>Examineur</b>	<i>Jean Francois LEROMANCER, Dr, KEYNERGIE</i>
<b>Directeur de thèse</b>	<i>Bruno FRANÇOIS, Dr, Maître de Conférences HDR, Ecole Centrale de Lille, L2EP</i>

Thèse préparée dans le Laboratoire L2EP, EA2697  
Ecole Doctorale SPI 072

## **Preface**

The work, which is presented in this PhD thesis, has been done at the “Laboratoire d'Electrotechnique et d'Electronique de Puissance de Lille” (L2EP), from October 2007 to October 2010. This work has been carried out as a part of a research project “ANR–SUPERENER”, at Ecole Centrale de Lille with the support of the French National Research Agency (ANR).

## **Acknowledgements**

This dissertation is not only a result of my own dedication and perseverance, but is largely a credit to the patient and helpful people that I have worked with and to the supporting of understanding people that I have lived with over these past three years. I would like to take this opportunity to express my gratitude to everyone who contributed to this work.

My sincere thanks go to my supervisor, Dr. Bruno FRANCOIS, for his confidence in me throughout this project and for his valuable guidance during the study.

For their participation in the scientific evaluation of this work, I would also like to thank members of the jury, Professor Pascal MAUSSION, Dr. Hamid BEN AHMED, Professor Jean-Luc THOMAS, Professor Christophe FORGEZ, Dr Antoni ARIAS PUJOL, Professor Vladimir LAZAROV and Dr Jean François LE ROMANCER for their valuable discussions and insightful comments during the writing of the manuscript.

Many thanks go also to Xavier CIMETIERE, Simon THOMY, Christophe RYMEK and Hicham FAKHAM for their enormous help on implementation of the experimental test bench at Ecole Centrale de Lille. Equally, I am very grateful to the Professor Xavier GUILLAUD and Frédéric COLAS for their constructive suggestions and continuous help during my work on the platform « Energies Réparties » at the L2EP research center: Arts & Métiers Paristech.

I would like also to thank my colleagues in the Grid Network Team (Hicham FAKAM, Peng LI, Tao ZHOU, He ZHANG, Vincent COURTECUISSSE, Gauthier DELILLE, Amir AHMIDI, Arnaud VERGNOL, Fouad SALHA, Firas ALKHALIL, Ling PENG, Ye WANG) and my colleagues in the L2EP (Xavier MARGUERON, Guillaume PARENT, Francois GRUSON, Souleymane BERTHE, Jinlin GONG, Wenhua TAN, Aymen AMMAR, Ramzi BEN-AYED, Alexandru Claudiu BERBECEA, Martin CANTEGREL, Nicolas BRACIKOWSKI, Mathieu ROSSI, Sophie FERNANDEZ) for their infinite friendship and encouraging supports.

Finally, I am infinitely grateful to all my friends and my families for their moral support, to my parents for their continuous encouragement, and also to my girlfriend Yu ANLU for being supportive and understanding during these three years.

# Contents

<b>General introduction.....</b>	<b>1</b>
<b>Chapter I. Renewable energy based active generator.....</b>	<b>7</b>
I.1. Introduction.....	11
I.2. Renewable energy.....	11
I.2.1. Benefits of renewable energy.....	11
I.2.2. Dispatchable renewable energy based generators.....	12
I.2.3. Non-dispatchable renewable energy based generators.....	13
I.2.4. Renewable energy development.....	13
I.2.5. Constraints.....	14
I.3. Energy storage.....	15
I.3.1. Different kinds of energy storage.....	16
I.3.2. Long term energy storage and fast dynamic power storage.....	16
I.4. Hybrid power generator.....	17
I.4.1. Interest.....	17
I.4.2. Configuration of an hybrid power generator.....	17
I.4.3. Structure of the studied hybrid power generator.....	21
I.5. Modeling of the studied hybrid power generator.....	22
I.5.1. Presentation.....	22
I.5.2. PV panels.....	23
I.5.3. Lead-acid battery.....	31
I.5.4. Ultracapacitor.....	34
I.6. Conclusion.....	36
<b>Chapter II. Control system of the active PV generator.....</b>	<b>37</b>
II.1. Introduction.....	41
II.2. Modeling of the PV active generator.....	42
II.2.1. Methods.....	42
II.2.2. PV power conversion system.....	43
II.2.3. Batteries energy storage system.....	44
II.2.4. Ultracapacitors.....	45
II.2.5. Grid connection.....	46
II.2.6. DC bus.....	47

II.2.7. Modeling of the entire PV energy conversion system.....	48
II.3. Control of the active PV generator.....	49
II.3.1. Hierarchical control structure.....	49
II.3.2. Automatic Control unit.....	50
II.3.3. Power control unit .....	56
II.4. Power balancing strategies for the active PV generator.....	59
II.4.1. Role of the DC bus.....	59
II.4.2. Normal mode.....	60
II.4.3. PV limitation mode.....	63
II.4.4. Disconnection mode.....	64
II.4.5. Synthesis.....	66
II.5. Control of operating modes.....	69
II.6. Energy management of the embedded ultracapacitors.....	71
II.6.1. Energy level and management scheme.....	71
II.6.2. Full ultracapacitors mode.....	71
II.6.3. Empty ultracapacitors mode.....	72
II.7. Simulation and experimental results.....	72
II.7.1. Simulation results .....	72
II.7.2. Experimental results.....	75
II.8. Conclusions.....	77

### **Chapter III. Micro Grid framework for integrating DG in energy**

#### **management and control system of power network.....79**

III.1. Introduction.....	83
III.2. Architecture of future electrical systems.....	83
III.2.1. Issues.....	83
III.2.2. Interest of micro grids and specificities.....	85
III.2.3. Basic MG architectures.....	85
III.2.4. Operation modes.....	86
III.3. State of the art.....	88
III.3.1. In Europe.....	88
III.3.2. In the United States.....	92
III.3.3. In Japan.....	94

III.4. Dispatchable distributed generation for grid control.....	96
III.4.1. Interest.....	96
III.4.2. Classical isochronous speed control of conventional DGs.....	96
III.4.3. Energy storage requirements in power systems.....	97
III.4.4. Control functions for grid connected inverters.....	97
III.4.5. Control strategies for a grid-connected mode of the microgrid.....	98
III.4.6. Control strategies for a “Vf mode” in an islanded mode of the microgrid.....	101
III.4.7. Control capabilities of the PV based active generator.....	104
III.5. Control system for microgrids.....	104
III.5.1. Objectives and tasks.....	104
III.5.2. Communication system.....	105
III.5.3. Control functions and management tasks.....	105
III.5.4. Time scale analyzing and implementation constraints.....	106
III.5.5. Power management by sensing electrical quantities.....	107
III.5.6. Energy management by signal communication.....	109
III.6. Conclusion.....	115

## **Chapter IV. Planning and energy management system of a residential**

### **micro grid.....117**

IV.1. Introduction.....	121
IV.2. Residential network application.....	123
IV.2.1. Integration of the active generator in a home.....	123
IV.2.2. Residential network and electrical system organization.....	124
IV.2.3. Application of microgrid concepts and global objective.....	126
IV.2.4. Microgrid energy management.....	125
IV.3. Forecasting techniques and processing of data.....	129
IV.3.1. PV power prediction.....	129
IV.3.2. Load forecasting.....	131
IV.3.3. Energy estimation.....	134
IV.4. Daily power planning / Setting of half-hour power references.....	136
IV.4.1. Objectives.....	136
IV.4.2. Constraints.....	136

IV.4.3. Determinist algorithm.....	137
IV.4.4. Practical application.....	139
IV.5. Medium-term energy management.....	141
IV.5.1. Reduction of the uncertainty (MGCC).....	141
IV.5.2. Energy management of batteries (LC).....	142
IV.6. Short-term power management.....	143
IV.6.1. Primary frequency regulation.....	143
IV.6.2. Power balancing strategies for the active generator.....	144
IV.7. Experimental tests through Hardware in the Loop simulations.....	147
IV.7.1. Description of the experimental platform.....	147
IV.7.2. Analysis of the self consumption of one house.....	150
IV.7.3. Increasing the penetration ratio in a residential network.....	155
IV.8. Conclusions.....	161
<b>General conclusion</b> .....	163
<b>Appendix</b> .....	171
<b>General Bibliography</b> .....	203

# *General Introduction*





## **Targets for future sustainable electrical networks**

The electricity is suffering from a constraint irrefutable: At any moment, electrical systems must ensure a balance between production and consumption, while maintaining a satisfactory voltage. Historically, grid reliability was mainly assured by having excess capacity in the system with unidirectional flow to dispersed consumers from centrally dispatched large power plants. To combat climate change and increase the EU's energy security while strengthening its competitiveness, the EU Heads of State and Government have set a series of demanding climate and energy targets to be met by 2020, known as the "20-20-20" targets:

- A reduction in EU greenhouse gas emissions of at least 20% below 1990 levels,
- A 20% reduction in primary energy use compared with projected levels, to be achieved by improving energy efficiency,
- 20% of EU energy consumption coming from renewable resources.

## **Current limitation of the PV resource**

Today, renewable energies are considered as a potential solution for greenhouse gases emissions reduction and energy safety. Fueled by economic, environmental and social drivers, the penetration of photovoltaic generators rises in distribution networks. Thanks to its operation without noise and gas emission, it can be easily installed outdoor and on roofs. But the development of grid-connected PV generation is limited by the intermittent power generation and time-lag between the PV electrical production and the real consumption. A massive deployment of PV systems complicate the balancing between production and consumption, that may cause blackouts if it is disturbed

## **A new concept: the PV based active generator**

Because of the intermittency of PV power generation, PV panels can not be used as a stable, reliable and controllable power source and can not provide ancillary services like conventional generators. The topic of this thesis is the transformation of a PV generator into an active generator by using an embedded energy storage system and a local energy management system for the coordination of inner sources. Long-term energy storage batteries are used to shave the midday PV power peak and provide a complementary power supply during the night. Fast dynamic ultracapacitors storage can smooth the generated PV power, compensate the power gap and absorb the instantaneous high power peaks.

## **Local controller for a dispatched management**

Three sources with different characteristics must be coordinated inside the PV active generator. So for ensuring an optimal operation, a local energy management system of the PV based active generator has to be developed to enable:

- the management of the renewable energy intermittency and resources,
- the quality of power supply,
- the energy level management,
- the power system protection,
- the provision of grid ancillary services.

This PV based active generator is then an additional controllable dispersed generation, which have to be dispatched. In the context of a large scale development of PV based active generators, the operation mode of the electric network will have to be changed.

## Dispersed generation in a centralized network

Another characteristic of PV generators is that they are decentralized as are consumers. Mini Combined Heat and Power (CHP) units have this same specificity and are also awaited to heat entire residential area and even our individual home in the future. Hence electricity becomes a by-product it will be fatal to absorb at the right time. As example the future development of electric vehicles offers the opportunity to intelligently manage the charging of their batteries in order to participate in the storage of the power generated by renewable sources.

Until recently such operational problems due to the large development of dispersed generators were solved at the planning stage through reinforcements to keep the system within deterministic operational limits. This method is limited by the extreme cost of these reinforcements in the network. Investments in the electric system were made to meet the increasing demand and the accommodation of dispersed stochastic generators; but not to change fundamentally the way the system works.

An evolution towards new electrical system architectures for distributed generation must be imagined for the future. A second method is to develop advanced management strategies of the power system and the dispersed generators in order to maintain their current reliability and the security of supply. A fundamental shift from passive to active network management is proposed by “smart grids” for the reduction of carbon dioxide emissions and the increasing power demand.

## Smarter grids

The concept of smart grid is based on the integration of a communication infrastructure and a variety of automation technologies and digital communication services into the electrical infrastructure. The Web can be used as a platform for the incremental addition of new grid applications and their integration with utility systems and external systems and users. The Smart Grid transforms the current grid to one that operates functions more cooperatively, responsively and organically [Url 10f]. Bidirectional flow of energy transfers and bidirectional flow of information, coupled with new management capabilities will pave the way for a range of new features and applications that will improve:

- the capacity through the supply of electricity by integration of renewable sources for the huge demand,
- the reliability, through a high quality electricity available whenever it is needed with no interruptions
- the efficiency, through the energy saving from production and transport to consumption of electricity and the best use of resources, i.e. maximize benefits and minimize costs,
- the sustainability, through the use of low carbon energy sources.
- For distribution system operators, first features concern the control of power flows for a better solicitation of assets, the peak shaving and the deployment of renewable energies. Three levels of innovation can be identified:
- the improvement of physical infrastructures,
- the development of customer interfaces in order to refine the management of small dispersed producers and the load demand (communicating meters, wired or not communication network, sensors, communication box, ...),
- the use of grid technologies to improve the energy management of the entire electrical system.

This last point and more precisely the design of advanced energy management systems for integrating more PV generators is the general topic of this PhD report.

## **New organization of the electrical system and application of micro grid concepts**

The cumulative installed PV capacity in March 2010 is 422 MW in the French distribution network that is 106% more than in December 2009 (200 MW) [ERD10]. This fact shows that PV generators will be soon the main dispersed generation technology closed to consumers. Moreover 2 953 MW are awaiting agreements for connection because the existing electric power system is not ready for a significant and large deployment of PV systems. Following the smart grid concept the distribution grid will need to be adapted to interact with DG and load demand and, in some cases, to control them. An organization must be imagined to make evolve the small PV energy market with passive PV generators to a larger market, where PV based active generators are used to sell energy for customers and services for the grid.

In this context, the presented research works have been oriented to the use of the PV based active generator in the management of a residential grid. A new organization of the power system is considered and is based on an aggregator, responsible for a cluster of producers and consumers. Its management system will be derived from concepts of micro grids. For this task radial distribution systems can be arranged into several micro grids including a group of consumers, a group of producers and an entire feeder. The interconnection of small production of different technologies concerns a vast research domain as sizing, control design of generators, design of power converters, coordination of generators, reactive power compensation, etc. Here the work is focused on the energy management and the coordination of multiple sources. This research topic can be decisive for the technically and economically integration of PV generators in distribution networks. The problem is an operational problem. It involves making the best environmental improvement of the installed production capacity while ensuring a proper operation of the network.

This work is an additional contribution in the topic of “Integration of Distributed Generation in the micro grid” within the research group “Electrical networks” from the Laboratory of Electrical Engineering and Power electronic (L2EP) of Lille.

## **Layout of thesis**

In the first part, the design of PV based active generator is introduced. The architecture and the configuration of the active generator are presented. The characteristics of each source (PV panels, lead acid batteries and ultracapacitors) are detailed. The system modeling is carried out with macroscopic energetic representation.

In the second part, a local controller for the PV based active generator is developed by a hierarchical structure of the control system and is organized in different levels. Each level is in charge of a specific control function. A local energy management system is developed for controlling the power flows inside the PV active generator. This management system implements several algorithms in order to supply the power demanded by the grid operator. In the same time it extracts the maximum PV power and respects the storage capacity and power limits. A low-pass filtering method for the inner dispatching of power references is detailed.

In the third part, the micro grid concept is described. The different functions of the smart grid with the renewable energies are developed. Several research examples will show the state of the art about MGs in the world. Then fundamental principles of grid management systems and classical practices are recalled in order to better highlight constrains, required control functions for the DG as well as control system and practical implementation for the grid.

In the last part, a residential smart grid with PV active generators is taken as example for presenting the energy management process. The long-term energy management (24-hour operational planning) and the medium-term energy management (half-hour power point setting adjusting) are implemented in a master centralized controller and are designed by a determinist approach from a forecasting of the PV power and the load demand. The short-term power management is implemented in local controllers of generators and is designed to compensate for uncertainties in loads and renewable energy. The coordination is performed by droop controllers.

---

# *Chapter I*

Renewable energy based active generator



## Contents

Chapter I. Renewable energy based active generator.....	11
I.1. Introduction .....	11
I.2. Renewable energy.....	11
I.2.1. Benefits of renewable energy.....	11
I.2.2. Dispatchable renewable energy based generators.....	12
I.2.3. Non-dispatchable renewable energy based generators .....	13
I.2.4. Renewable energy development .....	13
I.2.5. Constraints .....	14
I.3. Energy storage .....	15
I.3.1. Different kinds of energy storage.....	16
I.3.2. Long term energy storage and fast dynamic power storage .....	16
I.4. Hybrid power generator.....	17
I.4.1. Interest .....	17
I.4.2. Configuration of an hybrid power generator .....	17
I.4.3. Structure of the studied hybrid power generator.....	21
I.5. Modeling of the studied hybrid power generator .....	22
I.5.1. Presentation.....	22
I.5.2. PV panels .....	23
I.5.3. Lead-acid battery .....	31
I.5.4. Ultracapacitor.....	34
I.6. Conclusion.....	36





## **Chapter I. Renewable energy based active generator**

### **I.1.Introduction**

Faced with the challenges of energy, the demand for primary energy in the world wide is evolving. However, the stock of oil in our planet will soon be exhausted. Today global warming becomes more serious due to the greenhouse effect. Some emissions of greenhouse gases come from the human activity. The production and processing of electrical energy is one of the main sources of greenhouse gases. For reducing the greenhouse gas emission and assuring the energy security, renewable energy is promoted in the electrical power production.

However, an electrical generating system depending entirely on the renewable energy sources is not reliable because the availability of the renewable energy sources can not be constantly assured.

In this report a hybrid active generator is proposed to deal with the problem of the renewable energy intermittent power. A hybrid power system combing the renewable energy sources and the storage units can be considered as an active generator, which can provide the power that is demanded by the grid operator. Integrating photovoltaic power sources with batteries as storage, can lead to a long-term reliable energy source. The ultra-capacitors have fast dynamics, thus can be used to smooth fast fluctuations of the photovoltaic power and can ensure a good power quality.

In this chapter, different forms of renewable energy and different kinds of electrical storage technologies will be presented. A hybrid system based on PV panels, lead acid batteries and ultracapacitors will be proposed. In the end of this chapter, each source inside this hybrid generator is modeled.

### **I.2.Renewable energy**

Renewable energy is the energy generated from natural resources. Renewable energy flows involve natural phenomena such as sunlight, wind, tides and geothermal heat, as the International Energy Agency explains:

“Renewable energy is derived from natural processes that are replenished constantly. In its various forms, it derives directly from the sun or from heat generated deep within the earth. It includes the electricity and the heat generated from solar, wind, ocean, hydropower, biomass, geothermal resources and bio-fuels and hydrogen derived from renewable resources” [IEA 03].

#### **I.2.1.Benefits of renewable energy**

The potential contribution of renewable energies to IEA member countries (United Kingdom, Germany, France, United States, Japan...) is growing, as the technologies mature and there is an increasing awareness about the full contribution that renewable energies can make. Renewable energy sources contribute to the diversity of the energy supply portfolio and reduce the risks of continued (or expanded) use of fossil fuels and nuclear power. Distributed renewable energies provide options to consumers because of their deployment close to use. Renewable energy is also the most environmentally benign energy supply option available in current and near-term markets. Finally, renewable energies contribute to a healthy economy, both in their contribution to the efficiency of the energy system, and in the employment and

investment opportunities that arise from continued rapid market growth [URL 06b].

The primary benefits to us are the energy security, the environment protection and the economic growth.

**a. Energy security**

Faced with the energy challenges, the demand for primary energy in the world wide is evolving, particularly in fast developing countries like China. However, the stock of oil in our planet will soon be exhausted. Such dependency over an extended period is unsustainable. Renewable energy can relieve some of that increasing need for imported fossil fuels and reduce dependence on foreign sources.

The distributed capability of renewable energies brings the electrical production closer to the end-use, thus minimizing energy transport concerns and costs. The Renewable Energy Working Party also believes that a greater use of renewables in the energy portfolio can minimize overall generation costs relative to the risk [IEA 03]. Energy policies should focus on developing efficient generating portfolios that do not solely rely on stand-alone costs but also on expected portfolio risk, including year-to-year cost fluctuations.

**b. Environment protection**

Moreover, today global warming becomes more serious due to the greenhouse effect. Some emissions of greenhouse gases come from the human activity. The production and processing of electrical energy is one of the main sources of greenhouse gases. Directly or indirectly, environmental concerns dominate the thrust for an expanded deployment of renewable energy technologies. Climate change concerns, which arose during the late 1980s, have created a new input for clean, low-carbon energy technologies, such as renewable energy technologies. In December 1997, the Kyoto protocol has been established in order to reduce global emissions of greenhouse gases. In the area of power generation, this protocol promotes renewable energy sources [KYO 09].

**c. Economic growth**

Renewable energy has several important economic benefits. In IEA (International Energy Agency) countries, the main economic benefits are employment creation and increased trade of technologies and services.

**1.2.2. Dispatchable renewable energy based generators**

The renewable energy based generation can be divided into two kinds: dispatchable production and non-dispatchable production. Dispatchable production refers to sources of electricity that can be dispatched at the request of power grid operators. They are able to change their power production upon demand.

**a. Water power**

Water power can be exploited in a form of kinetic energy. Since water is about 800 times denser than air, a slow flowing stream of water can yield considerable amounts of energy. Water power exists in many forms. Hydroelectric energy is a term, which is usually reserved for large-scale hydroelectric dams. Micro hydro systems are hydroelectric power installations that typically produce up to 100 kW of power, which are often used in water rich areas as a Remote Area Power Supply. Ocean energy describes all the technologies to harness energy from the ocean and the sea including marine current power, ocean thermal energy conversion, wave power and etc.

**b. Biofuel**

Plants use photosynthesis to grow and produce biomass. Also known as biomatter, biomass can be used directly as fuel or to produce biofuels. Agriculturally produced biomass fuels, such as biodiesel, ethanol and bagasse (often a by-product of sugar cane cultivation) can be burned in internal combustion engines or boilers. Typically biofuel is burned to release its stored chemical energy.

**c. Geothermal energy**

Geothermal energy is from the heat of the earth itself, both from kilometers deep into the Earth's crust in some places of the globe or from some meters in geothermal heat pump in all the places of the planet. Geothermal technology is mostly used for thermal power production, the space heating is becoming increasingly important. Geothermal electricity production is a base load technology, and can be a low-cost option if the hot water or steam resource is at a high temperature and near the earth's surface.

**I.2.3.Non-dispatchable renewable energy based generators**

**a. Wind power**

Wind energy is considered as one of the most promising technologies for electricity production and the costs, with good wind regimes, are comparable to fossil alternatives, particularly when the environmental benefit is considered. Airflow can run wind turbines for generating electricity. The rated power of modern wind turbines ranges from 600 kW to 5 MW [EWE 07]. The power output of a turbine depends on the wind speed and so, as the wind speed increases, the power output increases. The location of wind turbine installation is usually chosen in the areas where winds are strong and constant, such as offshore and high altitude sites. Offshore resources experience have shown that mean wind speeds are about 90% greater in onshore, so offshore resources may contribute more significantly to the supply of energy. Globally, the long-term technical potential of wind energy is believed to be five times equal to the total current global energy production, or equal to the 40 times current electricity demand [URL 06a].

**b. Solar power**

Solar energy comes from the radiant light and heat of the sun. Sunlight can be converted directly into electricity by using PhotoVoltaic (PV) panels or indirectly with Concentrating Solar Power (CSP). CSP normally focuses the sun's energy to boil water, which is then used to provide electrical power. Photovoltaic (PV) technologies use semiconductor materials to convert sunlight directly into electricity. They have dropped in price to between one-third and one-fifth their cost in 1980 [URL 06b]. PV is now widely viewed as cost competitive for many grid-connected, building-integrated uses and for off-grid applications as in telecommunications, power supply of village power.

**I.2.4.Renewable energy development**

Today different kinds of renewable energy technologies have been established in world markets. Some renewable energy technologies are becoming quickly competitive in growing markets, and some are widely recognized as the lowest cost option for stand-alone and off-grid applications. The capital costs of certain renewable energy technologies have been obviously reduced over the last decade and it is possible to be halved again over the next decade.

From the end of 2004 to the end of 2008, the PV power has increased six times and now is more than 16 Gigawatts (GW), wind power capacity has increased 250 percent to 121 GW, and the total power capacity from new renewable energies has increased to 75 percent to 280 GW (Figure I.1) [URL 09a].

The IEA's World Energy Outlook 2000 (WEO 2000), in its reference case, estimates that the non-hydro share of renewables will grow from the current 2 percents of TPES (Total Primary Energy Supply) to 4 percents of TPES by 2020 in the OECD (Organization for Economic Cooperation and Development) region. Non-hydro renewables are expected to be the fastest growing primary energy sources, with an annual growth rate averaging 2.8 per cent over the outlook period. Throughout the world, hydroelectricity is expected to increase by 50 per cent between 2000 and 2020, even though its overall share of TPES will decrease. More than 80 per cent of the increase will take place in developing countries [REN 09].

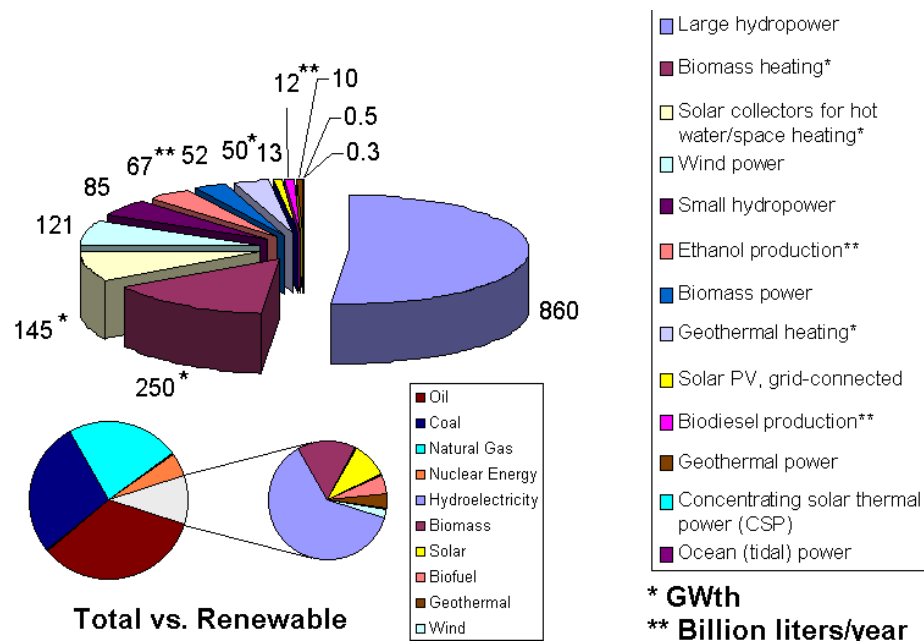


Figure I.1 2008 worldwide renewable-energy sources [URL 09a]

### 1.2.5. Constraints

The development of the different renewable sources is limited by different constraints depending on their intrinsic characteristics.

Hydropower and geothermal power are naturally limited because of the lack of geographic sites. Biomass requires large storage places for the natural resources.

This is the reason why a large development of PV and wind turbines is waited. Unfortunately these renewable energy sources are intermittent power sources (Figure 2.a). The production of electricity from solar sources depends on the amount of light energy in a given location. Solar output varies throughout the day and through the seasons, and is affected by cloud cover. Wind-generated power is a variable resource, and the amount of produced electricity will depend on wind speeds, air density and turbine characteristics (among other factors). If the wind speed is too low (less than about 2.5m/s) then the wind turbines will not be able to make electricity. If it is too high (more than about 25m/s) the turbines will have to be shut down to avoid damage. As this primary source is uncertain these kinds of renewable energy sources may produce a large amount of power when loads in the grid are very low.

And they are not always available when it is necessary, such as solar in the night and wind power when the wind is not blowing.

The addition of intermittent resources causes large amounts of variable power. Renewable energy based generations with intermittency decrease the reliability of a power system. The nature of the intermittency is, of course, different for the respective renewable energy technologies and this difference could be a relevant factor so far as mitigating the impacts of intermittency is concerned. As the percentages of intermittent generation capacity increase and become more significant, additional uncertainty is created in the management of the electrical system balance in real time the demand and generation. This requires the increasing amounts of conventional power reserve capacity that can be made available immediately (spinning reserve) and of plants capable of providing ancillary services (frequency response and voltage control as example), which are required to manage the electrical power system securely [Pea 08].

Actual wind and PV generators must be considered as passive generators because they can not participate to the grid management, because they are dependent on the availability of the primary renewable source. Most of the time, they work far below their nominal capacity (Figure I.2a). Moreover, the reliability and efficiency of the power system can not be ensured. Therefore, they can not provide ancillary services to the grid, like power balance between the production and the consumption. They are not dispatched by a grid system operator because their output active and reactive powers are not controllable.

In contrary conventional power plants are controllable and can supply necessary powers to satisfy the grid requirements. They are considered as active generators because they can usually provide some ancillary services to the grid, basically frequency regulation by active power control, voltage regulation by reactive power control, etc. They are mostly fossil and nuclear fuelled and rely on the abundant fuel supply like coal, oil, natural gas or nuclear fuels. Most of the time, they can work at any power level below its nominal power (Figure I.2b) by controlling the fuel supply.

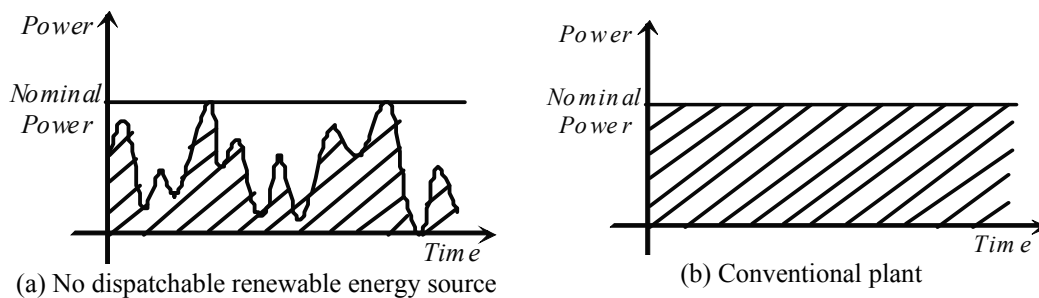


Figure I.2: Characteristic of different kinds of energy sources

### I.3. Energy storage

Facing to the problem of the power intermittency from renewable energy sources, different kinds of technological solutions have been proposed. The use of electrical energy storages is considered as an effective solution. The electrical energy storages can balance the intermittency of power supply, which is caused:

- by the renewable energy sources
- by the operating error, unplanned outage, component failures and etc.

They can help to provide ancillary services in an electrical network such as frequency regulation, voltage regulation and etc.

### I.3.1. Different kinds of energy storage

All forms of energy are either potential energy (e.g. chemical, gravitational or electrical energy) or kinetic energy (e.g. thermal energy). Energy can be stored in different forms:

- Chemical: Hydrogen, biofuels, liquid nitrogen, oxyhydrogen ...
- Electrochemical: Batteries, flow batteries, fuel cells ...
- Electrical: Capacitor, supercapacitor, superconducting magnetic energy storage, ...
- Mechanical: Compressed air energy storage, flywheel energy storage, hydraulic accumulator ...
- Thermal: Ice storage, air-conditioning... [URL 09g]

For electrical applications, according to the different requirements, various kinds of storage technologies are used with specific characteristics such as the rated current /voltage, the capacity of electrical power/energy, the maximum current, the minimum voltage, the weight, the volume and etc. The Figure I.3 shows the characteristics of the energy density and the power density for different electrical storage technologies.

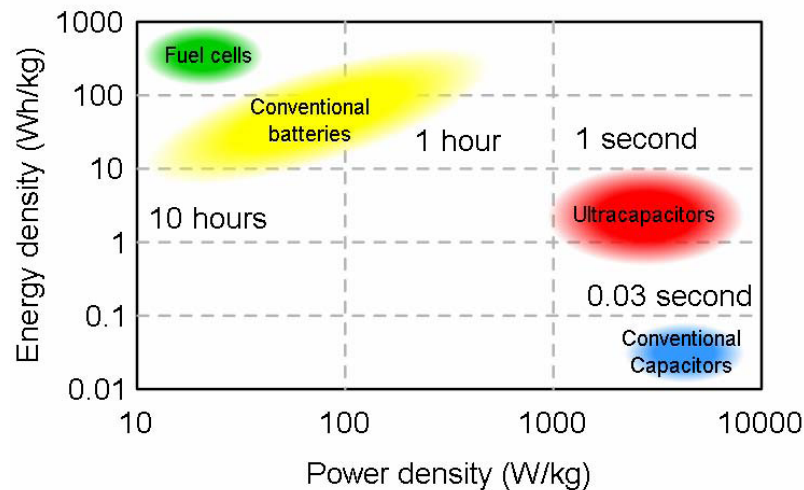


Figure I.3 Energy and power density of different storage technologies Source: Maxwell [URL 06c]

### I.3.2. Long term energy storage and fast dynamic power storage

According to the different energy and power densities, the energy storage technologies can be classified into two types: long term energy storage and fast dynamic power storage.

The long term energy storage units have the higher energy density. They are usually used as an energy reserve for a long time (several hours or several days). And long term energy storage units can continually release the electrical power during a relatively long period (from dozens of minutes to several hours). The different battery technologies, the hydrogen storage and the compressed air storage system are considered as the long term energy storage. This kind of long term energy storage units can be used in Uninterrupted Power Supply (UPS) systems and for providing ancillary services in an electrical grid [Pen 07] [Bar 09] (Figure I.4). Recently long term energy storages have been also proposed for solving the problem of the intermittent power supply of renewable energy sources [Bha 05] (Figure I.5).

Compared to the long term energy storage, the fast dynamic power storage units have higher power density. They are suitable for the fast balancing of high power. Their period of electrical power release and restoration is significantly less than the long term energy storage (from several milliseconds to minutes). This kind of power storage can perform a good dynamic characteristic in the application of hybrid electric vehicle [Lho 05]. In the domain of renewable energy based power production, they can also provide an improvement of the

power quality.



Figure I.4 NaS battery installation at Tokyo Electric Power Co.'s Ohito (6MW/48 MWh) [www.powermag.com]

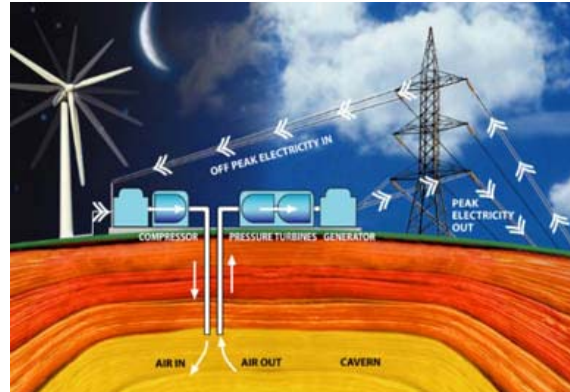


Figure I.5 Compressed Air Energy Storage (CAES) system with wind turbines, Huntorf, Germany [Gaelectric Energy Storage Ltd]

## I.4. Hybrid power generator

### I.4.1. Interest

Wind and solar energy based generators are passive generators since they can not participate in the energy management of a grid. Their power production depends on the availability of the primary renewable source. So a high reliability with a good efficiency for a power system can not be ensured with 100% of renewable energy based generators.

In contrast, conventional power generators (fossil fuel generators, nuclear fuels...) are controllable and can supply the necessary power to satisfy the grid power requirements. Moreover, this controllable power can provide some ancillary services to the grid, basically frequency regulation by active power control, voltage regulation by reactive power control, etc... However, conventional power generators must face to the fossil exhaustion and environmental challenge.

Energy storage devices can serve as backup power plants. They can be used to store or to release electrical power like an energy buffer, supporting the operation of sources, transmission, distribution and loads. Therefore, they can help to solve the problems of renewable energies' intermittent availabilities and fast transients.

The combination of energy storage devices and a renewable energy based generator constitutes a hybrid power generator. It provides not only a clean energy but also a high power quality. Moreover, this hybrid power system becomes an active generator, which can supply ancillary services to the grid as conventional generators.

Previously, at the L2EP lab, a PhD has worked on the use of hydrogen storage and fuel cells within a wind generator to design an active wind generator [Zho 09]. In a similar way one challenge of this research work is to upgrade actual passive PV generators to active PV generators.

### I.4.2. Configuration of an hybrid power generator

#### a. Improvement of reliability and erasing the intermittency

In our study, photovoltaic panels work as the main power source in this hybrid power generator. A set of lead acid batteries is chosen as the long term energy storage device for



shaving the PV power peak during the daytime and restoring it during sun unavailability. There sizing will depend on the wanted reliability for the active generator. In order to smooth the transient PV power fluctuations a bank of ultracapacitors is used for the fast dynamic power regulation. Components are now presented.

### b. Photovoltaic technology

Solar cells are classified into three generations. At present there are concurrent researches on all three technology generations while the first PV generation is the most highly represented in commercial production, accounting for 89.6% of the 2007 production.

First generations of PV cells consist of large-area, high quality and single junction devices. First technologies involve high energy and huge inputs, which prevent any significant progress in reducing production costs. Single junction silicon devices are approaching the 31% theoretical limiting efficiency and achieve an energy payback period of 5–7 years (Figure I.6a).

The second generation has been developed to address energy requirements and production costs of solar cells. Alternative manufacturing techniques, such as solution deposition, vapour deposition, electroplating, and use of Ultrasonic Nozzles, are advantageous as they reduce high temperature processing significantly. It is commonly accepted that, as manufacturing techniques evolve, production costs will be dominated by constituent material requirements, whether this be a silicon substrate or glass cover (Figure I.6b).

Third generation technologies aim to enhance the poor electrical performance of the second generation (thin-film technologies) while maintaining very low production costs (Figure I.6c). Current research is targeting conversion efficiencies of 30-60% while retaining low cost materials and manufacturing techniques [Gup 09] [Gre 06] [ISE 09].

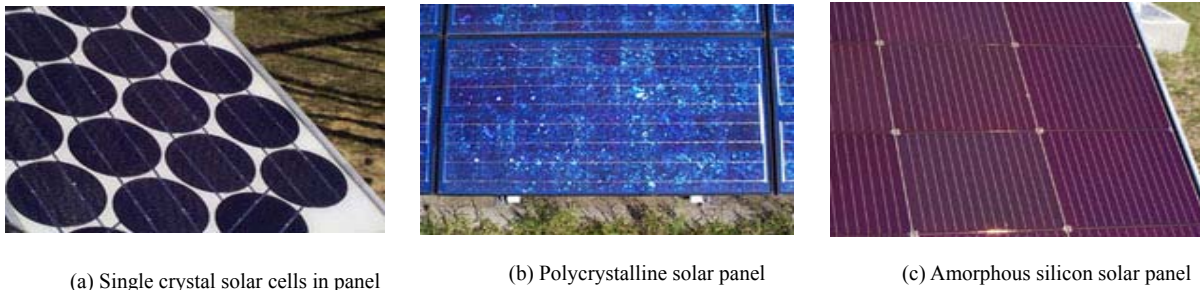


Figure I.6 Different types of silicon solar cells

PV cells consist of two types of material, often the P-type and N-type silicon ((Figure I.7). Light of certain wavelengths are able to ionize the atoms in the silicon (causing atoms to either gain or lose electrons) and the internal field produced by the junction separates some of the positive charges ("holes") from the negative charges (electrons) within the photovoltaic device. The holes are swept into the positive or p-layer and the electrons are swept into the negative or n-layer. Although these opposite charges are attracted to each other, most of them can only recombine by passing through an external circuit outside the material because of the internal potential energy barrier. Therefore if a circuit is made (Figure I.7), power can be produced from the cells under light because the free electrons pass through the load to recombine with the positive holes.

Why do we choose the photovoltaic cells as the main power source in a renewable energy based active generator? The 89 Petawatt ( $10^{15}$  W) of sunlight reaching the Earth's surface is plentiful, almost 6,000 times more than the 15 terawatts of average electrical power consumed by humans [URL 09b] [URL 09c]. Additionally, solar electric generation has the highest power density (global mean value of  $170 \text{ W/m}^2$ ) among renewable energies. PV installations

can operate for many years with little maintenance or intervention after their initial set-up, so after the initial capital cost of building any solar power plant, operating costs are extremely low compared to existing power technologies.

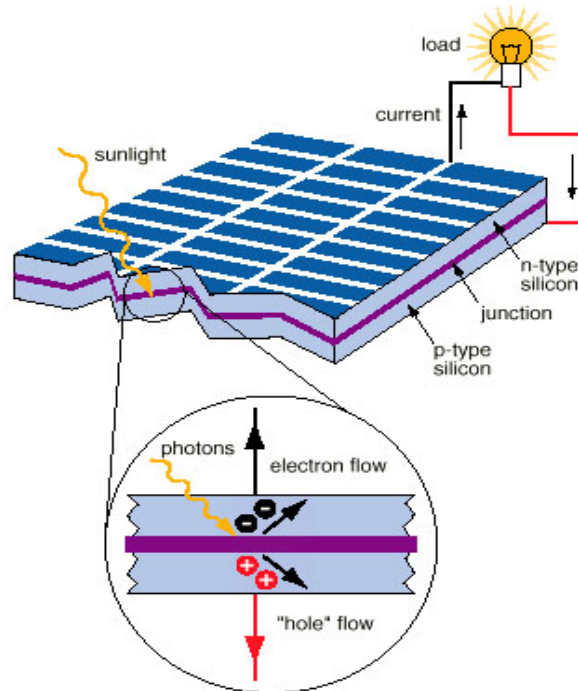


Figure I.7 Photovoltaic effects in a solar cell [URL 09b]

### c. Lead-Acid battery

Lead-acid batteries, invented in 1859 by the French physicist Gaston Planté, are the oldest type of rechargeable battery. Despite having the second lowest energy-to-weight ratio (after the nickel-iron battery) and a corresponding low energy-to-volume ratio, their ability to supply high surge currents means that the cells maintain a relatively large power-to-weight ratio [URL 09d].

Batteries use a chemical reaction to do work on charge and to produce a voltage between their output terminals. A lead-acid battery uses lead and lead oxide for electrodes and sulfuric acid for the electrolyte solution (Figure I.8). The reaction of lead and lead oxide with the sulfuric acid electrolyte produces a voltage. The discharge reaction can be reversed by applying a voltage from a charging source. The supplying of energy to an external resistance discharges the battery. The discharge reaction can be reversed by applying a voltage from a charging source. With the energy for charging battery, the lead sulfate is broken down and with oxygen from ionized water, lead oxide is deposited on the positive electrode and lead is deposited on the negative electrode.

For isolated PV applications, lead-acid batteries are yet used as an energy buffer. Because of their low cost and also because lead recycling is a well-established industry we will consider this storage technology for our study [URL 09e].

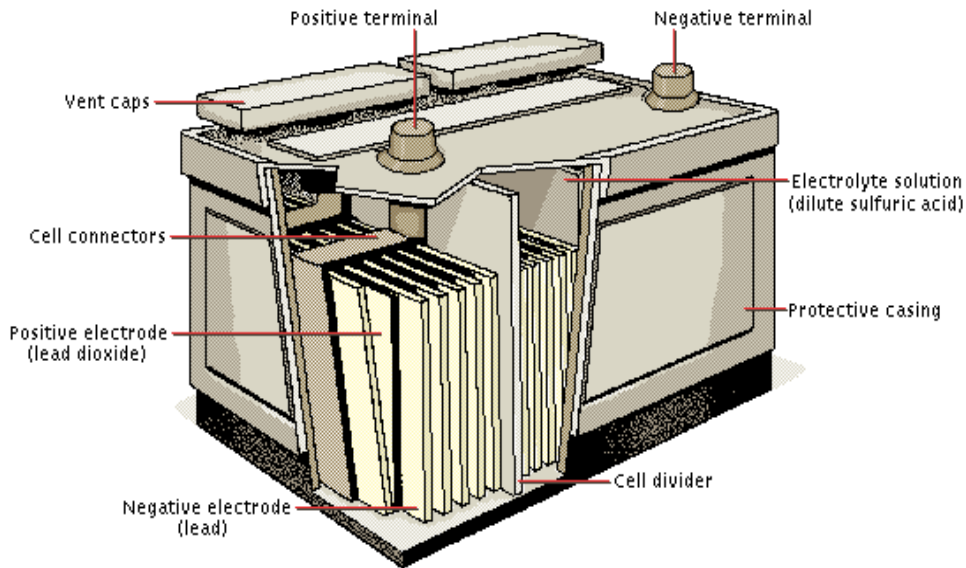


Figure I.8 Lead acid batteries [URL 09d]

#### d. Ultracapacitor

Ultracapacitors are electrochemical capacitors that have an unusually high energy density when compared to common capacitors. In an ultracapacitor charge are stored at the interface of the solid electrodes and the liquid electrolyte, forming a double layer [End 01]. So the two monolayers form a capacitance. The distance between the charge layers is only a few atomic diameters; hence an improvement of about two or three orders of magnitude in capacitance is obtained, but usually at a lower working voltage. A double layer is formed at each electrode. Larger, commercial electric double-layer capacitors have capacities as high as 5,000 Farads. The highest energy density in production is 30 Wh/kg [URL 09f].

Ultracapacitors have a variety of commercial applications, especially in "energy smoothing" and momentary-load devices. Some of the earliest uses were motor startup capacitors for large engines in tanks and submarines (Figure I.9). As the cost has fallen, ultracapacitors have started to appear on diesel trucks and railroad locomotives. Recently their ability to store energy quickly made them particularly suitable for regenerative braking applications, whereas batteries have difficulty in this application due to slow charging rates.



Figure I.9 Ultracapacitors (Maxwell)

Due to the ultracapacitor's high number of charge-discharge cycles (millions or more compared to 200–1000 for most commercially available rechargeable batteries) there are no limit parts during the whole operating life of the device, which makes the device environmentally friendly. Other advantages of ultracapacitors are: the extremely low internal resistor, the high efficiency (up to 97-98%), the high output power, extremely low heating levels and the improved safety. According to ITS (Institute of Transportation Studies, Davis, CA) test results, the specific power of electric double-layer capacitors can exceed 6 kW/kg with 95% efficiency [Zub 00].

In our study, the ultracapacitors are used for implementing the fast dynamic power compensations thanks to their high power density.

### I.4.3. Structure of the studied hybrid power generator

The structure that has been widely used for isolated power systems is based on the direct connection of a battery bank to the dc-bus of the grid-connected inverter (Figure I.10). A PV controller is used to extract the Maximum Power from PV panels and send it to the battery bank. However, the stochastic nature of the PV power output and power demand leads to a fast charge/discharge action of batteries and a fast battery ageing.

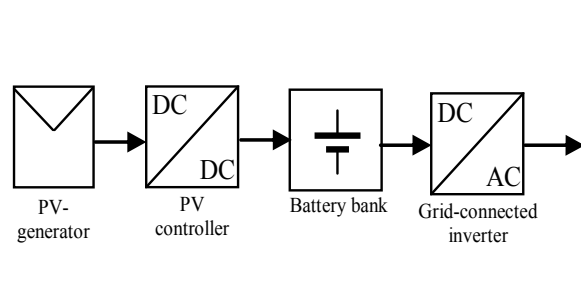


Figure I.10 Cascade coupled structure

To enable a more efficient use of batteries, AC coupled and DC-coupled structures can be considered in order to have control abilities of the exchanged powers with the batteries.

In an AC-coupled Hybrid Power Generators (HPG), all sources are connected to a main AC-bus (Figure I.11.a) [Bas 06] [Li 08a]. This AC-bus can be the utility network. In AC-coupled structure, different sources of HPG can be located anywhere in the grid with a long distance from each other. However, the voltage and the frequency of the main AC bus should be well controlled in order to ensure the stability of the distributed sources and the compatibility with the utility network.

In a DC-coupled HPG, all sources are connected to a main DC-bus before being connected to the grid through a main inverter (Figure I.11.b) [Yu 04]. In a DC-coupled structure, the voltage and the frequency of the grid are independent from those of each source. A first interest is that the battery bank is connected to the dc-bus via a DC/DC converter. This DC/DC converter can be used to implement an optimized charge/discharge operation mode. A second advantage is that a super capacitor bank is added and is also connected to the dc-bus via another DC/DC converter. The PV array is connected to the dc-bus via a PV converter.

Apart from these two coupling structure, a mixed structure can be also used to build a HPG (Figure I.11.c) with some advantages taken from both of DC and AC coupled structures.

In our study, a DC-coupled structure is chosen because it is flexible and expandable since the number and the type of the energy sources can be freely chosen. Moreover, the grid frequency is independent from the sources through a DC bus. The grid voltage is also

independent from the DC bus voltage and for each source's voltage through different power converters.

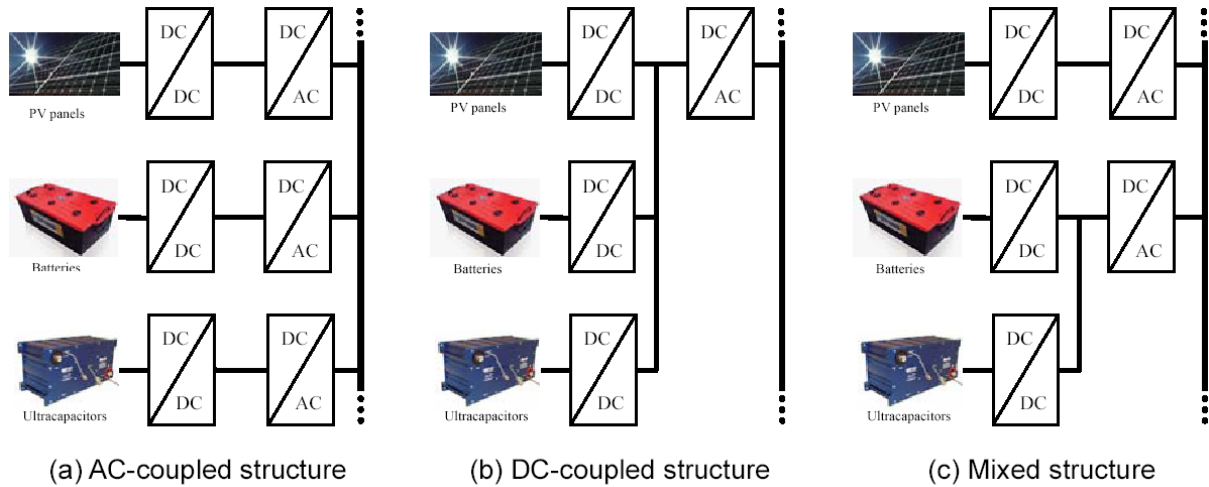


Figure I.11 Structure of hybrid power generator for distributed generation

## I.5. Modeling of the studied hybrid power generator

### I.5.1. Presentation

A domestic 3kW PV installation is considered. A set of 106Ah lead-acid batteries is used to enable at least four hours power supply. The ultracapacitors are sized to welcome the PV peak current as well as to supply the peak power (3kW) during 12 minutes in case of PV shortage. (Appendix I) Photovoltaic panels, batteries and ultracapacitors are coupled to a common 48V DC voltage bus by three DC/DC power electronic converters (Figure I.12).

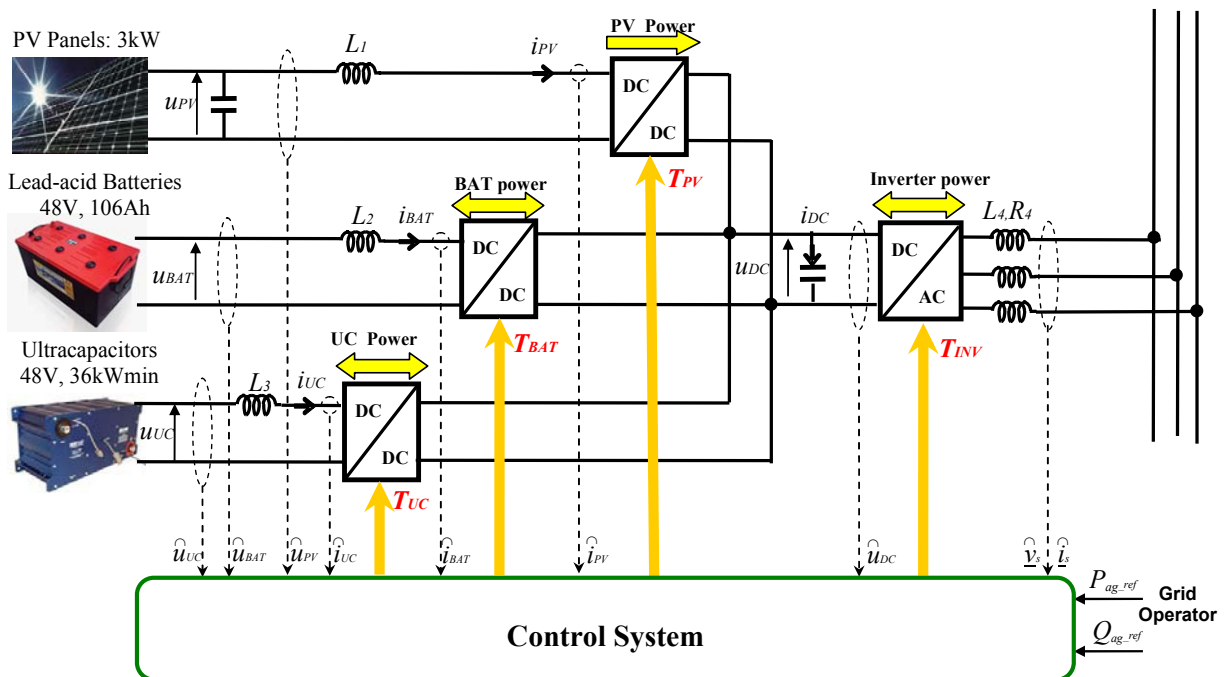


Figure I.12 PV based hybrid power generator

These converters are used for the power control of each source. The grid connection is performed by a three-phase inverter. In order to satisfy the power demand from the grid operator and to provide several ancillary grid services, the control system sends control

signals to each power electronic converter. In order to design the power management and the control system for this grid-connected PV generator including both storage units (see Chapter III) the mathematical modeling the HPG is now presented.

### I.5.2.PV panels

#### a. Modeling of a PV cell

##### **P-N junction**

Today, the most used photovoltaic cell consists of large-area P-N junctions, which are made from silicon. As a simplification, one can imagine bringing a layer of N-type silicon into direct contact with a layer of P-type silicon. In practice, P-N junctions of silicon solar cells are not made in this way, but rather, by diffusing a N-type dopant into one side of a P-type wafer.

In a P-N junction, the piece of P-type silicon and the piece of N-type silicon are intimately contacted. The electrons diffuse from the N-type side of the junction (high electron) into the P-type side of the junction (low electron concentration). When the electrons diffuse across the P-N junction, they recombine with holes on the P-type side. The diffusion of carriers does not happen indefinitely however, because of an electric field, which is created by the imbalance of charge immediately on either side of the junction. The electric field across the P-N junction creates a diode that promotes a charge flow, known as the drift current that opposes and eventually balances out the diffusion of electron and holes. This region where electrons and holes have diffused across the junction is called the depletion region because it no longer contains any mobile charge carriers. It is also known as the space charge region.

##### **Equivalent circuit of a solar cell**

In order to analyze the electronic behavior of a solar cell, an electrical equivalent model is considered. An ideal PV cell may be considered as a current source in parallel with a diode. In practice a PV cell is not ideal, so a shunt resistance and a series resistance component are added to the model [Xia 04]. The resulting equivalent circuit is shown on the Figure I.13.

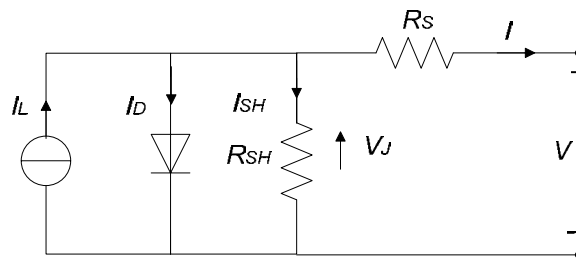


Figure I.13 Equivalent circuit of a solar cell

##### **Characteristic equations**

In this equivalent circuit, the PV cell is considered as a current source with the photovoltaic effect. The output current is expressed as:

$$I(t) = I_L(t) - I_D(t) - I_{SH}(t) \quad (R.I-1)$$

where

- $I$ : output current (amperes),
- $I_L$ : photogenerated current (amperes),

$I_D$ : diode current (amperes),

$I_{SH}$ : shunt current (amperes).

The current through these elements is governed by the voltage across them:

$$V_j(t) = V(t) + I(t)R_s \quad (\text{R.I-2})$$

where

$V_j$ : voltage across the diode and the resistor  $R_{SH}$  (volts),

$V$ : voltage across the output terminals (volts),

$I$ : output current (amperes),

$R_S$ : series resistor ( $\Omega$ ).

With the Shockley diode equation, the current through the diode is expressed as:

$$I_D(t) = I_0 \left\{ \exp \left[ \frac{qV_j(t)}{nkT} \right] - 1 \right\} \quad (\text{R.I-3})$$

where

$I_0$ : reverse saturation current (amperes),

$n$ : diode ideality factor (1 for an ideal diode),

$q$ : elementary charge ( $1.6022 \times 10^{-19}$  coulomb),

$k$ : Boltzmann's constant ( $1.3806 \times 10^{-23}$  J/K),

$T$ : absolute temperature and  $\frac{kT}{q} \approx 0.0259$  Volt at  $25^\circ\text{C}$ .

With the Ohm's law, the current through the shunt resistor is expressed as:

$$I_{SH}(t) = \frac{V_j(t)}{R_{SH}} \quad (\text{R.I-4})$$

Where  $R_{SH}$ : shunt resistor ( $\Omega$ ).

Substituting equations (R.I-4), (R.I-3) and (R.I-2) into the first equation gives the characteristic equation of a PV cell, which relates PV cell parameters to the output current and voltage:

$$I(t) = I_L(t) - I_0 \left\{ \exp \left[ \frac{q(V(t) + I(t)R_s)}{nkT} \right] - 1 \right\} - \frac{V(t) + I(t)R_s}{R_{SH}} \quad (\text{R.I-5})$$

For a given voltage ( $V(t)$ ) the equation may be solved to determine the output current ( $I(t)$ ). Because the equation involves the current on both sides in a transcendental function the equation has no general analytical solution. However it is easily solved by using numerical methods.

Since the parameters  $I_0$ ,  $n$ ,  $R_S$ , and  $R_{SH}$  cannot be measured directly, a characteristic equation is generally used with a nonlinear regression to extract the values of these parameters on the basis of their combined effect on the PV cell behavior.

### **Photovoltaic cell model**

When the cell is operated in short circuit,  $V = 0$  and the current  $I(t)$  through the terminals is defined as the short-circuit current ( $I_{SC}(t)$ ). For a high-quality PV cell (low value of  $R_S$  and  $I_0$ , and high value of  $R_{SH}$ ) the short-circuit current  $I_{SC}$  is expressed as:

$$I_{SC}(t) \approx I_L(t) \quad (\text{R.I-6})$$

By taking into account the effect of the irradiance and the temperature, the current  $I_{SC}$  is expressed as:

$$I_{SC}(t) = I_{SCS} \frac{G(t)}{G_s} [1 + \Delta I_{SC}(T(t) - T_s)] = I_L(t) \quad (\text{R.I-7})$$

With  $G$ : irradiance ( $\text{W} / \text{m}^2$ ),  
 $T$ : cell temperature ( $\text{K}$ ),  
 $I_{SCS}$ : short circuit current measured in Standard Test Conditions (STC),  
 $G_s$ : Standard illumination:  $1000 \text{ W} / \text{m}^2$ ,  
 $T_s$ : standard temperature:  $298.15 \text{ K}$ .  
 $\Delta I_{SC}$ : temperature coefficient of short circuit current

When the cell is operated in open circuit and  $I = 0$ , the voltage across the output terminals is defined as the open-circuit voltage ( $V_{OC}$ ). Assuming the shunt resistor ( $R_{SH}$ ) is high enough to neglect the final term of the characteristic equation (R.I-5), the open-circuit voltage is expressed as:

$$V_{OC}(t) \approx \frac{kT}{q} \ln\left(\frac{I_L(t)}{I_0} + 1\right) \quad (\text{R.I-8})$$

In an open-circuit condition:  $V = V_{OC}$  and  $I=0$ , the equation (R.I-1) can be written as:

$$I_L(t) = I_D(t) + I_{SH}(t) = I_{sat} \left[ \exp\left(\frac{V_{oc}(t)}{V_t}\right) - 1 \right] + \frac{V_{oc}(t)}{R_{SH}} \quad (\text{R.I-9})$$

With  $V_t = \frac{AkT}{q}$  and  $A$  the Ideal factor of the diode,

The saturation current is defined as:

$$I_{sat} = \frac{I_L(t) - \frac{V_{oc}(t)}{R_{SH}}}{\exp\left(\frac{V_{oc}(t)}{V_t}\right) - 1} \quad (\text{R.I-10})$$

The open-circuit voltage is expressed as:

$$V_{OC} = V_{OCS} + \Delta V_{OC}(T - T_s) \quad (\text{R.I-11})$$

With  $V_{OCS}$ : open-circuit voltage in STC,

$\Delta V_{OC}$ : temperature coefficient of open circuit voltage.

Note: The resistors and the ideal factor are influenced by the temperature [Sha 04]. In order to simplify the model, these values are set in STC.



### b. Maximum Power Point Tracking (MPPT)

A solar cell may operate over a wide range of voltages ( $V$ ) and currents ( $I$ ). By increasing the voltage of an irradiated cell continuously from zero (a short circuit) to a very high value (an open circuit) the maximum-power point can be determined. The point that maximizes the product  $V, I$  is achieved when the cell delivers the maximum electrical power for the received level of irradiation (Figure I.14).

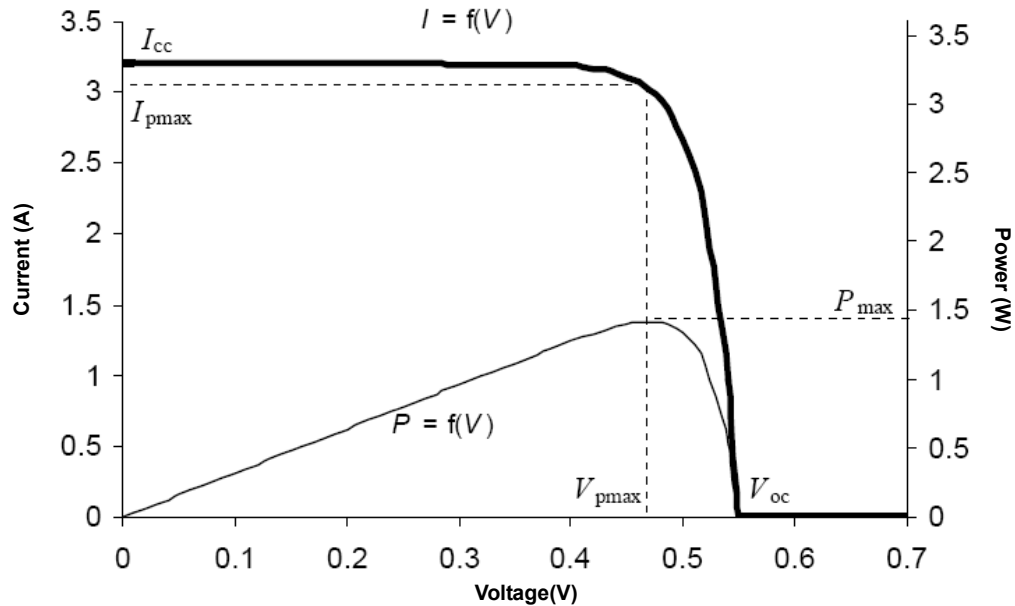


Figure I.14  $I=f(V)$  and  $P=f(V)$  characteristics of a PV Cell

The maximum power point varies with the incident illumination. For large PV systems, a maximum power point tracker tracks the instantaneous power by continually measuring the voltage and current. It uses this information to dynamically adjust the voltage so that the maximum power is always transferred, regardless of the variation in lighting.

The MPPT control may be processed by using different algorithms [Cha 05]. Perturbation and observation (P&O) and Incremental conductance are the most used algorithms.

- Perturbation and observation (P&O) algorithm

Thanks to its ease of implementation, the P&O algorithm is widely used. However, it does not follow exactly the point of maximum power when the solar radiation varies quickly because of its low speed. Figure I.15 shows the operating principle of the P&O algorithm.

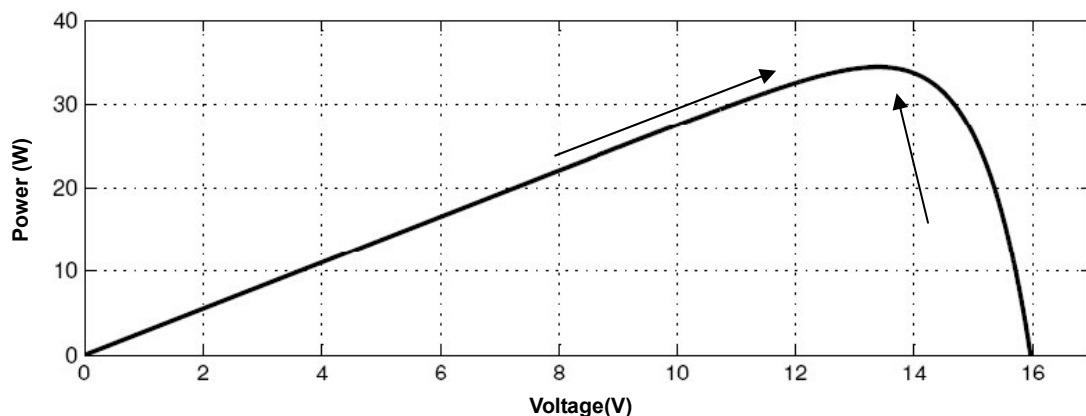


Figure I.15 Perturbation and observation method

In this algorithm, a slight disturbance is introduced in the PV voltage. Because of this disturbance, the power of the solar panel changes its value. If the power variation is positive ( $\Delta P > 0$ ), the research of the point of maximum power is in the good way. If  $\Delta P < 0$ , the search must be done in the reverse path.

- Incremental conductance algorithm

For the search of the maximum power point, this algorithm uses the equation:

$$P_{PV} = V_{PV} \cdot I_{PV} \quad (\text{R.I-12})$$

By differentiating equation (R.I-12) versus voltage  $V_{PV}$ , we get:

$$\frac{dP_{PV}}{dV_{PV}} = I_{PV} + V_{PV} \cdot \frac{dI_{PV}}{dV_{PV}} \quad (\text{R.I-13})$$

At the maximum power point, we get:

$$\frac{dP_{PV}}{dV_{PV}} = 0 \quad (\text{R.I-14})$$

$$\frac{dI_{PV}}{dV_{PV}} = -\frac{I_{PV}}{V_{PV}} \quad (\text{R.I-15})$$

As shown in Figure I.16, the algorithm seeks the point at which the conductance ( $\frac{I_{PV}}{V_{PV}}$ ) is equal to the conductance increment ( $\frac{dI_{PV}}{dV_{PV}}$ ).

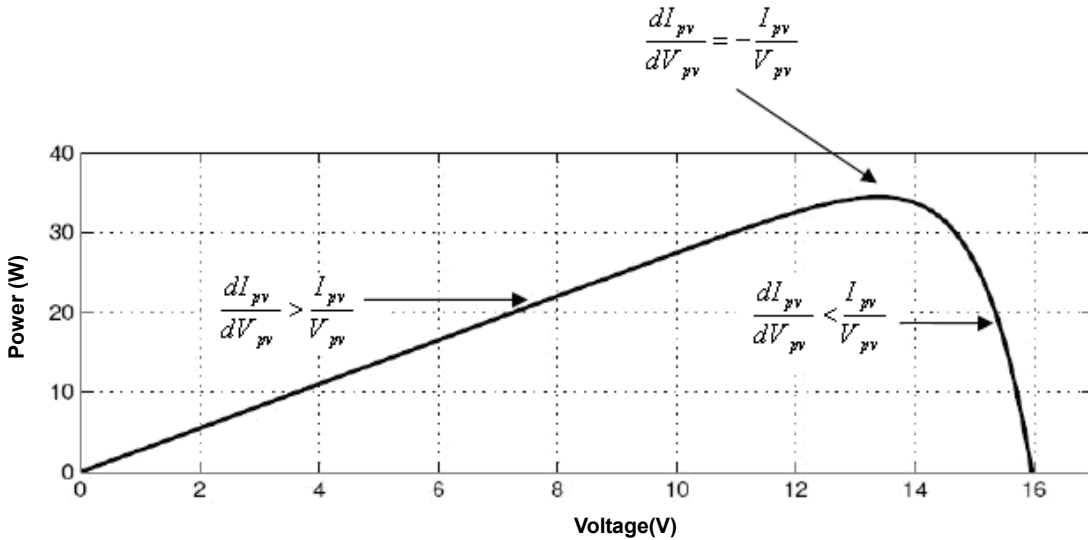
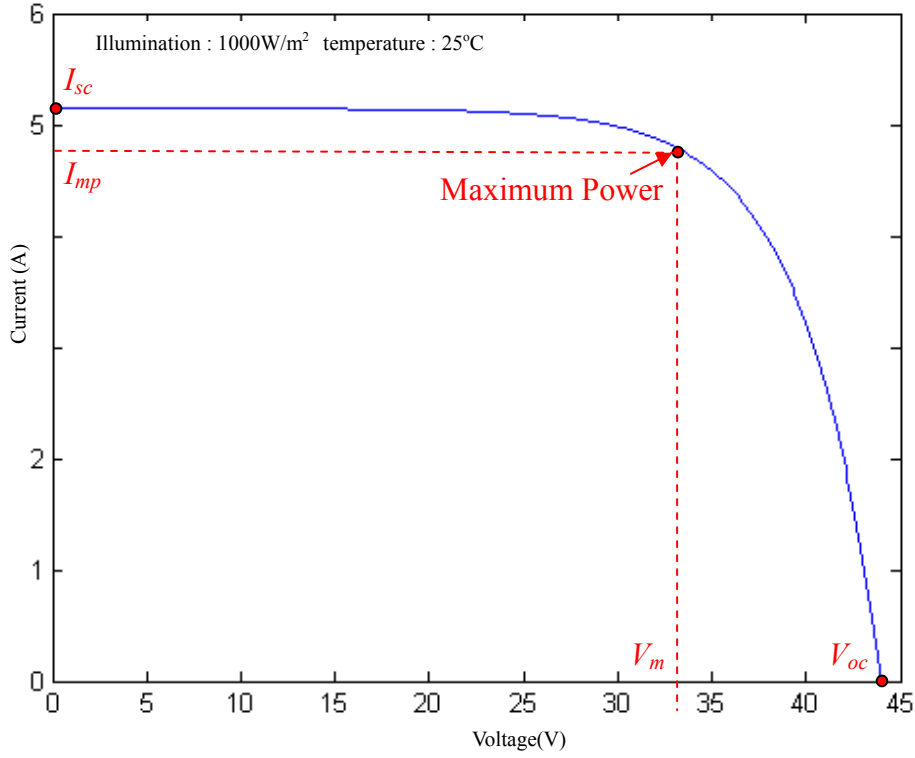


Figure I.16 Conductance increment method

### c. Simplified model with MPPT

The  $I(f, V)$  characteristic shown in Figure I.17 consists of 4 important values:

- $I_{SC}$ : short-circuit current,
- $V_{oc}$ : open-circuit voltage,
- $I_{mp}$ : current at the maximum power point,
- $V_{mp}$ : voltage at the maximum power point.


 Figure I.17  $I$  ( $V$ ) characteristic of a PV panel

Rauschenbach [Rau 80] has developed equations that generate the I-V characteristic curve of a cell according to these 4 values as:

$$I = I_{sc} \left[ 1 - C_1 \left( \exp\left(\frac{V}{C_2 V_{oc}}\right) - 1 \right) \right] \quad (\text{R.I-16})$$

$$C_1 = \left( 1 - \frac{I_{mp}}{I_{sc}} \right) \exp\left(-\frac{V_{mp}}{C_2 V_{oc}}\right) \quad (\text{R.I-17})$$

$$C_2 = \frac{\frac{V_{mp}}{V_{oc}} - 1}{\ln\left(1 - \frac{I_{mp}}{I_{sc}}\right)} \quad (\text{R.I-18})$$

The current corresponding to the maximum power is expressed as:

$$I_{mp} = I_{mps} \frac{G}{G_s} \left[ 1 + \Delta I_{mp} (T - T_s) \right] \quad (\text{R.I-19})$$

With  $I_{mps}$  the current at maximum power point is measured in standard test conditions (STC: standard test conditions) and  $\Delta I_{mp}$  the temperature coefficient of the current at the maximum power point.

The voltage corresponding to the maximum power is calculated by using [Ger 03]:

$$V_{mp} = V_{mps} \left[ 1 + \Delta V_{mp} (T - T_s) \right] + K_1 V_t \ln\left(\frac{G}{G_s}\right) + K_2 \left[ V_t \ln\left(\frac{G}{G_s}\right) \right]^2 \quad (\text{R.I-20})$$

With  $V_{mps}$  the voltage at the point of maximum power in STC,  
 $\Delta V_{mp}$ : temperature coefficient of the voltage at the maximum power point,

$K_1, K_2$ : constant parameters.

In a normal operation of the photovoltaic system, the MPPT inverter search always for the maximum power point. This allows us to simplify this model with only the current and the voltage at the maximum power point ( $I_{mp}$  and  $V_{mp}$ ).

The parameter identification has been done by using the data of the photovoltaic system at the “Arts & Métiers Paristech” research center of the L2EP (Figure I.18).



Figure I.18 PV panels at L2EP

Experimental data are chosen for constant temperature and illumination.

The characteristic parameters of the BP3160 panel can be found in Table I-1.

$V_{ocs}$	43,9 V
$I_{scs}$	5,1 A
$R_s$	1,2 $\Omega$
$R_{sh}$	161 $\Omega$
$V_{mp}$	34,5 V
$I_{mp}$	4,6 A
$\Delta V_{oc}$	160 mV/ $^{\circ}$ C
$\Delta I_{sc}$	0,065 %/ $^{\circ}$ C
$N_s$ : number of cells in series	72
$N_p$ : number of cell in parallel	1

Table I-1 Identified parameters

Obtained coefficient values and constant parameters are detailed in Table I-2:

Constant parameters	value	Constant parameters	value
$\Delta I_{mp}$	2,4e-3	$K_1$	-10
$\Delta V_{mp}$	-4,58e-3	$K_2$	- 1851

Table I-2 Constant parameters (simplified model)

The manufacturer characteristic curve is compared with the characteristic curves, which are simulated with the model. The given manufacturer curve is only valid for a 25°C cell temperature and a 1000W/m<sup>2</sup> irradiance. Obtained simulation results are much closed with the experimental results (Figure I.19).

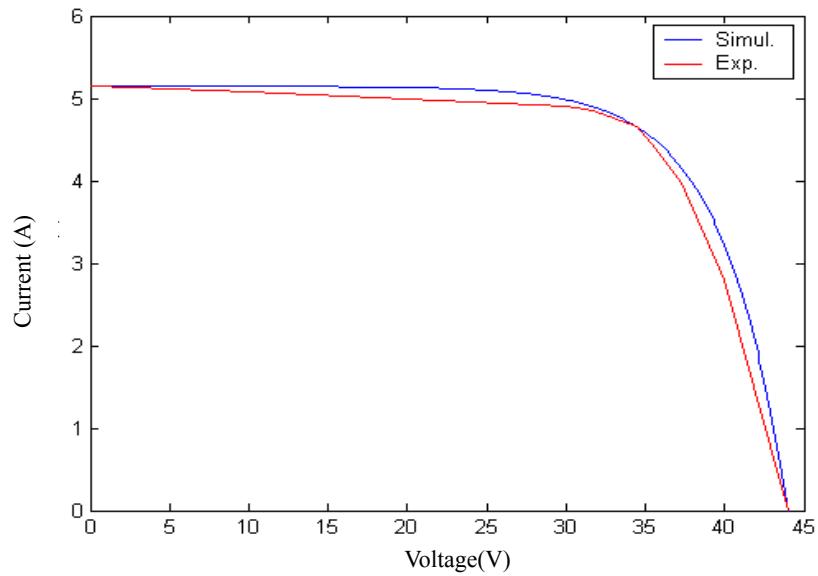


Figure I.19 Simulation results (V-I) of a simplified model for a PV panel

The powers characteristics for different illuminations and temperatures are shown on Figure I.20. For any value of the temperature and of illumination the MPPT algorithm achieve the maximum power by varying the voltage.

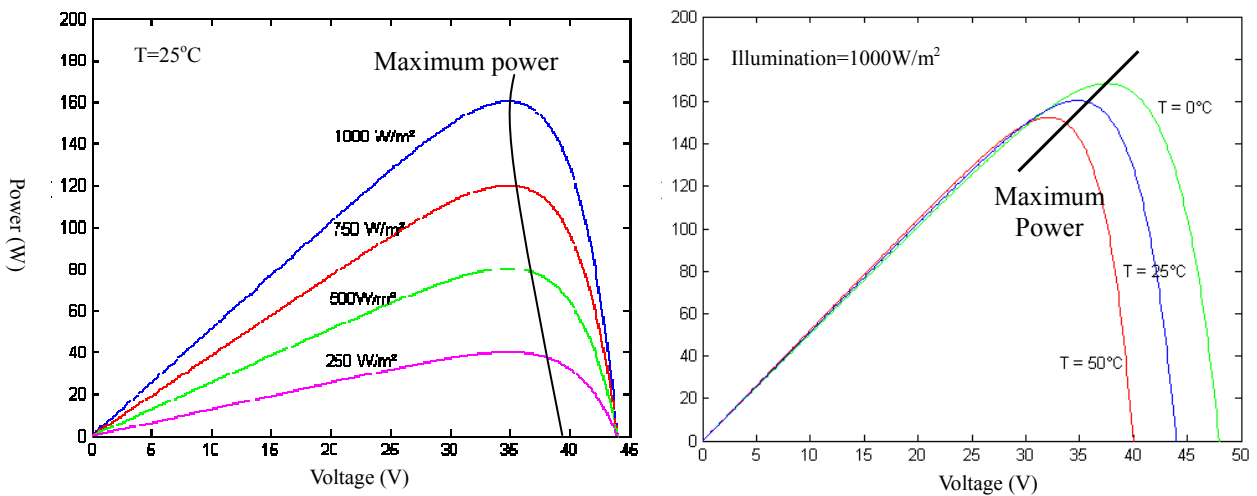


Figure I.20 P-V characteristic of a PV panel with a simplified model under different conditions

### I.5.3. Lead-acid battery

#### a. Basic cell model

An equivalent electrical circuit of the CIEMAT battery model [Ger 03] is shown in Figure I.21.

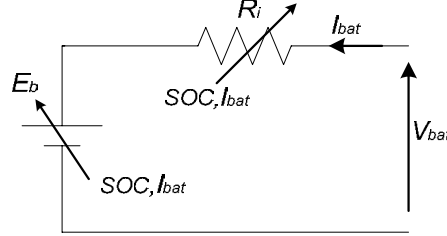


Figure I.21 Equivalent electrical circuit of the CIEMAT battery model

This model consists of a voltage source  $E_b$ , and an internal resistor  $R_i$ . This model includes the main variables of the system: the battery State Of Charge  $SOC$ , the current flowing across the battery  $I_{bat}$ , the temperature  $T$  and the number of cells in series  $n_b$ . The circuit equation is expressed as:

$$V_{bat} = n_b E_b + n_b I_{bat} R_i \begin{cases} E_b = f(SOC) \\ R_i = f(I_{bat}, SOC, T) \end{cases} \quad (R.I-21)$$

The voltage source  $E_b$  represents the voltage in open circuit across the battery terminals. This voltage is due to the stored energy into the battery through the electrochemical reactions. Obviously, this term depends directly on the stored energy.  $R_i$  is a resistor and represents the losses. This resistor value includes the effects of the working point ( $I$ ,  $SOC$ ,  $T$ ) and the health of the battery. A damaged battery has a high value of resistor irrespective of its working point. Also, the resistor is inversely proportional to the state of charge. Furthermore, at the same time as the battery is discharging, the resistor value is increasing. Note that all physical effects are expressed into electrical equations and are modeled in these terms.

The state of charge must be considered as an indicator of the electrical charge stored in the battery. The value range is  $0 < SOC < 1$ . The following equations describe the behavior of this indicator.

$$SOC(t_i) = \frac{1}{C(t_i)} \int_{-\infty}^{t_i} \eta_c I_{bat}(t) dt \quad (R.I-22)$$

$$C(t) = \frac{C_{no\ min\ al} C_{tcoef}}{(1 + A_{cap} \left(\frac{|I_{bat}(t)|}{I_{no\ min\ al}}\right)^{B_{cap}})(1 + \alpha_c \Delta T(t) + \beta_c \Delta T(t)^2)} \quad (R.I-23)$$

$$I_{no\ min\ al} = \frac{C_{no\ min\ al}}{n} \quad (R.I-24)$$

Terms involved are:  $C(t)$  the battery capacity,  $\eta_c$  the charging efficiency and  $I_{bat}(t)$  the current flowing through it.  $C_{nominal}$  is the rated battery capacity (at  $n$  hours),  $C_{tcoef}$ ,  $A_{cap}$  and  $B_{cap}$  are model parameters,  $\Delta T$  is the temperature variation from the reference value at  $25^\circ C$ ,  $I_{nominal}$  the discharge current corresponding to the  $C_{nominal}$  rated capacity,  $n$  is the time in hours,  $\alpha_c$  and  $\beta_c$  are the temperature parameters [Gua 03].

The SOC must be understood as the relation between the accepted energy and the available capacity at all times. The inner integral term models the accepted energy over the battery working life. Also, the outer integral term models the battery capacity due to the

working point environment at any given time. Both terms are functions of time and are evolving continuously. When the *SOC* is unity the battery cannot accept more energy from the system, because the stored energy fills all the battery capacity. And when the *SOC* is null the battery has no energy.

For a more intuitive use of the *SOC* concept in photovoltaic applications, a new indicator has been introduced: *LOE*, the Level Of Energy. This indicator shows the amount of energy available in the battery under normal working conditions. Equations (R.I-25, R.I-26) define the *LOE*, where  $T_1$  and  $T_2$  define the known temperature range of battery operation. Note that *LOE* depends only on the constitutive parameters of the device and the accumulated charge over time, not on the working environment of the battery. The *LOE* calculus may be carried out by considering the maximum available battery capacity  $C_n$ , obtained by taking into account the range of possible current and temperature values. So,  $C_n$  is evaluated from Equation (R.I-26), with battery current equal to zero and maximum temperature value (if a standard temperature range  $[-40^\circ\text{C}, 40^\circ\text{C}]$  is considered for a first theoretical approach, then  $T=40^\circ\text{C}$ ). Thus, *LOE* is not limited to the higher limit of unity, but *LOE* values near or greater than unity are undesirable in order to avoid damaging the battery.

$$LOE(t_i) \equiv \frac{1}{C_n} \int_{-\infty}^{t_i} \eta_c I_{bat}(t) dt \quad (R.I-25)$$

$$C_n \equiv \max(C(t)) \Big|_{\substack{I_{bat} = 0 \\ T \in [-T_1, T_2]}} \quad (R.I-26)$$

*LOE* represents directly the stored energy in the battery ( $C_n$  is constant). Therefore the *SOC* and the *LOE* are complementary. Furthermore, a battery can have  $SOC=1$  and  $LOE \neq 1$ ; this indicates that the battery is saturated, but only at a percentage of the nominal capacity.

Figure I.22 illustrates the time variation of the battery voltage evolution due to the current flowing through it. Thus, different possible working zones for a 2V element can be observed. For the first 16 hours the current is flowing inside the battery, and it evolves into different zones: charging, overcharging and saturation zones. From 16 hours to 27 hours the current is flowing outside the battery and it evolves into discharging, over discharging and exhaustion zones.

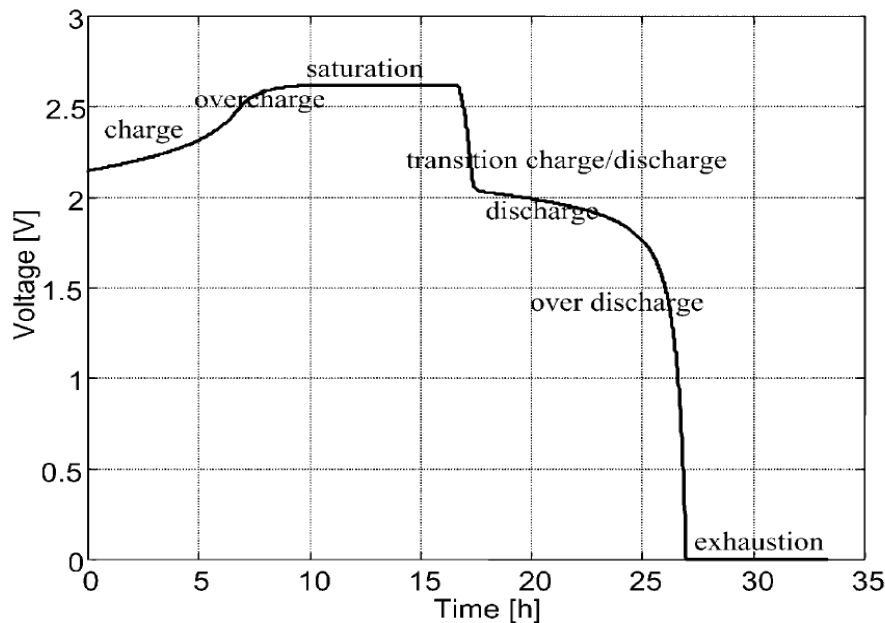


Figure I.22 Working areas of a battery

### b. Simplified model

In the studied case, a simplified model is used by considering a constant internal resistor  $R_i$ . The resistor is supposed to be constant during the charge and the discharge cycles and does not vary with the magnitude of the current. When this preset model is used in the SimPowerSystem software, a generic value is loaded, corresponding to the nominal voltage and the rated capacity of the battery. The battery voltage is expressed as:

$$E_b = E_0 - K \cdot Q \cdot \frac{1}{(Q - i_t)} + A e^{-B \cdot i_t} \quad (\text{R.I-27})$$

$$i_t = \int_{t_0}^t i_{bat}(t) dt \quad (\text{R.I-28})$$

with

$E_0$  = Fully charged voltage (V)     $Q$  = Battery capacity (Ah)

$A$  = Exponential voltage (V)     $B$  = Exponential capacity (Ah)

$K$  = Polarization voltage (V)

All parameters of this equivalent circuit can be identified, by considering the discharge characteristics with a nominal current. A typical discharge curve is composed of three sections (Figure I.23):

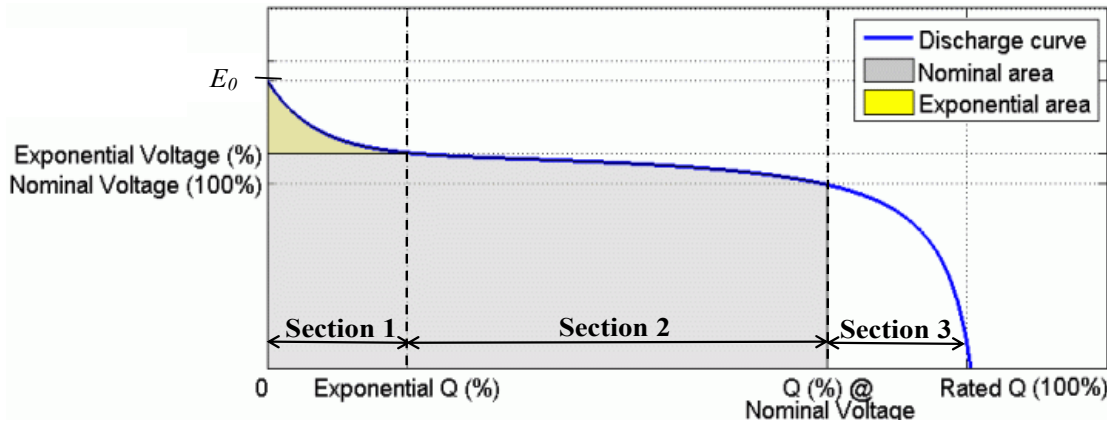


Figure I.23 Discharge curve (Q-V) of a battery

The first section represents the exponential voltage drop if the battery is initially fully charged. The width of this region depends on the battery type. The second section represents the charge that can be extracted from the battery until the voltage drops below the battery nominal voltage. Finally, the third section represents the total discharge of the battery, when the voltage drops quickly.

### c. Parameters determination

A STECO 3000 lead-acid battery is used for practical experimentations. Its nominal voltage is 12 volts ( $E_0$ ) with a 106 Ah capacity ( $Q$ ), a 5A rated current and a 2.8m $\Omega$  internal resistor  $R_i$ . From the rated current discharge characteristic curve (Figure I.24), the parameters of the battery model are estimated.



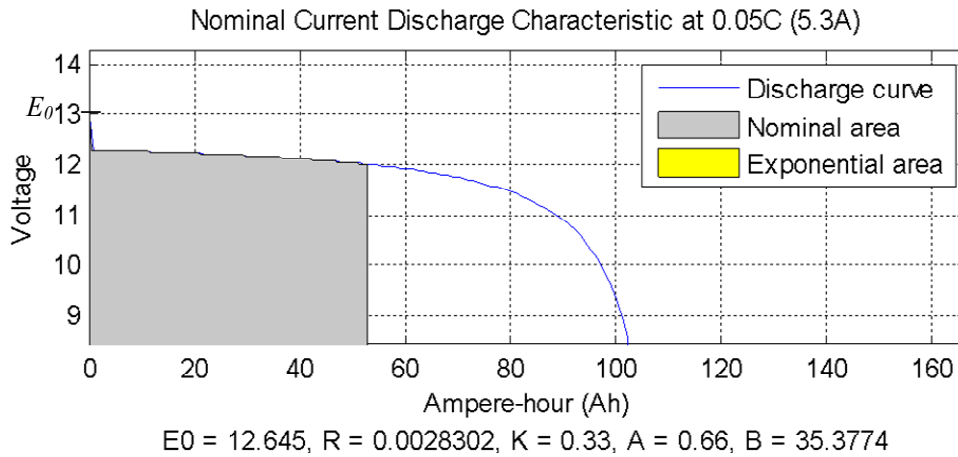


Figure I.24 Discharge curves of the lead acid battery STECO 3000

From the discharge curves of the lead acid battery STECO 3000, the following detailed parameters are deduced:

- Fully charged voltage factor: 13 Volt/12 Volt=108.33%
- Nominal Discharge current: 5.3A/ 106Ah=20%
- Capacitor @Nominal Voltage: 3.6 hours/ 5.2hours= 69%
- Exponential Voltage factor: 12.4 Volt/ 12 Volt=103.3%
- Exponential capacity factor: 0.15 hours/ 5.2 hours=2.88%

From the rated current discharge curve, all model parameters are determined with a graphic estimation:  $K=0.33$  Volt,  $A=0.66$  Volt,  $B= 35.38$  Ah.

#### I.5.4.Ultracapacitor

There are several different models describing the characteristics of ultracapacitors. The various equivalent electrical circuits of ultracapacitor model can be ranged according to the complexity.

##### a. Transmission line model

The transmission line model is currently the most used model for ultracapacitor. The ultracapacitor exhibits a non-ideal behavior, mainly because of the porous material, which is used to form the electrodes. This causes the resistance and capacitance to be distributed in such a way that the electrical response of the ultracapacitor can be described by the behavior of a transmission line [Zub 00].

A five stage model has a good accuracy for most applications and accounts for frequencies up to 10 kHz (Figure I.25). The transmission line model physically mimics the ultracapacitor distribution and has a good accuracy over a wide range of frequencies. The capacitance in the highly porous electrodes results in each of the pores is modeled as a transmission line. The model gives the double layer capacitance and the electrolyte resistor that extends deep into the pores of the material. The resistor of the electrode material is taken to be much smaller than the electrolyte resistance and the capacitors behave like small impedance elements at high frequencies. The current mainly flows among  $R_l$  and  $C_l$  into the electrode material and almost no current flows deep into the pore. The resistor and the double layer capacitance are reduced at high frequencies.

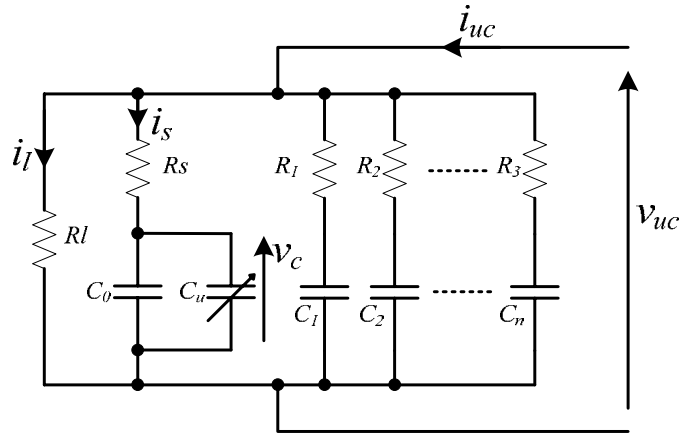


Figure I.25 Transmission line model of an ultracapacitor

### b. 3 branch model

The number of RC branches chosen for the model depends on the duration of the required time response. The 3-branch model covers a time range of up to approximately 30 minutes (Figure I.26.) [Spy 00]. Each branch has a different time constant. The first or immediate branch gives the behavior in the order of a few seconds. The second (delayed branch with  $R_{del}$  and  $C_{del}$ ) gives the behavior over the range of a few minutes, while the third (long term branch with  $R_{long}$  and  $C_{long}$ ) gives the behavior of the ultracapacitor for a time longer than 10 minutes. A leakage resistance  $R_l$ , is also included in the equivalent circuit and represents the self discharge of the ultracapacitor. Finally the voltage dependency of the ultracapacitor is modeled by a voltage dependent capacitor in the first branch of the model for simplicity.

Each of the branches has a different time constant, therefore the transient process of each branch can be observed independently from the others by measuring the terminal voltage as a function of time. This allows the model parameters to be calculated by using a single fast current controlled charge [Spy 00].

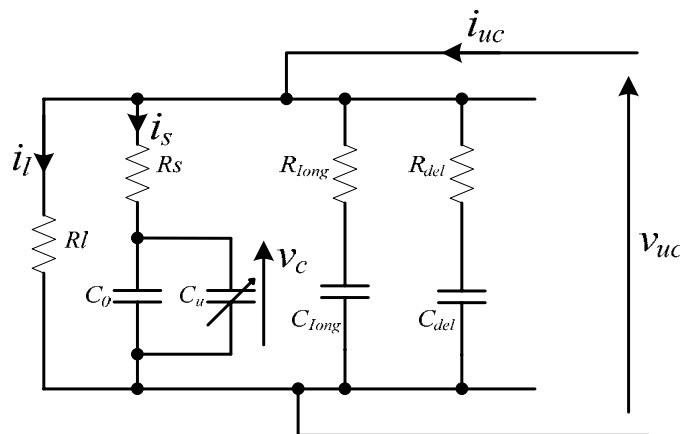


Figure I.26 3-branch model of an ultracapacitor

### c. Classical equivalent circuit model

The classical equivalent circuit model in Figure I.27 is used to describe the capacitor performances in fast discharge applications (in the order of a few seconds). The variable capacitor ( $C_u$ ) depends on the technology and the used equipment. It may be neglected. It consists of an equivalent series resistance ( $R_s$ ), which represents losses and models the internal heating in the capacitor. It is important during charging and discharging. The

equivalent parallel resistance ( $R_l$ ) models the current leakage effect.  $C_0$  is the capacitance.

**d. Simplified model**

In our application, the charging and discharging cycles are enough fast to ignore the phenomenon of relaxation. The leakage resistance  $R_l$  is also neglected because of its great value. The simplified model (sical equivalent circuit model Figure I.28) includes the final capacitor  $C_0$  in series with a resistance  $R_s$  [Li 08b].

All internal electrical relations are expressed in the following equation:

$$\frac{dv_c}{dt} = \frac{1}{C_0} i_{uc}(t) \tag{R.I-29}$$

$$v_R(t) = R_s i_{uc}(t) \tag{R.I-30}$$

$$v_{uc}(t) = v_c(t) + v_R(t) \tag{R.I-31}$$

With the ultracapacitor current  $i_{uc}$  and the output voltage  $v_{uc}$ .

Comparison of model simulation results and the experimental results have validated this model (Appendix II).

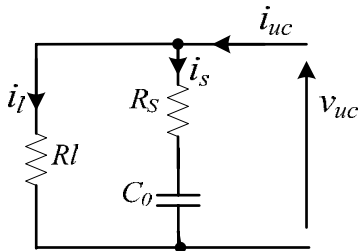


Figure I.27 Classical equivalent circuit model

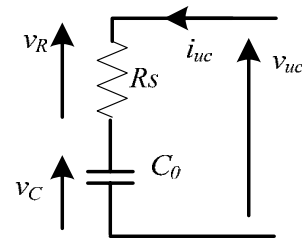


Figure I.28 Simplified model of ultracapacitor

**I.6. Conclusion**

In this chapter, the different kinds of renewable energy sources are presented. This part details the characteristics of different forms of renewable energy. Then, the interests of renewable energy are shown in different aspects: energy security, environment protection and economic development. In the same time, the constraints about the use of renewable energy in an electrical power system are discussed.

Facing to the problem of the power intermittency with the renewable energy sources, we propose to design a hybrid power generator with embedded energy storage units. The electrical energy storages can deal with not only the intermittency of power supply, but also they can help to provide the ancillary services in an electrical network. Several long term energy storage and fast dynamic power storage technologies are introduced in this chapter.

In order to transform PV panels in an active generator, a hybrid system is designed with PV panels, batteries and ultracapacitors. The photovoltaic panels, the batteries and the ultracapacitors are coupled to a common DC voltage bus by three DC/DC power electronic converters. The model description of each source is detailed. From the different models, a simplified model is chosen. In the next chapter the modeling of this active generator will help to analysis its characteristics for the design of the control system.

# *Chapter II*

## Control system of the active PV generator



## Contents

Chapter II. Control system of the active PV generator.....	41
II.1. Introduction.....	41
II.2. Modeling of the PV active generator.....	42
II.2.1. Methods.....	42
II.2.2. PV power conversion system.....	43
II.2.3. Batteries energy storage system.....	44
II.2.4. Ultracapacitors.....	45
II.2.5. Grid connection.....	46
II.2.6. DC bus.....	47
II.2.7. Modeling of the entire PV energy conversion system.....	48
II.3. Control of the active PV generator.....	49
II.3.1. Hierarchical control structure.....	49
II.3.2. Automatic Control unit.....	50
II.3.3. Power control unit.....	56
II.4. Power balancing strategies for the active PV generator.....	59
II.4.1. Role of the DC bus.....	59
II.4.2. Normal mode.....	60
II.4.3. PV limitation mode.....	63
II.4.4. Disconnection mode.....	64
II.4.5. Synthesis.....	66
II.5. Control of operating modes.....	69
II.6. Energy management of the embedded ultracapacitors.....	71
II.6.1. Energy level and management scheme.....	71
II.6.2. Full ultracapacitors mode.....	71
II.6.3. Empty ultracapacitors mode.....	72
II.7. Simulation and experimental results.....	72
II.7.1. Simulation results.....	72
II.7.2. Experimental results.....	75
II.8. Conclusions.....	77



## Chapter II. Control system of the active PV generator

### II.1. Introduction

In the previous chapter, the interest of a PV based hybrid active generator and the need for grid operator to get more dispatched distributed generators have been justified. In order to have a local energy reserve and to filter fast PV power fluctuations, lead-acid batteries and ultracapacitors are used to build a PV/batteries/ultracapacitors hybrid power system in a DC coupled structure. Lead-acid batteries and ultracapacitors have been separately studied and modeled.

The power flows between the different sources must be controlled in order to supply the real and reactive power required by the grid operator ( $P_{ag\_ref}, Q_{ag\_ref}$ ). This is performed by the control of the different power electronic converters, which must be then coordinated (Figure II.1). Different control strategies have been presented to design the energy management of hybrid power systems and for various applications. These strategies are based on the evolution of the state of the system [Aya 07], on the fuzzy control or the neural network control [Haj 07] [Mor 06], on the DC-bus regulation [Mar 06] [Tho 09], on the passivity and the flatness systems [Pay 07] [Bec 06]. In order to achieve the previous objectives, several specific problems have to be overcome, e.g. the fast and exact power control of each source with the power electronic converters; power dispatching of storage units according to their different technological characteristics for ensuring their optimal use of each storage device (life of the batteries, energy limit of the ultracapacitor).

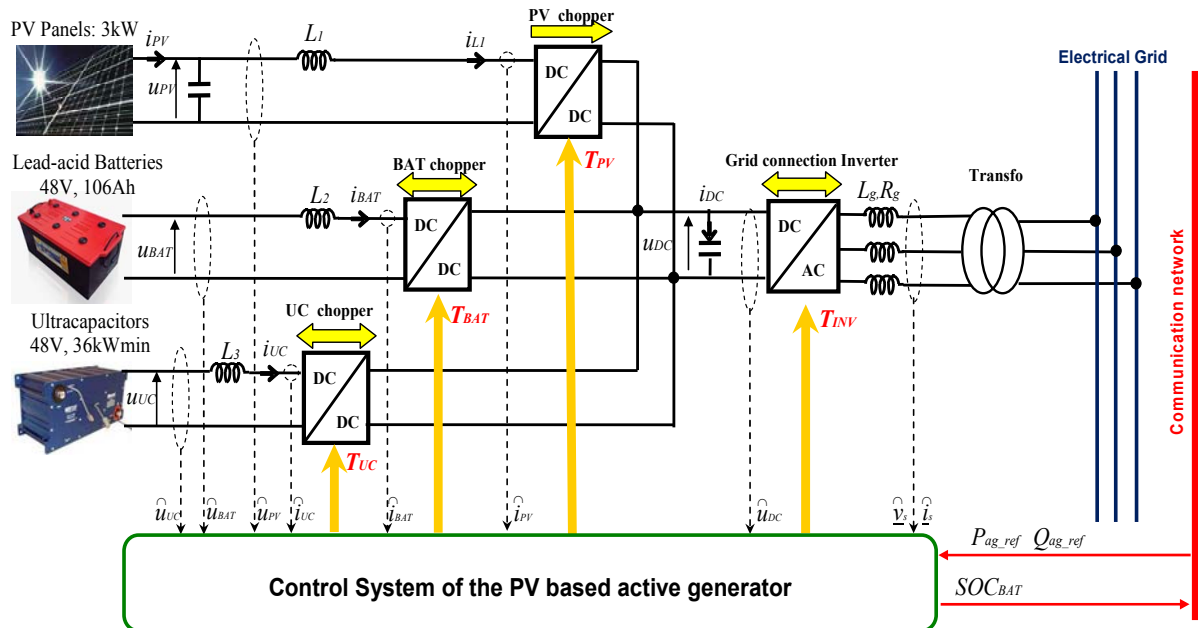


Figure II.1 Grid-connected PV based active generator with the control system

In this chapter, the presented study consists in the modeling in mean values of the entire PV based active generator. Then a hierarchical control structure is used and the design of the control system, including the power balancing and energy management strategies are detailed. The objective is to set up an active PV generator, which can work like a classical power plant; e.g. it must supply the power references from an electrical grid operator.



## II.2. Modeling of the PV active generator

### II.2.1. Methods

In order to design the control system of the PV active generator, the model of this entire system has to be analyzed. An equivalent average modeling of the power converters is enough for the design of the power control and the energy management moreover the harmonic analysis and the modulation techniques are not the scope of this study. Moreover, this characteristic can reduce significantly the simulation time for pre-validation. So, for the modeling of the PV based active generator, all the modulated values are replaced by their average values during the modulation period (Appendix III). So each power electronic converter can be replaced by an equivalent double modulated generator (Figure II.2).

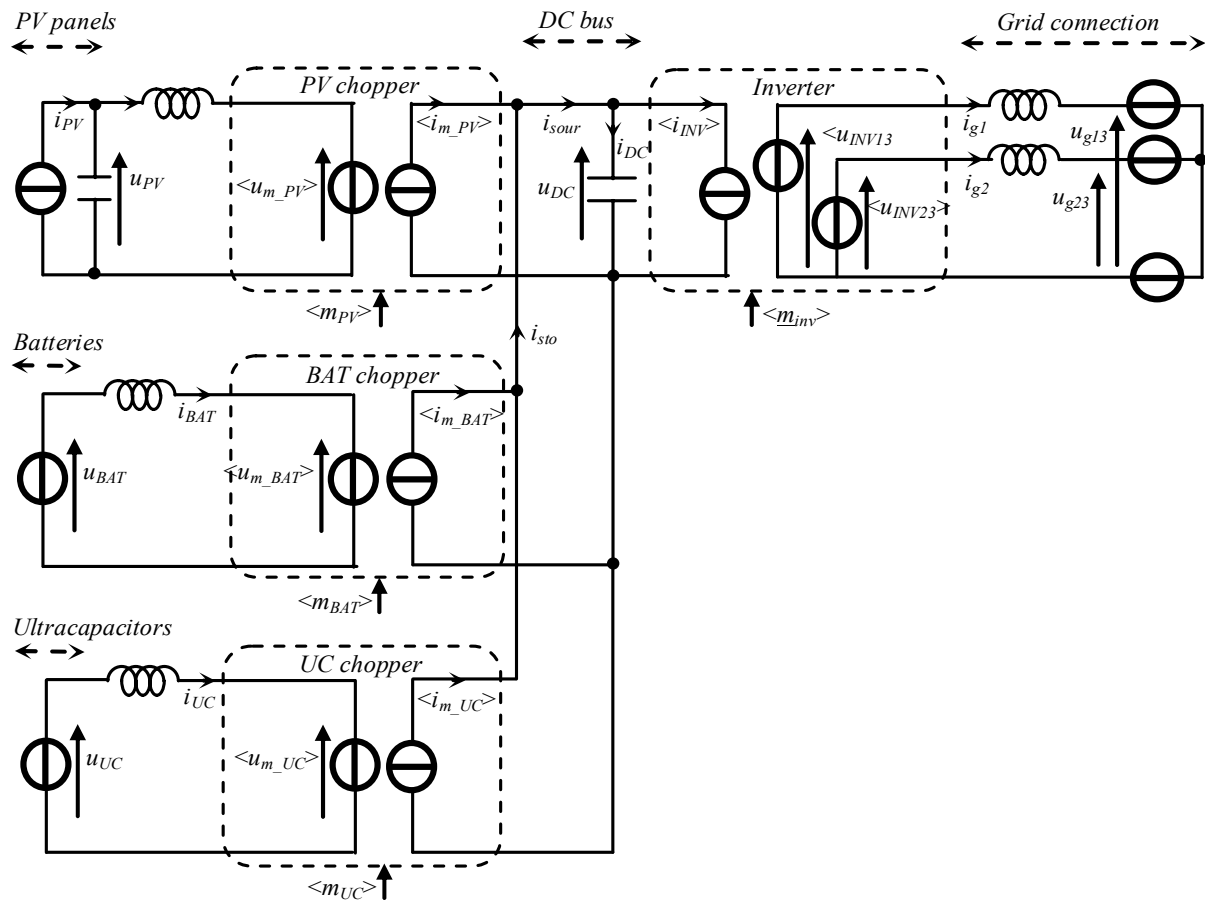


Figure II.2 Equivalent electrical diagram of the PV based active generator

The equivalent electrical diagram with the equivalent average modeling of power electronic converters makes appear five parts corresponding to the PV conversion system, the batteries, the ultracapacitors, the grid connection and the DC bus. These four power converters are used to introduce control inputs for each power conversion system, in order:

- to control the power generated by the PV panels;
- to maintain a constant DC bus voltage;
- to supply the required power exchange with the grid;
- to ensure the power buffering of each energy storage unit.

In order to illustrate the processing of the power conversion, the Energetic Macroscopic Representation (EMR) is used to model the whole PV based active generator (Appendix IV). The EMR is a synthetic graphical tool and is based on the principle of action and reaction

between connected elements. It leads to a synthetic description of the overall conversion system. In such a representation, coupling devices distribute the different electrical quantities from upstream or downstream elements. A first interest of the EMR is that an overview of all interaction of physical quantities is given and action chains can be found. A second one is that the structure of the control system can be deduced by using inversion rules in order to obtain a Maximum Control Structure (MCS). This will be used in part II.3.

### II.2.2. PV power conversion system

The modeling of PV panels has been introduced in the first chapter. In the whole PV power conversion chain, the photovoltaic panels are considered as a current source ( $i_{PV}$ ) and it must be supplied by a voltage ( $u_{PV}$ ) (Chapter 1, Part 1.5.2.b). The voltage comes from a filter ( $C_1, L_1$ ), which is fed by the modulated voltage (Figure II.3).

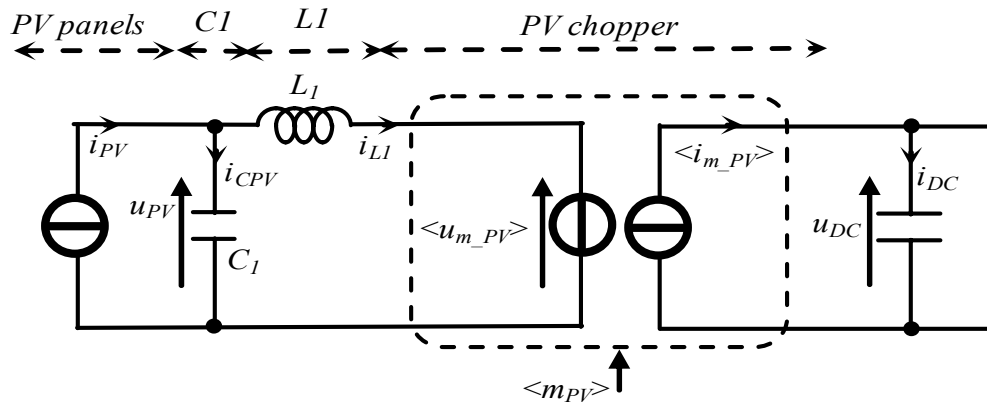


Figure II.3 Equivalent electrical diagram of PV power conversion system

The choke is also modeled as a current source ( $i_{L1}$ ). This current depends on the PV voltage and the modulated voltage of the chopper output ( $u_{m\_PV}$ ):

$$\frac{di_{L1}}{dt} = \frac{1}{L_1} (u_{m\_PV}(t) - u_{PV}(t)) \quad (\text{R. II-1})$$

Losses in the filter and the capacitor are neglected. The capacitor ( $C_1$ ) can stabilize the voltage ( $u_{PV}$ ) across the terminals of the PV panels. This capacitor can be modeled by using the PV current ( $i_{PV}$ ) and the filtered current ( $i_{L1}$ ):

$$\begin{cases} \frac{du_{PV}}{dt} = \frac{1}{C_1} i_{CPV}(t) \\ i_{CPV}(t) = i_{PV}(t) - i_{L1}(t) \end{cases} \quad (\text{R. II-2})$$

$i_{CPV}$  is the injected current in capacitor. The mean value of the terminal voltage of the chopper ( $u_{m\_PV}$ ) is obtained from the DC voltage ( $u_{DC}$ ) and the duty cycle ratio ( $m_{PV}$ ):

$$\begin{cases} \langle u_{m\_PV} \rangle = m_{PV} \cdot u_{DC}(t) \\ \langle i_{m\_PV} \rangle = m_{PV} \cdot i_{L1}(t) \end{cases} \quad (\text{R. II-3})$$

Comment:

Formerly the notation  $\langle x \rangle$  means “the average values of the instantaneous electrical quantities”  $x(t)$  (Appendix III). As all quantities are in fact in mean values the notation  $\langle x \rangle$  will not be used later.

In the EMR, the PV panels are an electrical current source and are represented as a green oval (PV) (Figure II.4). The capacitor and the inductor of the filter are two elements with energy accumulation, which are represented as two orange rectangles ( $C_1$  and  $L_1$ ). The PV chopper is an electrical converter without energy accumulation, which is represented as an orange square. Between each block exchanged electrical quantities are depicted.

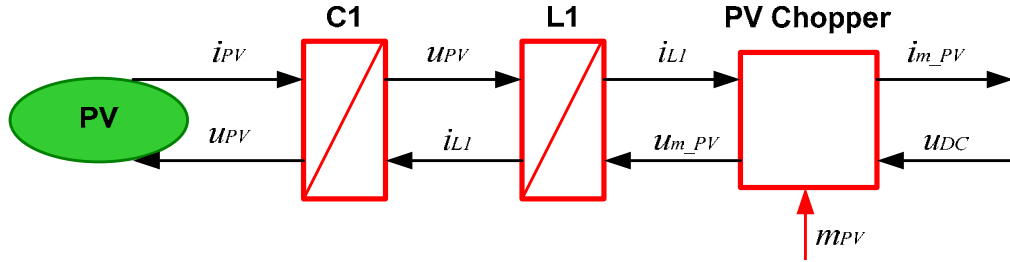


Figure II.4 EMR of the PV power conversion system modeling

### II.2.3. Batteries energy storage system

The modeling of lead acid batteries has been also introduced in the first chapter. In the whole batteries energy storage system, the batteries are considered as a voltage source ( $u_{BAT}$ ), which is connected to a choke filter ( $L_2$ ) (Figure II.5).

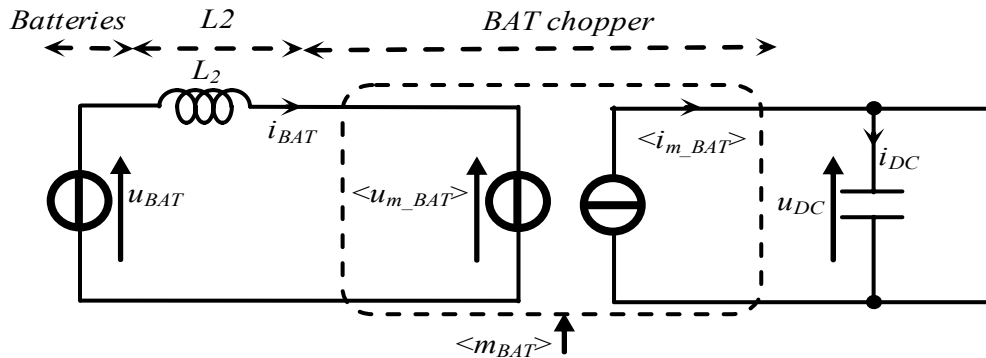


Figure II.5 Equivalent electrical diagram of the batteries energy storage system

By neglecting losses in the filter, the dynamic equation of the filtered current ( $i_{BAT}$ ) is expressed with the battery voltage ( $u_{BAT}$ ) and the modulated voltage ( $u_{m\_BAT}$ ):

$$\frac{di_{BAT}}{dt} = \frac{1}{L_2} \cdot (u_{BAT}(t) - u_{m\_BAT}(t)) \quad (\text{R. II-4})$$

where  $L_2$  is the inductor of the filter.

The mean value of the terminal voltage of the battery chopper ( $u_{m\_BAT}$ ) is obtained from the DC voltage and the duty cycle ratio ( $m_{BAT}$ ):

$$\begin{cases} u_{m\_BAT} = m_{BAT} \cdot u_{DC}(t) \\ i_{m\_BAT} = m_{BAT} \cdot i_{BAT}(t) \end{cases} \quad (\text{R. II-5})$$

In a same way, the filtered current ( $i_{BAT}$ ) is modulated by the chopper, and then this

modulated current ( $i_{m\_BAT}$ ) is injected into the common DC bus. The average value of the output current ( $i_{m\_BAT}$ ) of the chopper is equal to the battery current ( $i_{BAT}$ ) multiplied by the duty cycle ratio ( $m_{BAT}$ ).

The modeling of the batteries system is described by using the EMR (Figure II.6).

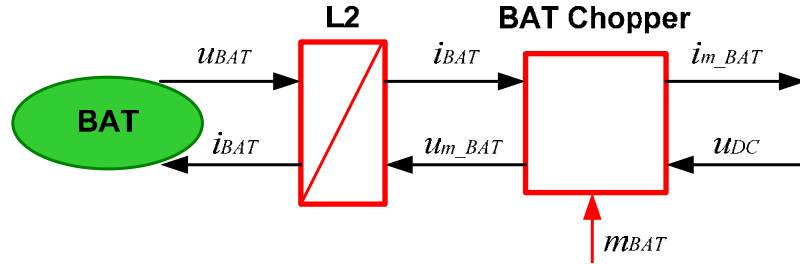


Figure II.6 EMR of the batteries energy storage system modelling

### II.2.4. Ultracapacitors

The modeling of ultracapacitors has been also introduced in the first chapter. In the whole ultracapacitor power storage system, the ultracapacitors are considered as an ideal voltage source ( $u_{UC}$ ), which is connected to a choke filter ( $L_3$ ) (Figure II.7).

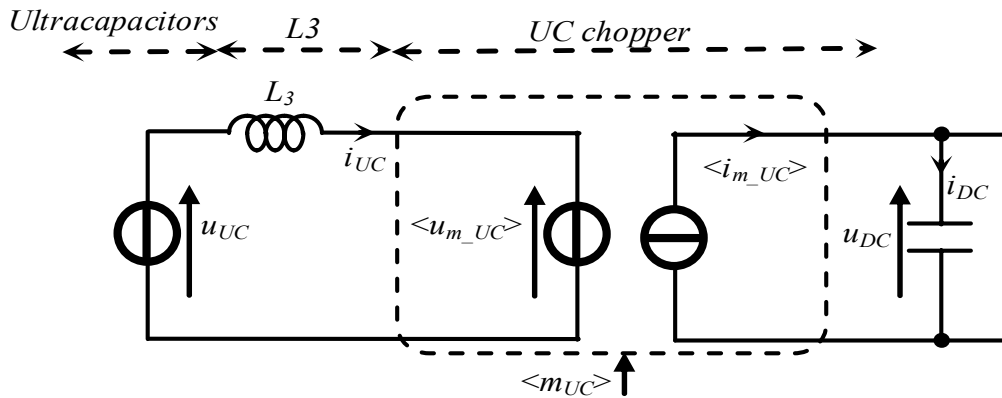


Figure II.7 Electrical diagram of the ultracapacitor power storage system

By neglecting losses, the filter current ( $i_{UC}$ ) is expressed with the following differential equations:

$$\frac{di_{UC}}{dt} = \frac{1}{L_3} \cdot (u_{UC}(t) - u_{m\_UC}(t)) \quad (\text{R. II-6})$$

The mean value of the modulated voltage is obtained with the DC voltage ( $u_{DC}$ ) and the duty cycle ratio ( $m_{UC}$ ):

$$\begin{cases} u_{m\_UC} = m_{UC} \cdot u_{DC}(t) \\ i_{m\_UC} = m_{UC} \cdot i_{UC}(t) \end{cases} \quad (\text{R. II-7})$$

The filtered current ( $i_{UC}$ ) is modulated by the chopper, and then this modulated current ( $i_{m\_UC}$ ) is injected into the common DC bus. The output current ( $i_{m\_UC}$ ) of the chopper is equal to the ultracapacitor current ( $i_{UC}$ ), which is multiplied by the duty cycle ratio ( $m_{UC}$ ). The ultracapacitors system is described by using the EMR in Figure II.8.

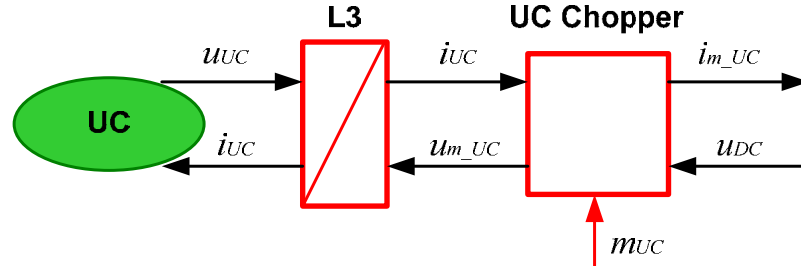


Figure II.8 EMR of the ultracapacitors power storage system modeling

### II.2.5. Grid connection

A three-phase inverter within a choke as filter is used for the grid connection. Hence, an equivalent mean modeling of this three-phase inverter is sufficient for representing fundamental components of voltage/current (Figure II.9) as dependent phase to phase voltage sources ( $u_{INV\_13}$  and  $u_{INV\_23}$ ) with the DC bus voltage ( $u_{DC}$ ) through modulation indexes ( $m_{INV\_13}$  and  $m_{INV\_23}$ ) and a dependent current source ( $i_{INV}$ ) with AC currents through the same modulation indexes.

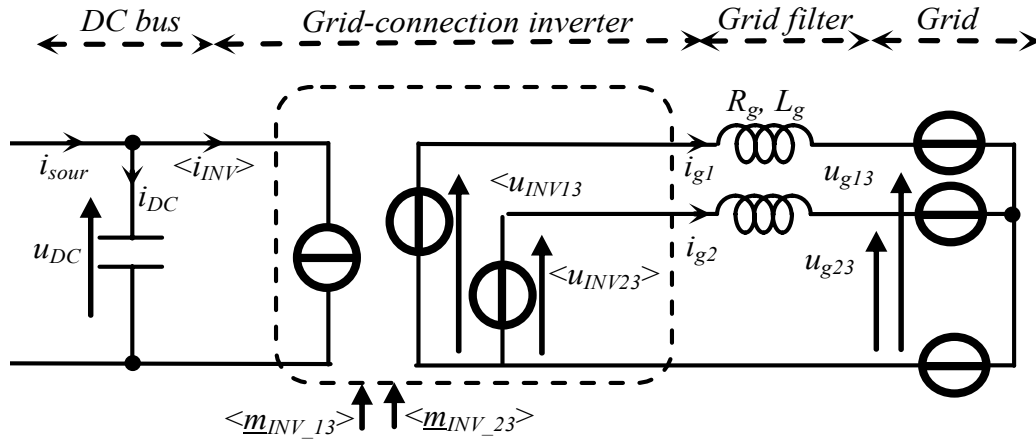


Figure II.9 Electrical diagram of the grid connection

Then mean values of modulated phase to phase voltages and of the average currents are expressed as:

$$\begin{cases} u_{INV\_1} = m_{INV\_13} \cdot u_{DC} \\ u_{INV\_23} = m_{INV\_23} \cdot u_{DC} \end{cases} \quad (\text{R. II-8})$$

$$\langle i_{INV} \rangle = m_{INV\_13} \cdot i_{g1} + m_{INV\_23} \cdot i_{g2} \quad (\text{R. II-9})$$

By assuming that grid voltages are balanced, line voltages are obtained through:

$$\begin{cases} v_{INV1} = \frac{2}{3} \cdot u_{INV\_13} - \frac{1}{3} \cdot u_{INV\_23} \\ v_{INV2} = -\frac{1}{3} \cdot u_{INV\_13} + \frac{2}{3} \cdot u_{INV\_23} \end{cases} \quad (\text{R. II-10})$$

The filter currents are deduced from following differential equations:

$$\begin{cases} \frac{di_{g1}}{dt} = \frac{1}{L_g} (v_{INV1} - R_g \cdot i_{g1} - v_{g1}) \\ \frac{di_{g2}}{dt} = \frac{1}{L_g} (v_{INV2} - R_g \cdot i_{g2} - v_{g2}) \end{cases} \quad (\text{R. II-11})$$

Three-phase inverter voltages, grid voltages, currents and duty cycles can be expressed as vectors, respectively by:

$$\underline{v}_{INV} = \begin{bmatrix} v_{INV1} \\ v_{INV2} \\ v_{INV3} \end{bmatrix}, \quad \underline{v}_g = \begin{bmatrix} v_{g1} \\ v_{g2} \\ v_{g3} \end{bmatrix}, \quad \underline{i}_g = \begin{bmatrix} i_{g1} \\ i_{g2} \\ i_{g3} \end{bmatrix}, \quad \underline{m}_{INV} = \begin{bmatrix} m_{INV\_13} \\ m_{INV\_23} \end{bmatrix} \quad (\text{R. II-12})$$

The grid connection part is described by using the EMR on Figure II.10.

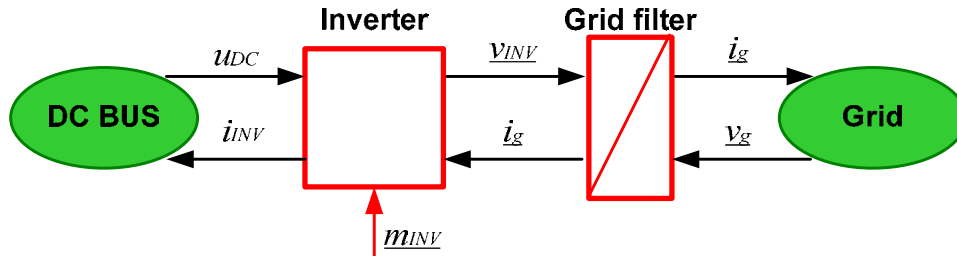


Figure II.10 EMR of the grid connection modeling

### II.2.6.DC bus

In this hybrid generating system, four energy sources (PV panels, batteries, ultracapacitors and the electrical grid) are all connected to the common DC bus via different power electronic converters (Figure II.2). So according to this DC-coupling, the capacitor current of the DC bus ( $i_{DC}$ ) is expressed as:

$$i_{sto}(t) = i_{m\_BAT}(t) + i_{m\_UC}(t) \quad (\text{R. II-13})$$

$$i_{sour}(t) = i_{sto}(t) + i_{m\_PV}(t) \quad (\text{R. II-14})$$

$$i_{DC}(t) = i_{sour}(t) - i_{INV}(t) \quad (\text{R. II-15})$$

with  $i_{m\_PV}$ : the modulated current from the PV chopper;  
 $i_{m\_BAT}$ : the modulated current from the BAT chopper;  
 $i_{m\_UC}$ : the modulated current from the UC chopper;  
 $i_{INV}$ : the modulated current from the grid inverter.

The DC bus voltage is expressed as:

$$\frac{du_{DC}}{dt} = \frac{1}{C_{DC}} i_{DC}(t) \quad (\text{R. II-16})$$

$C_{DC}$  is the capacitor of the DC bus.

The EMR is obtained by using double squares for current node equations and one square

for the voltage equation (Figure II.11).

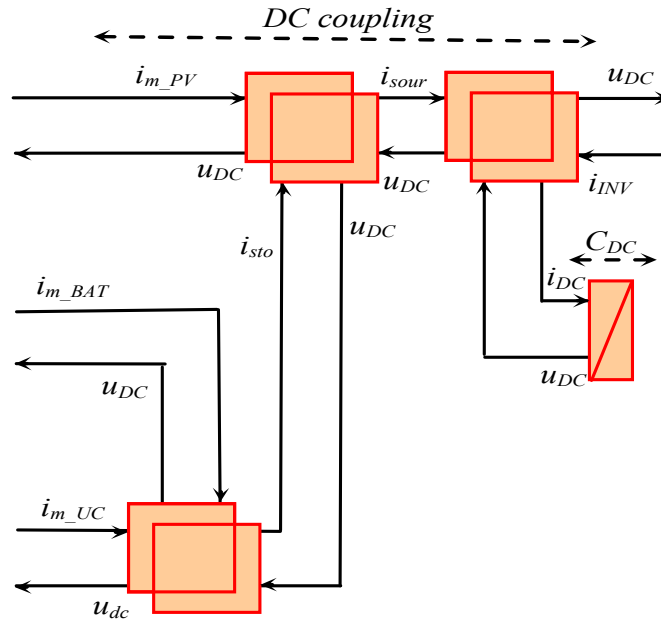


Figure II.11 EMR of the DC bus modeling

### II.2.7. Modeling of the entire PV energy conversion system

The EMRs of each source's power conversion system modeling have already been presented in the previous sections (Figure II.4, Figure II.6, Figure II.8, Figure II.10, Figure II.11). By combining these EMRs, the EMR of the entire active PV generator is obtained (Figure II.12). Four action paths appear from the control inputs of the four power converters to the different electrical quantities ( $u_{PV}$ ,  $i_{BAT}$ ,  $i_{UC}$ ,  $i_g$ ):

- from the PV chopper ( $m_{PV}$ ) to the PV panels terminal voltage ( $u_{PV}$ ) in yellow;
- from the BAT chopper ( $m_{BAT}$ ) to the batteries current ( $i_{BAT}$ ) in green;
- from the UC chopper ( $m_{UC}$ ) to the ultracapacitor current ( $i_{UC}$ ) in magenta;
- from the grid connection three-phase inverter ( $m_{INV}$ ) to the line currents ( $i_g$ ) in blue.

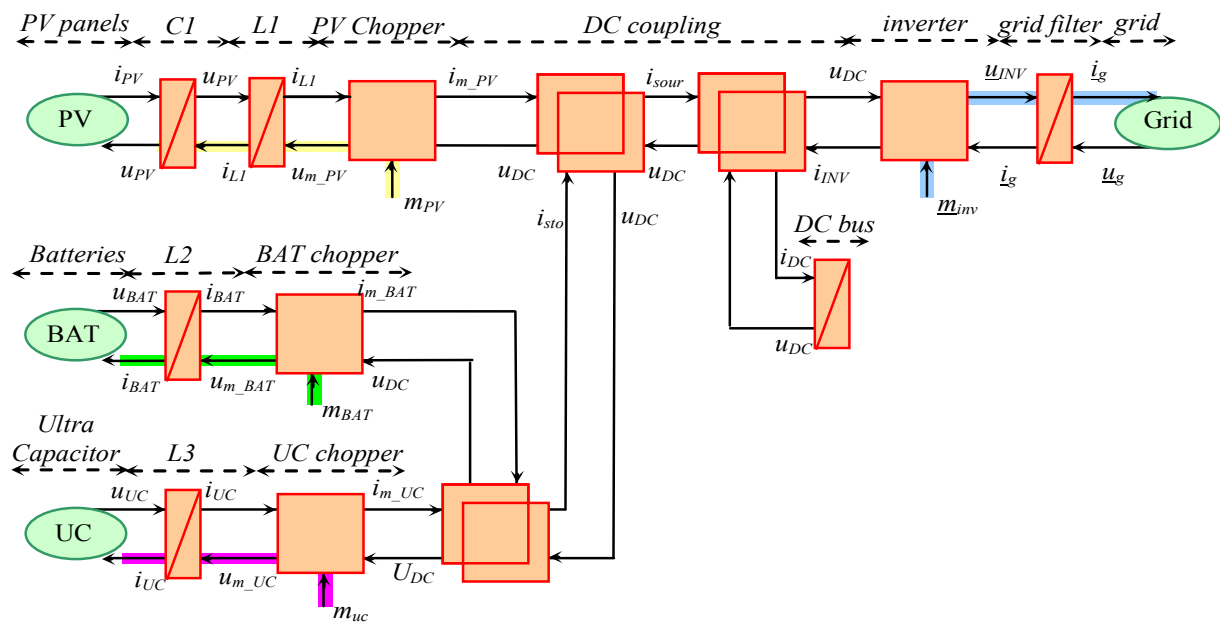


Figure II.12 EMR of the PV active generator

## II.3. Control of the active PV generator

### II.3.1. Hierarchical control structure

A hierarchical structure of the control system is proposed for this active PV generator. The structure of this hierarchical control system includes 4 levels (Figure II.13). Each one has precise control tasks depending on its hierarchical position:

- Switching Control (SC);
- Automatic Control (AC);
- Power Control (PC);
- Mode Control (MC).

The MC level decides the operating mode for the whole hybrid generator according to the availability of the PV production, the states of each storage unit and the actual power demand from the grid. The PC level calculates the power reference for each source according to the sensed values and the selected operating mode from the MC level. The AC level applies the control algorithm to meet the current or voltage references. The SC level implements the modulation technique to each converter and generates the semiconductor signals ( $\{-5, +15\}$ ) to apply wished ideal states ( $\{0, 1\}$ ).

In the studied active PV generator, four sources are considered: the PV panels (PV), the ultracapacitors (UC), the batteries (BAT) and the grid connection (GC). Four power electronic converters are used to regulate the power exchanges among them. So in the control system, four SCs and four ACs are used for the control of the four sources, a common PC and a common MC are used for the power dispatching among the different sources, the real time power balancing and the long term energy management of the entire active generator (Figure II.13).

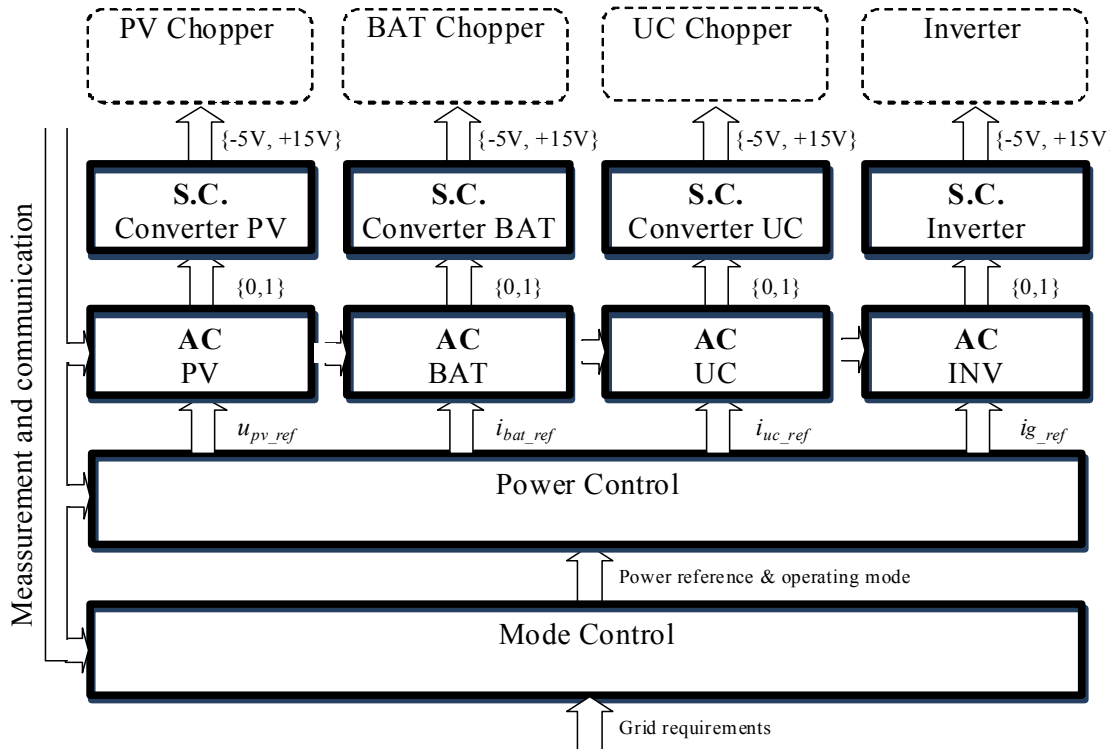


Figure II.13 Hierarchical control structure for the active PV generator

In the SC level of each power electronic converter, the IGBT and PWM techniques are used to control the switching legs. These units are not the main concerns of the study, so they



will not be detailed here. However, the control algorithms in the AC level should be presented in order to highlight the physical quantities, which can be used for the power flow control among the different energy sources.

### II.3.2. Automatic Control unit

#### a. Task and method

The task of the Automatic Control units is to calculate duty cycles for each SC in order to set dynamical quantities equal to their references (current and voltage), which are coming from the Power Control level. They will be designed by applying inversion rules to the EMR. A Maximum Control Structure (MCS) is obtained and can be later reduced if necessary. From the MCS a schema bloc representation can be easily found.

#### b. PV controller

The AC of the PV power conversion system must regulate the terminal voltage across the PV panels in order to implement a Maximum Power Point Tracking (MPPT) strategy or a Power Limitation (PL) strategy. The variation of this voltage will modify the generated PV power (Figure II.14).

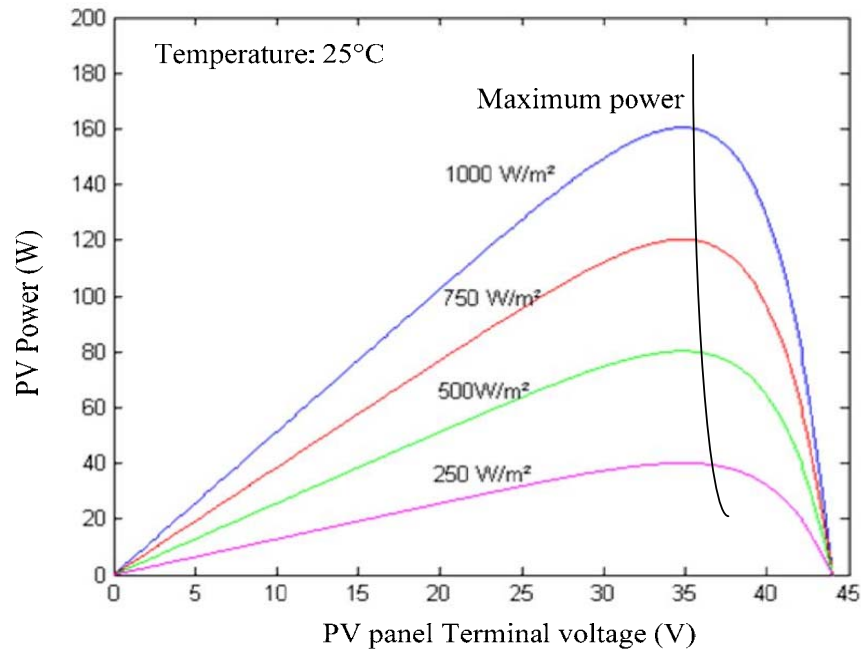


Figure II.14 Power characteristics of one PV module

From the Energetic Macroscopic Representation of the PV power conversion system (Figure II.15), an action chain from the duty cycle ratio ( $m_{PV}$ ) and pointing to the PV terminal voltage ( $u_{PV}$ ) appears and has been highlighted in yellow. A control chain is obtained by inverting this action chain. The controllers are depicted by parallelograms with an oblique bar.

According to the inversion rules of the Maximum Control Structure (MCS), the automatic control system is achieved by:

- a closed loop control ( $LI'$ ) of the filtered current ( $i_{LI}$ ) with a IP controller ( $C_{LI}$ ) (detailed in Appendix VIII),

$$u_{m\_PV\_ref} = C_{L1}(i_{L1\_ref} - i_{L1\_mes}) + u_{pv\_mes} \quad (R. II-17)$$

- a closed loop control ( $C1'$ ) of the terminal voltage ( $u_{PV}$ ) with a IP controller ( $C_{CI}$ ),

$$i_{L1\_ref} = C_{C1}(u_{PV\_ref} - u_{PV\_mes}) + i_{pv\_mes} \quad (R. II-18)$$

- a converter control ( $PVC'$ ) for the calculation of the duty cycle, which will be sent to the SC level:

$$m_{PV\_reg} = \frac{u_{m\_PV\_ref}}{u_{DC\_mes}} \quad (R. II-19)$$

The design of the IP correctors is detailed in the Appendix V.

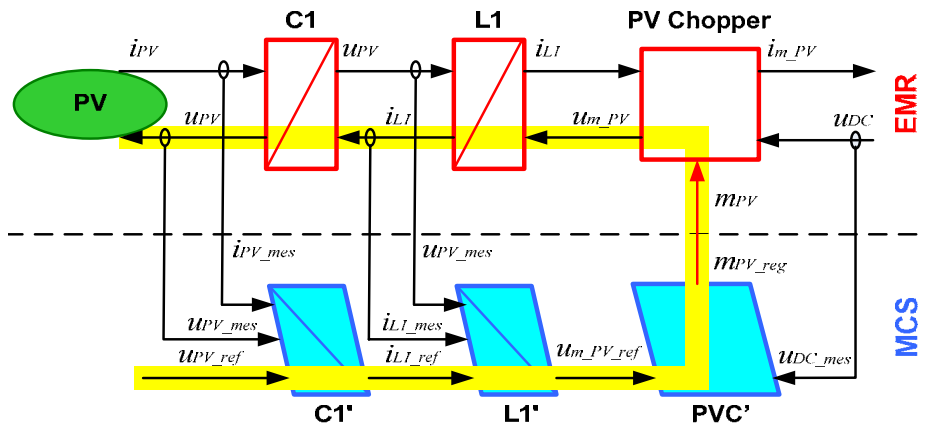


Figure II.15 EMR and MCS of the PV power conversion system

### c. Batteries controller

From the Energetic Macroscopic Representation of the batteries energy storage system, an action chain from the duty cycle ratio ( $m_{BAT}$ ) and pointing to the battery current ( $i_{BAT}$ ) appears and has been highlighted in green (Figure II.16).

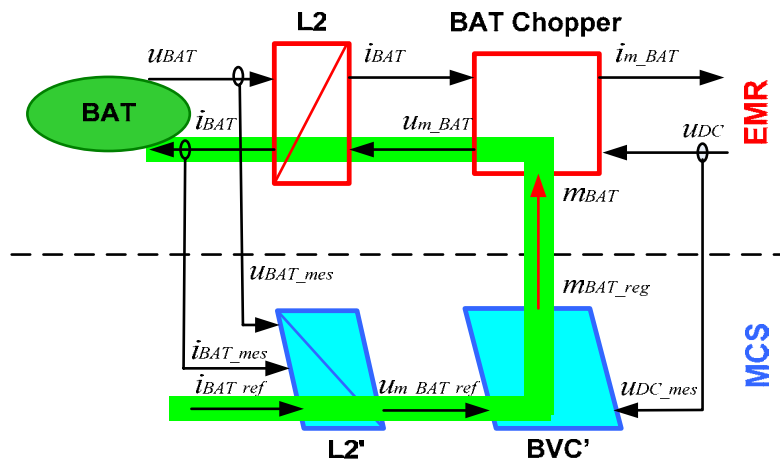


Figure II.16 EMR and MCS of the BAT energy storage system

A control chain in blue is obtained by inverting this action chain. The inversion rules of the Maximum Control Structure (MCS) yields to two control functions:

- a closed loop control ( $L2'$ ) of the current with a PI controller ( $C_{L2}$ )

$$u_{m\_BAT\_ref} = C_{L2} (i_{BAT\_ref} - i_{BAT\_mes}) \quad (R. II-20)$$

- a converter controller ( $BVC'$ ) to calculate the duty cycle ratio, which will be sent to the SC level:

$$m_{BAT\_reg} = \frac{u_{m\_BAT\_ref}}{u_{DC\_mes}} \quad (R. II-21)$$

#### d. Ultracapacitors controller

From the Energetic Macroscopic Representation of the ultracapacitor power system, an action chain from the duty cycle ratio ( $m_{UC}$ ) and pointing to the ultracapacitor current ( $i_{UC}$ ) appears and has been highlighted in magenta (Figure II.17). A control chain is obtained by inverting this action chain.

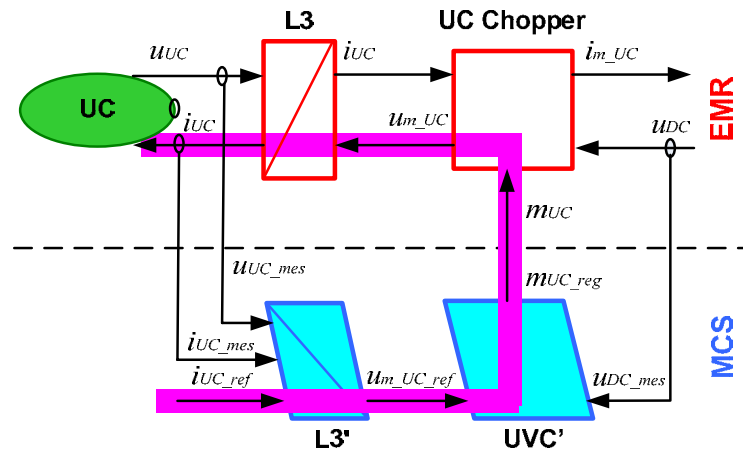


Figure II.17 EMR and MCS of the UC power storage system

The objective of the control of the ultracapacitors power storage system is to make equal the ultracapacitor current to a reference ( $i_{UC\_ref}$ ) by varying the duty cycle ( $m_{UC}$ ). According to the inversion rules of the Maximum Control Structure (MCS), the automatic control system is achieved by:

- a closed loop control ( $L3'$ ) of the current in the blue block  $L3'$ , with a PI controller ( $C_{L3}$ ) is used:

$$u_{m\_UC\_ref} = C_{L3} (i_{UC\_ref} - i_{UC\_mes}) \quad (R. II-22)$$

- a converter controller ( $UVC'$ ) calculates the duty cycle ratio, which will be sent to the SC level:

$$m_{UC\_reg} = \frac{u_{m\_UC\_ref}}{u_{DC\_mes}} \quad (R. II-23)$$

#### e. Grid connection control

The EMR of the grid connection system modeling makes appear a path in blue from the control inputs ( $\underline{m}_{inv}$ ) of the inverter to the line currents ( $\underline{i}_g$ ) in Figure II.18.

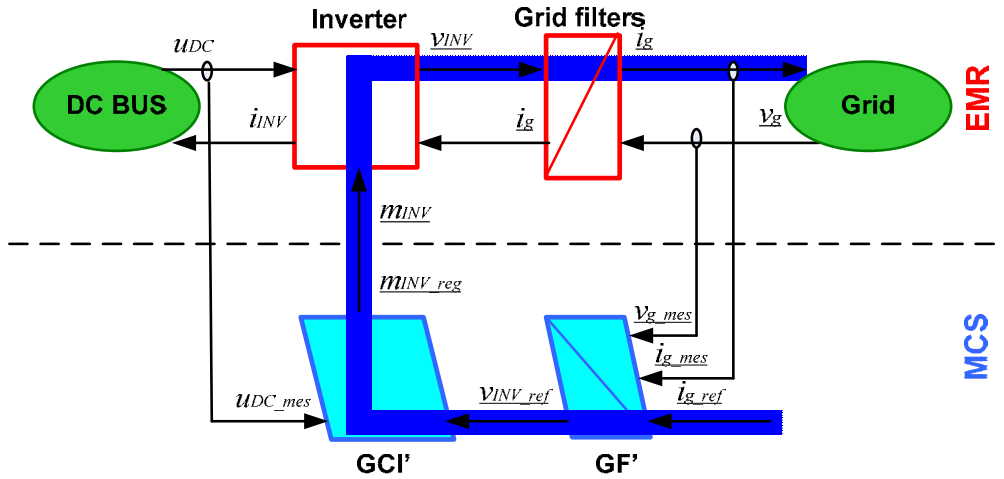


Figure II.18 EMR and MCS of the grid connection

The control scheme of the grid connection system is obtained by inverting this path. It consists to calculate the reference of the inverter's duty ratios ( $m_{inv\_ref}$ ) according to the line currents' references ( $i_{g\_ref}$ ). The objective of the grid connection control is to regulate the delivered active power and reactive power to the grid. The grid is a voltage source ( $u_{grid}$ ), so the line current should be controlled in order to regulate the exchanged power with the grid. Hence, the delivered power control is based on the grid current control. According to the inversion rules of the Maximum Control Structure (MCS), the automatic control system is achieved by an inverter controller (block GCI') and a closed loop control of currents (block GF'). This grid current controller is presented as a blue block (GF') in the MCS (Figure II.18).

For the design of the controllers, a Park transform is used. The voltages and currents in the three-phase frame ( $a,b,c$ ) can be transformed to two voltages and two currents in the two-phase rotating frame ( $d,q$ ) with synchronization with the first line voltage:

$$\begin{cases} v_{INV\_dq} = [P]v_{INV} \\ v_{g\_dq} = [P]v_g \\ i_{g\_dq} = [P]i_g \end{cases} \quad (\text{R. II-24})$$

$[P]$  is the matrix of the Park transformation.

$$[P] = \frac{2}{3} \begin{bmatrix} \cos \theta & \cos(\theta - \frac{2\pi}{3}) & \cos(\theta + \frac{2\pi}{3}) \\ \sin \theta & \sin(\theta - \frac{2\pi}{3}) & \sin(\theta + \frac{2\pi}{3}) \\ \frac{1}{2} & \frac{1}{2} & \frac{1}{2} \end{bmatrix} \quad (\text{R. II-25})$$

Hence in this frame, filter current equations are expressed as:

$$\begin{cases} \frac{di_{g\_d}}{dt} = \frac{1}{L} (v_{INV\_d} - v_{g\_d} - R_g i_{g\_d} - L_g \cdot \omega_s \cdot i_{g\_q}) \\ \frac{di_{g\_q}}{dt} = \frac{1}{L} (v_{INV\_q} - v_{g\_q} - R_g i_{g\_q} + L_g \cdot \omega_s \cdot i_{g\_d}) \end{cases} \quad (\text{R. II-26})$$

$\omega_s = 2\pi f$ , with  $f$  the grid frequency.

So the control of these currents is organized in three parts: a current decoupling, a compensation of grid voltages and a closed loop control (Figure II.19). The modulated voltage references of the inverter outputs can be expressed as:

$$\begin{cases} v_{INV\_d\_ref} = C_{igd} (i_{g\_d\_ref} - i_{g\_d\_mes}) + v_{g\_d\_mes} - L_g \cdot \omega_s \cdot i_{g\_q\_mes} \\ v_{INV\_q\_ref} = C_{igq} (i_{g\_q\_ref} - i_{g\_q\_mes}) + v_{g\_q\_mes} + L_g \cdot \omega_s \cdot i_{g\_d\_mes} \end{cases} \quad (\text{R. II-27})$$

with two current PI correctors ( $C_{igd}$ ,  $C_{igq}$ ).

The obtained voltage references in the  $dq$  frame can be transformed to the three voltage references in the  $abc$  frame with an inverse Park transformation:

$$\underline{v}_{INV\_ref} = [P]^{-1} \underline{v}_{INV\_dq\_ref} \quad (\text{R. II-28})$$

Phase to phase voltages are obtained with the following equations:

$$\begin{cases} u_{INV13\_ref} = v_{INV1\_ref} - v_{INV3\_ref} \\ u_{INV23\_ref} = v_{INV2\_ref} - v_{INV3\_ref} \end{cases} \quad (\text{R. II-29})$$

Mean values of the modulation functions are calculated by using the inverse equation (R. II-8):

$$m_{INV13\_reg} = \frac{u_{INV13\_ref}}{u_{DC\_mes}}, \quad m_{INV23\_reg} = \frac{u_{INV23\_ref}}{u_{DC\_mes}} \quad (\text{R. II-30})$$

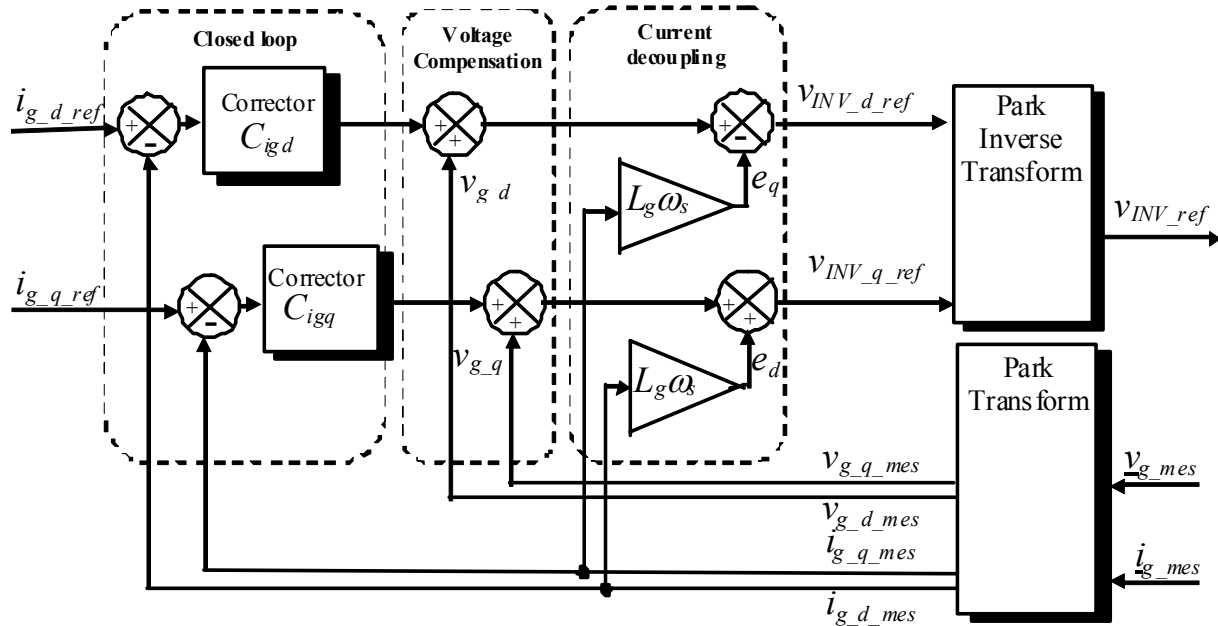


Figure II.19 Block diagram of the grid current controller

### f. DC bus control

The decomposition into the different subsystems relies on the assumption that the DC-bus voltage ( $u_{DC}$ ) is constant. The control scheme of the DC bus is obtained by inverting the EMR of the system modeling (Figure II.20) and requires a closed loop control of the DC bus voltage ( $u_{DC}$ ) with a PI corrector ( $C_{CDC}$ ):

$$i_{DC\_ref} = C_{CDC}(u_{DC\_ref} - u_{DC\_mes}) \quad (\text{R. II-31})$$

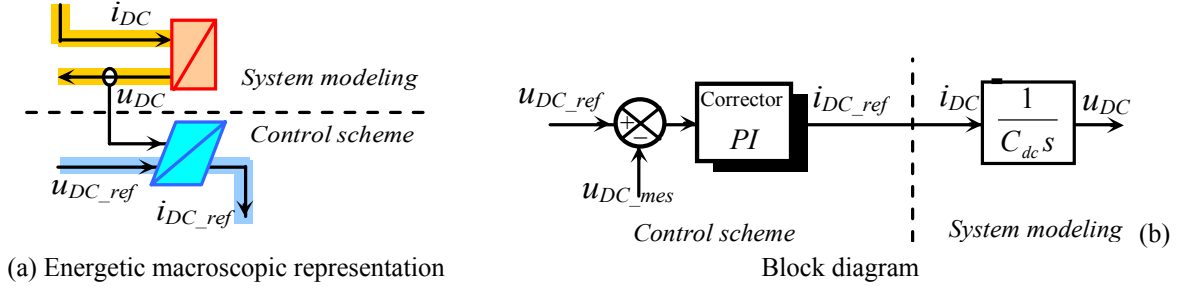


Figure II.20 Control scheme of the DC bus

The current flowing the capacitor of the DC bus ( $i_{DC}$ ) can be expressed (Figure II.20) as:

$$i_{DC} = i_{m\_PV} + i_{m\_BAT} + i_{m\_UC} - i_{INV} \quad (\text{R. II-32})$$

So the regulation of the current in the capacitor can be achieved by controlling the currents of each source (PV panels, batteries and ultracapacitors) corresponding to the power control of each source. It is detailed in the next section.

### g. Control of the entire PV energy conversion system

The global control scheme of the entire active PV generator is obtained by combining all control schemes, which have been presented in the previous parts. A block diagram of all control functions inside the Automatic Control Units (ACU) is presented on Figure II.21. Five references ( $i_{DC\_ref}$ ,  $i_{g\_ref}$ ,  $u_{PV\_ref}$ ,  $i_{UC\_ref}$ ,  $i_{BAT\_ref}$ ) must be set to interface the automatic control units with the power control unit.

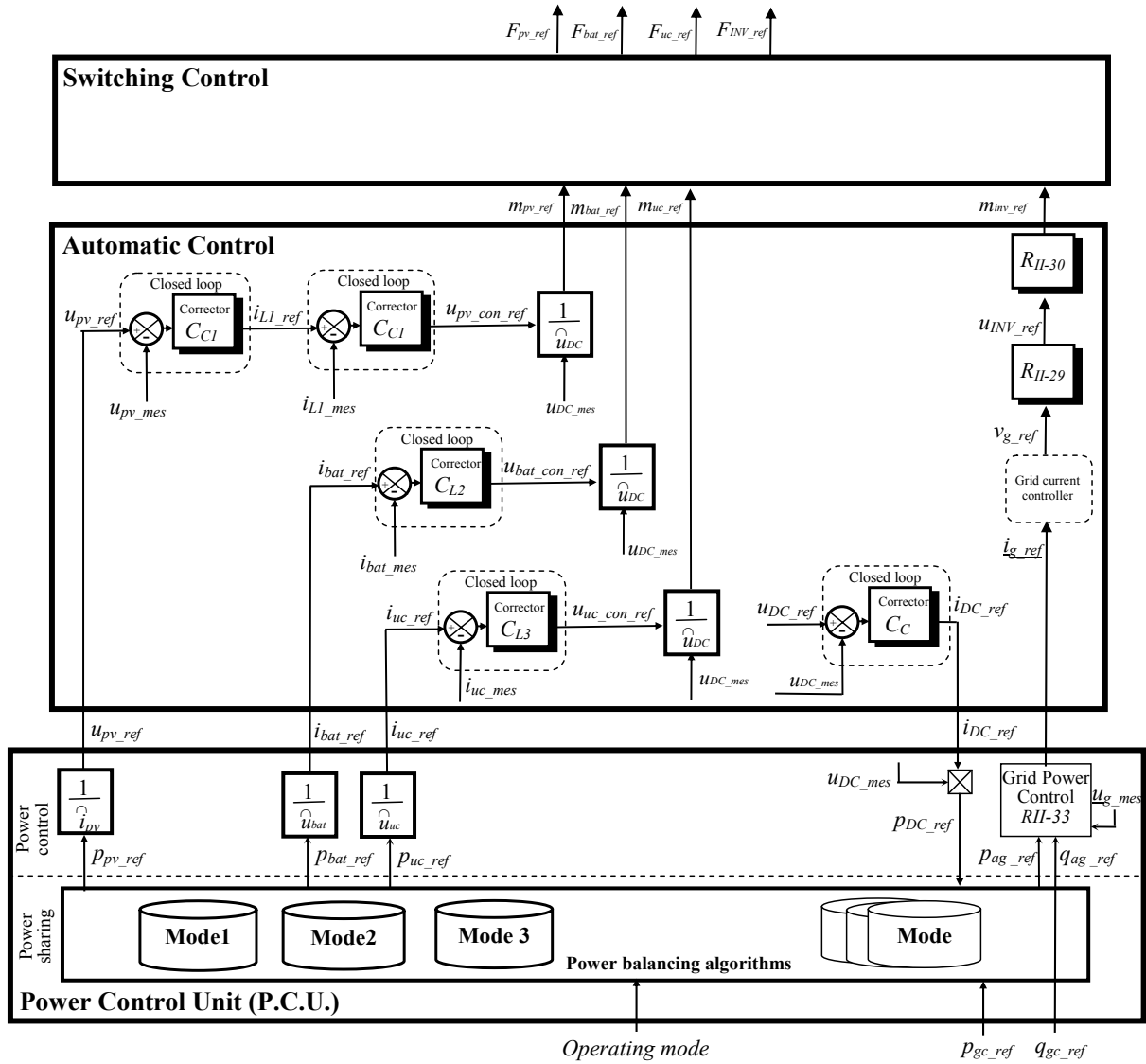


Figure II.21 Block diagram of the automatic control units for the active PV generator

### II.3.3. Power control unit

#### a. Layout of the Power Control Unit

The Power Control Unit is divided into two levels: the Power Control Level and the Power Sharing Level.

The Power Control Level consists to calculate the reference quantities ( $i_{g\_ref}$ ,  $u_{PV\_ref}$ ,  $i_{UC\_ref}$ ,  $i_{BAT\_ref}$ ) from power references.

The Power Sharing Level coordinates the power flow exchanges among the different energy sources with different power balancing strategies (Figure II.22). They are presented here in details with the help of the Multi-Level Representation, which has been developed by Peng LI in 2008 [Li 08c] (Appendix VI).

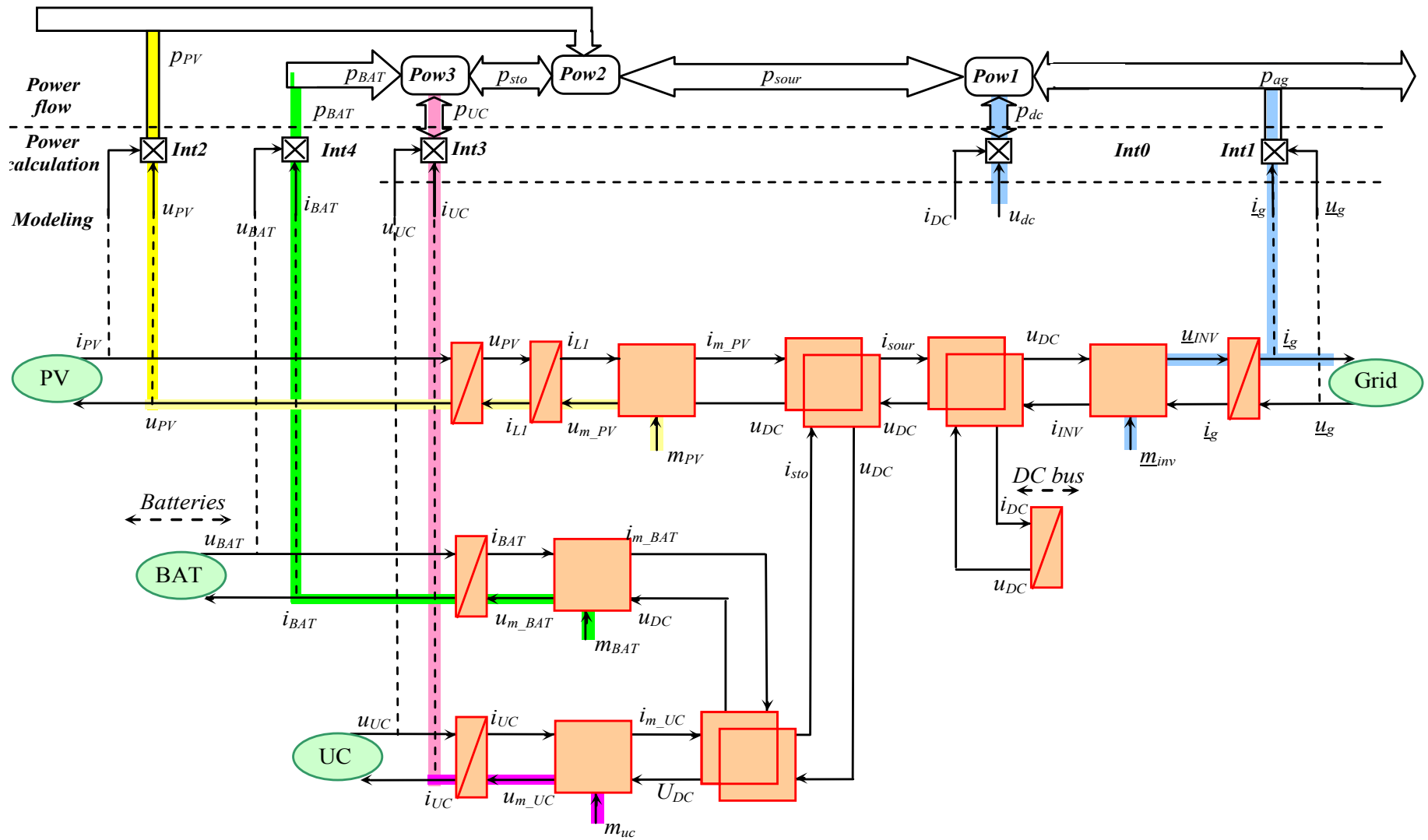


Figure II.22 Multi-Level Representation of the power modelling of the active PV generator



### b. Power calculation

In order to implement the power control, the inner power flow of the active generator has to be calculated. In order to focus on the power exchanges with the different sources around the DC bus, the instantaneously exchanged power with the choke, the losses in the filters and the losses in the power converters are neglected. Only the sources' powers and the exchanged power with the DC-bus capacitor are taken into account here (Figure II.23). Powers in the DC part are easy calculated by multiplying dc currents and dc voltages (Table II-1). All the variables with hat symbol are the sensed variables.

Table II-1: Power calculation and power control algorithms for the active PV generator

Energy source	Power calculation	Power control
DC-bus capacitor	<b>Int0:</b> $p_{DC} = u_{DC} i_{DC}$	<b>Int0e:</b> $p_{DC\_ref} = \hat{u}_{DC} i_{DC\_ref}$
Grid connection	<b>Int1:</b> $\begin{cases} p_{ag} = u_{g13} \cdot i_{g1} + u_{g23} \cdot i_{g2} \\ q_{ag} = \sqrt{3}(u_{g13} \cdot i_{g1} - u_{g23} \cdot i_{g2}) \end{cases}$	<b>Int1c:</b> $\begin{cases} i_{g1\_ref} = \frac{(2\hat{u}_{13} - \hat{u}_{23})p_{ag\_ref} + \sqrt{3}\hat{u}_{23}q_{ag\_ref}}{2\hat{u}_{13}^2 - 2\hat{u}_{13}\hat{u}_{23} + 2\hat{u}_{23}^2} \\ i_{g2\_ref} = \frac{(2\hat{u}_{23} - \hat{u}_{13})p_{ag\_ref} - \sqrt{3}\hat{u}_{13}q_{ag\_ref}}{2\hat{u}_{13}^2 - 2\hat{u}_{13}\hat{u}_{23} + 2\hat{u}_{23}^2} \end{cases}$
PV panels	<b>Int2:</b> $p_{PV} = u_{PV} i_{PV}$	<b>Int2c:</b> $u_{PV\_ref} = \frac{1}{\hat{i}_{PV}} p_{PV\_ref}$
Ultracapacitors	<b>Int3:</b> $p_{UC} = u_{UC} i_{UC}$	<b>Int3c:</b> $i_{UC\_ref} = \frac{1}{\hat{u}_{UC}} p_{UC\_ref}$
Batteries	<b>Int4:</b> $p_{BAT} = i_{BAT} u_{BAT}$	<b>Int4c:</b> $i_{BAT\_ref} = \frac{1}{\hat{u}_{BAT}} p_{BAT\_ref}$

### c. Power control

The expressions of the powers are inverted to obtain the control equations (Figure II.23).

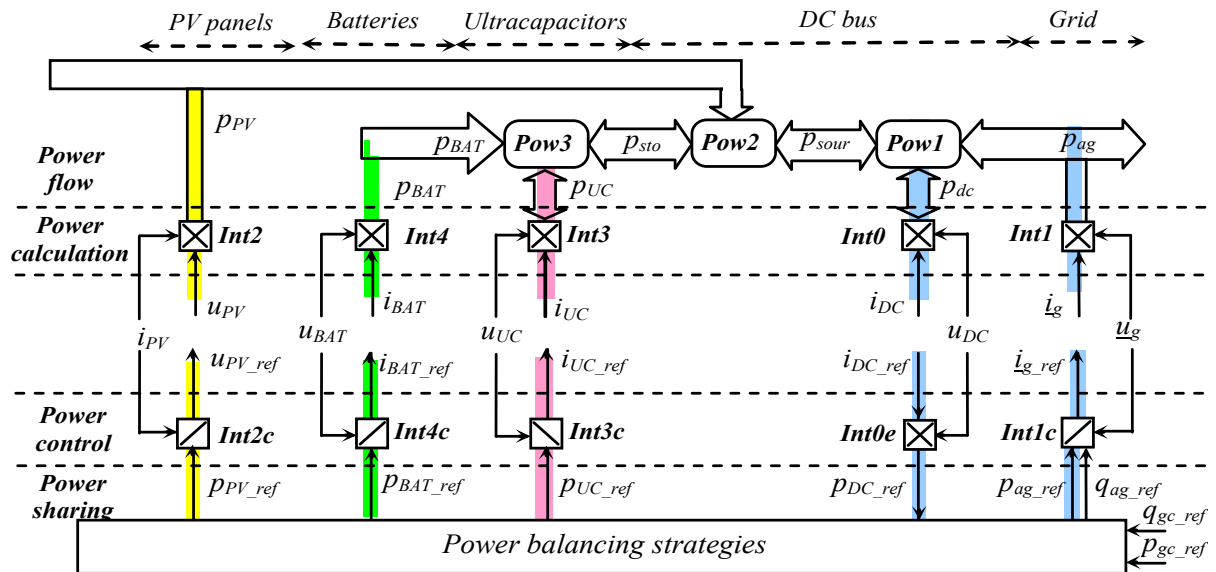


Figure II.23 Multi-Level Representation of the power modelling and control

### **Power control of PV panels**

A reference value for the PV power can be set by calculating the PV voltage reference ( $u_{PV\_ref}$ ) with the sensed PV current:

$$u_{PV\_ref} = \frac{P_{PV\_ref}}{i_{PV\_mes}} \quad (\text{R. II-33})$$

### **Power control of storage units**

For the storage systems, the powers are calculated by multiplying currents with the voltages (*Int3* and *Int4* in Table II-1). The current references are given by dividing corresponding power references with the sensed voltages (*Int3c* and *Int4c* in Table II-1).

### **Power control of the Grid connection**

The powers, which are exchanged with the grid, can be calculated through the “two-wattmeter” method (*Int1* in Table II-1). According to the grid power reference and the measured phase to phase voltages of the grid, the current references for the inverter can be deduced by inverting this equation (*Int1c* in Table II-1).

### **Power control of the DC bus**

The output of the DC-bus voltage control loop is the current reference ( $i_{DC\_ref}$ ) of the DC-bus capacitor, and its product with the measured DC-bus voltage gives the power reference ( $p_{DC\_ref}$ ) for the DC-bus voltage regulation (*Int0e*).

*Comment:* This regulation power for the DC bus voltage control can be satisfied by the difference between the sources power and the grid power.

The reference of the controllable variable should be limited while the powers are divided by a too small value. A look-up table can sometimes be used to avoid division by zero.

#### **d. Power sharing level**

The power sharing level is used to implement the power balancing strategies in order to coordinate the various sources in the hybrid power (Figure II.21). The power references for each source are set according to different power control strategies, which are specific to different operating modes. Operating modes are defined according to the various conditions (the power demand from the grid, the availability of the PV power, the state of the energy storage units ...). In order to set the power reference of each source, the power flow between each source should be determined and balanced. So a modeling of the power flow in the active generator for each mode is necessary. Here three typical operating modes (mode1, mode2, mode3) are studied in normal operation, in PV power limited mode and disconnected from the grid [Lu 09a].

## **II.4. Power balancing strategies for the active PV generator**

### **II.4.1. Role of the DC bus**

The DC bus leads directly to the stability of the generator. All power exchanges are performed via the DC-bus and have an impact on the DC-bus voltage ( $u_{DC}$ ):

$$C_{DC} u_{DC} \frac{du_{DC}}{dt} = \frac{dE_{DC}}{dt} = P_{DC} = P_{sour} - P_{ag} = P_{UC} + P_{BAT} - P_{ag} \quad (\text{R.II-34})$$

with  $E_{DC}$ : the energy stored in the DC-bus capacitor;  
 $p_{DC}$ : the resulted power into the DC-bus capacitor;  
 $p_{pv}$ : the power, which is injected into the DC bus from the PV generator;  
 $p_{BAT}$ : the power, which is exchanged between the batteries and the DC bus;  
 $p_{UC}$ : the power, which is exchanged between the ultracapacitors and the DC bus;  
 $p_{ag}$ : the power, which is extracted from the DC bus into the grid;  
 $p_{sour}$ : the total power from the sources.

So to get a constant DC bus voltage, the instantaneous powers must be balanced. For the different studied modes, the power flow must be then modeled in order to be controlled in a second step.

## II.4.2. Normal mode

### a. Power flow modeling

In a normal mode, the PV panels work always in MPPT for obtaining a maximum power from the solar energy. The two types of storage units are always available to enable a charge or discharge action of power.

For the theoretical analysis, batteries and ultracapacitors are assumed to be in generating mode. The power flow from sources to the grid is described in Figure II.24.

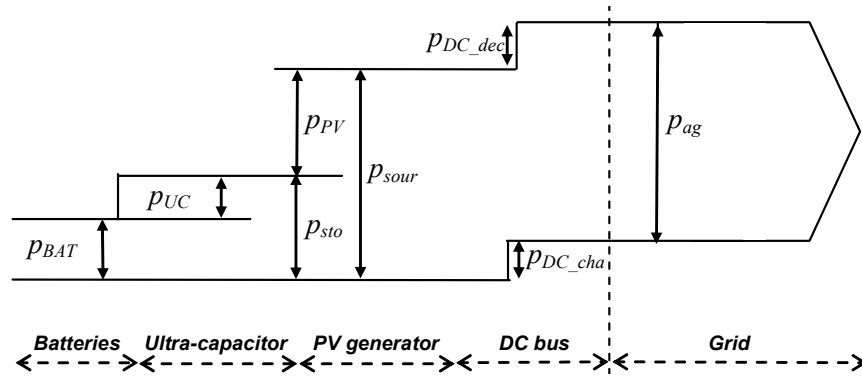


Figure II.24 Power flow in normal mode

The exchanged power with batteries ( $p_{BAT}$ ) and with ultracapacitors ( $p_{UC}$ ) constitutes the total exchanged storage power ( $p_{sto}$ ).

$$\text{Pow3: } p_{sto} = p_{BAT} + p_{UC} \quad (\text{R. II-35})$$

The total exchanged storage power can be used for compensating or absorbing the produced photovoltaic power ( $p_{pv}$ ). The resulting power is named ( $p_{sour}$ ).

$$\text{Pow2: } p_{sour} = p_{sto} + p_{PV} \quad (\text{R. II-36})$$

By taking into account the power for the DC bus voltage regulation ( $p_{DC}$ ), the output power to the electrical grid ( $p_{ag}$ ) is found:

$$\text{Pow1: } p_{ag} = p_{sour} - p_{DC}, \quad (\text{R. II-37})$$

On Figure II.24, the DC bus power is decomposed into two terms:  $p_{DC\_cha}$  if the DC capacitor is loaded ( $p_{DC} = p_{DC\_cha}$ ) and  $p_{DC\_dec}$  if the capacitor is unloaded ( $p_{DC} = p_{DC\_dec}$ ). By deducing losses in the filter ( $l_f$ ), the supplied power ( $p_{ag}$ ) is obtained:

The grid power ( $p_{ag}$ ) must be equal to the power reference ( $p_{gc\_ref}$ ) sent by the microgrid system operator.

The DC power ( $p_{DC}$ ) must be equal to the required value ( $p_{DC\_ref}$ ) to regulate the DC-bus voltage ( $u_{DC}$ ) to a constant value. Hence the sources' total power ( $p_{sour}$ ) can be adjusted by regulating the total power exchanged with storage units ( $p_{sto}$ ). So the power flows must be supervised with power references, which must be calculated by the Power Sharing Level of the Power Control Unit (Figure II.21).

In this PV/batteries/ultracapacitor hybrid power system, four power electronic converters are used to regulate the power transfer with each source. The PV chopper is used to control the PV generator with a MPPT strategy. The three-phase inverter in the grid connection system and the DC choppers in the other power conversion systems can be used for the DC-bus voltage regulation and the grid power control. According to the chosen power flow, two power balancing strategies can be implemented [Zho 09a]:

- **The grid following strategy** uses the line current loop to regulate the DC-bus voltage, then the total power from sources ( $p_{sour}$ ) can be dispatched by a grid operator;
- **The power dispatching strategy** uses the line current loop to control the grid active power, and the DC-bus voltage is regulated with the PV generator and storage units.

The power dispatching strategy is useful for islanding operation. The grid following strategy is the control scheme, which is used in classical "passive" PV generators. Here, we consider an upgraded PV generator that is dispatched by a microgrid operator. So the grid following strategy is modified to take into account storage units and this new task.

### b. Grid following strategy

With the grid following strategy, the DC-bus voltage is regulated by adjusting the exchanged power with the grid, while the PV generator works in MPPT strategies.

$$P_{PV\_ref} = P_{PV\_MPPT} \quad (\text{R. II-38})$$

In Figure II.25, it is depicted by a closed loop ( $p_{DC\_ref} \rightarrow p_{ag\_ref} \rightarrow p_{ag} \rightarrow p_{DC}$ ). So the required power for the DC-bus voltage regulation ( $p_{DC\_ref}$ ) is used to calculate the grid power reference ( $p_{g\_ref}$ ) with an estimation equation,

$$\text{Pow1e: } p_{ag\_ref} = \tilde{p}_{sour} - p_{DC\_ref} \quad (\text{R.II-39})$$

The sources' total power ( $p_{sour}$ ) is a disturbance and should also be taken into account by using estimations of the PV power and the storage' power:

$$\text{Pow2e: } \tilde{p}_{sour} = \tilde{p}_{sto} + \tilde{p}_{pv} \quad (\text{R. II-40})$$

$$\text{Pow3e: } \tilde{p}_{sto} = \hat{p}_{UC} + \hat{p}_{BAT} \quad (\text{R. II-41})$$

The energy storage systems help the PV energy conversion system to satisfy the power references, which are asked by the microgrid operator. In steady state, the DC-bus voltage is regulated and the averaged power exchange with the DC-bus capacitor ( $p_{DC}$ ) can be considered as zero in the equation (**Pow1**). Hence in steady state, the grid power ( $p_{ag}$ ) is equal to the total power from the sources ( $p_{sour}$ ).

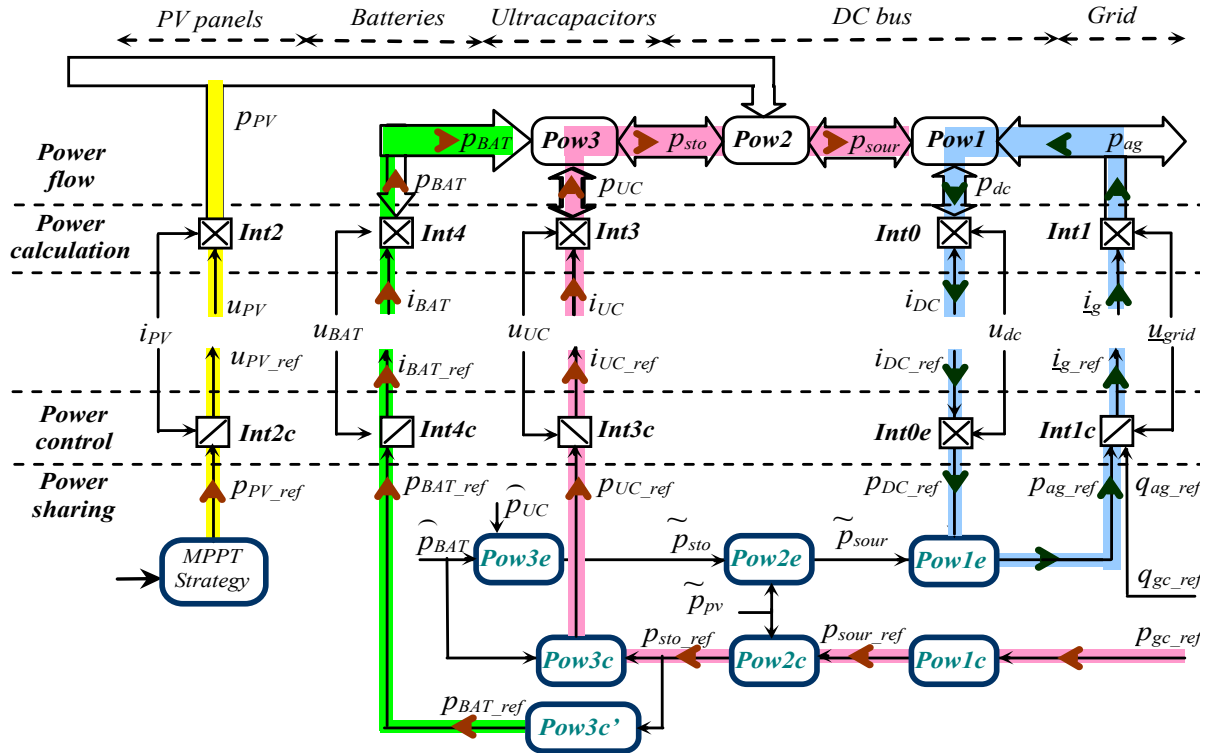


Figure II.25 Multi-Level Representation of the grid following strategy

If the microgrid system operator sets a power requirement ( $p_{gc\_ref}$ ), it must be equal to the sources' power reference ( $p_{sour\_ref}$ ) as shown in Figure II.25:

$$\mathbf{Pow1c}: p_{sour\_ref} = p_{ag\_ref} = p_{gc\_ref} \quad (\text{R. II-42})$$

In order to help the PV energy conversion system to respect the active power requirement, the energy storage systems should be coordinated to supply or absorb the difference between this power requirement ( $p_{gc\_ref}$ ) and the fluctuant PV power ( $p_{pv}$ ) as shown in Figure II.25:

$$\mathbf{Pow2c}: p_{sto\_ref} = p_{sour\_ref} - \tilde{p}_{pv} \quad (\text{R. II-43})$$

However, the power reference ( $p_{sto\_ref}$ ) is a fast varying value due to the fluctuant PV power ( $p_{pv}$ ) and the varying grid power ( $p_{ag}$ ). Moreover, the batteries have relatively slow power dynamics, fast varying power reference are not welcome for their operating lifetime. For the first step of the tests, a simple method to dispatch the power between batteries and ultracapacitors is used with a Low-Pass Filter (LPF) [Lu 08a]:

$$\mathbf{Pow3c'}: p_{BAT\_ref} = \frac{1}{1 + \tau s} p_{sto\_ref} \quad (\text{R. II-44})$$

where  $\tau$  is the time constant of the LPF. Its value should be set large enough according specific application by taking into account the power dynamics of the batteries as well as the size of the super-capacitors.

The ultracapacitors are not a long-term energy backup unit because they have limited energy storage capacities due to their low energy density. However, they have very fast power dynamics and can supply fast varying powers and power peaks. They can be used as an auxiliary power system of the batteries to fill the power gaps during their transients:

$$\text{Pow3c: } p_{UC\_ref} = p_{sto\_ref} - \hat{p}_{BAT} \quad (\text{R. II-45})$$

The block diagram of the grid following strategy for the active PV generator is shown on Figure II.26.

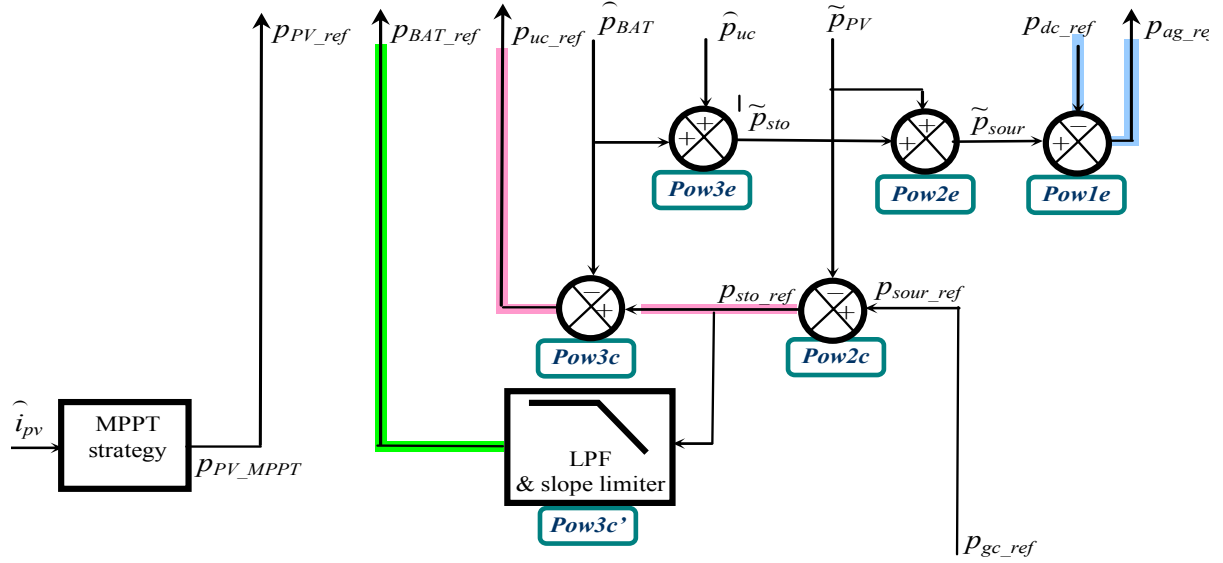


Figure II.26: Block diagram of the grid following strategy

### II.4.3. PV limitation mode

Figure II.23 shows that the PV power can be evacuated to storage units or to the grid. If both ways out can not be used then the PV power must be limited. This case appears when the energy storage units can not be charged and the PV power is greater than the grid power reference.

The power references for storage units must be calculated according their characteristics. There are two restrictions.

The first one is the rated power limit. For any kind of energy storage device, its rated power must be considered. The exchanged power with the energy storage unit must be in a certain range according to its characteristics. To detect a limitation mode, the exchanged power with the storage unit (ultracapacitors) has to be first considered:

$$p_{sto\_required} = p_{ag\_ref} - \tilde{p}_{DC} - \tilde{p}_{PV} \quad (\text{R. II-46})$$

If this power is higher than the rated value ( $p_{sto\_rated}$ ), then the PV power has to be limited to the following value (Figure II.27):

$$p_{PV\_ref} = p_{ag\_ref} + p_{DC\_ref} - p_{sto\_rated} < \tilde{p}_{PV} \quad (\text{R. II-47})$$

The second one is the energy capacity limit. If the energy storage units (batteries) are fully charged, they cannot absorb more energy in case of PV production. If they are empty, they cannot compensate the power gap in case of a PV power shortage. The management of the stored energy must be performed in coordination within the missed PV energy and it is implemented in the central microgrid management in the next chapter.

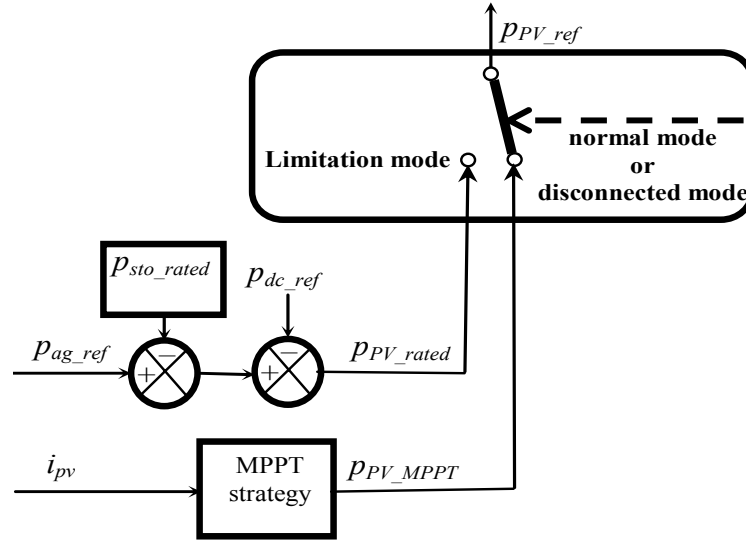


Figure II.27 Principle of the PV limitation

### II.4.4. Disconnection mode

#### a. Power flow modeling

Under certain conditions, the PV active generator must be disconnected from the electrical grid and must work in an isolated mode. In this mode, the whole active generator does not deliver any power into the electrical grid. Hence the modeling equation **Pow1** is simplified since:

$$Pow1: p_{sour} = p_{DC} \tag{R. II-48}$$

But the PV panels go on and its generated power can be stored in the energy storage units if they are available ((Figure II.29, Figure II.29).

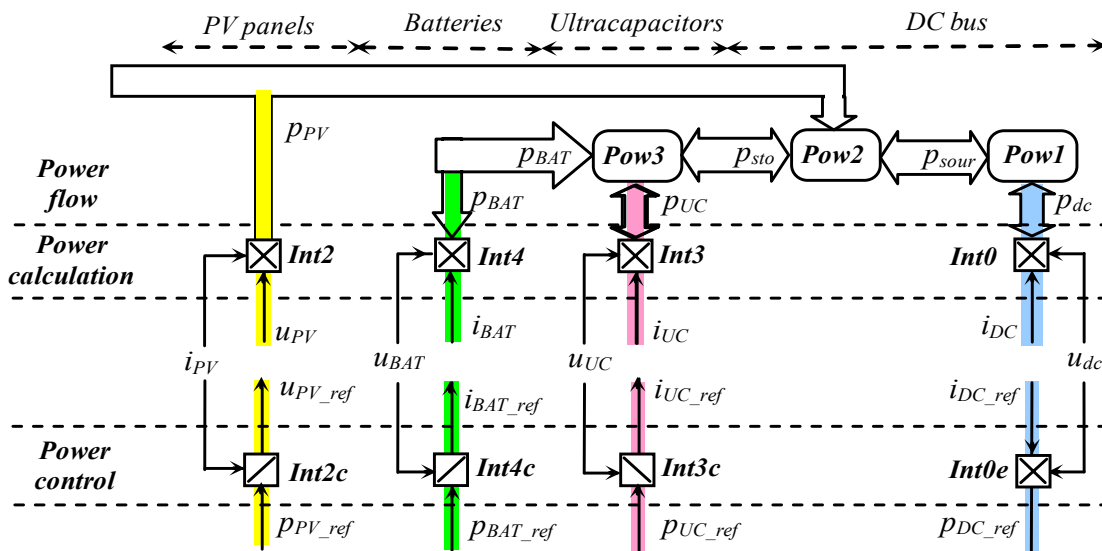


Figure II.28 Multi-Level Representation of the power modelling and control in the disconnection mode

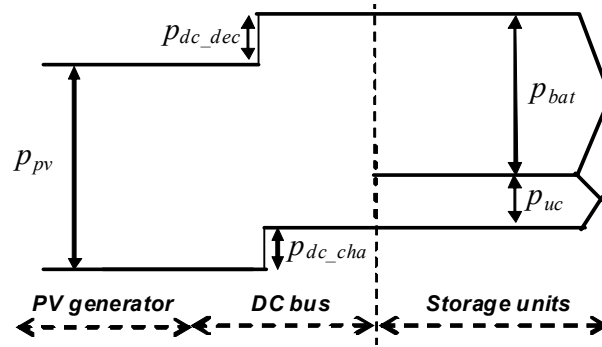


Figure II.29 Power flow in the disconnection mode

### b. Autonomous charging strategy

If the grid is disconnected, the active generator is not dispatched and then the local control objectives change. Moreover the DC-bus voltage can not be regulated by adjusting the exchanged power with the grid and so the grid following strategy can not be used. The only way to control the DC bus voltage is a combined use of the PV and storage units' power. In Figure II.30, it is depicted by a closed loop:  $p_{DC\_ref} \rightarrow p_{sour\_ref} \rightarrow p_{sto\_ref}$  and then a dispatching of the storage power is performed between the batteries and the ultracapacitors.

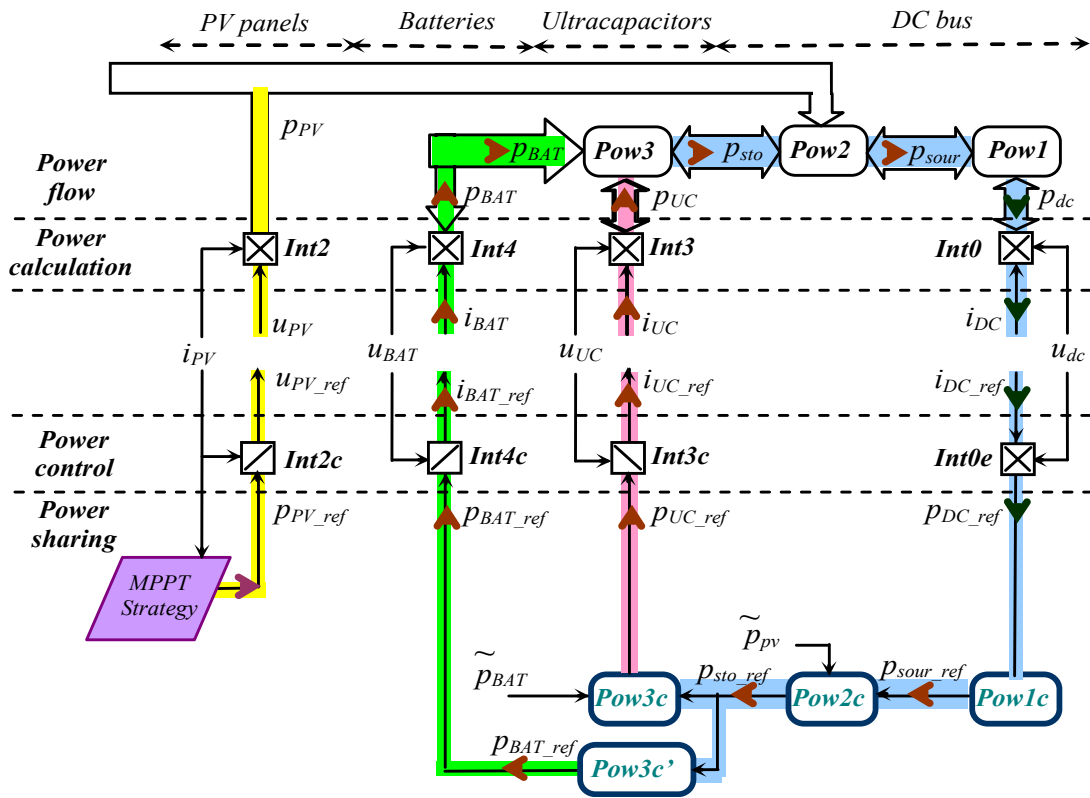


Figure II.30 Multi-Level Representation of the power dispatching strategy

In this case, the necessary total power reference ( $p_{sour\_ref}$ ) is equal to the required power for the DC-bus voltage regulation ( $p_{DC\_ref}$ ):

$$\mathbf{Pow1c: } p_{sour\_ref} = p_{DC\_ref} \quad (\text{R.II-49})$$

Then the total power reference of the storage systems is deduced by taking into account the fluctuant PV power with the inverse equation of **Pow2** (Figure II.31):



$$\mathbf{Pow2c}: p_{sto\_ref} = p_{sour\_ref} - \tilde{p}_{pv} \quad (\text{R. II-50})$$

This power reference is shared among the batteries and the super-capacitors in the same way as explained above with equations **Pow3c'** and **Pow3c**. The block diagram of the grid following strategy for the active generator is shown in Figure II.31. If the storage units are not fully charged, the PV panels can work in MPPT:

$$p_{PV\_ref} = \tilde{p}_{PV\_MPPT} \quad (\text{R. II-51})$$

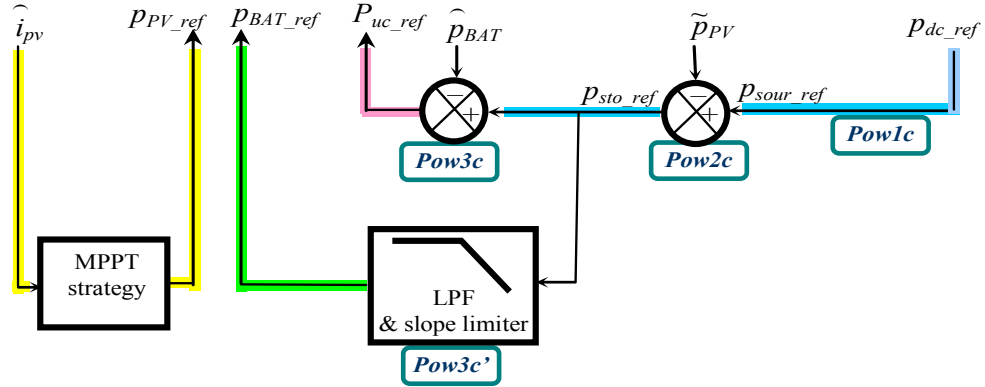


Figure II.31 Block diagram of the autonomous charging strategy

#### II.4.5.Synthesis

To enable the operating of the PV based generator in a normal mode and in a disconnected mode, two different control algorithms must be used: the grid following strategy and the power dispatching strategy. A better organization of the power sharing relies on a single strategy, which can be easily used for both operating modes. This one has been designed from the power dispatching strategy by making appear the power flow corresponding to the inverter:  $p_{gc\_ref} \rightarrow i_{g\_ref} \rightarrow i_{g\_ref} \rightarrow p_{ag}$  (Figure II.32).

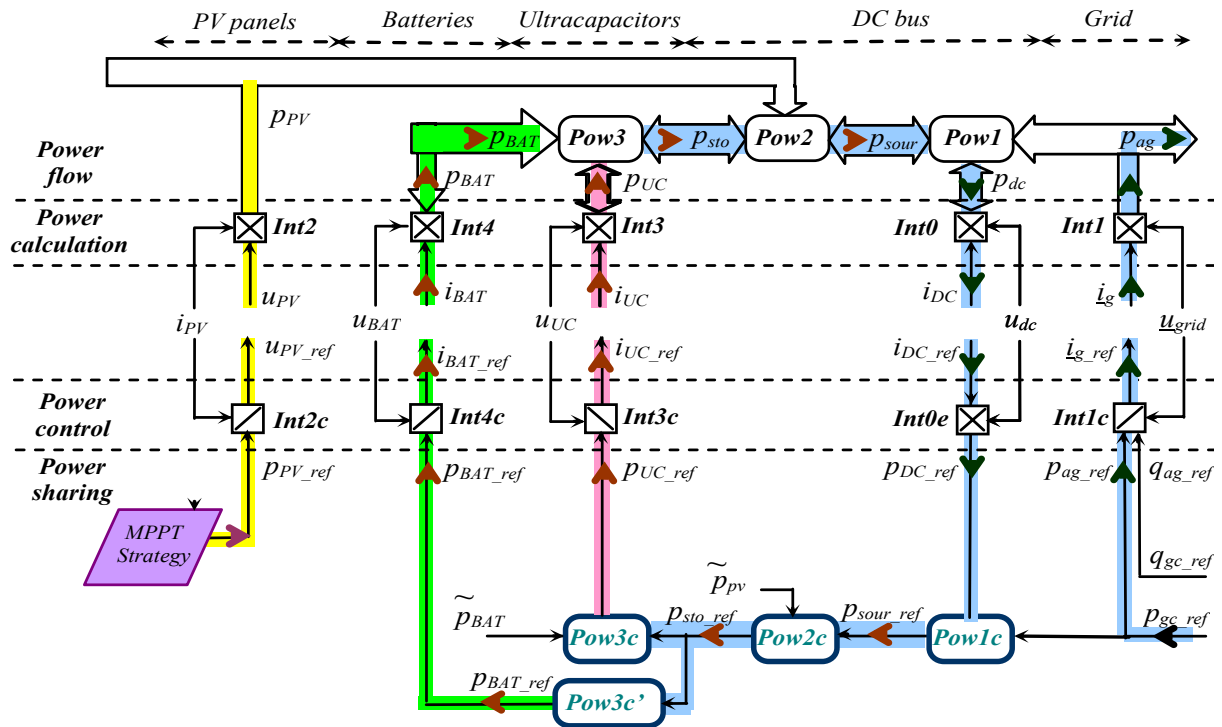


Figure II.32 Multi-Level Representation of the power dispatching strategy

The power sharing level can be depicted by using block diagrams and by highlighting a switching between them in Figure II.33.

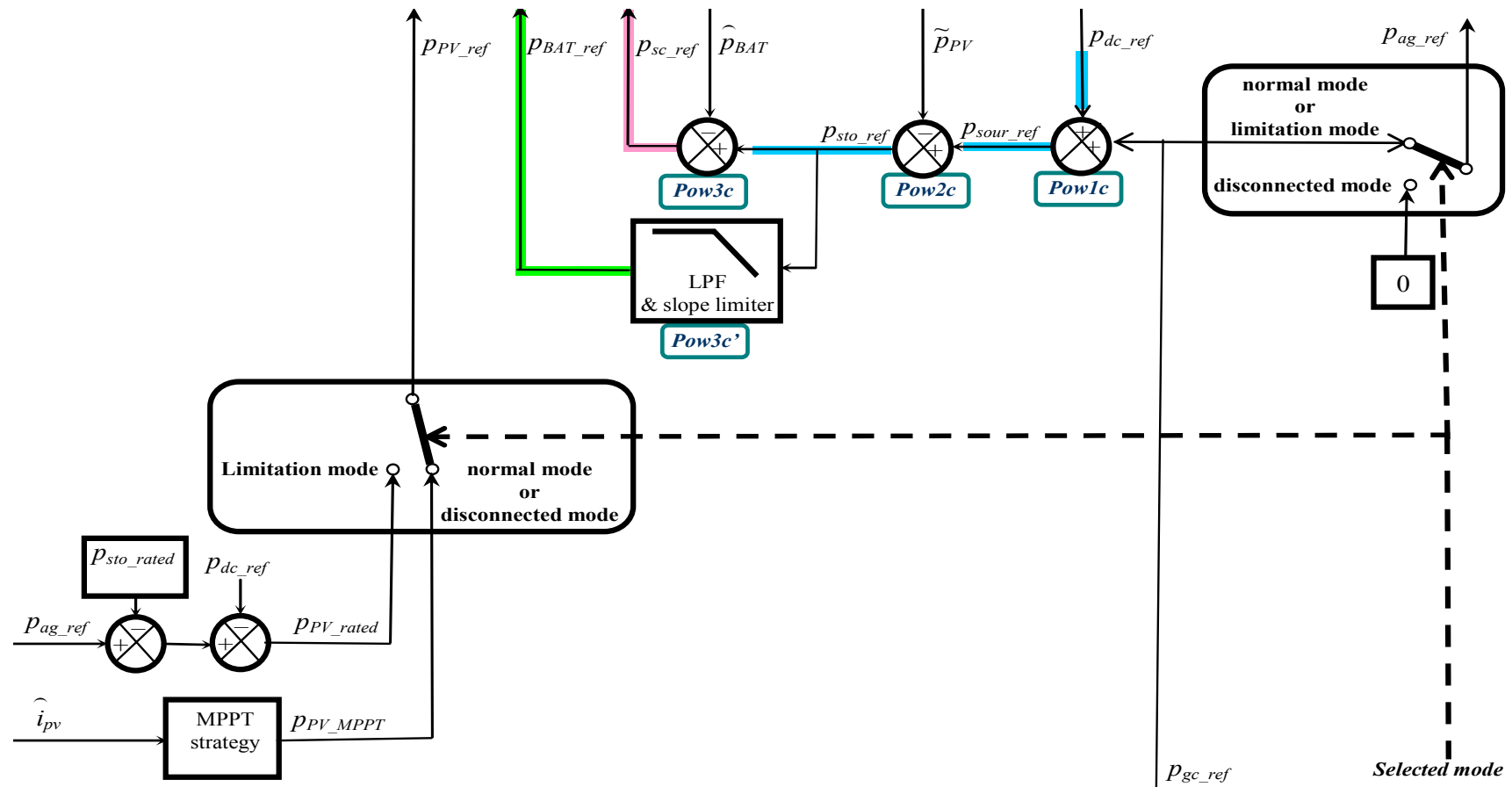


Figure II.33: Block diagram of the power sharing level

## II.5. Control of operating modes

The up grating of the PV generator to active generator depends on the state of both storage units.

Lead acid batteries are used as an energy buffer. Hence if they are full they can not be used if the PV production is higher than the requested grid power reference. So the State Of Charge of the batteries is calculated by using equations (R. I-22).

If it is over the maximum value, the active generator must be operated in the “PV limitation mode” since the over energy can not be stored and neither sent to the grid.

If batteries are empty they can not be used to perform the energy balancing in order to supply the grid power reference. Hence the active generator must be operated in the “Disconnection mode”.

When the  $SOC$  of the batteries is between  $SOC_{min}$  and  $SOC_{max}$ , batteries can be used as an energy buffer in a normal operating.

The selection of the operating mode (“Selected mode”) can then be implemented by the synoptic of Figure II.34.

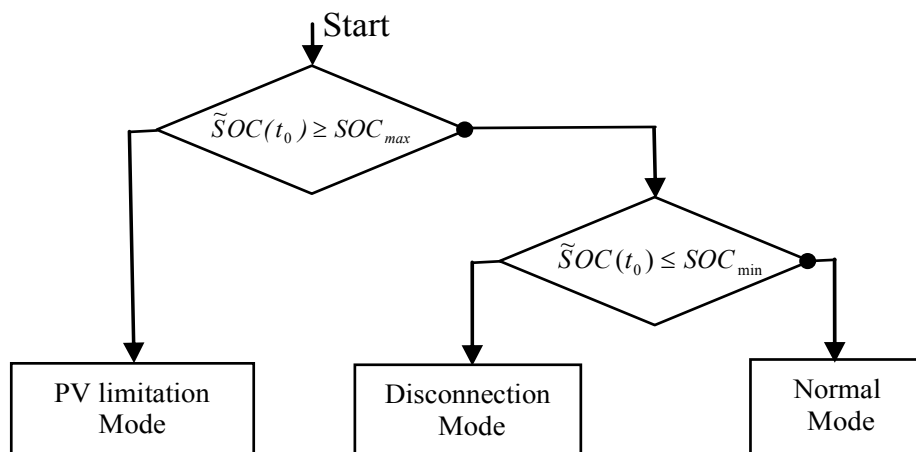


Figure II.34: Synoptic for the selection of the operating modes

Figure II.35 shows the integration of the control operating mode in the control system.

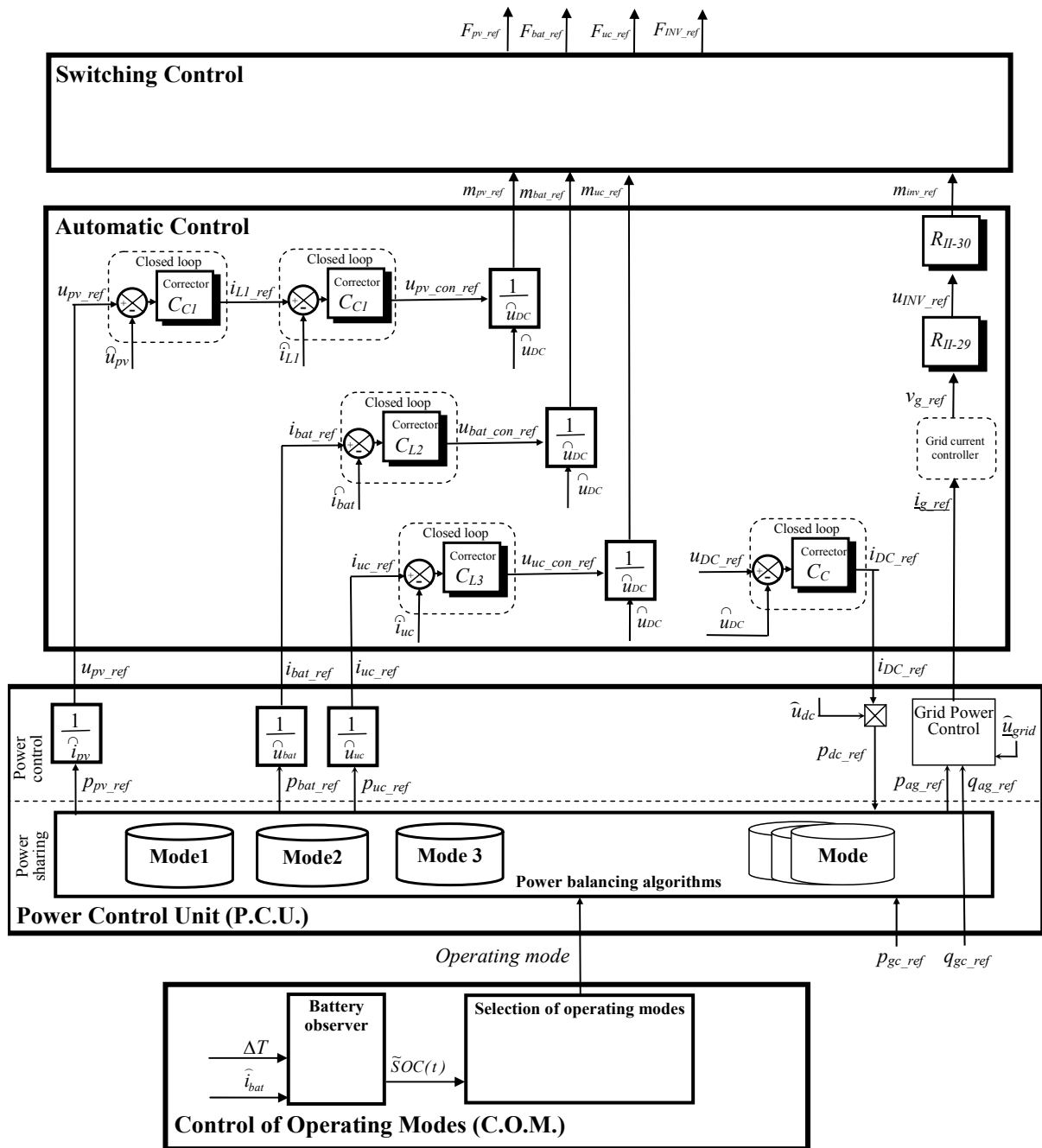


Figure II.35 Integration of the control of operating modes

In the PV based active generator ultracapacitors are used to perform the power balancing inside the generator. When both energy storage systems are available (with their storage levels in a good range), the PV based active generator works in the previous presented “normal operating mode”. The power balancing algorithms can be directly used without any modification.

Ultracapacitors are fast power units and so their state of charge can be managed directly in the balancing algorithms.

## II.6. Energy management of the embedded ultracapacitors

### II.6.1. Energy level and management scheme

The energy level of the ultracapacitors can be expressed with the ultracapacitors voltage and is indicated in percentage:

$$Level_{uc} = \frac{E_{uc}}{E_{uc\_max}} = \frac{C_{uc}u_{uc}^2/2}{C_{uc}u_{uc\_max}^2/2} = \frac{u_{uc}^2}{u_{uc\_max}^2} \quad (\text{R. II-52})$$

with  $E_{uc}$ : the energy, which is stored in the ultracapacitors;

$E_{uc\_max}$ : the maximal energy, which can be stored in the ultracapacitors;

$u_{uc}$ : the voltage across the ultracapacitors;

$u_{uc\_max}$ : the maximum voltage across the super-capacitors bank;

$C_{uc}$ : the equivalent capacitance of the ultracapacitors bank.

For efficiency and security reasons, the energy level must be limited from 25% to 95%. It corresponds to an operating voltage from 50% to 97.5% of the maximal voltage. In our study, BOOSTCAP 48V ultracapacitors modules are used in series and the rated voltage is 48V. So the operating voltage range of the super-capacitors is from 24V to 46.8V.

In order to avoid the chattering phenomena, two hysteresis operators are used to define the supercapacitor storage state ( $State_{uc}$ ) as  $Empty_{uc}$  or  $Normal_{sc}$  or  $Full_{uc}$  (Figure II.36).

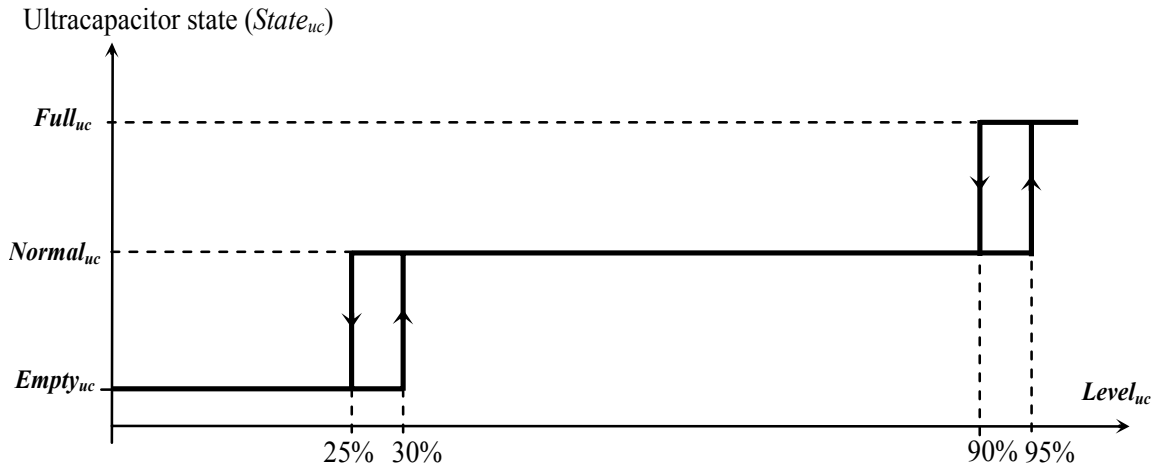


Figure II.36 Hysteresis control of the ultracapacitor energy management.

### II.6.2. Full ultracapacitors mode

When the ultracapacitors voltage increases above 46.8V, the ultracapacitor energy storage level is too high ( $Level_{uc} > 95\%$ ). If the battery energy storage level is still in a good range, the active PV generator begins to work in the “full ultracapacitors mode”. A special energy management strategy should be performed to recover the supercapacitor storage level ( $Level_{uc}$ ) as soon as possible, while the PV power and the real grid power are always well regulated to achieve the power requirements. The strategy consists not to use batteries in generating mode. As result, the ultracapacitors start to be discharged and return back to the normal state. With the same power control algorithms for the other sources, the ultracapacitors will be automatically discharged.

### II.6.3. Empty ultracapacitors mode

When the ultracapacitors voltage decreases below 24V, the supercapacitor energy storage level is too low ( $Level_{uc} < 25\%$ ). If the battery energy storage level is still in a good range, the active PV generator begins to work in the “empty ultracapacitors mode”. A special energy management strategy should be performed to recover the supercapacitor storage level as soon as possible, while the PV generator the active grid power are always well regulated to achieve the power requirements.

The strategy consists not to use the batteries to store the over power then super-capacitors start to be recharged for returning back to its normal state (Figure II.37).

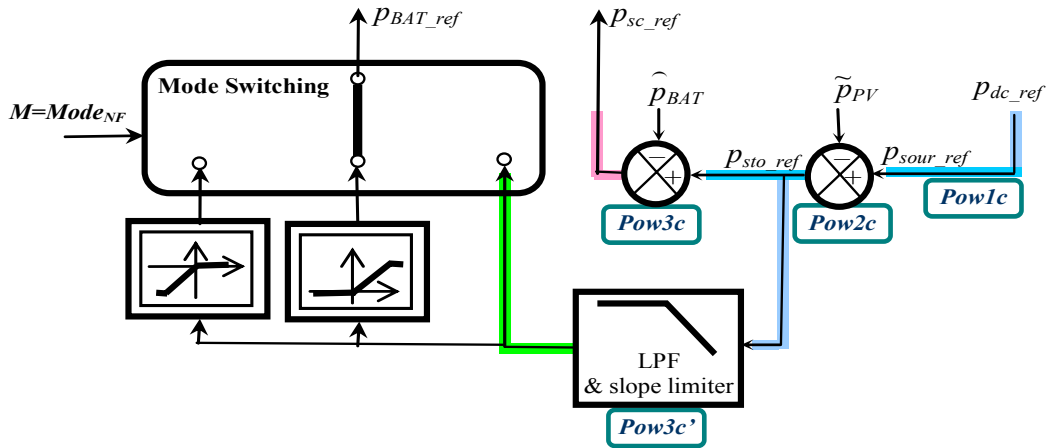


Figure II.37 Energy management of ultracapacitors

## II.7. Simulation and experimental results

### II.7.1. Simulation results

#### a. Scheme

In order to validate the models of each element in the PV active generator and to test the control design, a simulation for the operation of the PV active generator system is implemented with the Matlab/Simulink Software. Figure II.38 and Figure II.39 show the considered power production plan. Here we consider a change each ten seconds in order to have a better view on electrical waveforms during the transient states.

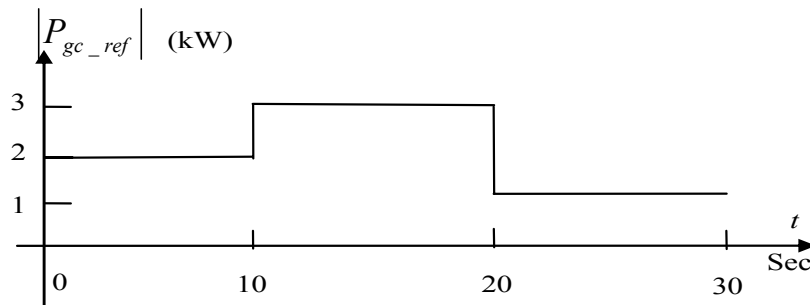


Figure II.38 Active power reference for the active PV generator

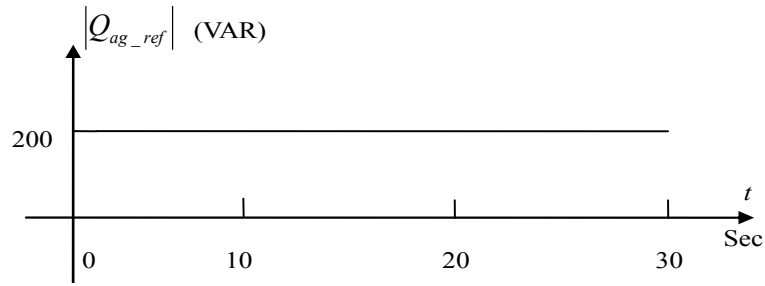


Figure II.39 Reactive power reference for the active PV generator

Three simulation tests have been done under the three different operating modes.

**b. Normal mode**

In Figure II.38, at 10<sup>th</sup> second, the grid power reference ( $p_{ag\_ref}$ ) increases very quickly to 3kW according to the power production plan. The generated power from the PV panels ( $p_{pv}$ ) is about 2.5kW and is not sufficient (Figure II.40). The batteries cannot provide the missing power because the batteries have low dynamics. We show that the ultracapacitors are well used to compensate the power gap. Unless the fluctuations of the produced PV power, a good coordination of both storage units is achieved. The generated powers ( $p_{ag}$ ,  $q_{ag}$ ) meet the requested references ( $P_{ag\_ref}$ ,  $Q_{ag\_ref}$ ).

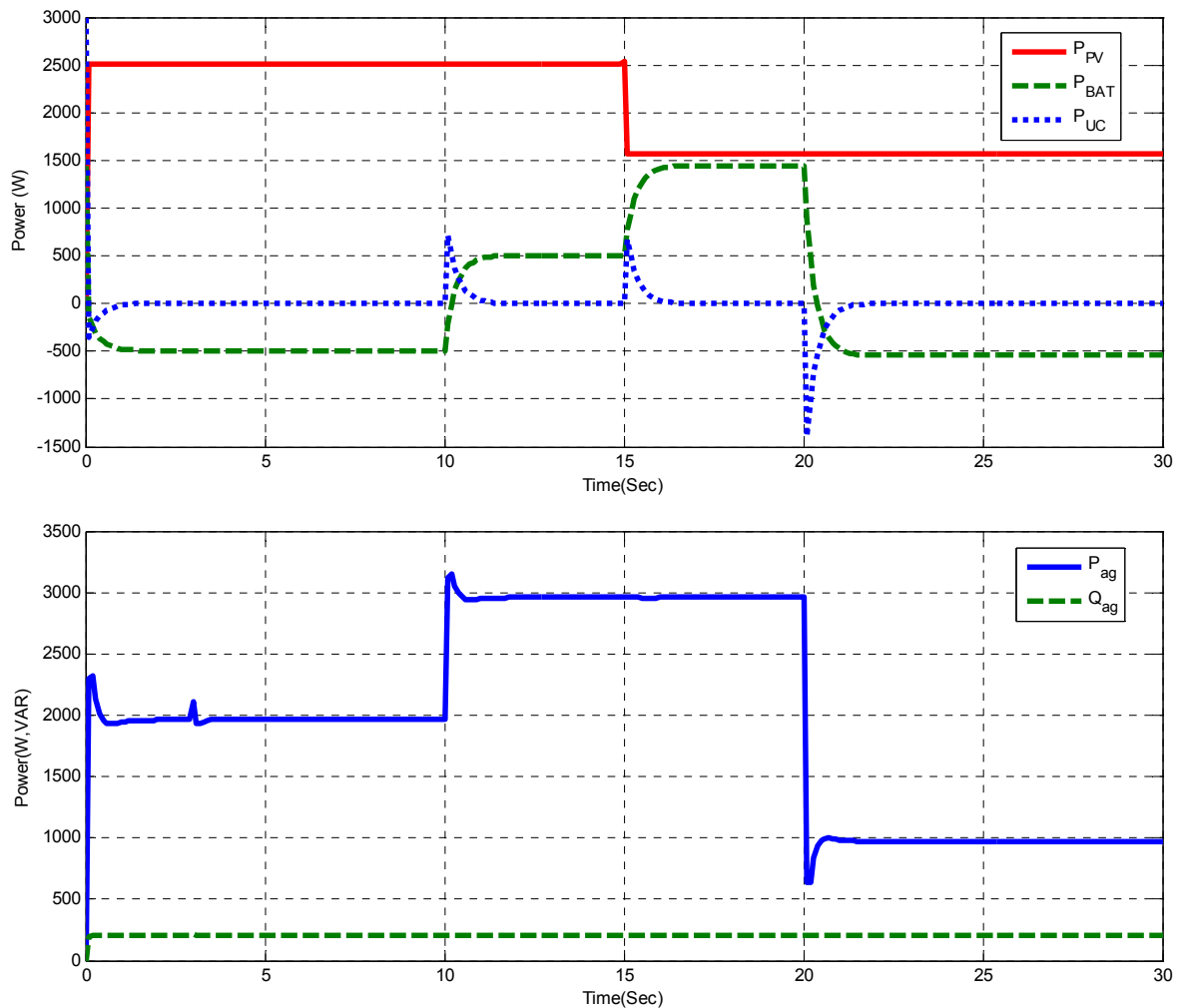


Figure II.40 Simulation results in normal mode



### c. Limitation mode

In this simulation test, the weather is very sunny. The generated power from the PV panels can satisfy the grid power demand. But the surplus power can not be injected into storage units, which are already fully charged. Thus the exchanged power with batteries and ultracapacitors is null and we can see that the PV panels are controlled in a dynamic limitation mode (Figure II.41).

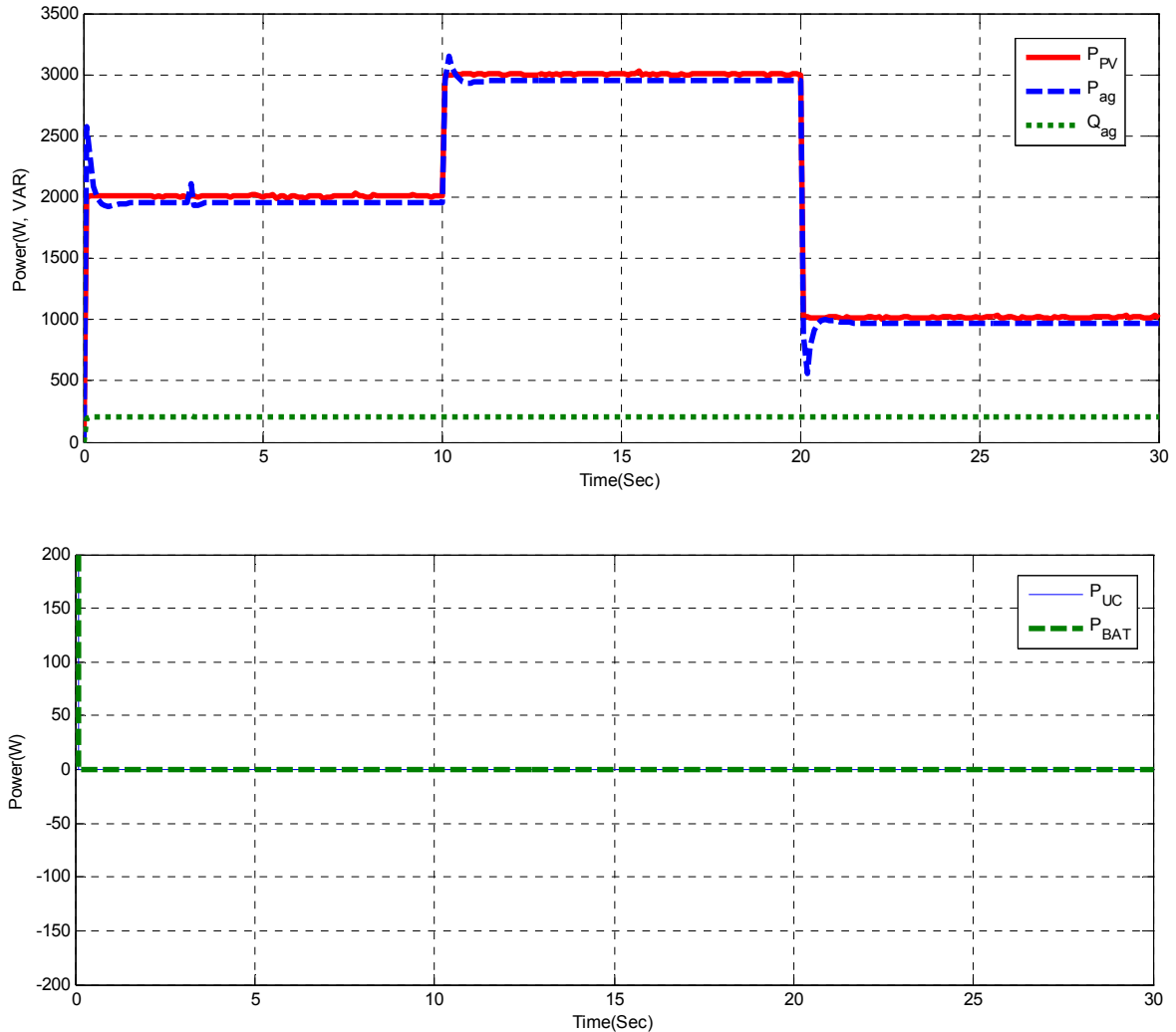


Figure II.41 Simulation results in limitation mode

### d. Disconnection mode

In this test, the weather is very cloudy. The generated power by the photovoltaic panels is insufficient. In Figure II.42 Simulation results in disconnection mode, we can see that the batteries are charged with the available PV power. Ultracapacitors are used to limit the battery current during the starting and to filter the PV power fluctuations.

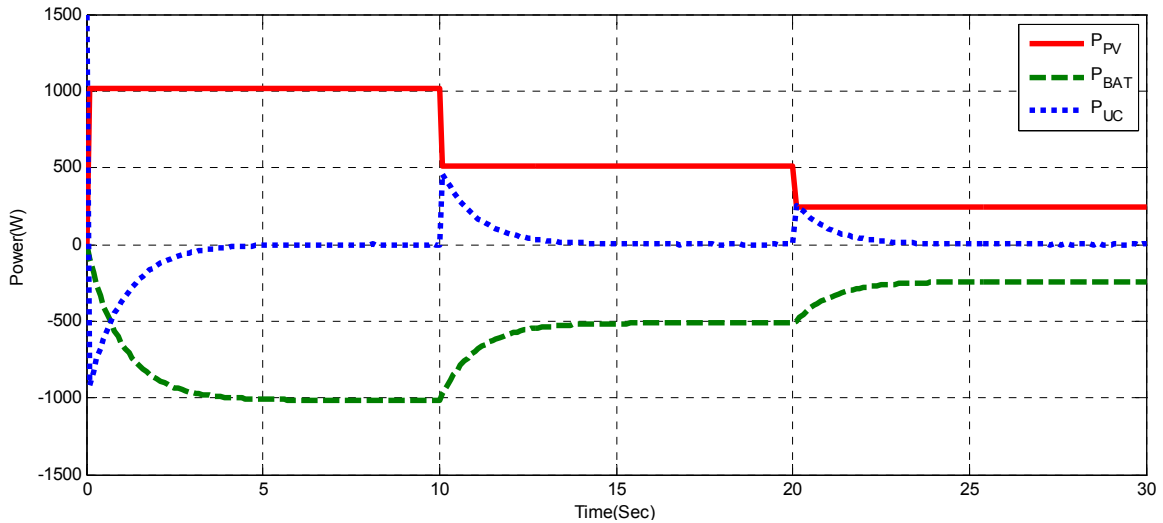


Figure II.42 Simulation results in disconnection mode

### II.7.2. Experimental results

In order to test our power control system, a prototype system of the PV based active generator has been built. A set of 106Ah batteries and 112kWp ultracapacitor modules are used as storage components. A DC current source is used for simulating PV panels. The control system is implemented into a DSpace card (Figure II.43).

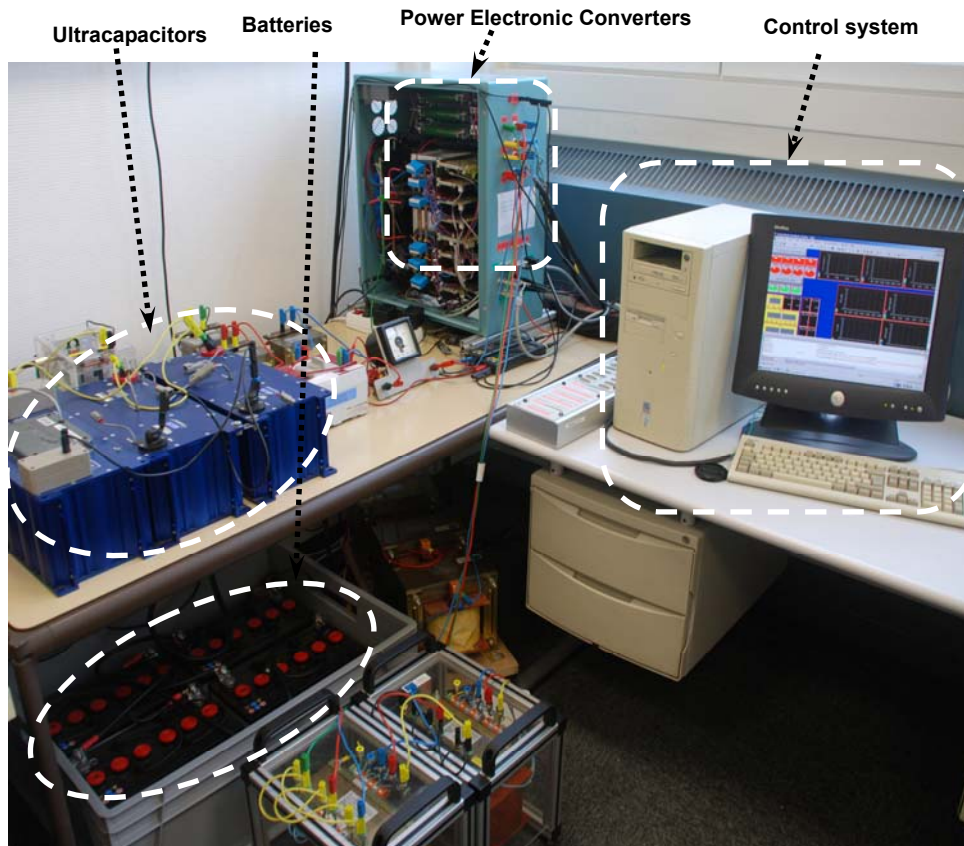
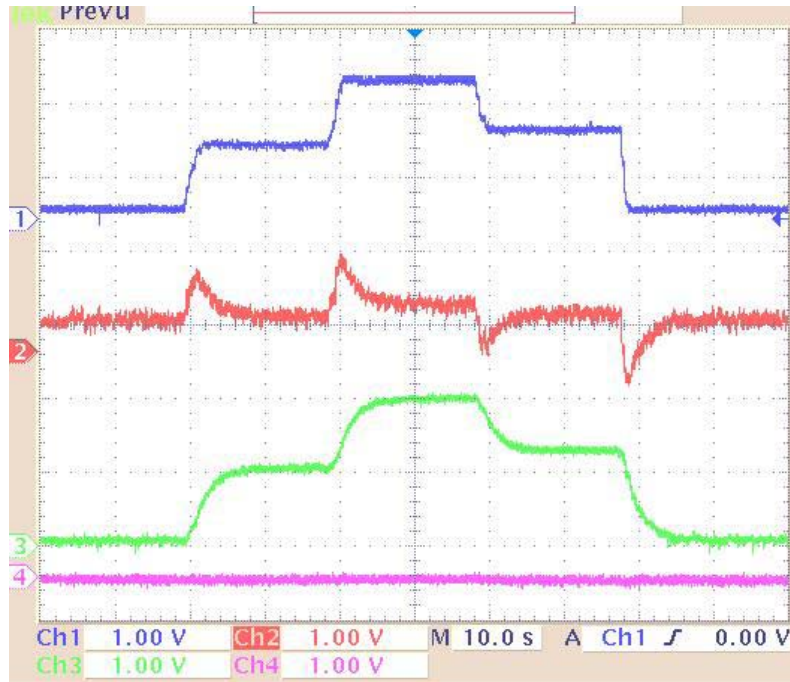


Figure II.43 Prototype PV based generator for the experimental test

Two experimental tests are presented.

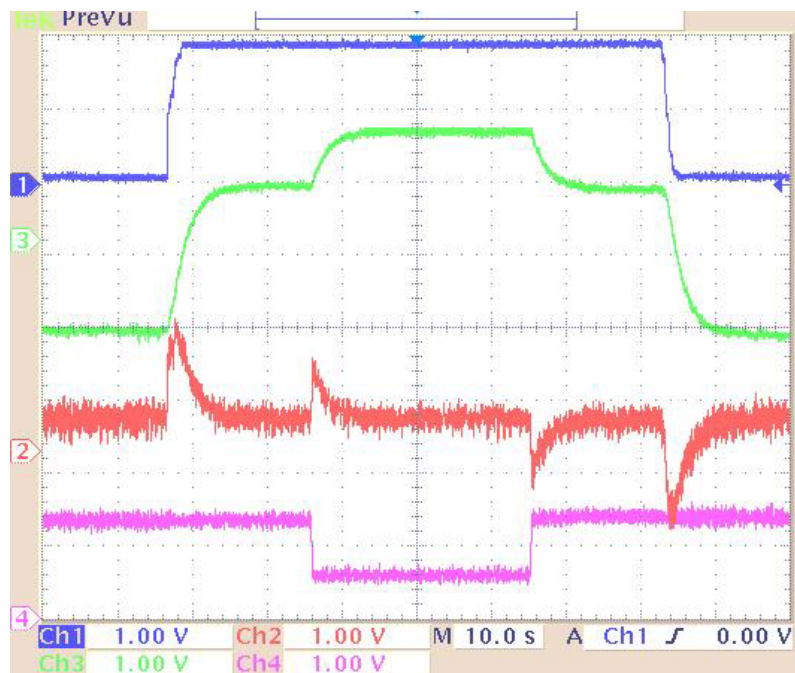
First in the night, there is no electrical production from PV power. Figure II.44 shows the variation of the grid power and the dynamic currents from both storage units. When a step change from 0 to 200W occurs in the grid load demand ( $p_g$ ), at the 19 second the batteries are discharged with a slow power increase and, in the same time, the ultracapacitors are instantaneously discharged with a high current to meet the grid load demand (Figure II.44).

The second presented experimental test corresponds to the day time operating. A 400W power demand from the grid ( $p_g$ ) between the 17 to the 82 second during this test (Figure II.45).



Ch1 (200W/div):  $p_g$ ; Ch2 (200W/div):  $p_{uc}$ ; Ch3 (200W/div):  $p_{bat}$ ; Ch4 (200W/div):  $p_{pv}$ .

Figure II.44 Experimental results in the night test



Ch1 (200W/div):  $p_g$ ; Ch2 (200W/div):  $p_{uc}$ ; Ch3 (200W/div):  $p_{bat}$ ; Ch4 (200W/div):  $p_{pv}$ .

Figure II.45 Experimental results in the day test

The PV power production changes between 4<sup>th</sup> and 7<sup>th</sup> second from 250W to 100W. Powers from both storage units are shown in Fig.15. When the PV production decreases fastly, the batteries can not immediately supply all the surplus production, the ultracapacitors help to perform the power balancing while charging more power with a higher power appears at 4<sup>th</sup> second.

## II.8. Conclusions

In this chapter, an average model of a PV based active generator in a DC-coupled structure has been detailed. The modelling of this complex generation system is led by considering each source with the dedicated power electronic converter. The EMR of the system model is used to make appear power conversion chains.

The objective is to control the different sources in order to satisfy the microgrid power requirements, in spite of the fluctuations of the PV power. For the design of the control system, a hierarchical structure including four levels has been used.

Control algorithms are obtained by inverting the EMR and are implemented in the Automatic Control level. The modelling of the possible power flows inside the active generator is presented and various operating modes are introduced. The Multi-Level Representation is used to show the different power paths. For a dedicated operating mode, the inversion principle helps to find all control equations of the different powers in the Power Control level. From the calculated power references, electrical references (voltages, currents) are deduced for the various control algorithms.

A part of the power is required to regulate the DC bus. The regulation scheme of the DC bus depends on the chosen operating mode. A grid following strategy is used when the active generator is connected to the microgrid. In this mode grid power references are received and supplied by the generator. An autonomous charging strategy is used to load storage units when the active generator is disconnected. A synthesis is performed to design an unique control strategy for any operating modes.

The reference of the exchanged power with both storage units has been calculated by using an estimation of the produced PV power. For the first step of the tests, a simple method to dispatch the power between batteries and ultracapacitors is used with a low-pass filter. Ultracapacitors are controlled to supply the required transient power from storage units.

Several simulations show the performances of the control system.

Experimental test results verify the effectiveness of the proposed control and show the good dynamic performances thanks to the coordination of each source embedded the PV based active generator.



# *Chapter III*

Micro Grid framework for integrating DG  
in energy management and control system  
of power networks



## Contents

Chapter III. Micro Grid framework for integrating DG in energy management and control system of power networks.....	83
III.1. Introduction .....	83
III.2. Architecture of future electrical systems .....	83
III.2.1. Issues .....	83
III.2.2. Interest of micro grids and specificities.....	85
III.2.3. Basic MG architectures.....	86
III.2.4. Operation modes.....	87
III.3. State of the art.....	88
III.3.1. In Europe .....	88
III.3.2. In the United States.....	92
III.3.3. In Japan.....	94
III.4. Dispatchable distributed generation for grid control.....	96
III.4.1. Interest .....	96
III.4.2. Classical isochronous speed control of conventional DGs.....	96
III.4.3. Energy storage requirements in power systems.....	97
III.4.4. Control functions for grid connected inverters.....	97
III.4.5. Control strategies for a grid-connected mode of the microgrid.....	98
III.4.6. Control strategies for a “Vf mode” in an islanded mode of the microgrid..	101
III.4.7. Control capabilities of the PV based active generator.....	104
III.5. Control system for microgrids.....	104
III.5.1. Objectives and tasks .....	104
III.5.2. Communication system .....	105
III.5.3. Control functions and management tasks.....	105
III.5.4. Time scale analyzing and implementation constraints .....	106
III.5.5. Power management by sensing electrical quantities .....	107
III.5.6. Energy management by signal communication.....	109
III.6. Conclusion.....	115





## **Chapter III. Micro Grid framework for integrating DG in energy management and control system of power networks**

### **III.1. Introduction**

In the previous chapter power fluctuations of a PV generator have been compensated by integrating storage units. The local controller has been enhanced in order to perform the independent and simultaneous control of the generated active and reactive power. Hence, the PV based active generator is able to generate a predetermined real and reactive power. These new control capabilities have been developed in order to create new possibilities to manage a power system in presence of renewable energy based generators.

Continuously small and smart grid energy systems are under development to integrate massively renewable resources, micro generators, small energy storage systems, critical and non-critical loads in the control system of grids. In this chapter, the context of future electricity system development is first presented and the interests for Micro Grids (MGs) are exposed specifically for integrating renewable and non conventional energy resources.

Then several demonstration projects will show the state of the art about MGs in the world.

The PV based active generator uses a power electronic converter for the grid connection and so dedicated control functions are required for a better integration into the micro grid management system. Different control schemes are reviewed and classified in order to highlight the required interface with the grid control system to make it operate as a classical dispatchable distributed generator.

Then fundamental principles of grid management systems and classical practices are recalled in order to better highlight:

- \_ constraints,
- \_ required control functions for the DG as well for the grid control system and
- \_ practical implementation.

### **III.2. Architecture of future electrical systems**

#### **III.2.1. Issues**

The different scenarios for future architecture of electricity systems recognize the fundamental fact that with increased levels of distributed generation penetration, the distribution network can no longer be considered as a passive appendage to the transmission network. The entire distributed system has to be designed and operated as an integrated unit. In addition this increased complex operation must be undertaken by a system under a multi-level management electrical system.

The growing share of DG in the electricity system may evolve in three distinct stages [Kok 05]: the accommodation step, the decentralization step and then the dispersal stage.

First, at the accommodation step, the DGs are accommodated in the current market. Distributed units are running free while the operating of the network is performed through the conventional production units. In this scheme Renewable Energy Based Generators (REBG) must not be dispatched and so classical wind generators and PV generators are connected.

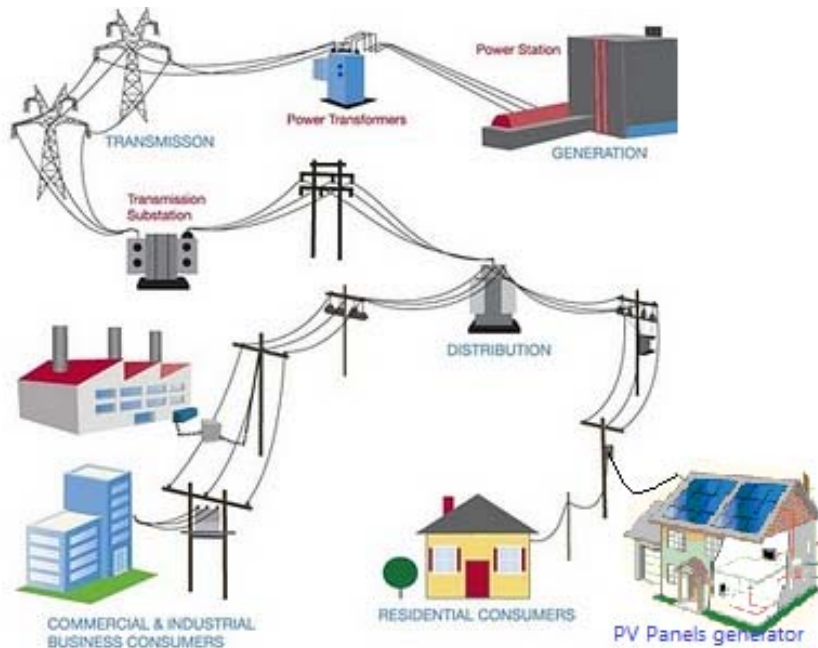


Figure III.1 Integration of DG in the actual electrical network [Url 10c]

If the share of DG increases massively, the decentralization step is achieved. Then virtual utilities optimize the services of decentralized providers through the use of common ICT-systems. A virtual utility is view as a flexible collaboration of independent, market-driven entities that provide efficient energy service demanded by consumers without necessarily owning the corresponding assets. Central monitoring and control is needed. In this scheme REBG and DG must be dispatched with a virtual utility and receive power references.



Figure III.2 Massive DGs in the electrical network with the virtual utilities [Url 10c]

At the last dispersal stage, local low-voltage network segments (here microgrids) provide their own supply with limited exchange of energy with the rest of the distribution network. The distribution network operator operates more like a coordinating agent between separate power systems (different microgrids) rather than a controller of the system. This kind of electrical network is smarter; can provide more different services based on intelligent appliances.

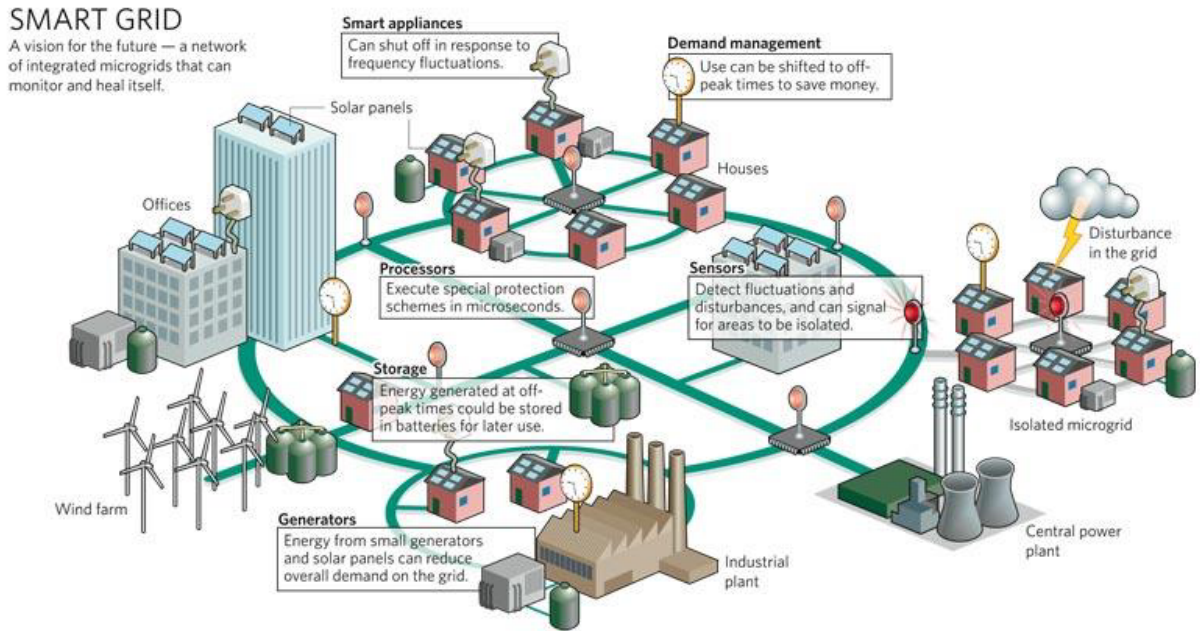


Figure III.3 Future electrical network based on smart grid [URL 10a]

For the integration of our PV based generator, we consider a micro grid organization to implement the virtual utility inside the MG central controller like in the decentralization step and also to enable a possible islanding operation as required in the dispersal stage.

### III.2.2. Interest of micro grids and specificities

MGs are small electrical distribution systems that connect multiple customers to multiple distributed sources of generation and storage. MGs are typically characterized by multipurpose electrical power services to communities with overall energy demands ranging up to several thousand kWh per day and are connected via low voltage networks. A great interest is that these hybrid power systems have the potential to provide reliable power supply to remote communities where connection to transmission supply is uneconomic.

In general, the MG concept assumes a cluster of loads and DERs operating as a controllable system that provides both power and heat to its local area. The benefits of MG, such as, the enhancement of the local reliability, the reduction of feeder losses, the control of the local voltage, provide an increased efficiency through the using of waste heat from Combined Heat and Power (CHP) generators, the voltage sag correction or the provision of uninterruptible power supply functions.

Generally, a MG is centrally controlled and managed by a MG Central Controller (MGCC) installed at the Medium Voltage/Low Voltage substation. The MGCC includes several key functions, such as economic managing functions and control functionalities and is the head of the hierarchical control systems. The MG is intended to operate in the following two different operating conditions: the normal interconnected mode with a distribution network and the emergency mode in islanding operation via a central switch, which must also implement the synchronization between both power systems.

As example Figure III.4 shows the MG concept of ABB where Micro-source Controllers (MC) are similar to Local Controllers for DG and Load Controllers are similar to Local Controllers for dispatched loads.

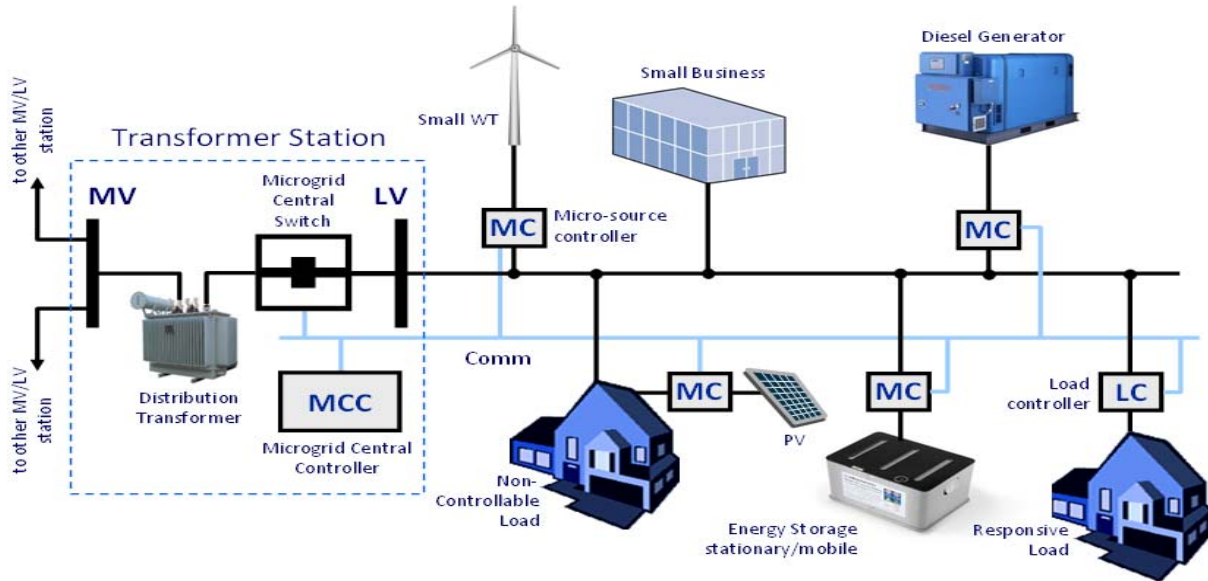


Figure III.4 A control architecture for a MG [ABB]

Most DERs that can be installed in a MG are not suitable for the direct connection to the electrical network due to the characteristics of the energy produced. Therefore, power electronic interfaces (DC/AC or AC/DC/AC) are required. Inverter control is thus an important concern in MG operation.

When the total number of MGs reaches a significant high share in Low Voltage substations, similar technical benefits can be expected in upstream grids as a consequence of multi-Microgrid operation.

### III.2.3. Basic MG architectures

The basic MG network is assumed to be radial with several feeders and a collection of loads Figure III.5). The radial system is connected to the distribution system through a separation device, usually a static switch at the PCC. Each feeder has a circuit breaker and a power flow controller [Hua 08].

In the EU project “Microgrids”, an operational architecture has been developed. It consists of a LV network, loads (some of them are interruptible), both controllable and non-controllable power generators, energy storage units and a hierarchical-type management. The control scheme is supported by a communication infrastructure used to monitor and control power generators and loads. The centre of the hierarchical control system is the Micro Grid Central Control (MGCC). At the low hierarchical control level, Local Controllers (LC) of loads and DGs exchange information with the MGCC for managing the MG operation by providing set-points to LCs. The exchanged information includes mainly messages about power reference setting for each source; MG switches orders that are sent by the MGCC to LC and the sensed voltage/current information to MGCC from each local capture.

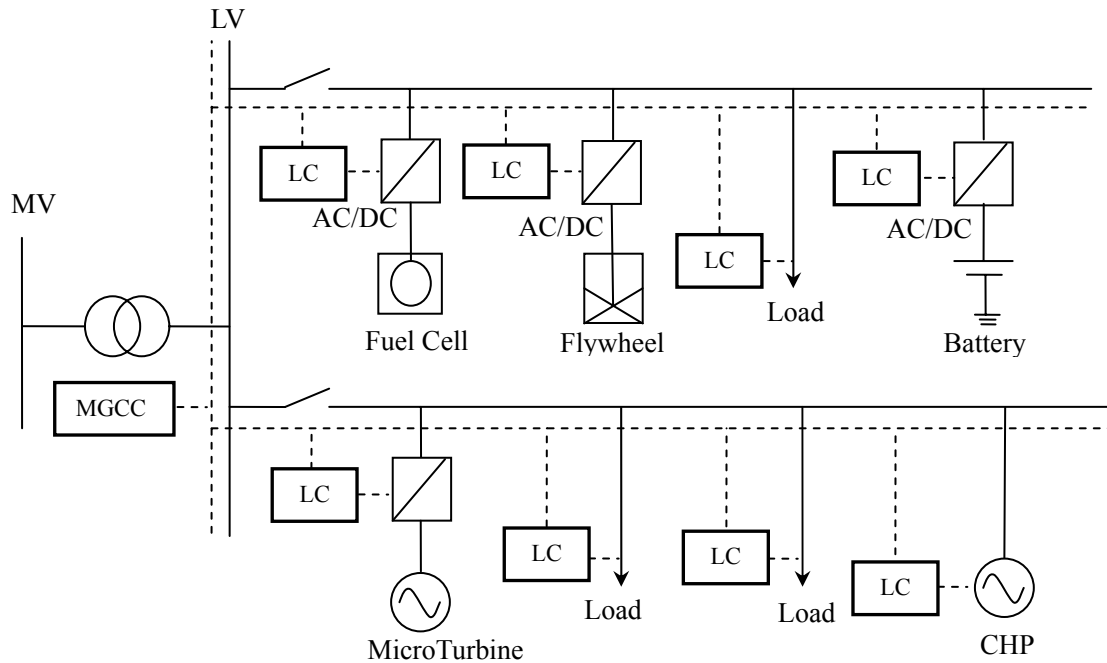


Figure III.5 Basic MG architecture with a MGCC

### III.2.4. Operation modes

#### a. Normal operation in a grid-connected mode

MG flexibility can be achieved by allowing its operation under two different conditions. In the normal operation, the MG is connected to a main MV grid being either partially supplied from it or injecting some amount of power into it. Depending of the custom desire, in this grid-connected mode, the main grid and local DGs may send power to the loads. As the MV grid sets the RMS voltage, all DGs inside the MG can only generate currents but can be dispatched by the MGCC in order to provide power references. The control system into the LC of the DG is known as “PQ inverter control” and the DG is said to be in “PQ mode”. Corresponding local controllers for DGs, which are connected to the grid with power electronic converters, will be detailed in paragraph III.4.5.

#### b. Emergency operation in an islanded mode

If any events in the main grid appear, an islanded operating mode can be implemented because the electrical system is organized in the form of a MG with a MGCC. The MG islanding process may result from an intentional disconnection from the MV grid (due to maintenance needs) or from a forced disconnection (due to a fault in the MV network such as voltage dips). The disconnection is performed by a static bypass switch opening itself as a controllable load or source.

The emergency operation of MG consists of the disconnection but also of the operation in the islanded mode. Hence, one DG in the MG should be in charge of maintaining the frequency and the voltage. The corresponding local controller must implement a Voltage Source Inverter (VSI) control with an inner RMS voltage reference and frequency set point and so compensate the power unbalancing between loads and other DG produced power (paragraph 4.6). The DG is said to be in “Vf mode” and is defined as the “Master Source”. Other DGs are “Slave Sources”, whose local controllers must operate in a PQ mode (paragraph 4.5). The MGCC share the total amount of real power to produce among the “Slave Sources” and send them PQ references. It is important to avoid the overload of

inverters and to ensure that load changes are controlled in a proper form. So in an islanded mode, one DG must be in “Vf mode” and the others in a “PQ mode”.

### **c. Fault detection**

When the MG is operating in islanded mode, any current fault must be covered by generators inside of the MG. These fault currents may have low values. But compared with the current limit of the power electronic converters for the generators, these fault currents are relatively too high. This margin is insufficient to trip conventional over-current protection and therefore other protection techniques have to be found.

One approach proposed by Lasseter [Las 04], that is quite powerful, is to develop a real-time fault location technique that will identify the exact location of the fault much more accurately than the classical relaying is capable of doing under any circumstances. These methods may be too costly. Low cost approach such as a Current Transformer (CT) based zero sequence detection, and differential current and/or voltage methods also show promise.

Hernandez-Gonzalez and Iravani [Her 06] have presented an active islanding detection technique for a DER at the distribution voltage level, which uses a three-phase, voltage-sourced converter (VSC) as the interface unit. The proposed method is based on injecting a disturbance signal into the system through either the direct axis (d-axis) or the quadrature axis (q-axis) current controllers of the interface voltage-sourced converter. Signal injection through the d-axis controller modulates the amplitude of the voltage at the PCC, whereas signal injection through the q-axis controller causes a frequency deviation at PCC, under islanded conditions.

### **d. Safety analysis**

A fault in a MG may cause a ground potential rise, even if the energy sources operate at LV. Thus grounding the distributed energy sources and the transformer connecting the MG to the utility network must be carefully analyzed and appropriate rules need to be developed.

LV earthing systems are defined according to the earthing techniques of the secondary side of the MV/LV transformer and the frame of the load equipment. Besides, a grounding system for a typical MG has been designed in [Jay 05] and its adequacy during fault conditions studied from an electrical safety point of view.

## **III.3.State of the art**

Intense research activities on various aspects related to micro grids have been launched in Europe, in the United States and in Japan. In this part we focus the attention on technological aspects and the market organization is not discussed here.

### **III.3.1.In Europe**

In the EU, two major research efforts have been devoted exclusively to micro grids: the project “Microgrids” and the project “More Microgrids”. Main general results are exposed and three specific European applications of the microgrid concept are presented.

#### **a. Project Microgrids (1998-2002)**

In the 5<sup>th</sup> Framework Program the project “Microgrids: the large-scale integration of micro-generators for low voltage networks” was led by the National Technical University of Athens (NTUA), with 14 partners from seven EU countries [Haz 07]. The objectives of this project were:

- to study the operation of microgrids to increase penetration of renewable and other DERs while reducing carbon emissions,
- to study the operation of microgrids in parallel with the grid and in islanded mode, as may follow faults,
- to define and develop control strategies to ensure efficient, reliable, and economic operation and management of microgrids,
- to define appropriate protection and grounding policies to assure safety, fault detection, separation, and islanded operation,
- to identify and develop the required telecommunication infrastructures and protocols,
- to determine the economic benefits of microgrid operation and propose systematic methods to quantify them,
- to simulate and demonstrate microgrid operation on laboratory scales.

This project has proposed several solutions and innovative techniques:

- DER models and steady-state and dynamic analysis tools enabling simulation of LV asymmetrical, inverter dominated microgrid performance,
- islanded and interconnected operating philosophies both hierarchical and distributed (agent based) control algorithms,
- local blackstart strategies,
- definitions of DER interface response and intelligence requirements grounding and protection schemes,
- methods for quantification of reliability benefits,
- laboratory microgrids of various complexities and functionalities.

Several levels of centralized and decentralized control have been developed by participating laboratories: ISET (Germany), University of Manchester (UK), School of Mines (France) and NTUA (Greece).

#### **b. Projet More Microgrids (2002-2006)**

A follow-up project titled “More Microgrids: Advanced Architectures and Control Concepts for More Microgrids” within the 6<sup>th</sup> Framework Programme was aiming to increase micro-generation systems in electric power systems by broadening the original concept of microgrid. This second consortium, again led by NTUA, comprises manufacturers, including Siemens, ABB, SMA, ZIV, I-Power, Anco, Germanos, and EmForce; power utilities from Denmark, Germany, Portugal, the Netherlands, and Poland; and research teams from Greece, the United Kingdom, France, Spain, Portugal, and Germany. The new objectives include:

- the investigation of new DER controllers to provide effective and efficient operation of microgrids,
- the development of alternative control strategies using next generation information and communications technology,
- the creation of alternative network designs, including application of modern protection methods, modern solid-state interfaces, and operation at variable frequencies,
- the technical and commercial integration of multiple microgrids, including interface of several microgrids with upstream distribution management systems, plus operation of decentralized markets for energy and ancillary services,
- the standardization of technical and commercial protocols and hardware to allow easy installation of DERs with plug-and-play capabilities,
- the study of the impact on power system operation, including benefits quantification of microgrids at regional, national, and EU levels of reliability improvements, reduction of network losses, environmental benefits, etc,



- the exploring of the impact on the development of electricity network infrastructures, including quantification of the benefits of microgrids, to the overall network, and to the reinforcement and replacement strategy of the aging EU electricity infrastructure,
- the executing extensive field trials of alternative control strategies in actual installations, with experimental validation of various microgrid architectures in interconnected and islanded modes, and during transition testing of power electronics components and interfaces and of alternative control strategies, communication protocols, etc.

### c. Agent based control of the Kythnos Island Microgrid

The island operation of the Gaidouromandra microgrid in Kythnos (Greece) has been designed, installed and operated by IWES through two European Joule Projects "PV-Mode" and "MORE" [Gei 09], [Par 09]. In this microgrid, six PV generators (10kW) at different locations feed in AC current. 12 vacation houses (12 kVA) by a combination of three parallel battery inverters (53 kWh). A 5 kW diesel generator set is available as a back-up unit. Additional 2 kW PV array, mounted on the roof of the control system building, is connected to a SMA inverter and a 32 kWh battery bank to provide power for monitoring and communication (Figure III.6)

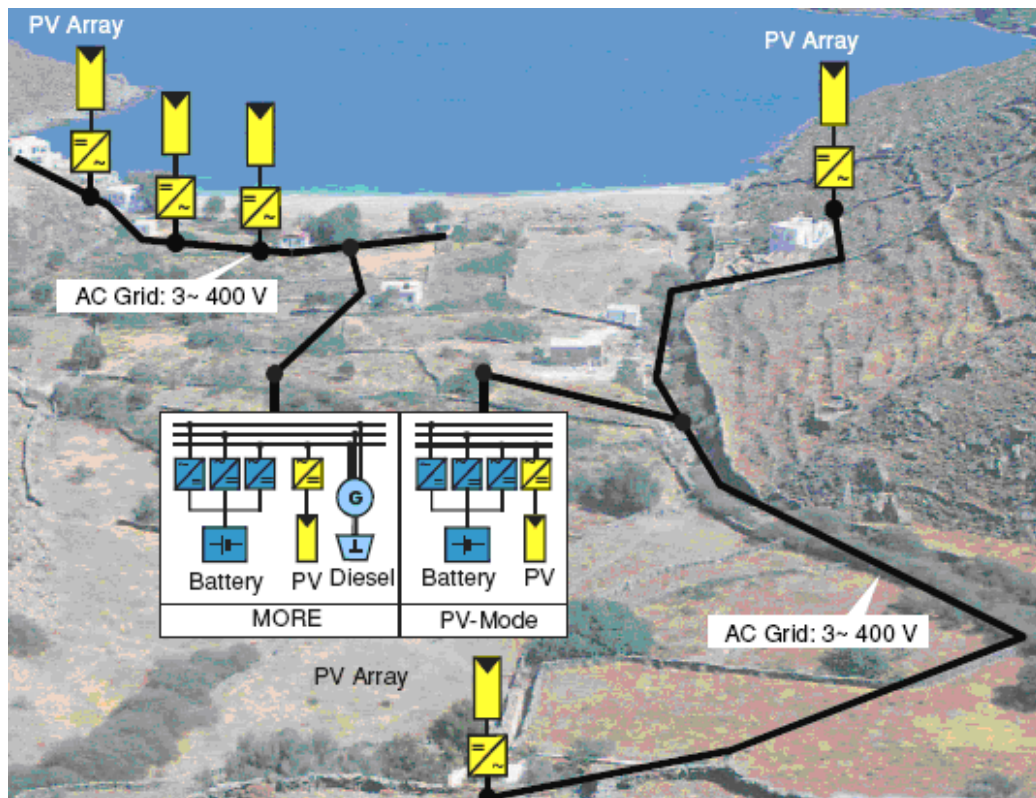


Figure III.6 Kythnos microgrid [Van 08] [Cob 08]

Residential service is powered by three SMA battery inverters ("Sunny Island") connected in a parallel master-slave configuration forming one strong single-phase circuit. More than one of the 3.6 kW battery inverters is used only when more power is demanded by consumers. The battery inverters can operate in frequency droop mode (paragraph III.5.5.a), allowing information flow for switching load controllers if the battery state of charge is low, and limiting the power output of the PV inverters when the battery bank is full.

An innovative centralized supervisory system was designed in order to monitor individually all generators and users, in real time and with a time resolution of up to 1 sec. First, ANCO intelligent Load Controller units (AN-ILC-01) are used to monitor the status of

power lines and to sense voltages, currents and the frequency. In addition it can remotely control up to PLC (Power Line Communication) load switches connected to the power line. Hence each DER/RES as well some of the loads are considered as intelligent agents and are managed with a Multi Agent System approach. An agent has the ability to take autonomously decision and to communicate with other agents (paragraph III.3.5.6.b). The agents may cooperate or compete according to their internal goals and behaviors. A flexible controller, based on an embedded processor, the Java based platform for agents called Jade host the Java based platform for agents called Jade.

This project has demonstrated the possible optimization of the operation in islanded mode by using agent based control of non-critical loads.

#### **d. Improvement of the voltage quality with energy storage**

The Bronsbergen holiday resort near Zutpen, the Netherlands, is equipped with a vast amount of PV systems [Cob 08]. During the summer the electricity generated by the solar panels (315 kW) is more than twice the peak consumption of the 210 cottages (150 kW). Moreover the PV inverters cause specific harmonic problems and asymmetries in the network. Over 700 kWh of electricity storage is installed. Two 200 kVA inverters have been connected to the main LV busbar. Each inverter is connected to a set of 360 battery cells. A Battery Monitoring System monitors and logs the voltage across each set of six cells, so that failing cells can be quickly identified.

An automatic disconnection/reconnection switch was installed between the transformer and the main LV busbar of the network. The MGCC has its own voltage measurements on both sides of the disconnection/reconnection switch to support the resynchronization process.

Battery inverters have droop controllers (paragraph III.5.5.a) for automatic parallel operation with distribution grid. Automatic sharing of active and reactive power between inverters in the network is ensured by a systematic application of droop control.

Communication between a central controller and the individual inverters is needed only for the transfer of setpoints and to prepare an islanded microgrid for reconnection to the public network. In grid-connected operation, the active compensation has shown to reduce the 5<sup>th</sup> and 7<sup>th</sup> harmonic voltages originating from the public grid by at least a factor 2.

In order to fully support islanded operation, the following capabilities have been implemented and demonstrated:

- Black start of the complete microgrid from a single battery inverter,
- Clearing a feeder fault by blowing a 200 A feeder fuse with a single battery inverter,
- Automatic islanding on an open-circuit fault in the external public network,
- Automatic islanding on a short-circuit fault in the external public network,
- Automatic synchronization and reconnection of the islanded microgrid to the external public network.

#### **e. Reliability and economic issues in a microgrid**

The MG at the research center IKERLAN (Mondragón, Spain) contains residential loads, the PV, a microturbine (CHP), a Stirling engine (CHP) and a storage system based on batteries. The microgrid is controlled by a centralized energy management system in order to optimize the microgrid operation both in grid-connected and in stand-alone modes. In grid-connected mode the optimization of the economic exploitation of the microgrid is privileged by applying optimization techniques. In stand-alone mode, management functions are applied to improve the reliability of the facility by means of islanding operation capability. An optimization analysis has been carried out in simulation while the reliability improvement of the microgrid

operation has been analyzed and proven experimentally [MIL 09].

#### **f. Micro Grids in France**

At the Laboratory of Electrical Engineering and Power electronics (L2EP) of Lille, an experimental platform « Distributed Energy» has been developed to study electrical networks and systems in presence of small dispersed generators. It is composed of several generation systems, storage systems and loads; as examples a monitored 18kW photovoltaic plant, super capacitors as well as static and dynamic hardware in the loop emulators of generations and loads. Furthermore, the central core of the platform is a real-time simulator that can be connected to hardware equipments through power amplifiers. Using this experimental platform, several control techniques for the coordination of various generation systems can be studied. This platform will be used in the last chapter to test an energy management system. Micro grid concepts will be derivate to design an energy management system of a small residential network with a gas micro turbine and PV based generators. This platform will be used to test it.

The center PREDIS (ENSE3 and G2Elab) meets a set of technology platforms centered on the production, the distribution and energy uses. PREDIS is a demonstration tool on the intelligent management of energy, closed to the real networks, connecting different modes of decentralized energy production to different uses through an expert supervision system. It includes a hybrid real-time simulator, a PV generator, a CHP micro turbine, a fuel cell, controllable loads, systems, emulators wind generators, control systems and control of a supervisor driving and driving and other charges controllable.

At the laboratory SATIE (Système et Applications des Technologiess de l'information et de l'énergie) at Antenne de Bretagne of ENS (Ecole Normale Superieure) de Cachan, a power generation system of PV panels and wind turbines with lead-acid battery storage on a common DC bus has been set up in 1999. The research works concern the development of energy models in view to optimize the design and sizing of such systems based on economic criteria, the consummation management, the Li-ion technology evaluation and etc [Thi 10].

### **III.3.2. In the United States**

The United States has a modest but slowly expanding microgrids research program for a number of years, supported both by the U.S. Department Of Energy under the Office of Electricity Delivery and Energy Reliability and by the California Energy Commission through its Public Interest Energy Research Program. Heightened demand for high Power Quality Requirement (PQR) in the U.S., primarily to match the high end of heterogeneous end-use requirements, has naturally led to increased focus on enhancing PQR locally using microgrids.

#### **a. CERTS Microgrid**

The most well-known U.S. microgrid R&D effort has been pursued under the Consortium for Electric Reliability Technology Solutions (CERTS) [URL 10b], which was established in 1999 to explore implications for power system reliability of emerging technological, economic, regulatory–institutional and environmental influences. The specific concept of the CERTS Microgrid (CM) was fully developed in 2002. Subsequently, building physical examples was undertaken.

The CM, as for other microgrid paradigms, is intended to, as seamlessly as possible, separate from normal utility service during a disruption and continues to serve its critical internal loads until acceptable utility service is restored. The CM provides this function for relatively small sites (~<2MW peak power) without need for costly fast controls or expensive site-specific engineering. No single device is essential for operation, creating a robust system.

Figure III.7 shows a part of the CM, whose salient features are:

- The operation of generators is controlled locally by power electronic devices incorporating droop characteristics that respond to locally monitored frequency and voltage. Consequently, some devices that naturally require a power electronic interface, e.g., dc sources, are particularly amenable to incorporation in a CM.
- There is a single Point of Common Coupling (PCC), and without export. To the utility the CM appears as a single controlled load, similarly as “customers.”
- There is an explicit design to provide heterogeneous PQR. As example the architecture on Figure III.5 shows a varying reliability on the three circuits. Circuit C is exposed to normal grid power; however, in the event of inadequate grid power quality, e.g. voltage sag, the static switch opens and circuits A and B are served as an intentional island until acceptable power quality is restored.
- This is a dispersed plug-and-play system. No custom engineering is required for interconnection of any single device, making system configuration flexible and variable. Generators may not only be spread across circuits, they may be physically placed around the site, quite possibly co-located with convenient heat sinks that offer economically attractive CHP opportunities.

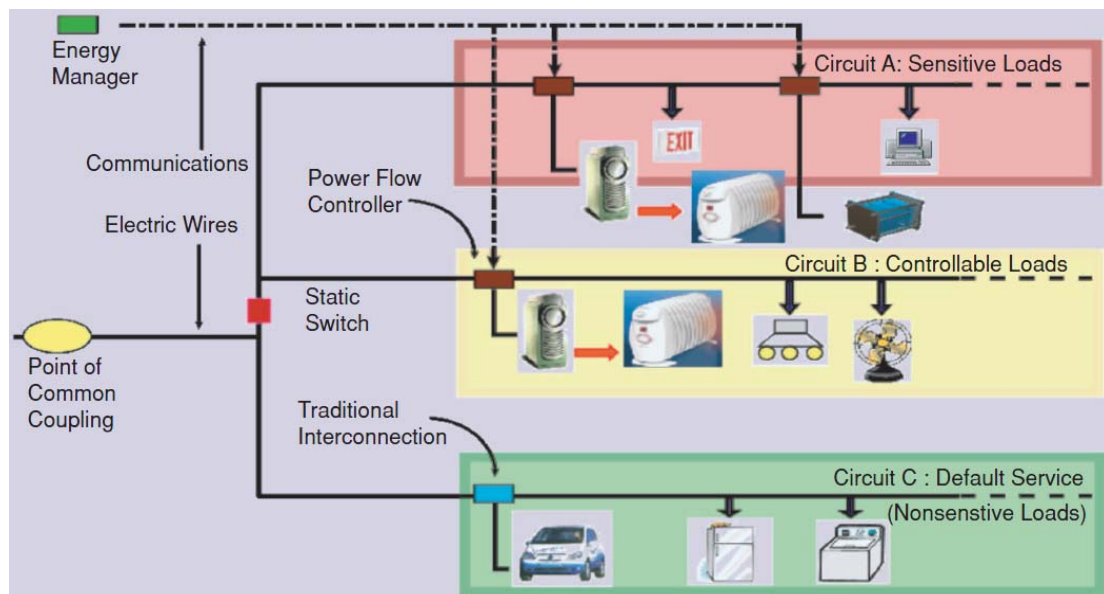


Figure III.7 Schematic of an example CM (source: CERTS).

### b. General Electric (GE) global research Microgrid

GE aims to develop and demonstrate a Microgrid Energy Management (MEM) framework for a broad set of microgrid applications that provides a unified control, protection and energy management platform (Figure III.8) [Hat 07]. At the asset level, MEM is intended to provide advanced controls for both generation and load assets that are robust with respect to low-inertia environments. At the supervisory level, MEM will optimize the coordinated operation of interconnected assets in the microgrid to meet customer objectives such as maximizing operational efficiency, minimizing cost of operation, minimizing emissions impact, etc., and is also intended to enable integration of renewable energy generators and microgrid dispatchability.

The program is executed in two phases. The completed Phase I of the program focused on fundamental controls and energy management technology development guided through the use of case studies considered to have market potential. These technologies were validated in simulation on a detailed model of a microgrid field demonstration to be executed in Phase II.

A multi-building campus is selected to demonstrate the technologies in a real-world application. Upon installation of equipment, validation and verification experiments to prove the advanced microgrid functionality is executed in mid 2008[Hat 07].

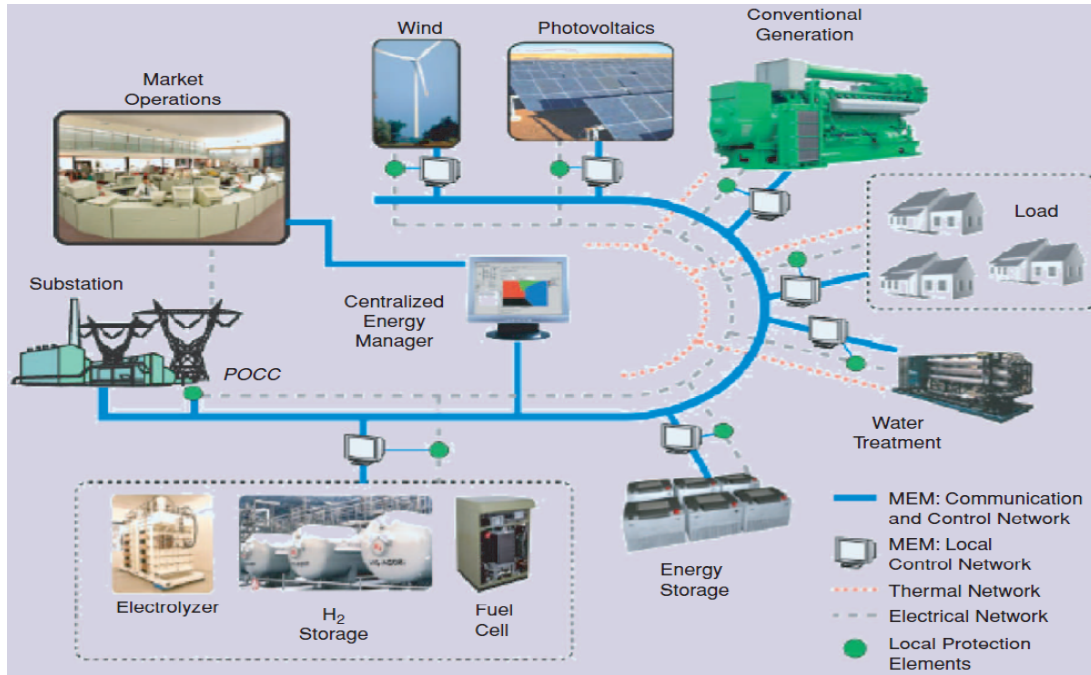


Figure III.8 GE MEM framework (source: GE Global Research)

Another project of General Electric at its research labs will let homeowners cut annual energy consumption to zero by 2015. This will be done by combining on-site power generation through solar panels or wind turbines with energy efficient appliances and also on-site storage. Home Energy Manager will give consumers to get detailed energy data and also control appliances. This device will cost between \$200 and \$250 which is a fair enough price for getting the power bills to zero. GE is piloting the in-home products and expects to have the appliances and energy display available in the future. A net-zero energy home would cost about 10 percent more by 2015. So as an investment basis, it is sure a higher end home like this would pay back the investment if there is nothing to pay on energy bills every month.

### III.3.3. In Japan

Japan is the current world leader in microgrid demonstration projects. The Japanese government has set ambitious targets for increasing the contribution of renewable energy sources, such as Wind Turbines (WT) and PV, but the fluctuating power of renewable energy sources might degrade the country's outstanding PQR. Traditionally, customers that operate fossil fuel-fired DERs, such as natural gas gensets with Combined Heat Power (CHP) do so baseloaded at rated power. Others that use intermittent renewable sources balance supply and demand through purchased grid power. In either case, residual purchases from the grid are volatile. Conversely, a microgrid can contribute to the load-following capability for a utility grid by balancing its own energy requirement using controllable prime movers to balance fluctuating load and renewable output. For example, a microgrid with electrical storage and/or gensets can potentially fully compensate its intermittent renewable supply and so is presented itself to the grid as a constant load. This principle has motivated much of the R&D in Japan, and has led to an emphasis on controls and electrical storage.

### a. The Aomori project in Hachinohe

This microgrid was put into operation in October 2005 and is being evaluated for PQR, cost effectiveness, and GHG (Green House Gases) emission reductions over a planned demonstration period lasting until March 2008 [Mar 07].

Figure III.9 gives an overview of the microgrid. A central feature of the system is that only renewable energy sources, including PV, WTs (100 kW) and biomass are used to supply electricity and heat. The controllable DGs consist of three 170 kW gensets (510 kW total) burning sewage digester gas, a 100 kW lead-acid battery bank and a 1.0 t/h woody biomass boiler. The microgrid serves seven City of Hachinohe buildings. These facilities are interconnected through a 6kV, 5.4km duplicate distribution line, with the whole system connected to the commercial grid at a single PCC.

The energy management system developed through this project optimally meets building demands for electricity and heat by controlling the output of the gensets and boilers, together with the charging and discharging of the battery bank. The control objective is to minimize operating costs and CO<sub>2</sub> emissions while maintaining a constant power flow at the PCC. From November 2005 and July 2006, primary energy consumption was reduced by 57.3%, thanks to reduced electricity purchases, while carbon emissions were also reduced by 47.8%.

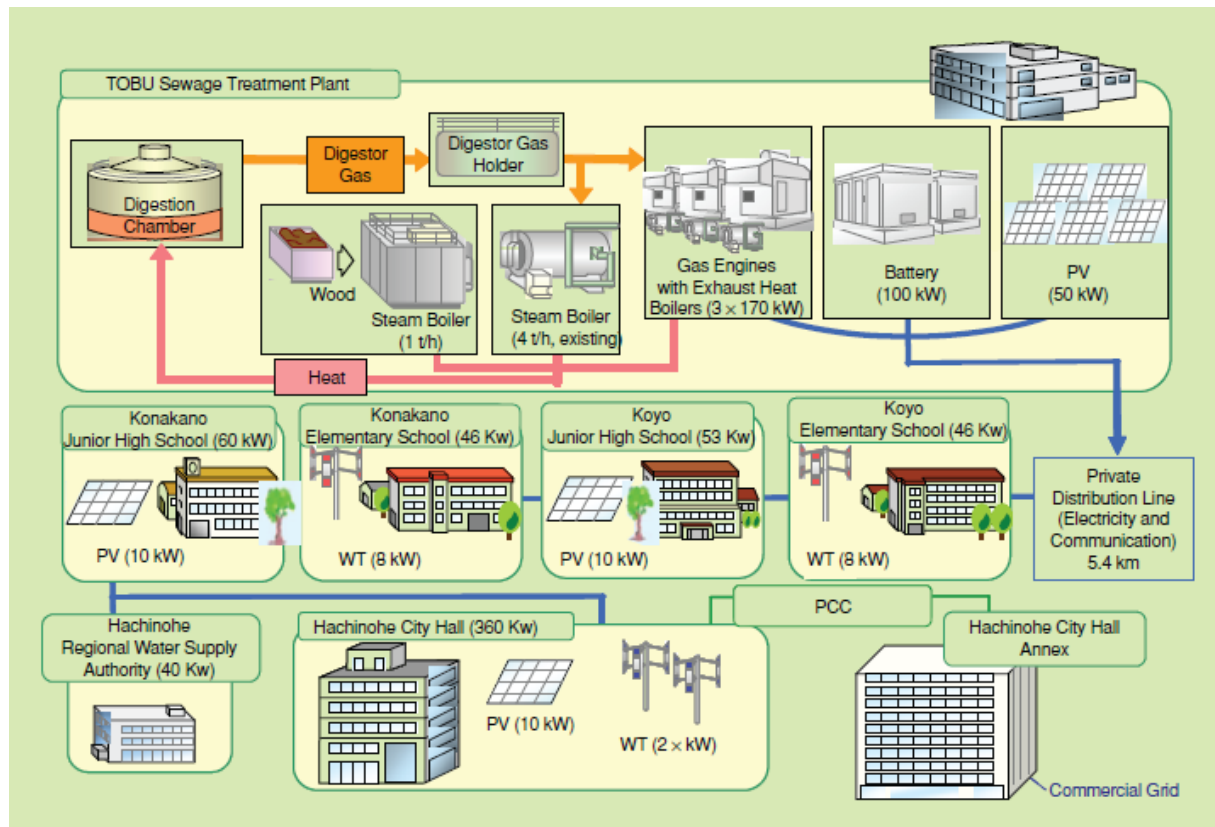


Figure III.9 Overview of the Aomori project

### b. The Aichi Project near the Central Japan Airport

The first NEDO demonstration project started operation at the site for the World Exposition in March 2005 [Mar 07]. The system was moved to the Central Japan Airport City near Nagoya in 2006, where it began operation in early 2007. It now supplies a Tokoname City office building and a sewage plant via a private distribution line. Its main feature is a combination of the following fuel cells as the main sources: 270 kW and 300 kW Molten Carbonate Fuel Cells (MCFC), four 200 kW Phosphoric Acid Fuel Cells (PAFC) and a 50 kW

Solid Oxide Fuel Cell (SOFC). The MCFCs use biogas generated from high temperature (1,200 °C) treatment of wood waste and plastic bottles. The MCFCs and SOFC are base-loaded while the PAFCs load follow. The total PV capacity is 330 kW and a 500 kW NAS battery is used for balancing. Experiment results of intentional islanding mode have also been obtained. The efficiency of this MG with Storage has been improved thanks to batteries in reliability, economy and environment assessments.

### III.4. Dispatchable distributed generation for grid control

#### III.4.1. Interest

Today, large centralized facilities provide most of the electrical power around the world with fossil fuel (coal, gas powered) or nuclear or hydropower plants. Normally, these large centralized plants have good economies of scale. But they usually have to transmit electricity to customers far away and so may affect the environment.

DG or DER is another approach. These sources are installed near customers end and reduce relatively the electrical power losses on transmission lines because the electricity is generated very close to the point of end use. This also decreases the size and number of power lines that must be constructed. DER appears as a faster, less expensive option to the construction of large, central power plants and high-voltage transmission lines. They offer consumers the potential for lower cost, higher service reliability, high power quality, increased energy efficiency, and energy independence. The use of renewable distributed energy generation technologies and "green power" can also provide a significant environmental benefit since they have few emissions.

As shown in chapter 1 (Section 2), DG can be or can not be dispatched. In our research study, an enhanced control organization of the power system is studied to make dispatchable DGs with a grid operator in the framework of a MG. The studied active generator in chapter 2 is considered as a dispatchable generator who participates to the management of the grid.

#### III.4.2. Classical isochronous speed control of conventional DGs

Isolated power systems and industrial microgrids are relatively small power systems. They are usually powered by an AC single generator, which is driven by a gas turbine or a diesel engine generator. The frequency of a synchronous AC generator is directly proportional to the speed of the rotating electrical field. Hence the power management relies on an isochronous speed control, which maintains the turbine at a constant speed. Hence the energy being admitted to the prime mover is regulated in response to changes in load, which would tend to cause changes in the speed as it is shown for a gas turbine in Figure.III.10. Any increase of loads would tend to cause the speed to decrease. The kinetic energy in the large inertia contributes to maintain constant the speed in the few instants. Moreover energy is quickly admitted to the prime mover to maintain the speed at the set point by the speed regulation. Any decrease in load would tend to cause the speed to increase, but energy is quickly reduced to the prime mover to maintain the speed at the set point.

An Automatic Voltage Regulator (AVR) is used to control the output RMS value of the machine ( $V_{mes}$ ) by regulating the voltage across the field exciter ( $V_{ref}$ ).

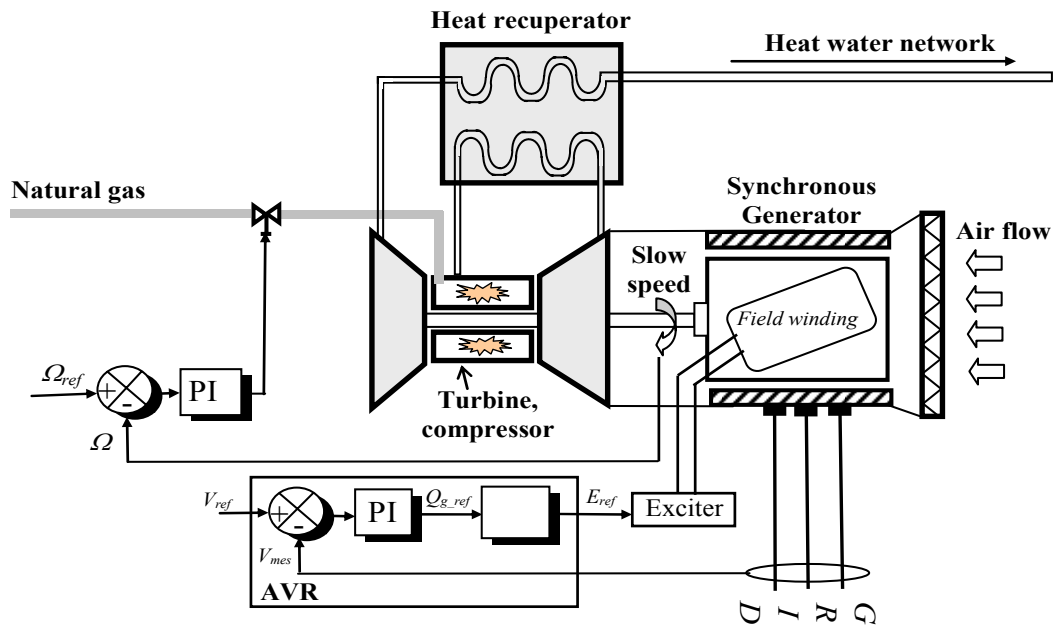


Figure III.10 Scheme of an isochronous speed control system of gas turbine

### III.4.3. Energy storage requirements in power systems

Current power systems can provide energy storage with the large inertia of all rotating conventional large power generation units. In case of a load change in the network, the power system's inertia can perform energy balance with detection of the variation of system frequency.

Lasseter [Las 02] points out that a system with clusters of small power DG (with small inertia) designed to operate in an islanded mode must provide some form of storage to insure initial energy balance. Due to the large time responses (from 10 to 200 s) of some small DG, such as fuel-cells, additional storage units may provide the amount of power required to balance the system following disturbances and/or significant load changes. For this operating, additional storage units must act as controllable ac sources to face sudden system changes. Anyway these devices have physical limitations and thus a finite capacity for storing energy may be considered.

In a MG, several forms and structures of energy storage can be considered as the use of traditional generator based DG with inertia, direct connection of additional ac storage systems (batteries, flywheels, etc.) and additional batteries or/and ultracapacitors coupled with a renewable energy source on a common dc bus (chapter 1, Section 3).

### III.4.4. Control functions for grid connected inverters

Because of their internal characteristics, the most of DERs is not suitable for a direct connection to an electrical network. Therefore, power electronic interfaces (dc/ac or ac/dc/ac) are required.

The most classical power electronic topology is a back to back structure with two Voltage Source Converters (VSC) (one for the generator-side converter and one for the grid-side converter). In PV generators and wind turbine applications, the generator side converters are usually controlled to implement a Maximum Power Point Tracking (MPPT) (and are usually a chopper for PV applications). The grid-side converter is usually a three-phased inverter.



Power electronic interfaces can provide more flexible operation compared to the direct connection of synchronous and induction generators to the grid [Las 03] [Zho 09e]. Functions that must be implemented by the control system of the inverter must be distinguished according to the operating mode of the microgrid (paragraph III.2.4). For a grid connected mode of the microgrid the ac voltage and frequency are supplied by the grid. So all dispatchable DG's inverters must be controlled in a "P/Q mode" to inject powers. For an islanded mode of the microgrid the inverter has to control the RMS value and the frequency of the ac voltage in a "Voltage Source Inverter mode".

### III.4.5. Control strategies for a grid-connected mode of the microgrid

#### a. Grid following strategy for passive generators

With a grid following strategy, the grid-side converter can control the voltage across the DC-link capacitor and control the reactive power exchanged with the grid.

This is the unique strategy for non-dispatchable DGs, as wind and PV generators because the primary energy resource is uncertain and can not enable a correct DC bus voltage control. Moreover if the DC-link voltage can be adjusted then different DC voltage values can be provided in order to MPPT for PV or wind turbines with synchronous generators and diode rectifiers [Bar 07] (Figure III.11).

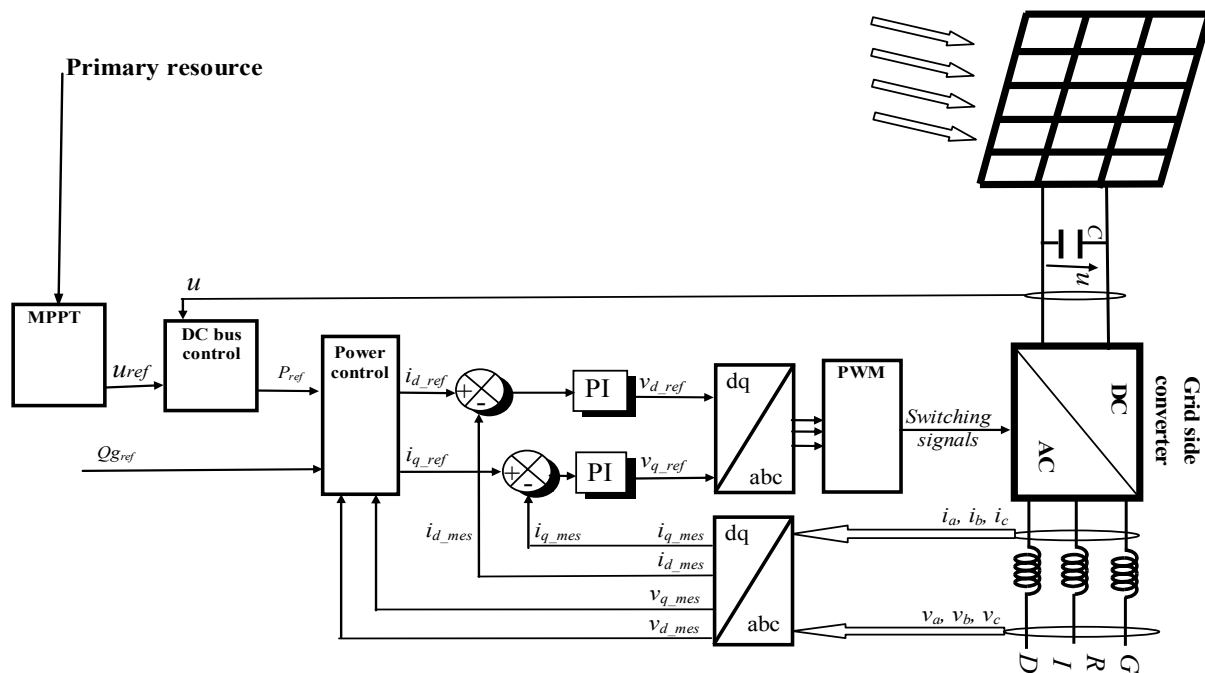


Figure III.11 Grid following strategy of a PV generator with a variable DC bus voltage for MPPT

This function can also be done by an additional generator side converter (Figure III.12). With a grid following strategy, the grid side inverter is controlled as a current-controlled voltage source because of the use of a choke filter. Direct and quadrature components of currents are calculated by a Park transformation for power calculation. Generated real power variations of the DG cause a DC-bus voltage error, which is corrected via the PI regulator by adjusting the magnitude of the currents injected to the grid. The reactive power output is also controlled by the PI regulator by adjusting the magnitude of the inverter reactive current output. This inverter can be operated with a unit power factor or can receive a set-point (from the MGCC) for the output reactive power.

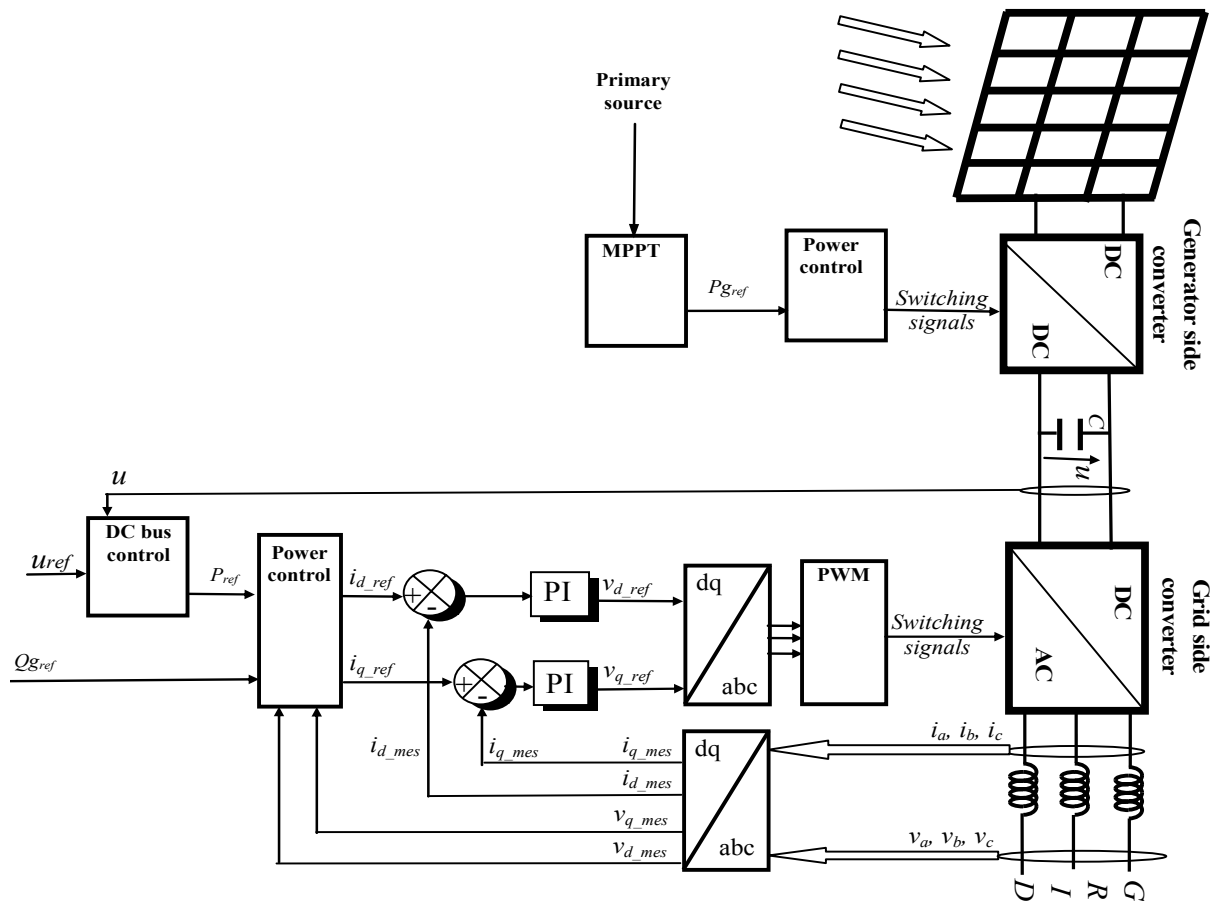


Figure III.12 Grid following strategy of a PV generator with a generator side converter for MPPT

**b. Grid following strategy for the “PQ mode”**

With a grid following strategy, the inverter operates by injecting into the grid the power available at the primary source because the DC bus voltage is constant. For PV generators or wind generators, this power is fluctuant. The DG is not dispatchable. For DG with possibilities to increase or to decrease the amount of the primary power, an additional active power reference can be used by the local controller or the MGCC to make variable the generated active power. These kinds of DG are dispatchable and their control system is known as “PQ control” (Figure III.13).

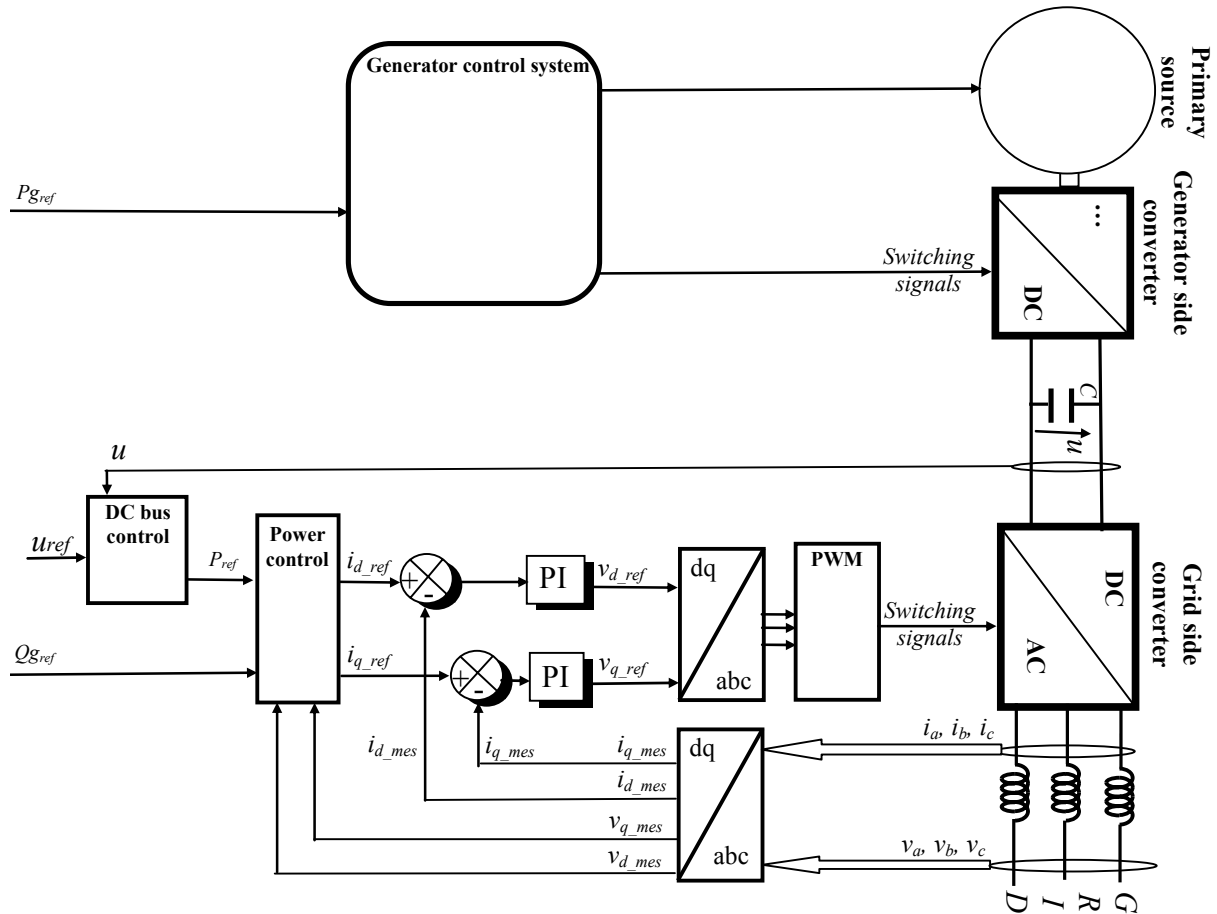


Figure III.13 Grid following strategy of a dispatchable generator in a PQ mode

### c. Power dispatching strategy for the “PQ mode”

With a power dispatching strategy, the voltage of the DC-link capacitor is maintained by controlling the generated power from the primary source (Figure III.13). The primary source is responsible for responding to this power demand in order to maintain a constant DC voltage bus. This is suitable for applications with controllable power generation such as hydro turbines, gas micro turbines and fuel cells as the availability of the primary energy is guaranteed. Then the voltage across the DC bus can be considered as constant and the grid-side converter can control the active and reactive power output [Tra 07]. These kinds of DG are dispatchable [Cal 03]. The “PQ inverter control” consists in an outer loop power that calculates current references for the current control inner loop (Figure III.14).

This control scheme is very similar to classical isochronous speed control of conventional DGs (Paragraph 4.2). If we consider that the role of the DC bus is equivalent to the inertia as the primary power is injected in order to regulate a constant DC voltage. In practice, performances are not similar because of the small value of the DC bus time response.

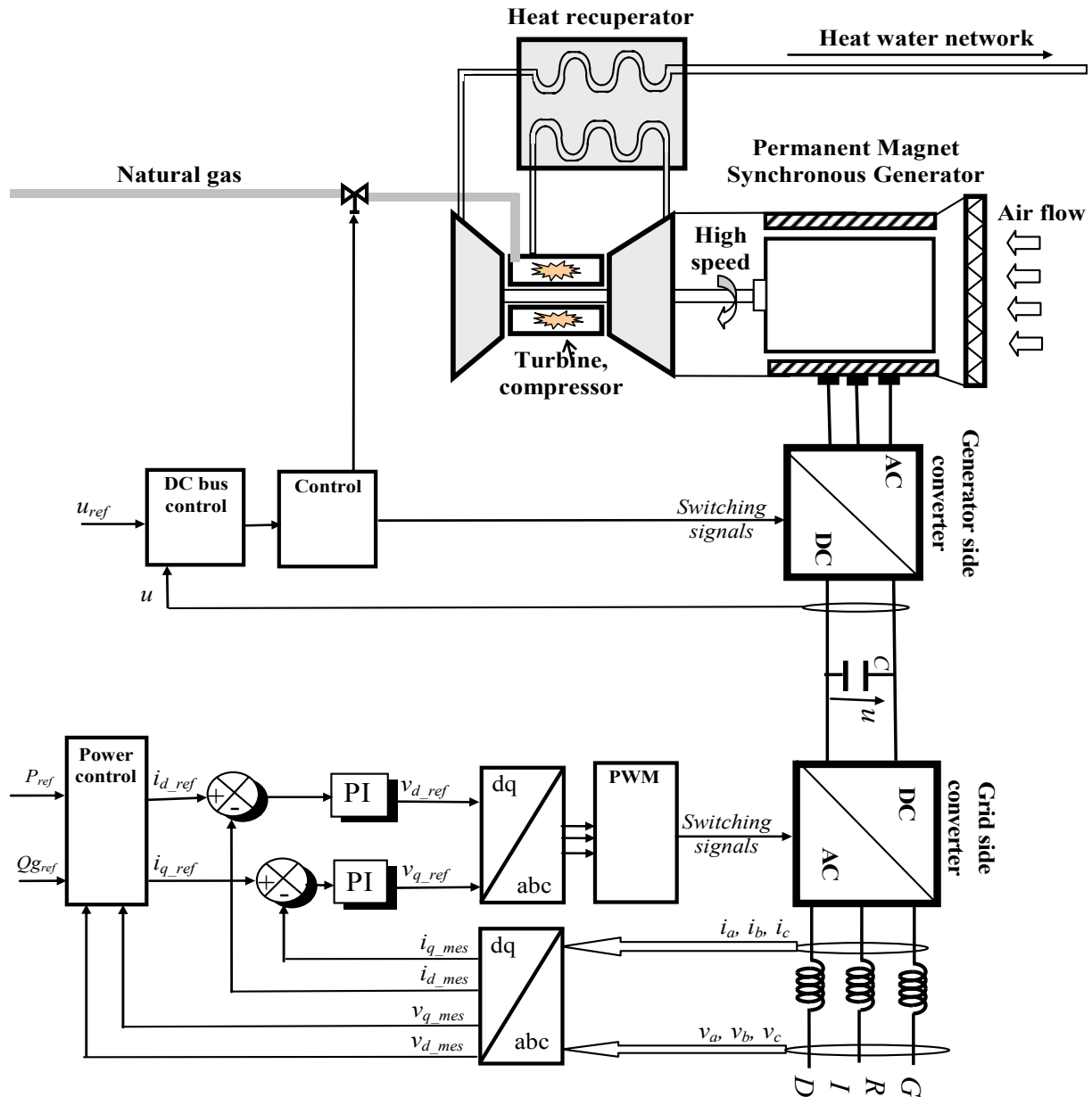


Figure III.14 Control strategy of a gas micro turbine with a PQ control system

### III.4.6. Control strategies for a “Vf mode” in an islanded mode of the microgrid

In an islanded mode one DG must “feed” the MG with predefined values for the voltage and the frequency (Paragraph III.2.4.b). In order to generate AC voltages, AC capacitors are required and so a LCL filter is used for the grid connection (Figure III.15).

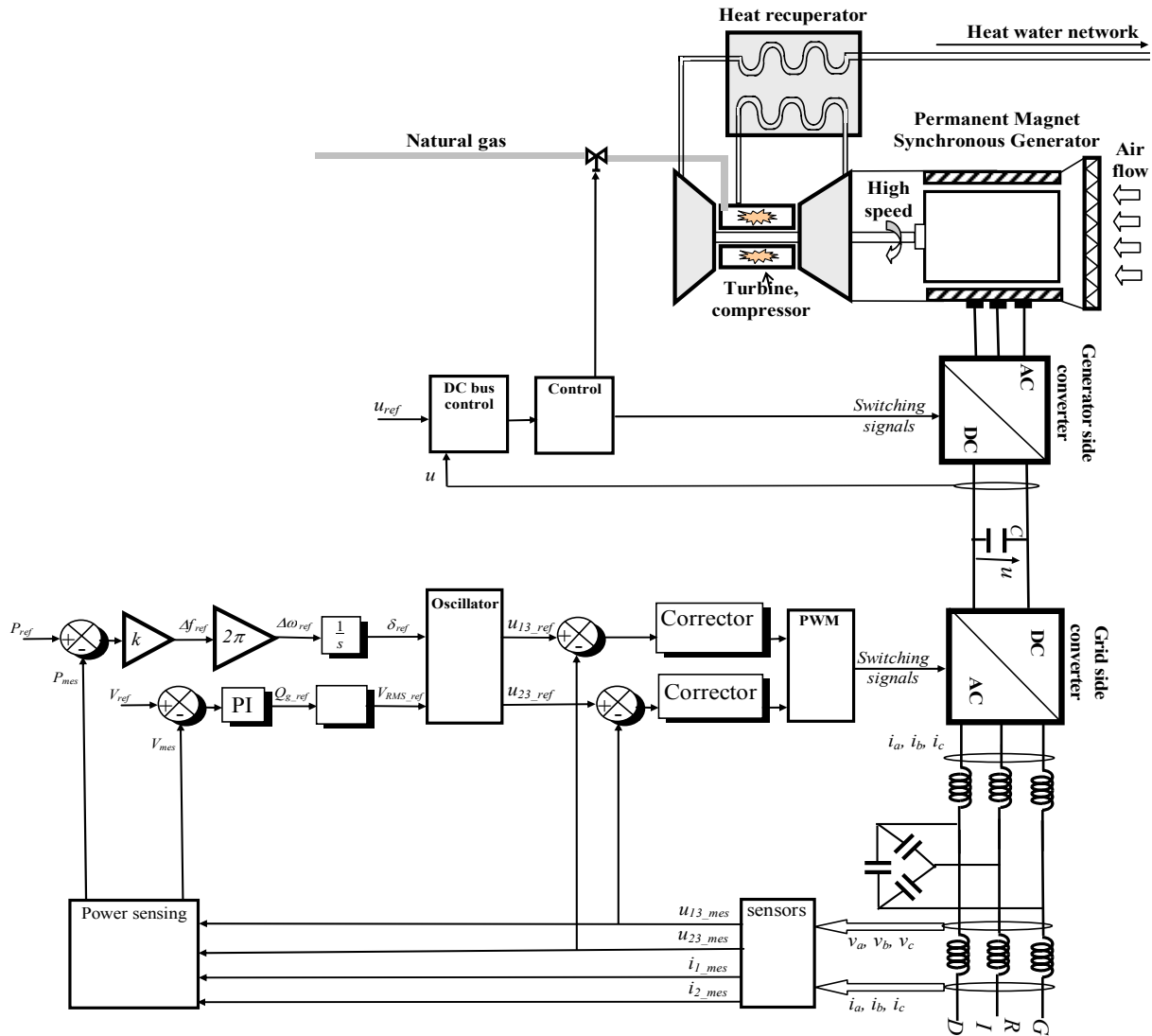


Figure III.15 Power dispatching strategy of a gas micro turbine for a VSI control system

With this power structure, the control strategy of the grid-side converter can control the voltage and the frequency at the PCC and thus can emulate the behavior of a synchronous machine [Las 03], [Awa 08], [Bar 07]. This control scheme is known as the “Voltage Source Inverter Control”. Phase to phase voltages are controlled by a closed loop control to be equal to following references:

$$\begin{cases} u_{13\_ref}(t) = V_{RMS\_ref} \sqrt{3} \sqrt{2} \sin\left(2\pi f \cdot t - \frac{\pi}{6} + \delta_{ref}\right) \\ u_{23\_ref}(t) = V_{RMS\_ref} \sqrt{3} \sqrt{2} \sin\left(2\pi f \cdot t - \frac{\pi}{2} + \delta_{ref}\right) \end{cases} \quad (\text{R.III-1})$$

Voltage references are generated by an oscillator, which is fed by the shift between the grid voltage and the modulated voltage ( $\delta_{ref}$ ) and the wished RMS value of line voltages ( $V_{RMS\_ref}$ ). In practice the inductance of the grid connected choke is low to minimize the voltage drop and so voltages across ac capacitors are nearly equal to grid voltages. Details about the calculation of the correctors can be found in [Dav 07].

By neglecting the filter losses (and so the equivalent resistor), the single-phase equivalent circuit of the grid connection is obtained (Figure III.16).

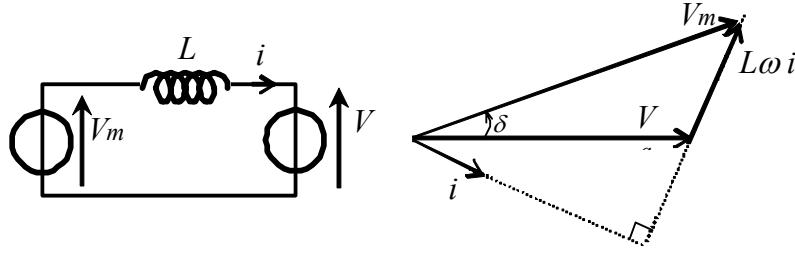


Figure III.16: Equivalent single-phase circuit of the grid connection and vector diagram.

In order to generate a current ( $i$ ) to the grid, the modulated voltage ( $V_m$ ) must be higher than the ac capacitor voltage ( $V$ ). Vectors  $V_m$  and  $V$  correspond respectively to the vector of the three modulated voltages and of the three grid voltages. The powers at the grid connection are expressed as follows [Bou 09]:

$$P_g = 3V \frac{V_m \sin \delta}{L\omega} \quad (\text{R.III-2})$$

$$Q_g = 3V \frac{(V_m \cos \delta - V)}{L\omega} \quad (\text{R.III-3})$$

With:

- $V$ : the line grid voltage RMS value,
- $V_m$ : the fundamental modulated voltage RMS value,
- $L\omega$  the reactance of the coupling reactor.

In practice the quantity  $3 \frac{V}{L\omega} V_m$  is large and so the quantity  $\sin \delta$  is very small. In this condition, we can assume:

$$\sin \delta = \delta, \quad \cos \delta = 1 \quad (\text{R.III-4})$$

Thus, the real power can be expressed as:

$$P_g = 3 \frac{V}{L\omega} V_m \cdot \delta \quad (\text{R.III-5})$$

The real power is classically controlled by a droop controller (paragraph III.5.a), which calculates the required frequency, the speed variation is calculated and the shift is obtained by an integration operator. Figure III.17 shows that the increase of the shift induces an increase of the generated power. Moreover the grid voltage ( $V$ ) must remain constant then the grid current ( $i$ ) must change and so the reactive power.

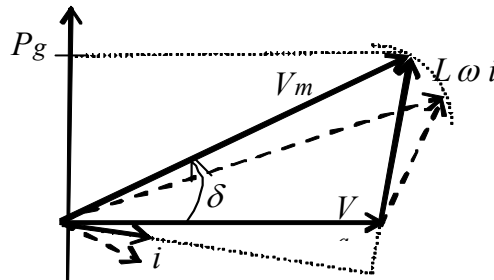


Figure III.17: Increase of the shift

The closed loop control of the grid voltage is used to calculate the required reactive power to be produced. The reactive power can be expressed as:

$$Q_g = 3 \frac{V}{L\omega} (V_m - V) \quad (\text{R.III-6})$$

The RMS value of the modulated voltage is obtained by inverting the equation.

$$V_{RMS\_ref} = \frac{1}{3} \frac{L\omega}{V} Q_{g\_ref} + V \quad (\text{R.III-7})$$

### III.4.7. Control capabilities of the PV based active generator

For dispatchable DGs the power reference is sent to the Local Controller of the generator. Inverter control is thus a very important main concern in MG operation since it will give or will not give new control flexibilities to the grid operator.

Classical PV generators are controlled with a grid following strategy since that their primary energy is volatile (Chapter 1, Section 5). The grid following control strategy has been applied for the studied PV based active generator in Chapter 2 (Section 2) for the normal operating mode. In a disconnected mode a “power dispatching strategy” must be used to control the DC bus voltage. Finally a “power dispatching strategy” for both operating modes has been developed to unify the local control system of the DG.

As the PV active generator has embedded batteries (energy storage units) the availability of enough energy can be guaranteed as long as the storage unit is not empty and can be used. In this condition a “power dispatching strategy” can be implemented for this DG and the availability of the embedded energy power must be known and managed by the MGCC. This organization will be detailed in the next chapter.

## III.5. Control system for microgrids

### III.5.1. Objectives and tasks

The energy control system should respect the following criteria, which govern the operation of an electric power system: Safety, quality, reliability, economy [Eih 00]. The safety is the first criterion and the most important criterion. The consideration of the safety covers the personnel, the environment, and the property in every aspect of system operations. Quality is defined in terms of variables, such as frequency and voltage that must conform to certain standards to accommodate the requirements for proper operation of all loads connected to the system. Reliability of supply does not mean a constant supply of power, but it means that any break in the supply of power is one that is agreed to and tolerated by both supplier and consumer of electric power. Making the generation cost and losses at a minimum motivates the economy criterion while mitigating the adverse impact of power system operation on the environment.

So, in order to the preceding criteria, the following tasks should be performed for an operating power system:

- The real power balancing between the generation and the load,
- the reactive power balancing for the voltage regulation,
- the optimum generation scheduling for limiting the cost and environment impact of the power generation,
- the security of the network against credible contingencies.

These tasks require protecting the network against reasonable failures of equipment or outage.

### **III.5.2. Communication system**

To automate the operation of an electric power system electric utilities rely on a high sophisticated integrated system for monitoring and control. Such a system has a multi-tier structure with many levels of elements. The bottom tier (level 0) is the high-reliability switchgear, which includes automatic equipment such as protective relays and automatic transformer tap-changers. Tier 1 consists of tele-control cabinets mounted locally to the switchgear, and provides facilities for actuator control, interlocking, and voltage and current measurement. At tier 2, is the data concentrators/master remote terminal unit, which typically includes a man/machine interface giving the operator access to data produced by the lower tier equipment. The top tier (level 3) is the supervisory control and data acquisition (SCADA) system. The SCADA system accepts tele-metered values and displays them in a meaningful way to operators, usually via a one-line mimic diagram. The other main component of a SCADA system is an alarm management subsystem that automatically monitors all the inputs and informs the operators of abnormal conditions.

### **III.5.3. Control functions and management tasks**

#### **a. Presentation**

Normally there are two types of control implemented in an electric utility. The EMS is for the operation of the generation-transmission system. And the distribution management is for the operation of the distribution system. The two systems are intended to help the dispatchers in better monitoring and control the power system. In this thesis, we focus on the EMS.

System dispatchers are required to make short-term and long-term decisions on operational and outage scheduling on a daily basis. Moreover, they have to be always alerted and prepared to deal with contingencies that may arise occasionally. We can classify these functions in the following manner: base functions, generation functions, network functions.

#### **b. Base functions**

The required base functions of the EMS include:

- the ability to acquire real time data from monitoring equipments throughout the power system,
- the processing of the raw data and the distribution of the processed data within the central control system.

So it consists of data acquisition, supervisory control, logical alarming, sequence of events function, historical database, automatic data collection, load shedding function, safety management and etc...

#### **c. Generation functions**

The main functions that are related to operational scheduling of the generating subsystem involve the following: load forecasting, unit commitment, economic dispatch and Automatic Generation Control (AGC), interchange transaction scheduling with the distribution grid.

#### **d. Network Functions**

Network applications can be subdivided into real-time applications and study functions. The real time functions are controlled by real time sequence control that allows for a particular function or functions to be executed periodically or by a defined event manually. The network study functions essentially duplicate the real time function and are used to study any number of "what if" situations. The functions that can be executed are:

- Topology processing (model update) function,



- State estimation function,
- Network parameter adaptation function,
- Dispatcher power flow,
- Network sensitivity function,
- Security analysis function,
- Security dispatch function,
- Voltage control function,
- Optimal power flow function.

### III.5.4. Time scale analyzing and implementation constraints

The microgrid supervision can be analyzed through various functions, which are classified in a timing scale (Figure III.18).

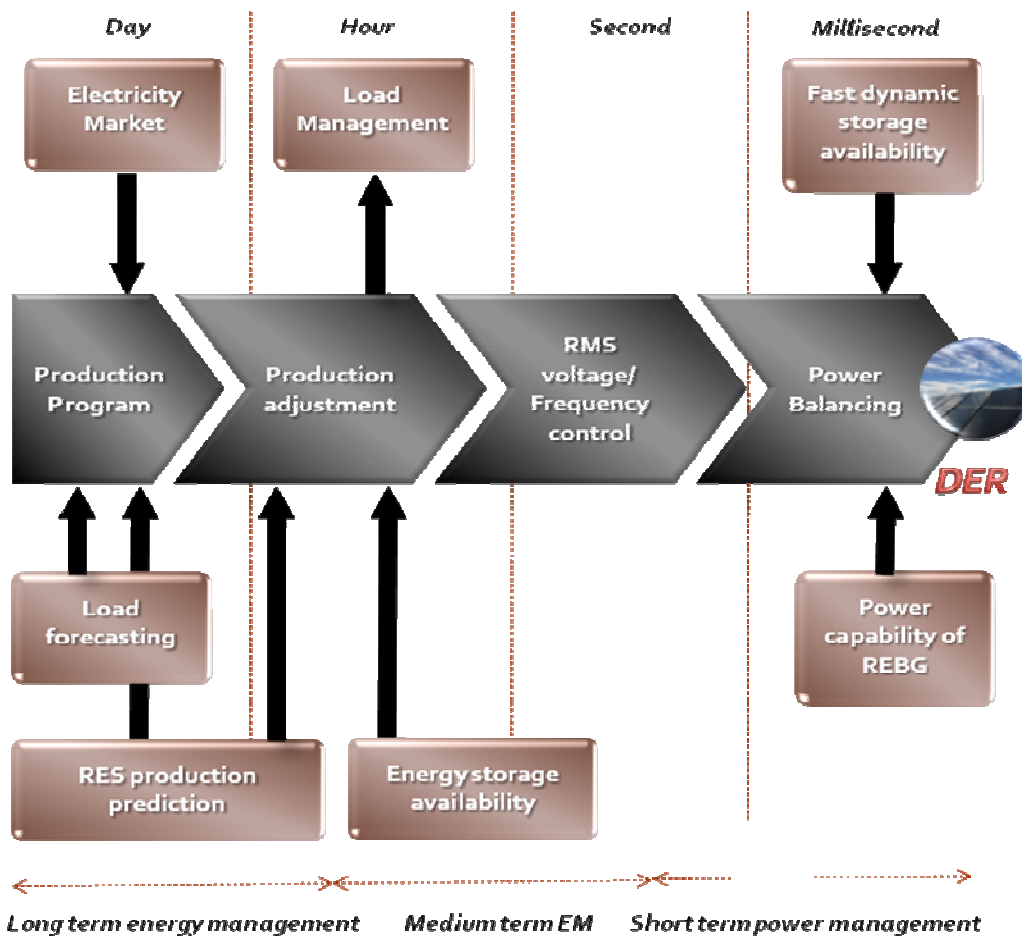


Figure III.18 Timing classification of control functions in the context of microgrid

The short-term power balancing corresponds to a primary control and includes:

- the real time “Balancing and power dispatching” among DG units and storage units according to the storage level capacity and to the specific requirements/limitations of each DG unit, including available power from Renewable Energy Based Generators (REBG),
- the RMS voltage regulation and primary frequency control.

The medium-term energy management includes:

- the adjustment of renewable energy source production and load prediction each half hour,
- the available storage energy estimation,
- the correction of power set-point of each source each half hour,
- the secondary regulation supply for the system ancillary services.

The long-term energy management corresponds to a secondary control and includes:

- the hourly “RES production forecast” including the time dependency of the prime source, environmental impacts and cost of generation,
- the management of non-sensitive loads that may be disconnected/shed according to the supervision requirement,
- the maintenance intervals,
- the provision of an appropriate level of power reserve capacity according to the electricity market and the load demand forecast.

In a classical vertical integrated electrical system, the long-term energy management is implemented by the Grid System Operator and the short term power balancing is implemented into generators.

For supplying these functions, DG’s must be coordinated either in a grid connected mode or an islanded mode of the microgrid. Two types of system managements exist [Kat 08] [Ped 08] [Li 09]:

- The short term power management by sensing electrical quantities is achieved by using the knowledge of physical quantities at the Point of Common Coupling (PCC) [Las 02] [Kat 06] and a droop characteristic control;
- The long term and medium-term energy management require a communication network to exchange information and control signals [Dim 05] [Bar 05] [Gaz 06] [Deg 06] [Dim 07].

The details of both control schemes are presented in the following paragraph. Discussions about the choice for our studied microgrid are carried out.

### III.5.5. Power management by sensing electrical quantities

#### a. Basic concept of droop controllers

In a power system all generators must respond in a coordinated manner to a variable load in real time: the global balance of power must be ensured at the same time as the main parameters (voltage, frequency) must be controlled. In Europe, existing electrical networks have been developed after the Second World War. At this time, communication infrastructures were limited. Coordination of all generators has been implemented through the measurement of two grid physical dynamic quantities: the frequency and the RMS value of the voltage [Las 02] [Kat 06]. With these data, a droop characteristic control performs the coordination of generators with a frequency/real power droop characteristic and voltage/reactive power droop characteristic in order to share the adjustment of the total demand for real and reactive power. This function is mainly provided by the speed governors and voltage regulators and ensures a stable operation of several DGs connected in parallel.

For example, when the frequency deviation exceeds a pre-defined threshold value, the characteristic modifies the power reference in order to increase or decrease the generated real power to restore the power balance. The primary frequency control contribution of a generator is based on a droop constant, which gives the additional power that is supplied as a function of the frequency deviation:

$$\Delta P_{g\_ref} = -k\Delta f = -k(f_0 - \hat{f}) \quad (\text{R.III-8})$$

$f_0$  is the frequency in the normal operation (50 Hz for the studied case),  $\hat{f}$  is the sensed value of the frequency. Hence the reference of the generated power will move from the value in normal conditions (point 1 in Figure III.19) to another value (point 2 in Figure III.19). After restoration of the power balance by the primary control, the system is stable (point 2 in Figure III.19) but at another frequency ( $f_1$ ).

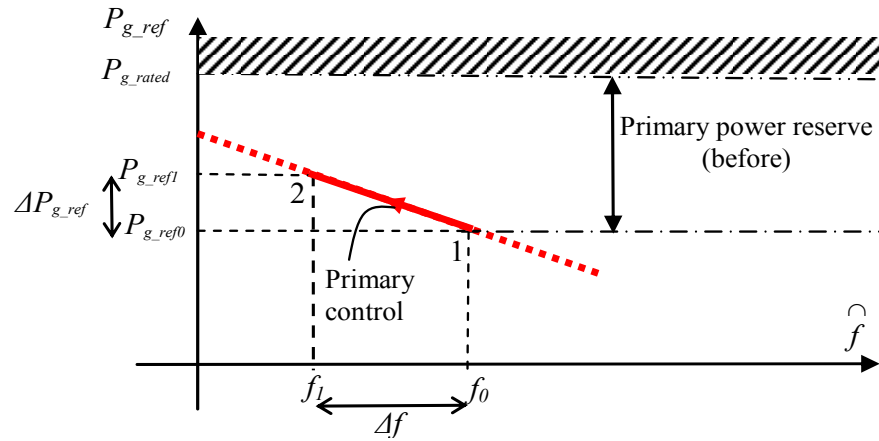


Figure III.19 Idealized static characteristic of the power/frequency control

The power/frequency constant is calculated as:

$$k = \frac{1}{s} \frac{P_{g\_rated}}{f_0} \quad (\text{R. III-9})$$

With the droop:  $s = 5\%$  and  $P_{g\_rated}$  is the maximum available power, which can be exported to the microgrid.

For the reliability and stability of a power network, a voltage/reactive power droop control is also necessary. With small errors in voltage set points, the circulating current can exceed the ratings of the DGs. This situation requires a voltage and reactive power droop control. The reactive power generated by the MS becomes more capacitive, the local voltage set point is reduced. Conversely, as reactive power becomes more inductive, the voltage is increased.

### b. Application to MG

Each grid connected inverter of DGs must have an external power loop based on a droop control, called also as autonomous or decentralized control, whose purpose is to share active and reactive power among DG units and to improve the system performance and stability, adjusting at the same time both the frequency and the magnitude of the output voltage.

As a real power reference is required, the only usable strategy is the « Power dispatching strategy » as shown on Figure III.20. Then the magnitude and frequency of the output voltage directly influence generated currents through droops. The “PQ mode” and the droop control are implemented in the Local Controller (LC) of the DG.

The main advantage of this method is its simple hardware implementations, since the development of central supervision devices is unnecessary. Moreover this local implementation enables a very fast response and then a good adequacy for frequency control and RMS voltage regulation.

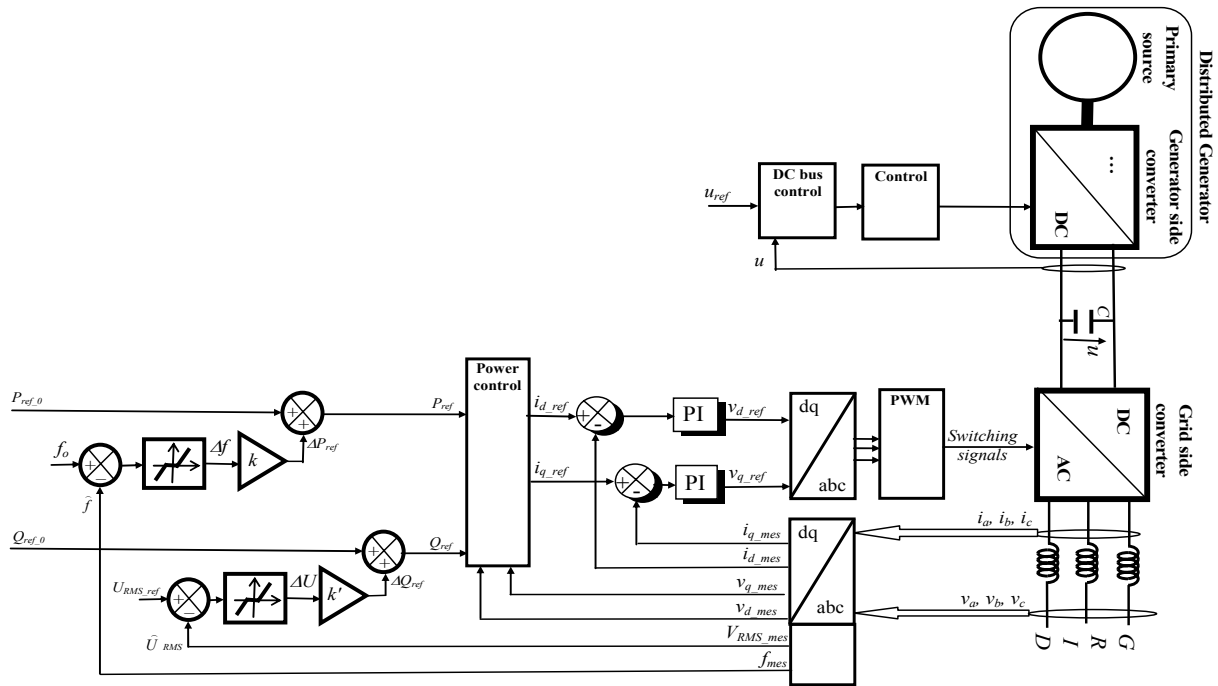


Figure III.20 Droop controllers for the « Power dispatching strategy »

This organization works in an autonomous way and sometimes is called “non interactive” (Figure III.21) since it is not coordinated with a higher control center. In this case power references  $P_{ref\_0}$  and  $Q_{ref\_0}$  in Figure III.21 are constant. The main disadvantage is the fact that an optimization function of the microgrid can not be designed with accuracy, since no sufficient information is known from operating points of other generators in the electrical system.

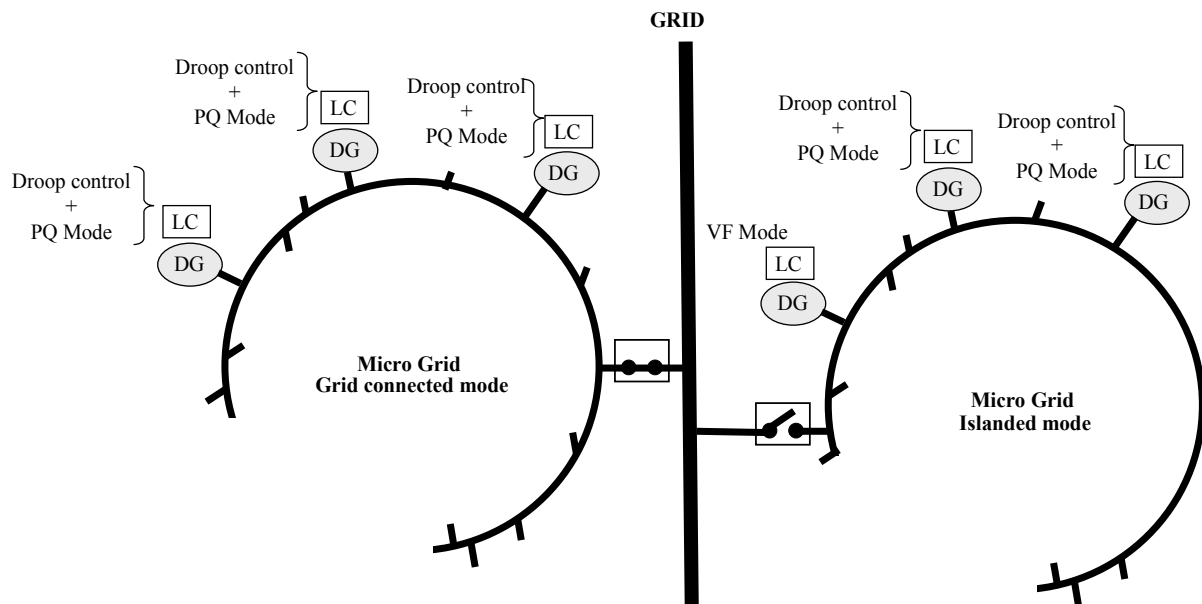


Figure III.21 Setting of DG control strategies in a “non interactive” organization

### III.5.6. Energy management by signal communication

#### a. Presentation

If a communication network can be used then power references (as example, references

$P_{ref\_0}$  and  $Q_{ref\_0}$  in Figure III.20) can be changed to implement an energy management of each DG in order to optimize the global operating of the microgrid. This “interactive“ control can be implemented with an enough low dynamic for the changes of power references in order to faithful the time delays of the communication network. So it is suitable for the long term energy management of DGs. Control by signal communication enables information exchange and includes three categories of controllers as described in [Kat 08]:

- Distribution Network Controller (DNC);
- Micro Grid Central Controller (MGCC);
- Local Controllers (LCs), which are associated with generators or loads.

This type of system organization implies either a centralized control achieved by a global supervision function [Deg 06], either a decentralized control, which uses the results of negotiations between agents of every LC functions (multi-agent systems) [Dim 05] [Dim 07].

The DNC is intended for an area in which more than one microgrid exists. It does not belong to the microgrid but is the delegate of the distribution network. The main interface between the DNC and the microgrid is the MGCC. The MGCC assumes different roles ranging from the maximization of the microgrid value to the coordination of LCs. In part III.4, several LC strategies in order to implement the received set points have been presented.

In a centralized operation, each LC receives set points from the corresponding MGCC. In this context the MGCC corresponds to a virtual utility or an aggregator at the decentralized step, as explained in paragraph II.2.1. In a decentralized operation, each LC makes decisions locally.

#### b. Centralized control: Micro Grid hierarchical control

The centralized approach suggests that a central processing unit collects all the measurement and decides next actions for a coordinated operation inside of the MG (Figure III.22). The goal is to coordinate and to schedule generators and controllable loads in order to maximize the revenues from energy market participations.

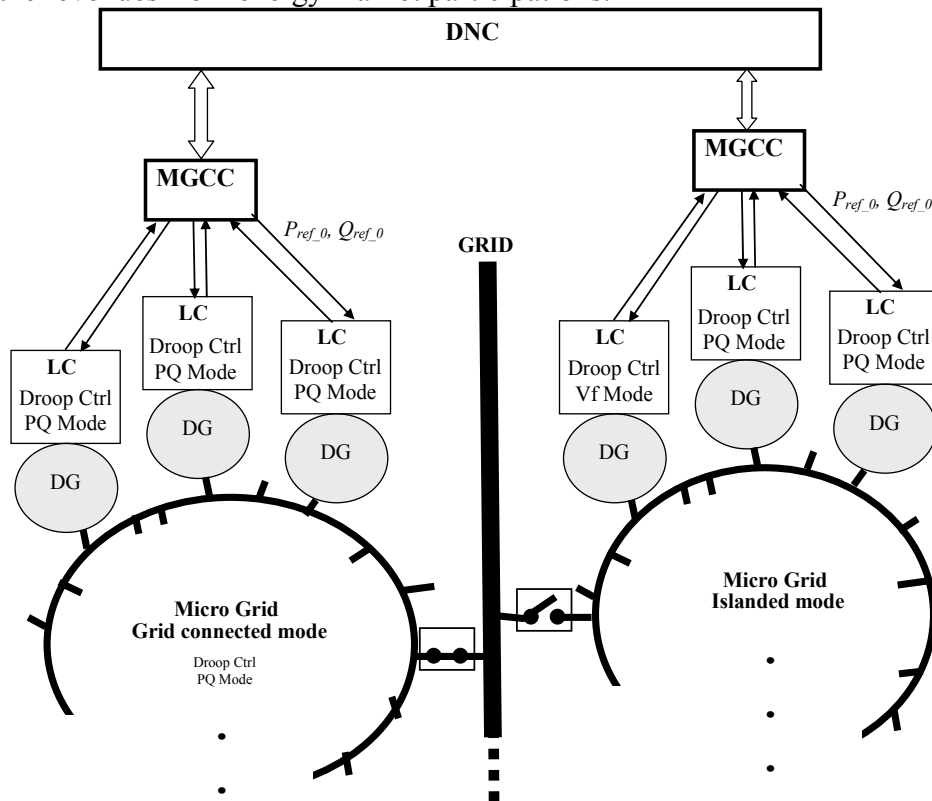


Figure III.22. Centralized control of a microgrid in an “interactive” organization

The MGCC is responsible for a real time provision of set points for micro sources and controllable loads. Here he is a virtual utility who manages a dedicated electrical network (here a microgrid) as explained at the decentralization step in paragraph III.2.1. The controller and communication infrastructure are constructed to allow optimal operation of the whole micro grid system. Real time information of the production and consumption in MG is collected at the central controller via a fast and reliable communication system. An advanced information and communication infrastructure is required, but an optimal operation economically and reliably can then be obtained. The central controller monitors the system frequency, real time production/consumption in the microgrid, and energy and ancillary service market information, calculates and communicates the appropriate set-points for each individual micro source and responsive load based on the available forecast of market prices and the availability of micro-sources and responsive loads. Nowadays most small scale generators do not have local frequency controller implemented. The communication system enables the exchange of the required data between the central controller and each source/load, playing a central role in such implementation.

With a centralized control method, the MGCC takes into account constraints in order to perform an optimization operating. The constraints can be:

- generators, dispatched DGs and loads operating points,
- market prices,
- network security constrains,
- demand and/or renewable production forecasts.

This optimization is achieved by receiving the information from LCs and by sending the control references to LCs.

The MGCC calculates the control reference and the necessary data for the optimization, such as:

- Power references for generators and dispatched DER units;
- Set points for the non-critical loads;
- Market prices for the next optimization period.

Therefore, the LCs can adjust their own operating points by using the reference signals send by the MGCC.

Based on management tasks (Chapter II.5.3), the MGCC is constructed by considering a formulation of constraints, an implantation of economic optimizations and an interface with LCs (Figure III.23)

The constraints depend on the weather forecasts, which have an impact on the daily load profiles and the energy potential of the intermittent renewable primary sources. The exploitation cost of microgrid generators is present in the constraints and also the environment impacts (by taking into account the generators using fossil energy, the efficiency of different generators...).

On the technical level, the ancillary services for the whole microgrid are quantified and dispatched to the different generators. Moreover, the function mode of every generator is also specified. From available information (the frequency, the AC bus voltage, the storage level, etc.), these algorithms make the necessary decisions for the generators, in order to provide a correct function of the microgrid.

The interface in the MGCC enables the real-time generation of the references for each generator according to a selected function mode. It shapes also the information of generators about their availability (set point, storage level, production potential, etc., an example is given

in the appendix 7 of the [Li 09]).

Figure III.23 illustrates the information exchange path in a central supervision and indicates that a two-way communication bus between the MGCC and each LC is required for control signals and information signals of the generator. The communication can be performed through electric cables, optic cable with photoelectric devices, telephone lines, power line carriers, or a wireless transmission, an intranet or the internet, etc. For our experimental work, an Ethernet communication system is used to communicate the signals between the central supervision and the LCs. The details will be given in the last chapter.

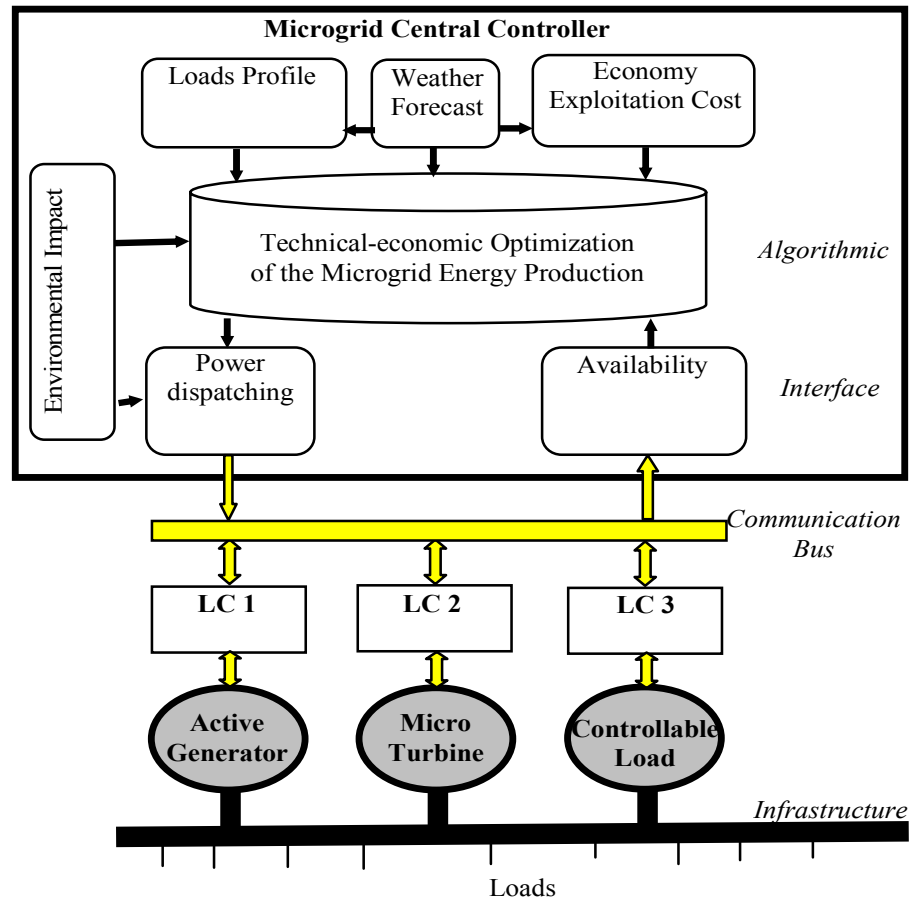


Figure III.23 Architecture of a MGCC

The economic considerations and the prevision are not in the scope of this PhD thesis. We will focus on the power dispatching, the energy management and the ancillary services supplies, which are the basic element to ensure the operation of our studied microgrid. Other considerations can be integrated by modifying our achieved fundamental functions.

The architecture of the MGCC for the grid connected mode with a distribution network will be detailed in chapter 4. The microgrid is then considered by the DNC as an independent electricity producer and a specific interface has to be developed in order to synthesis the necessary information for the MGCC (Figure III.23).

### c. Decentralized control: Multi-Agent System (MAS)

The decentralized approach suggests that advanced controllers are installed in each node forming a distributed control system.

This is the case for the primary control of the frequency and the voltage. The controllers are tuned with a predefined droop characteristic so that it can react to system frequency changes and voltage changes.

For implementing a full decentralized control concept, the intelligent Multi-Agent System (MAS) approach is a good solution [Dim 05]. The MAS approach can solve certain specific operational problems in the MG. Since the DERs have different owners and several decisions should be taken locally, an unique centralized control is difficult. Furthermore because of a liberalized market, the decisions of the controller of each unit concerning the market should have a function of intelligence. At last, for the local DERs besides deliver power to the grid, they have also other tasks: producing heat for local installations, keeping the voltage locally at a certain level or providing a backup system for local critical loads in case of a failure of the main system [Dim 04] [Hat 05]. These tasks suggest the importance of the distributed control and autonomous operation.

Dimeas and Hatziargyriou [Dim 05] have described four kinds of agents: production agent, consumption agent, power system agent and MGCC agent. The MGCC agent has only coordinating tasks and more specifically it announces the beginning and the end of a negotiation for a specific period and records final power exchanges between the agents in every period. In the market environment, three control levels are distinguished:

- Distribution Network Operator (DNO) and Market Operator (MO) at the level of the MV;
- MGCC;
- Local controllers (LC), which could be either micro source controllers or load controllers.

The main interface between the DNS/MO and the MG is the MGCC. The MGCC is the main responsible for the optimization of the MG operation, or alternatively, it simply coordinates the LC, which assumes the main responsibility for this optimization.

A main feature of the MAS is that the software within each agent can embed local intelligence. Each agent uses its intelligence to determine future actions and independently influences its environment [Reh 03] [Bar 05] [Dim 07] (Figure III.24).

An intelligent microgrid requires a fairly advanced communication system with capabilities similar to the human speech; for example, the Agent Communication Language (ACL) provides an environment for information and knowledge exchange. The need for a high-level communication environment can be shown by considering the communication needs of two agents within a microgrid. For example, at a given time one may have an instantaneous surplus of 1,500 W and the other may need 500 W. It is neither efficient nor required to provide the exact values, since the situation can change within a short time. The ACL provides the environment to exchange messages of the form “I have currently some watts and do not expect to use them in the next 30 minutes” or “I need a few extra watts in the next 30 minutes.”

The agents exchange not only simple values and on-off signals but also knowledge, commands, beliefs, and procedures to be followed through the ACL. For example, the agent that controls a load can participate in the local micro-grid market by sending a request message to all DER agents stating the amount of required energy. Furthermore, its object-oriented nature and data abstraction enables each agent to handle only the necessary or allowable information and knowledge.

Figure III.24 shows a decentralized microgrid control structure. The higher level (“Agent of DNC”) corresponds to a medium-voltage network (grid level) and its agent is responsible for communication between the microgrid and the DNC and the message exchange regarding the energy market. The medium level is the management level in which the agents of all MCCs coordinate:

- Controllers of DER/load units;
- Market participation;
- Possible collaborations with the adjacent microgrids.



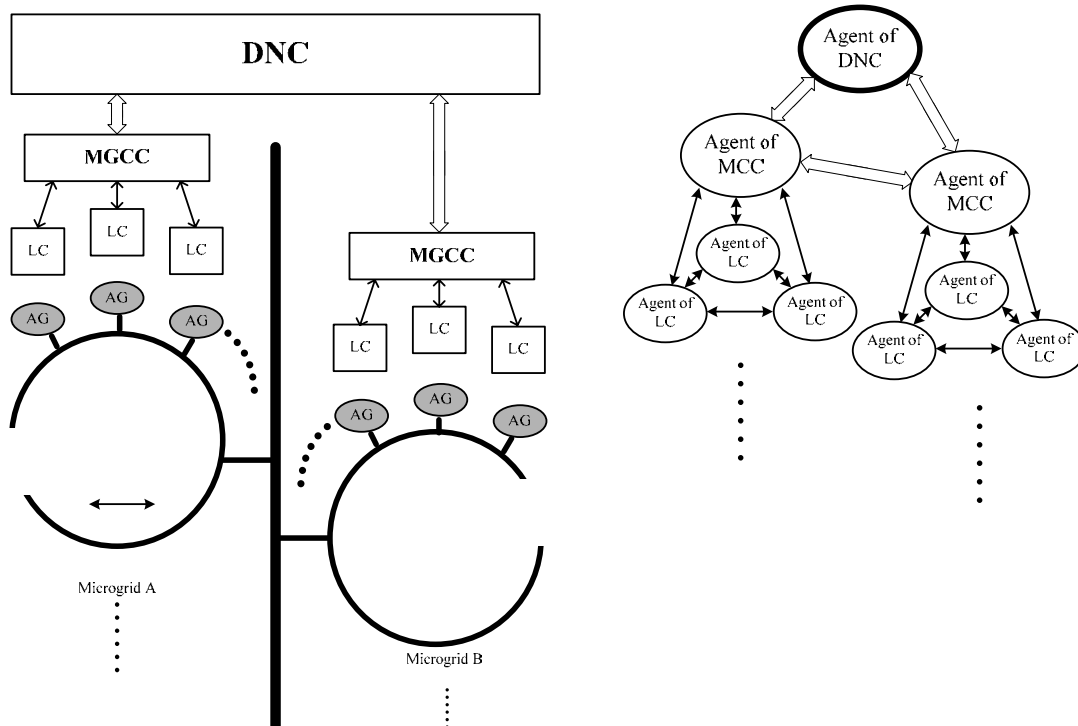


Figure III.24 MAS architecture for a decentralized control of a microgrid in an “interactive” organization

In Figure III.24, the left part shows multi microgrids connected to a distributed network and the topological structure of their controllers. In a micro grid, its MGCC is charged for the communication among all the controllers inside of this microgrid and also the external communication with the other MGCC and the DNC.

The right part of Figure III.24 shows the MAS architecture. In order to control all the DERs inside the microgrid and make the electrical system operate in an economic and environmental optimal mode, the discussions among the agent of each LC and the MGCC are implemented.

The bids and the offers result from negotiations among the local agents (“Agent of LC”). Operation of LCs requires an external part and an inner part. The external part provides interface with the microgrid and is identical for all LCs to exchange set points, bids and commands. The inner part is specific to each LC and responsible for translating orders and/or set points and applying them to the corresponding unit.

The main challenge of this method is to develop communication functions such that a new functionality requires minimum changes in the agent-based software. To add a new functionality, all that should be required is to train the agents to deal with a new type of message or a new object. The method is also used to coordinate a large amount of production systems whose task can not be easily clarified. However, in our studied microgrid, each of the three typical production systems has respectively specified task (a dispatchable generator for a long-term power management, a non-dispatchable generator for a MPPT power generation, and a storage system for a short-term power management). The method necessitates also the construction of a complicated communication interface. This is not the case of our application, in which only some simple communication interface devices are available.

Therefore, the centralized microgrid control is chosen for our study.

### III.6. Conclusion

In this chapter a cluster of DGs is proposed to form a micro grid in order to achieve technical and economic benefits. Through advanced control and communication, these integrated DGs should be more controllable, flexible for the grid operator and competitive for the economic market. Some research projects and practical demonstration with micro grids around the world are exposed.

Different control approaches for the grid connection can be implemented in a DG and are presented according to the operating mode of the microgrid. The islanded mode and the grid connected mode imply various control strategies for the DGs : the PQ mode (slave) mode and Vf (master). In a PQ mode, the generator controls the active and reactive power injected to the network. In a Vf mode, the generator controls voltage and frequency at its terminals. In a grid connected mode, all generators are in PQ mode and inject powers to the grid because the voltage and frequency of the electrical system are imposed by the main distribution network. In the islanded mode, one of the generators, the master, works in Vf mode by controlling both the voltage and frequency of the system and therefore absorbing the power imbalances that can occur, whereas others generators, slaves, working in PQ mode.

All generators in large electrical power systems are coordinated through droop characteristics without fast communication networks.

In a grid connected mode, the balancing between generators and loads and the control of main electrical parameters (voltage and frequency) are guaranteed by the main distribution network. Consequently, the generators can be operated to maximize the economic exploitation of the facility in terms of the sale of energy.

The organization of a micro grid control system is recalled as well as new requirements for welcoming DGs:

- The management of dispatchable real and reactive power,
- The voltage/frequency control and the utility controlled islanding.

In the next chapter, a centralized control system with a hierarchical structure for a Micro Grid will be proposed by using a communication bus for information exchanges between embedded Local Controllers in DG and a central Micro Grid Central Controller. The long-term energy management and short-term power management of the MGCC for the whole Micro Grid will be detailed.



# *Chapter IV*

## Planning and energy management system of a residential micro grid



## Contents

Chapter IV. Planning and energy management system of a residential micro grid ...	121
IV.1. Introduction.....	121
IV.2. Residential network application.....	123
IV.2.1. Integration of the active generator in a home.....	123
IV.2.2. Residential network and electrical system organization .....	124
IV.2.3. Application of microgrid concepts and global objective.....	126
IV.2.4. Microgrid energy management .....	128
IV.3. Forecasting techniques and processing of data.....	129
IV.3.1. PV power prediction .....	129
IV.3.2. Load forecasting.....	131
IV.3.3. Energy estimation.....	134
IV.4. Daily power planning / Setting of half-hour power references .....	136
IV.4.1. Objectives.....	136
IV.4.2. Constraints.....	136
IV.4.3. Determinist algorithm .....	137
IV.4.4. Practical application.....	139
IV.5. Medium-term energy management.....	141
IV.5.1. Reduction of the uncertainty (MGCC).....	141
IV.5.2. Energy management of batteries (LC).....	142
IV.6. Short-term power management.....	143
IV.6.1. Primary frequency regulation.....	143
IV.6.2. Power balancing strategies for the active generator.....	144
IV.7. Experimental tests through Hardware in the Loop simulations.....	147
IV.7.1. Description of the experimental platform .....	147
IV.7.2. Analysis of the self consumption of one house.....	150
IV.7.3. Increasing the penetration ratio in a residential network .....	154
IV.8. Conclusions.....	160



## **Chapter IV.Planning and energy management system of a residential micro grid**

### **IV.1.Introduction**

The building sector currently accounts for 18% of emissions of greenhouse gas emissions and 65% of the French electrical consumption [BEF 08]. Past oil crisis and more recently the risks of global warming caused by the massive release of greenhouse gas emissions, impose new obligations in energy saving and reduction of home electrical consumption. The evolution in the building industry tends to the construction of healthy buildings, intelligent, high environmental quality and with positive energy. The goal of positive energy buildings is to design long-term buildings that do not consume more than they produce, with a view to increase the energy autonomy of the individual home. Currently, the annual consumption in the residential sector is 250 kWh / year / m<sup>2</sup>, the objective for new homes are 80 kWh / year / m<sup>2</sup>. The research project at the European level sets as goals to reach 40 kWh / year / m<sup>2</sup> in 2025 and Positive Energy in 2050.

Another changing factor is the liberalization of the electricity market and the opening to new producers. Home sources (meeting the needs of the building sector) concerns only the modular small power generation (less than 1 kW to several tens of kW) and are connected to the grid at low voltage (LV). Most interesting technologies for the residential and tertiary sector concern PV generators and cogeneration. Photovoltaic systems have now a relative maturity even if new improvements of energy performances are awaited and that their current deployments will induce a significant reduction of costs. The increasing of PV generators connection and decentralized electricity producers into power grids is causing strong structural changes within the electrical energy supply. The number of new connections of PV facilities has increased dramatically in France since the new feed-in tariffs of PV based electricity in July 2006. In March 2010, a 422 MW amount of PV production was installed in the French distribution network that is 106% more than in December 2009 (200 MW) [ERD10]. In addition, the rated power of a single producer is generally less than 3kW and represents nearly 92% of the total PV producers connected to the low voltage distribution network. This increasing of decentralized PV producers generates locally many troubles in the grid. As explained in part III.2.1, their system-compliant integration into the supply process must be performed in order to enable their extensive expansion. As example, in a residential network with all homes equipped with PV panels, the total produced power may be higher than the consumed power and so induce overvoltage. In this case a part of the PV power has to be switched off by the grid operator. The PV power is no longer valued. Hence the arrival of 100% green energy production induces new requirements to manage technically and economically the network automation processes in an efficient manner.

Because of the intermittent and fluctuate power generation based on the renewable energy, these generators can not actually provide services to the electric network. As shown in chapter 2 integration of energy storage units in a renewable energy based power generation system makes these generators more active for the ancillary services supply.

Moreover, an international trend suggests feed-in tariffs will disappear with a price drop over a few years. A sale of the entire production would be less interesting in the future. It is already the case in Germany, with the new GET regulation tariff subsidizing self-



consumption of renewable energy systems for a rated power below 30 kW [EEG 09], [RIF 09]. A recommendation from European research groups [EUD 04] is the abandonment of fixed prices for electricity. Such abandonment would increase the interest among other smart control of the customer loads by using tariff changes in the day to optimize its own production and consumption. Dispersed generation brings benefits in particular the flexibility of production and consumption that can be adapted to price. As example, in chapter 2, a standardized interface of the active generator's local controller between the energy sources and the grid has been developed with the possibility to store locally a part of the PV electrical production or to generate more power as the one available from the renewable source if it is necessary.

This chapter describes a practical application concerning the energy management of active PV based generators for the buildings, as part of the ANR project SUPERENER: "Energy supervision of dispersed production plants for the provision of ancillary services in a microgrid". This project brought together different partners: Ecole Centrale de Lille, Arts et métiers ParisTech, Hautes Etudes d'Ingénieur. The application aims at establishing a smart electrical system for the management of energy in a residential district to better promote the use of PV energy produced locally. The project adopts a medium-term vision where purchase prices will be scaled back or disappears. To this end, the building has no incentive to inject all the energy produced. It will rather consume it locally or store it if there is a surplus to export it later or shed or defer controllable loads in case of peak demand. The PV active generator is linked directly to a central energy management system via an Internet-based communication network. This proposed smart grid organization is designed to facilitate the organization, operation, optimization and the clustering of DG's. Hence a main contribution of this chapter is to derivate microgrid concepts to implement an active participation of PV active generators via this system organization and control schemes previously presented in chapter 3.

So in section II, the integration of the presented active generator in a home is first presented. A cluster of producers-consumers is organized into a residential electrical network and are interfaced within an aggregator via a communication network. Then microgrid concepts are used to define control functions, to locate them and to organize the control of the residential microgrid system. Tasks of the microgrid energy management are recalled and the strategy is exposed.

In section III fundamental techniques for the PV power forecasting as well as for the load forecasting are presented. Then data are processed to estimate the different available and required energies.

The daily power planning for the different generators is detailed in section IV and a determinist algorithm is proposed to satisfy the different constraints.

Unavoidable forecasting deviations are taken into account each half of an hour by the medium-term energy management in section 5.

The control system of the active generator is modified in order to implement control functions for the short-term power management of the microgrid and the dispatching of the producer-consumer. Section VI describes the local controller in charge of the coordination of home energy resources whose function is to satisfy grid power references.

Finally, the implementation of the residential network on the L2EP experimental platform: "Distributed Energy" is presented and experimental results concerning the penetration ratio of PV production are given in the last section.

## IV.2. Residential network application

### IV.2.1. Integration of the active generator in a home

For several decades, utilities try to partially adjust loads to market constraints (economic) and network (technical) through a demand side management. A demand side management refers to a set of scenario whereby the consumer can reduce energy consumption during peak usage or other critical energy use periods. It is based on different payment/incentive schedules that can be classified into two families:

Demand response is based on price signals that are used to motivate customers to change its load profile. In this scheme customers manage voluntarily their loads by curtailing/shedding some electrical loads at peak times. The price is higher during peak hours for customers to move their loads during hours when electricity is cheaper. Demand response can be implemented by a dynamic pricing and then customers pay for the used electricity according to a specific pricing structure (hourly pricing, time of use, critical peak pricing, ...). Or, demand response can be also implemented by a (day-ahead) notification program and then customers are paid an incentive or pay a penalty based on a calculated load reduction.

Another option is the direct control of some loads. In this case customers offer the ability to switch ‘off’ and ‘on’ loads under certain circumstances.

In this context electrical vehicles and their batteries will play an important role in the future as a possible flexible load and a possible storage of the local PV electrical production.

Figure IV.1 shows a home application with PV panels and storage units and a demand side management capability via some controllable loads.

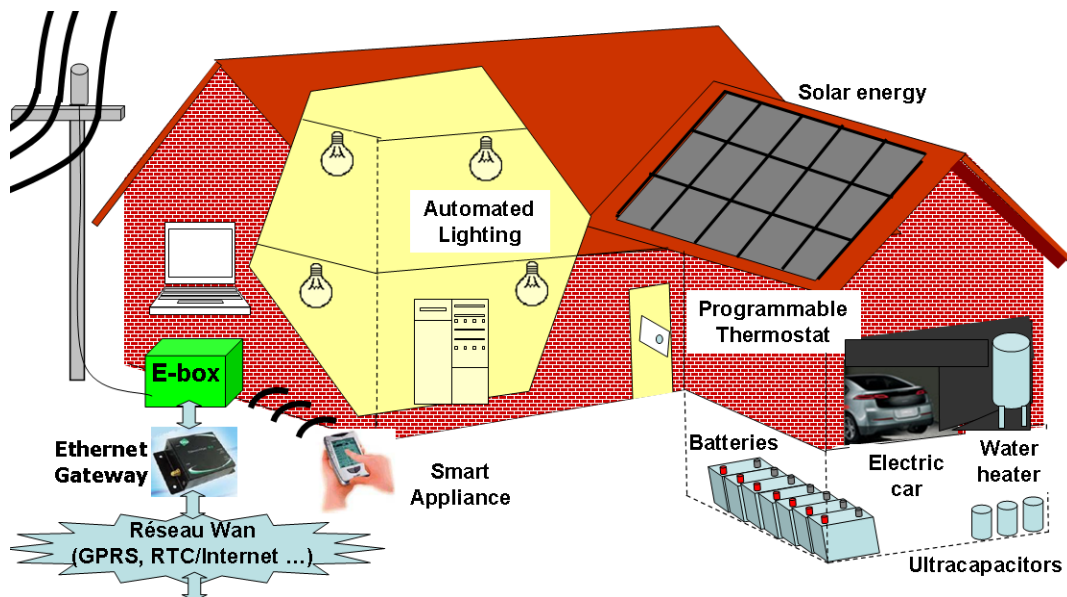


Figure IV.1 Prosumer with load demand response and electrical production capabilities.

During the day this home application may be a power producer or a consumer and is also known as a ‘prosumer’.

A few years ago, Energy-boxes (E-boxes) were developed in order to follow energy consumption. They have been upgraded to increase consumer satisfaction with various options for automatic control of some loads. This customer-enabled management provides opportunities for consumption adaptation to time pricing and new grid services for higher quality power supply (Yellow Strom’s meter, Linky meter ...). The concept of placing a smart driver at the grid coupling point allows the integration of all technical components

(processor card, relays, communication devices, sensors ...) required implementing strategies for energy management. This concept must be kept and upgraded to enable also the management of the storage and PV systems.

Here advanced E-boxes with on-board intelligence are considered. They receive signals from a grid operator and are able to reduce home demand or increase power production as in the NEDO project of Ohta City [Har 09],[Mar 07]. The home has a dedicated connection for the injection of energy to the distribution network (Figure IV.2). The E-box integrates at least three functions: a load manager, an advanced meter and a local energy management.

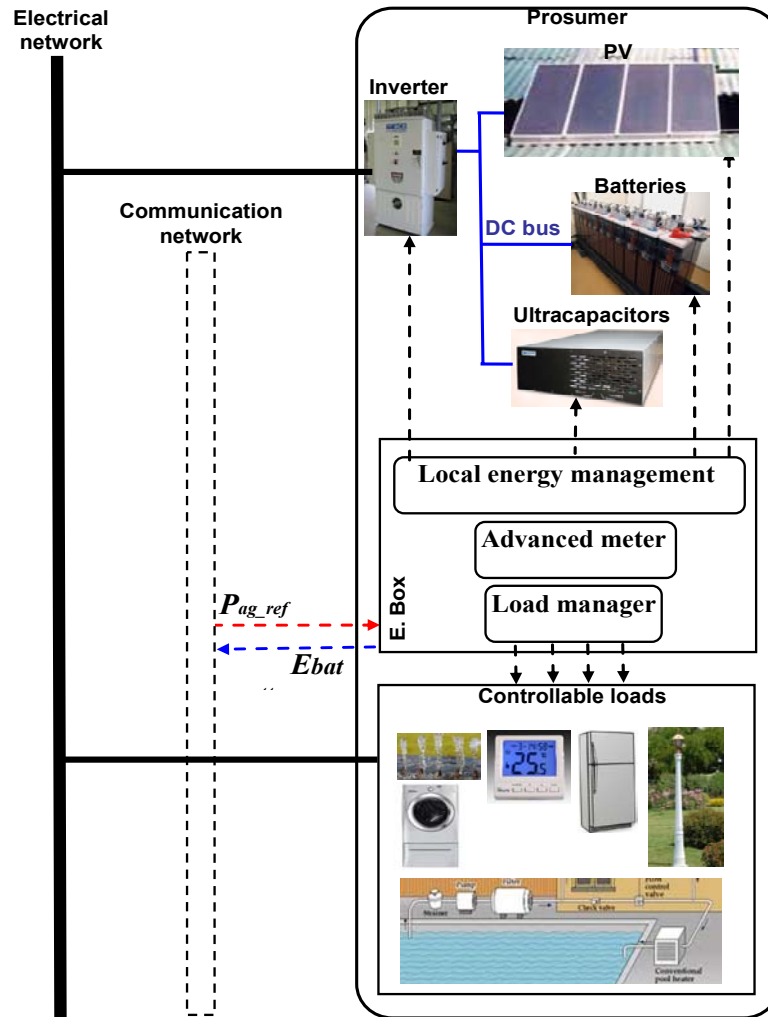


Figure IV.2 Advanced energy box

### IV.2.2. Residential network and electrical system organization

The load manager enables customers to automatically pre-program appliances to turn on when prices are lower or to create energy consumption habits, such as: uninterrupted supply of critical loads, time programmable use, etc. Moreover it can reduce a part of the home power demand when the grid is under stress by disconnecting offered controllable loads [Lu 09]. An advanced meter feeds the local energy management system as well as the load manager. Moreover the utility is able to ping the meter.

In this work a DC coupling of the PV system and storage systems is considered to form a home active PV generator (as presented in chapter 2). The interesting aspect of this hybrid generator is that it is able to deliver a prescribed power level ( $P_{ag\_ref}$ ) like a conventional

generator (for example, a gas micro turbine). The local energy management thus allows the use of PV energy according to the grid operator requirement also when the sun is not shining. In this case batteries are tapped to provide the required power. To highlight the difference with conventional PV panels, this concept is called an active generator. Excess PV energy is stored in batteries for use when needed and the local real time power control is performed with ultracapacitors. The local energy management corresponds to a Local Controller of a DG.

The E-box gives a remote control of facility to the grid operators. It enables faster adjustments to conditions and gives more flexibility to re-route power in a certain offered margin.

The idea is to install small PV panels on roofs of all houses in a residential area with the aim of:

- an energy optimization,
- an economic recovery through the sale of energy generated locally and the delivery of services to the system and
- the increase of the system reliability through the opportunity to work in islanded mode.

A residential network with several prosumers with PV active generators, several houses with controllable loads and a micro gas turbine is considered in order to optimize the electrical and environmental operating (Figure IV.3).

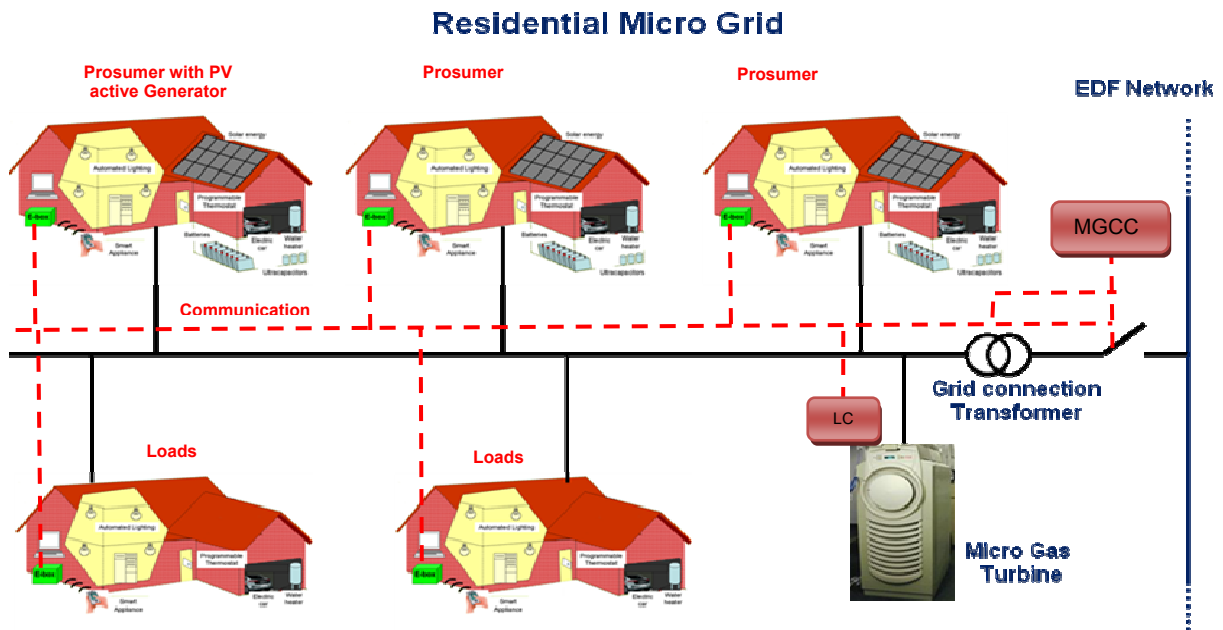


Figure IV.3 Residential network

This studied power system is in a certain small area, all power generators and electrical loads are locally connected. So line losses and voltage drops can be ignored.

All electrical power demands are based on the domestic loads of several residential homes. Loads are modeled by constant impedances. Loads are classified into critical loads and controllable loads in order to implement load shedding in islanded mode if necessary (as for the CERTS microgrid, Figure III.7). In this micro grid, the prime movers comprise the photovoltaic panels installed on the home' roofs and a gas turbine.

A considerable research activity is focused on the integration of large amounts of Distributed Energy Resources (DER) in the electrical system. The attention is now oriented toward the use of DER for improving grid operation by contributing to ancillary services,

increasing the energy reserve and reducing CO<sub>2</sub> emissions. In practice, new facilities are expected to reduce congestion, to minimize the production costs and to maintain the frequency and voltage.

These developments require a fundamental redesign of the grid control. Here an aggregated architecture of an urban power system is considered as a mean to facilitate the integration of distributed prosumers both in the electrical system and in the market. In this architecture, the aggregators are the key mediators between prosumers and consumers on one side and the markets and the other power system participants on the other side. The aggregators collect from the DSO (and the markets in future) the requests and signals for prosumers. They gather the “flexibilities” and the contributions provided by prosumers and consumers to form grid services and they offer these services to the different power system participants through various markets [PEE 09]. At the prosumers’ premises, electrical appliances, distributed generation can be controlled and optimized by the energy box, the interface with the external world. This business and market organization is an example of the “decentralization step” in the development of the future grid (Chapter 3, Paragraph II.2.1).

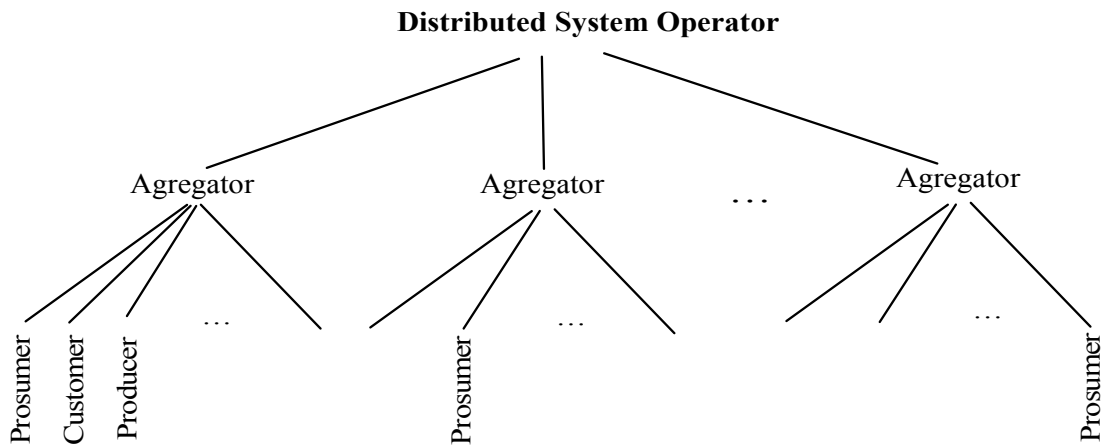


Figure IV.4 Example of a system organization for the decentralization step

### IV.2.3. Application of microgrid concepts and global objective

One way to apply the microgrid concept to the implementation of an aggregator is to coordinate home applications with conventional production units by a central Energy Management System (EMS) to form a microgrid (Figure IV.5). Here a centralized control of a microgrid in an ‘interactive’ organization (Figure. III.22) is derived for the organization of the energy management system. The global objective consists in matching the total power production to demand in an optimal way [Kro 08]. This concept is pertinent in the framework of smart grids through the combined use of an additional communication network within an intelligent energy management system and local controllers [Lu 08], [Zho 09]. This scheme is a step between current grid requirements and future needs.

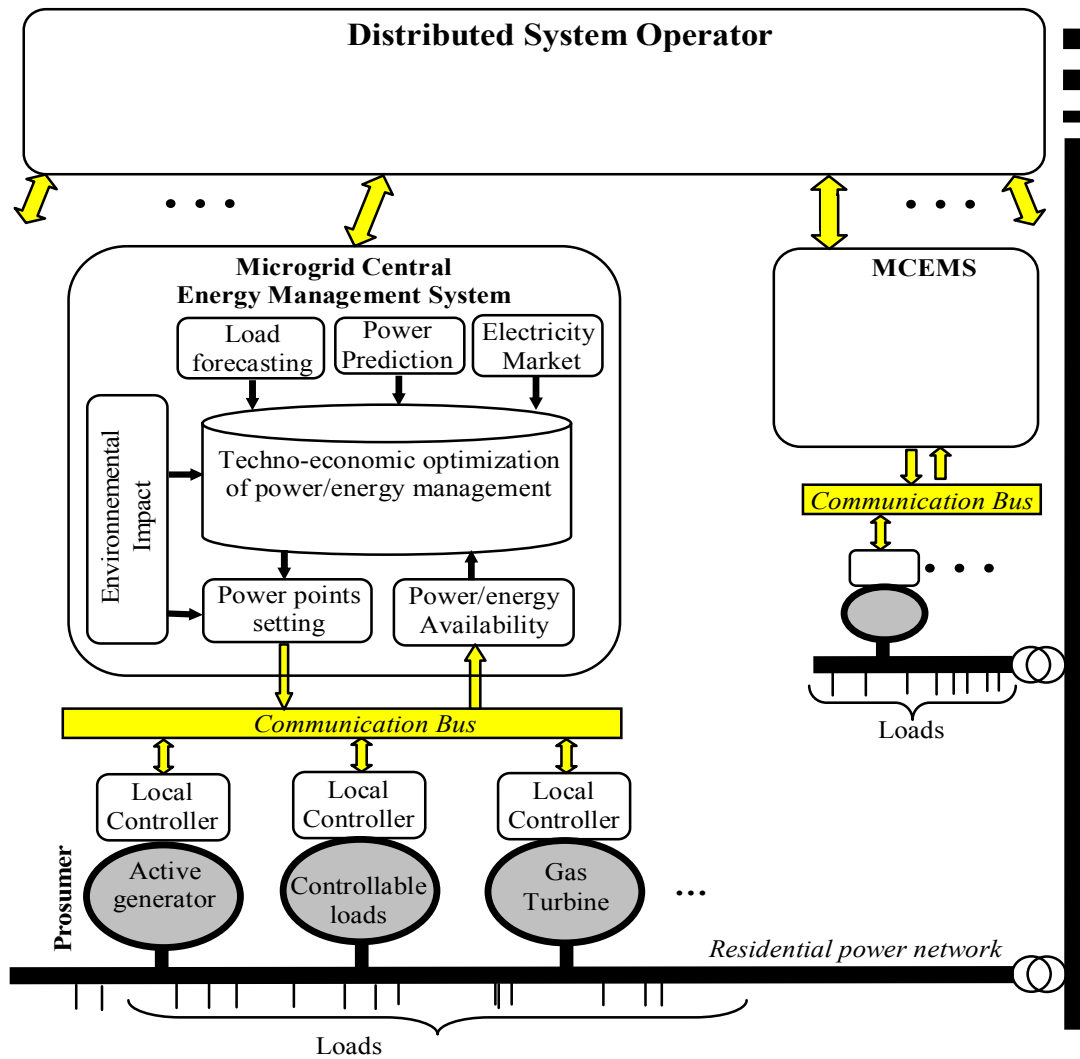


Figure IV.5 Framework of the central energy management system.

In this electrical system two types of generators are used: a gas microturbine and PV based active generators. All generators are grid connected with power electronic converters. Grid-inverter control is thus an important concern for the microgrid operation.

The residential microgrid can operate in two different modes: the islanded mode and the grid-connected mode. The control algorithms for these two operating modes are different. [Li 09].

In the islanded mode, all the power demand is satisfied by the local power generators (PV panels and micro gas turbine). The gas micro turbine is chosen as the single master generator in the microgrid system because it is the main source of energy. Hence it is controlled in a “V f mode” (Chapter 3, paragraph III.4.6). PV based active generators are controlled in a “PQ Mode” with droop controllers (Chapter 3, Paragraph III.4.5).

In a grid-connected mode, the residential network can provide or absorb the electrical power from the distribution grid and the voltage is imposed by the distribution grid. Then the micro turbine and the PV based active generators are controlled in a “PQ Mode” with droop controllers. A communication bus is used in order to share the grid control functions among all generators in an ‘interactive’ organization (Figure III.22). In this chapter, the grid-connected mode is detailed.

The microgrid central controller measures the microgrid state variables and dispatches

orders to micro sources through the communication bus. Local controllers (of the micro turbine and the PV based active generator) receive power set points from the micro grid central controller. In the same time they send various information, as example the sensed power production at the coupling point. Hence the MGCC has to manage the micro turbine and the PV active generator in order to control the microgrid.

The design of a centralized control strategy for this MG is presented in this chapter. The global objective is to use in priority PV based active generators to power the residential network as well as the gas micro turbine can be used as a backup generator. To facilitate the presentation of theoretical developments a single prosumer and a micro gas turbine are considered in this microgrid (Figure IV.6).

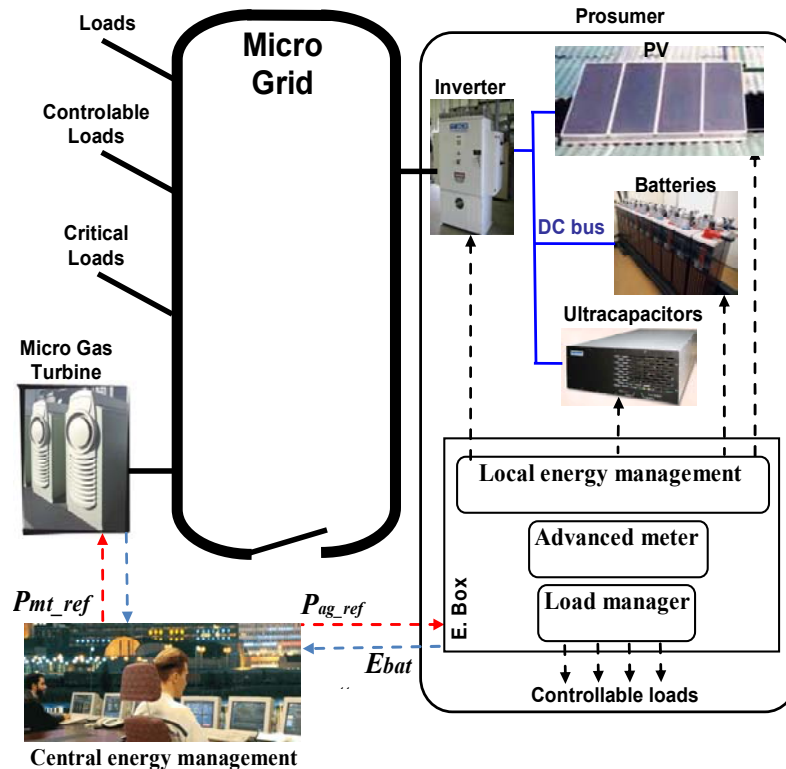


Figure IV.6 Microgrid integration of a prosumer and a micro gas turbine.

#### IV.2.4. Microgrid energy management

##### a. Tasks and organization

From a general point of view the task of the central EMS is to manage the power and the energy between sources and loads into the microgrid. The real and reactive power production must then be shared among the DG units (here a single prosumer) and the gas micro turbine. So the central energy management system must assign real and reactive power references and also other appropriate control signals to the DG units, conventional production units and controllable loads.

The microgrid management has been analyzed through three various grid management functions that are classified in a timing scale: the long-term energy management, the medium-term energy management and the short-term energy management (Chapter 3, Paragraph III.5.4). Each layer is characterized by its goals, its degrees of freedom, its response time and its time horizon.

According to the different management objectives, the proposed energy management

system is implemented in two locations: a central EMS of the whole micro grid for the long-term and medium-term energy management and a local energy management system in the E-box for the short-term power balancing (in real time).

A communication between these two management units is set up because the data acquisition and information about the states of each resource (such as the SoC and the real-time produced power ...) are very important for the central EMS of the microgrid. Control orders from the microgrid central energy management are also sent to the local controllers (Figure IV. 6).

### **b. Strategy**

In order to integrate active generators into the electrical system, the central energy management has to be upgraded. Control systems of electrical generators in a power system are characterized by adjustment criteria of the produced electrical power according to the request, depending on the economic value and under different constraints uncertainty. The design of a power planning should take into account many criteria for the operation, such as:

- The operating of generators; the reference provided to them should not cause a loss of performances or modify its characteristics, such as the reducing of the lifespan;
- The efficiency; references must use generators in their power range where the operating is optimal.

Finally, criteria to be considered are numerous and contradictory and therefore, the obtained planning is generally a compromise between performance and robustness.

The strategy adopted here is based on a prediction of loads and PV production. The load curve is not known a priori, it is predicted, the day-ahead from data sets of the past days, measurements and predictions of weather. The power planning must optimize the operation of the microgrid in terms of technical, economic or ecological on the basis of available information (network state, availability of generators, consumption forecasts, current rates, etc.) and determines the electrical production planning.

The medium term management monitors planned references and corrects each half of an hour deviations from the load predictions.

Several functions in the central EMS have to be modified or created as power prediction of the renewable energy, load forecasting, energy storage reserve, peak shaving, maximized use of renewable energy source, reduction of CO<sub>2</sub> emissions and new power planning. A deterministic approach is studied for the design of the microgrid energy management system, by having information on the load demand and PV production. So in the next section forecasting techniques are presented and the processing of data for the design of the long-term energy management is presented.

## **IV.3. Forecasting techniques and processing of data**

### **IV.3.1. PV power prediction**

In the studied case, the naturally poor predictability of the solar energy level is a weakness for the purpose of its use in an electric system. Photovoltaic panels provide electrical power only during the day with a power peak around the midday. Meanwhile huge production variations may occur.

As example, frequent huge fluctuations of the PV power production during 16h-18h can be shown on the recorded data at our laboratory (Figure IV.7). Moreover, one other disadvantage occurs during the winter, when the maximum power consumption peak in the grid meets with the moment of sunset. However, according to the historic data the obtained power prediction can be adapted more and more accurately to the real situation by means of



predictive models and studies.

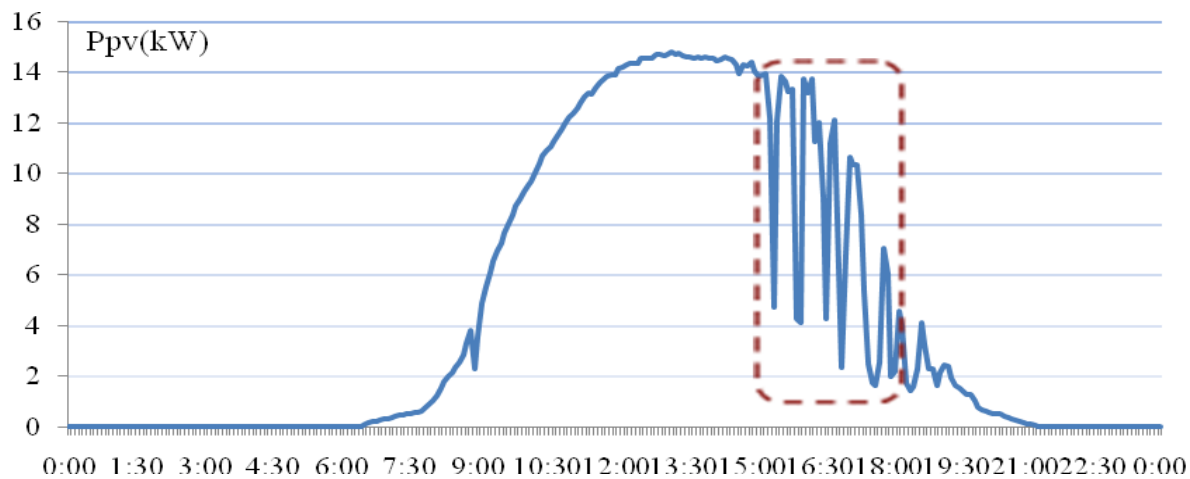


Figure IV.7 Recorded PV power production data at L2EP - Art et Métiers ParisTech (Lille, France) (11/05/2008)

The produced power output of PV panels as a function of time, can be written as the sum of two functions: on one hand, the “typical” curve that corresponds to an irradiation profile with a clear sky, and on the other hand, a “stochastic” curve that is a function of the cloud coverage [Cop 10].

The correlation is determined between weather predictions of the evening before and the measured PV power output. A least square method can be applied to calculate the best possible prediction of a local PV power production based on irradiation predictions of 4 meteorological stations. The success of the prediction is strongly dependent on the weather type. In 20% of the studied days in [Cop 10] the error between production and prediction was more than 100%.

The “typical” curves for two PV-systems at different locations correlate strongly, such that the total produced energy equals the sum of both systems. However, short-term fluctuations due to cloud coverage are not correlated for two different locations. In theory, two non-correlated signals are orthogonal and such the energy of the sum of two signals increases by a factor  $\sqrt{2}$  [Cop 10]. But in practice, the cloud influence is not easy to forecast.

In some applications, the sky photograph of a meteorological satellite is used for the cloud detection [Kle 08]. UC San Diego addresses forecasting of cloudiness through:

- a continuous collection of a 1 second global horizontal solar radiation data at 8 DEMROES stations located throughout the 1200 acre campus,
- a Total Sky Imager (YES TSI-440, Figure IV.8) that takes hemispherical sky photographs and compute cloud fraction every 30 seconds. Cloud motion vectors are determined through pattern matching analysis of subsequent images,
- a ceilometer to record cloud height and aerosol optical depth.

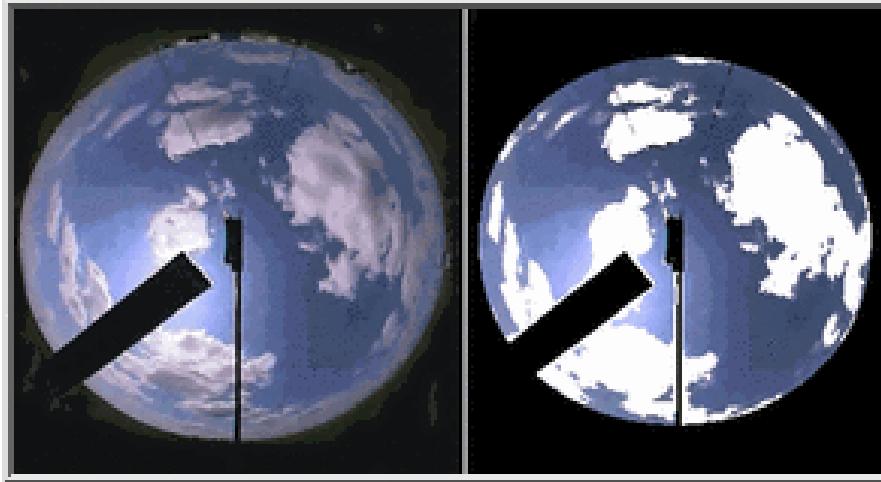


Figure IV.8 Hemispheric sky image showing raw sky image left and processed image with cloud identification (right). Yankee Environmental Systems

For our residential application, a one day ahead PV power forecasting and a real-time PV power forecasting are used.

The one day-ahead PV power forecasting is used for the 24-hours planning of the long-term energy management and is based on the one day-ahead weather forecasting and the historic data. The forecasting gives a 24 hours PV power prediction with a constant value for each half-hour (Figure IV.9).

The real-time PV power forecasting is used for the MPPT and for the real-time set point correction in the inner energy management of the short term energy management and for the real-time set point correction in the short term power management. The real-time PV power forecasting is based on the real-time weather condition detections (solar irradiation, panel temperature, cloud identification etc.).

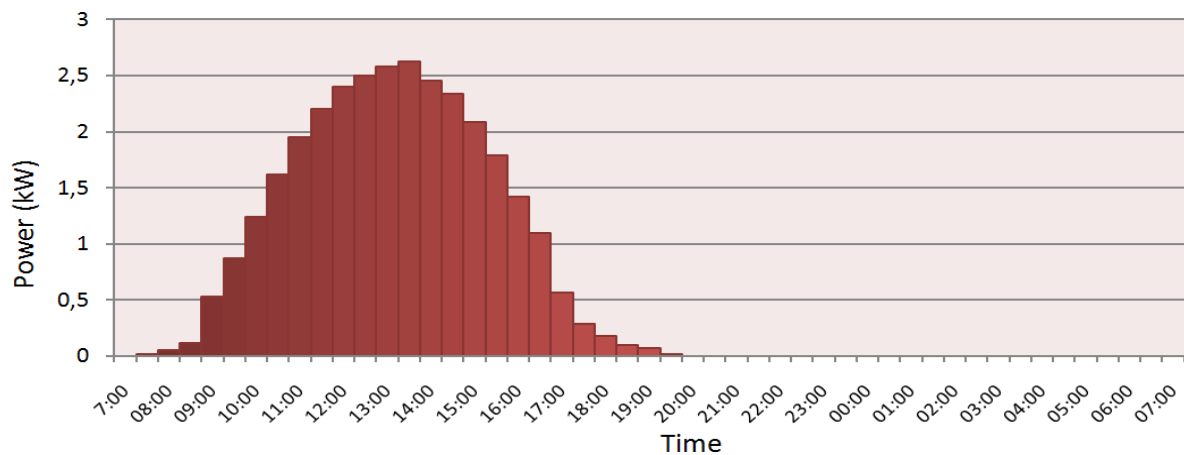


Figure IV.9 24 hours ahead PV power forecasting

### IV.3.2. Load forecasting

Load forecasting has many applications including energy purchasing and generation, load switching, contract evaluation, and infrastructure development. In this study, the load forecasting is used for the generation power planning and the energy management inside the micro grid.

Load forecasting can be performed during different time scales according to the needs [Fre 08]. A forecasting longer than a year is used for the sizing for power systems. The

purchasing, the generation of electricity and the energy management of a power system require a load forecasting from one hour to one week or a load forecasting from a week to a year.

The natures of these forecasts are different. For example, for a particular region, it is possible to predict the next day load with a 1-3% accuracy of approximately. However, it is impossible to predict 24h ahead the peak load with the similar accuracy since accurate long-term weather forecasts are not available.

Most forecasting methods use statistical techniques or artificial intelligence algorithms such as regression, neural networks, fuzzy logic, and expert system. Two methods, so-called end-use and econometric approach are broadly used for medium- and long-term forecasting. A variety of methods, which include the so-called similar day approach, various regression models, time series, neural network, statistical learning algorithms, fuzzy logic, and expert systems, have been developed for short-term forecasting [Mcm 98][ Mis 08].

As shown, a large variety of mathematical methods and ideas have been used for load forecasting. The development and improvements of appropriate mathematical tools will lead to the development of more accurate load forecasting techniques. The accuracy of load forecasting depends also on the accuracy of forecasted weather scenario.

### **Important factors for load forecasting**

For short-term load forecasting several factors should be considered, such as time factors, weather conditions, and customers' power demand behaviors.

The time factors include the season in the year, the day in the week, and the hour in the day. There are important differences in load between weekdays and weekends. The load in different weekdays can also behave differently. For example, Mondays and Fridays being adjacent to weekends, may have structurally different loads than Tuesday through Thursday. This is particularly true during the summer time. Holidays are more difficult to forecast than non-holidays because of their relative infrequent occurrence. [Fre 08]

Weather conditions are an important impact factor for the load. Forecasted weather parameters must be used for the short-term load forecasts. Various weather variables could be considered for load forecasting. Temperature and humidity are the most commonly used load predictors. An electric load prediction survey published in [Cho 96] indicated that in the studied 22 research reports, 13 use only the temperature, 3 use the temperature and humidity, 3 use additional weather parameters and 3 use only load parameters. Among the weather variables listed above, two composite weather variable functions, the THI (Temperature-Humidity Index) and WCI (Wind Chill Index), are broadly used by utility companies. THI is a measure of summer heat discomfort and similarly WCI is cold stress in winter.

Most electric utilities serve different types of customers such as residential, commercial, and industrial. The electric usage pattern is different for customers that belong to different classes but is somewhat alike for customers within each class. Therefore, most utilities distinguish load behavior on a class-by-class basis.

The following figures show the load forecasting curves and the real power consumption in France for several days [ERD 10].

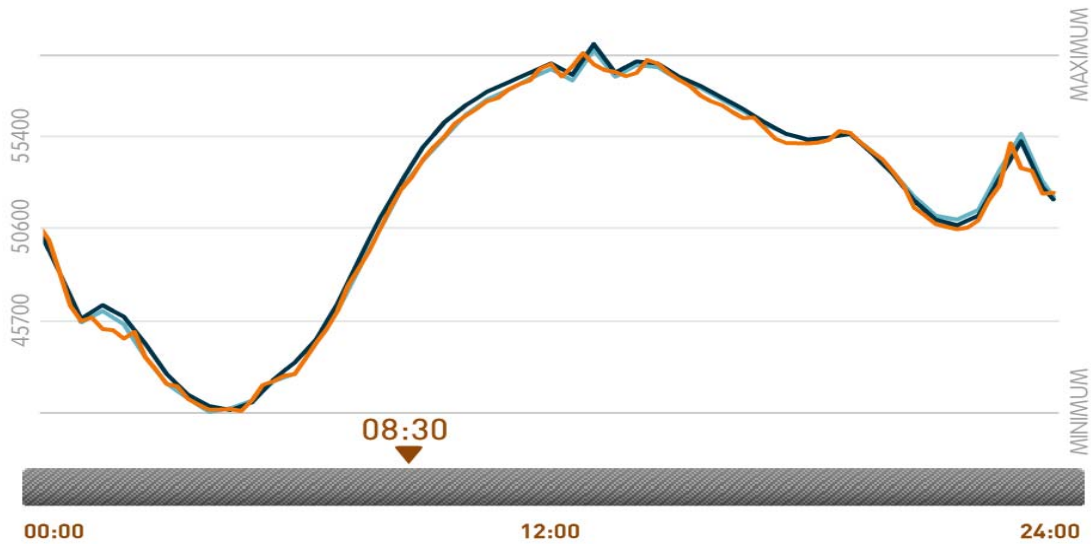


Figure IV.10 Load forecasting (orange curve) and real power consumption (blue curve) in France for July 20<sup>TH</sup> - 21<sup>TH</sup>, 2010 (MW)

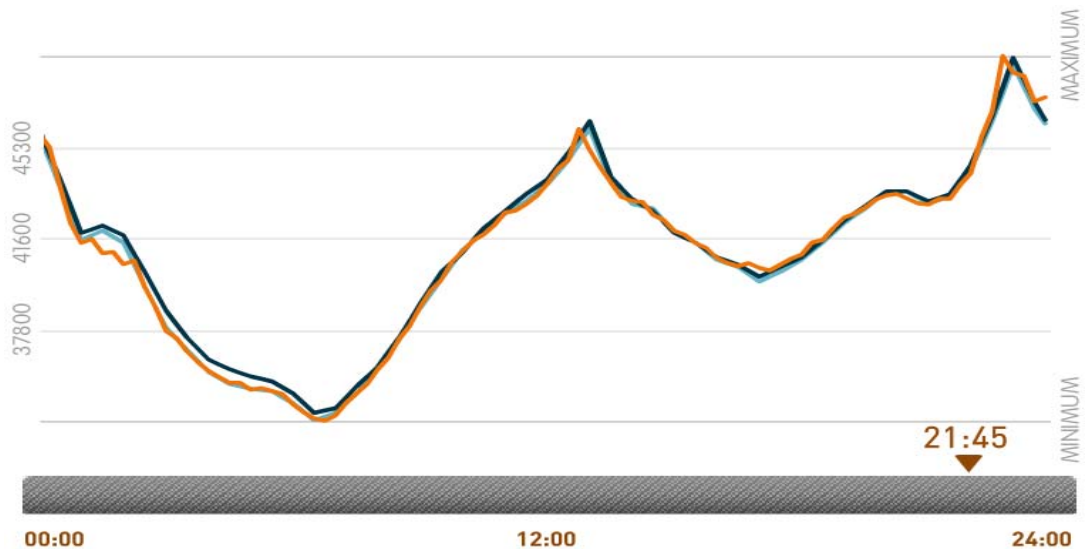


Figure IV.11 Load forecasting (orange curve) and real power consumption (blue curve) in France for July 18<sup>TH</sup> - 21<sup>TH</sup>, 2010 (MW)

From the above two figures, the load forecasting results are very close to the real power consumption. But the forms of these two curves are different. The first one (Tuesday 20 July, 2010) is a working day and the industrial loads and shops are a great part of the total power consumption. The second curve (Sunday 18 July, 2010) shows the situation without industrial loads. The first power peak is shifted to 13h00. For both days a peak appears at 23h00 in reason of electric water heaters.

During one year, differences are attributable to heating, which explains the difference in power peak levels between winter and other times in the year, and additional lighting consumption. In winter, the dark causes a peak around 19h later in the summer and mid-season. Similarly, the lighting need in the morning in the winter locates the maximum consumption at 9h00, while it tends to shift to 12h00 when the sun rises earlier.

For our residential studied case, the load forecasting is different from the RTE load curve because the industrial loads do not exist. A perfect knowledge of the residential consumption of the next day is unrealistic. Anyway a set of information can be used to estimate load profiles and can be used to determine decisions. Based on historic electrical

power production requirements for these residential homes in this region, the behavior of the loads in this micro grid can be forecasted and estimated. Several important factors influence the load in the electrical network: weather situation (temperature, cloudiness...), economic activity (huge modifications of load forecasting in the holidays), the legal working time and etc. The method of load forecasting is based on the meteorological data and the historical consumption data. About the availability of meteorological data, a similar service is already offered by Météo France, called "recepteurs météorologiques" with forecasts cut by quarter of a day, communicating with the METEO FRANCE centers through radio [MET 10].

A 24-hour-ahead load forecasting profile ( $\tilde{P}_{Load\_24h}$ ) is given in Figure IV.12 with data each half hour. For the study, the pattern of the studied home power consumption in a day has been characterized by five timing domains:

- the morning peak (Figure IV.12, Zone A) related to the resumption of activities in homes, rail transport, industry and tertiary sector,
- the lunch peak (Figure IV.12, Zone B), the sag in the afternoon (Figure IV.12, Zone C),
- the evening peak (Figure IV.12, Zone D) due to end activities of the day in the office, the recovery of the residential consumption and the activity transportation peak and
- the night sag (Figure IV.12, Zone E).

At that time, consumption is restricted to continuous industrial processes, public lighting, electronic stand by devices and the winter heating.

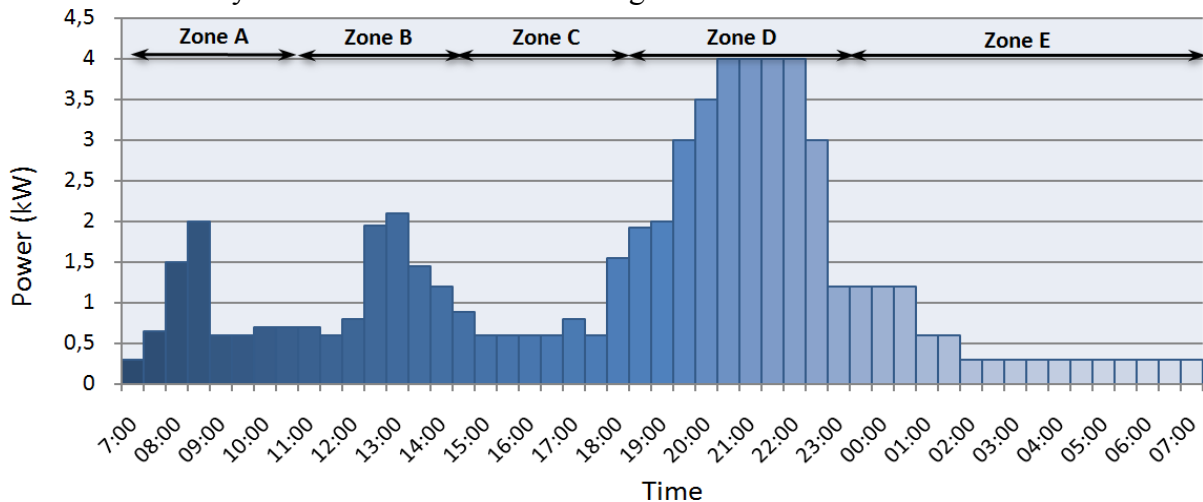


Figure IV.12 24-hour-ahead load forecasting ( $\tilde{P}_{Load\_24h}$ )

### IV.3.3. Energy estimation

#### a. Context

In order to plan the power generation and implement the energy management algorithms, an energy analysis is necessary. The maximum available energy generated by the PV panels during the daytime, the consumed electric energy during the daytime and the stored energy in the batteries are all estimated values and are used to decide how much complementary energy generated by the back-up generator (Micro Gas Turbine) is needed. Therefore, the energy estimation from the forecasting data (PV power prediction and load forecasting) is essential.

For the energy estimation the initial time point is the starting of the day ( $t_0$ ) and the day duration is named ( $\Delta t$ ) (Figure IV.13).

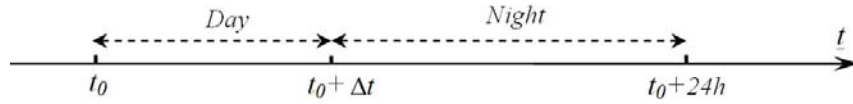


Figure IV.13 Time axis for the PV power application

The timing of sunrise is usually chosen as the initial time point ( $t_0$ ). However for cloudy days or raining days, the initial time point may be changed, because the solar irradiation and the temperature influence the PV power production. The duration of the sunshine is also always changed. Both parameters depend on the season and the weather conditions. So in the morning, when, the initial time of a day ( $t_0$ ) is set as soon as the PV panels start to generate the power for the first time. And the time  $t_0 + \Delta t$  is fixed at the start of sunset.

### b. Estimation of the available PV power

The long-term PV power prediction is based on a half hour forecasting (Fig. IV.9). The scheduled energy of the PV production during each 1/2h interval can be calculated with data from the PV power prediction as:

$$\tilde{E}_{PV\_1/2h} = \int_{t_0+nTe}^{t_0+(n+1)Te} \tilde{P}_{PV\_24h}(t) dt = Te \cdot \tilde{P}_{PV\_24h}(t_0 + nTe) \quad (\text{R. IV-1})$$

for  $t_0 + nTe \leq t \leq t_0 + (n+1)Te$  with  $Te=30\text{min}$  and  $n \in \{0,1,\dots,47\}$ .

The total PV energy for one day is the sum of all the previous calculated half hour PV energies:

$$\tilde{E}_{PV} = \sum_{n=0}^{n=23} \tilde{E}_{PV\_1/2h}(t_0 + nTe) \quad (\text{R. IV-2})$$

### c. Estimation of the required load energy

In order to plan the production program, the energy, which is demanded by the load is also estimated during the same interval:

$$\tilde{E}_{Load\_1/2h} = \int_{t_0+nTe}^{t_0+(n+1)Te} \tilde{P}_{Load\_24h}(t) dt = Te \cdot \tilde{P}_{Load\_24h}(t_0 + nTe) \quad (\text{R. IV-3})$$

### d. Estimation of the required stored energy

The energy demanded by the load during the daytime is also necessary to estimate the energy difference between the PV power and the demanded power. If the PV power is not enough, the micro gas turbine has to generate more power to assure the power supply in the micro grid. If the PV power is more than the load during the daytime, the surplus PV power can be stored in the energy storage units (batteries). The energy difference ( $\tilde{E}_{diff\_1/2h}$ ) for each half hour can be estimated from the PV power prediction and the load forecasting:

$$\tilde{E}_{diff\_1/2h}(t) = \tilde{E}_{PV\_1/2h}(t) - \tilde{E}_{Load\_1/2h}(t) \quad (\text{R. IV-4})$$

Thanks to the energy storage devices, this energy difference ( $\tilde{E}_{diff\_1/2h}$ ) can be absorbed or compensated. The size of the storage device determines the capacity of the power absorption and the power compensation. Because of the rated power limit, the exchanged energy with the batteries during the half hour is limited. If we consider a constant rated

value ( $P_{bat\_max}$ ), we get:

$$\tilde{E}_{bat\_1/2h\_max} = \int_0^{T_e} P_{bat\_max} dt = P_{bat\_max} \cdot T_e \quad (\text{R. IV-5})$$

## IV.4. Daily power planning / Setting of half-hour power references

### IV.4.1. Objectives

In this studied case two power sources are considered: the PV based active generator and a micro gas turbine. Because of the renewable energy benefits (less gas emission and low operating cost), the PV based active generator is considered as the prior source and the micro gas turbine as a back-up source for the missing energy. The objective of the daily power planning is to calculate the power reference setting for each generator and each controllable load. In our studies, controllable loads will not be considered but additional information may be found in [FOG 09]. In this part, we focus only on the system management functions directly related with technical information, while the remaining functions such as forecasting and economic information are considered as idealized.

### IV.4.2. Constraints

#### a. Battery power constraint

A first constraint concerns the optimal charging/discharging of the batteries to increase their lifetime. There are four basic methods for charging batteries [Url 10b]:

**Constant voltage:** A constant voltage charging is based on a stable DC power supply. The lead-acid cells used for cars and backup power systems typically use constant voltage charging.

**Constant current:** A constant current charging varies the voltage applied to the battery to maintain a constant current flow and is switched off when the voltage reaches the level of a full charge. This design is usually used for nickel-cadmium and nickel-metal hydride cells or batteries.

**Taper Current:** The charging is operated by a crude unregulated constant voltage source. The current diminishes as the cell voltage builds up. There is a serious danger of damaging the cells through overcharging. To avoid this, the charging rate and duration should be limited. This charging technique is suitable for SLA (Sealed Lead Acid) batteries only.

**Pulsed charge:** A pulsed charging feeds the charge current to the battery with pulses. The charging rate (based on the average current) can be precisely controlled by varying the width of the pulses, typically about one second. During the charging process, short periods of 20 to 30 milliseconds between pulses allow the chemical actions in the battery to stabilize by equalizing the reaction throughout the bulk of the electrode before starting a new charge cycle. This enables the chemical reaction to keep pace with the rate of inputting the electrical energy. It is also claimed that this method can reduce unwanted chemical reactions at the electrode surface such as gas formation, crystal growth and passivation.

Generally, battery cycle life is defined as the number of complete charge - discharge cycles a battery can perform before its nominal capacity falls below 80% of its initial rated capacity. Lifetimes of 500 to 1200 cycles are typical. The actual ageing process results in a gradual reduction in capacity over time. In our studied case the lead-acid battery cycle life is limited. So some algorithms of charging and discharging should be used for improving the

battery life.

The simplest and most obvious way of getting the maximum life out of a battery is to ensure that it always works well within its designed operating limits. There are however some further actions, which can be taken to increase the battery life. Most battery failures are due to an inappropriate charging. The use of a flexible charging algorithm and a protection system, which prevents the overcharging may not extend battery life but, at least, can prevent it from being cut short.

In PV application, the battery charging source is the PV panels, which are an intermittent current source. So the intermittency of the PV power can not ensure a continue complete process of charging because the charging current usually varies greatly. In the chapter 2, ultracapacitors are added and a low-pass filter is used to erase all fast transient components in the charging current of batteries. In this chapter, another technique is used by setting a constant charging current during each half hour. And for ensuring the battery cycle life, the batteries are not discharged during the daytime. Even although the PV power is not enough for the power supply, only the micro gas turbine is asked for the power compensation. In the night, the batteries are discharged. This charging and discharging algorithm assures not only a high charging/discharging efficiency, but also increases the battery cycle life (one cycle of charging and discharging each 24-hour) [LU 08]. The depth of discharge is maintained between 0% and 70% during a normal operation to increase the battery lifetime. Here the storage battery capacity is 106 Ah. Moreover the rated battery power ( $P_{bat\_max}$ ) is also considered. [Url 10b]

#### b. Micro gas turbine constraint

The rated power of the micro gas turbine ( $P_{MGT\_max}$ ) is 33kW.

A start of a micro gas turbine needs much more fuel than a continuous operation with a constant generated power and it causes a lot of air pollution. Moreover the start should take several minutes if the turbine is cold. [Pil 02]

In order to minimize energy losses and the gas emission at each start, the gas turbine should always work. Therefore, in the case of low power demand, the turbine is forced to work with a low power level ( $P_{MGT\_min}$ ), corresponding to the minimum energy:

$$\tilde{E}_{MGT\_1/2h\_min} = \int_0^{Te} P_{MGT\_min} dt = P_{MGT\_min} \cdot Te \quad (\text{R. IV-6})$$

### IV.4.3.Determinist algorithm

According to daily predictions of the available power and energy from the PV ( $\tilde{P}_{PV\_24h}, \tilde{E}_{PV\_1/2h}$ ) and the required power and energy of the loads ( $\tilde{P}_{Load\_24h}, \tilde{E}_{Load\_1/2h}$ ), a power production planning for the prosumer ( $P_{AG\_ref0}$ ) and for the micro turbine ( $P_{MGT\_ref0}$ ) must be determined. The central energy management system refreshes the power references each 30 minutes. As no power is available from PV panels during the night, power references are calculated separately for the night and for the day.

#### a. Day-time

In the day ( $t_0 < t < t_0 + \Delta t$ ), and for each 1/2h period, two cases are considered.

**Case 1:** If the available PV energy added with the minimum gas turbine energy is less than the demanded load energy ( $\tilde{E}_{PV\_1/2h} + \tilde{E}_{MGT\_1/2h\_min} < \tilde{E}_{load\_1/2h}$ ), the PV panels can work



with a Maximum Power Point Tracking (MPPT) algorithm and all PV power is injected in the grid. The micro gas turbine has to generate the missing power:

$$P_{AG\_ref0} = \tilde{P}_{PV\_24h} \quad (\text{R. IV-7})$$

$$P_{MGT\_ref0} = \tilde{P}_{Load\_24h} - P_{AG\_ref0} \quad (\text{R. IV-8})$$

with  $P_{AG\_ref0}, P_{MGT\_ref0}$  the initial power references of the 24-hours power planning, respectively, for the PV active generator and the micro gas turbine.

**Case 2:** Otherwise, the available PV energy added to the minimum gas turbine energy is more than the demanded load energy. The priority is then given to the renewable energy for the electrical production so that the micro gas turbine works with a minimum power and the active generator power is limited to the missing power:

$$P_{AG\_ref0} = \tilde{P}_{Load\_24h} - P_{MGT\_min} \quad (\text{R. IV-9})$$

$$P_{MGT\_ref0} = P_{MGT\_min} \quad (\text{R. IV-10})$$

with  $P_{MGT\_min}$  the minimum power production of the micro gas turbine.

The excess PV energy will be managed by the local controller.

#### b. Night-time

The energy management during the night ( $t_0 + \Delta t < t < t_0 + 24h$ ) depends on the available energy from batteries in homes. This energy ( $\tilde{E}_{bat}$ ) can be estimated or communicated by the E-box to the central energy management system. In the night two cases are distinguished. For both cases batteries have to be discharged in order to be ready for charging the next day at  $t_0$ . According to the stored energy ( $\tilde{E}_{bat}(t_0 + nTe)$ ) and the rated energy ( $\tilde{E}_{bat\_1/2h\_max}$ ), the available energy of batteries during the next 1/2h is obtained:

$$\tilde{E}_{bat\_1/2h\_rest}(t) = \min[\tilde{E}_{bat\_1/2h\_max}, \tilde{E}_{bat}(t_0 + nTe)] \quad (\text{R. IV-11})$$

with :

- $\tilde{E}_{bat\_1/2h\_rest}$ , the available battery energy for the next half hour,
- $\tilde{E}_{bat\_1/2h\_max}$ , the maximum battery exchanged energy for an half hour,
- $\tilde{E}_{bat}(t_0 + nTe)$ , the stored energy in the batteries.

**Case 3:** If the available stored battery energy, added to the minimum gas turbine energy is more than the demanded energy from loads ( $\tilde{E}_{bat\_1/2h\_rest} + \tilde{E}_{MGT\_1/2\_min} > \tilde{E}_{load\_1/2h}$ ), priority is given to the active generator for the electrical production since it has enough previously stored energy from PV panels. The gas turbine will work with a minimum power:

$$P_{AG\_ref0} = \tilde{P}_{Load\_24h} - P_{MGT\_min} \quad (R. IV-12)$$

$$P_{MGT\_ref0} = P_{MGT\_min} \quad (R. IV-13)$$

**Case 4:** Otherwise, the stored battery energy added with the minimum gas turbine energy is less than the demanded energy from the loads. Then the power reference of the active generator is calculated in order to discharge batteries and the gas turbine must generate the missing power:

$$P_{AG\_ref0} = \frac{\tilde{E}_{bat\_1/2h\_rest}}{Te} \quad (R. IV-14)$$

$$P_{MGT\_ref0} = \tilde{P}_{Load\_24h} - P_{AG\_ref0} \quad (R. IV-15)$$

The case where the battery energy is insufficient is then included.

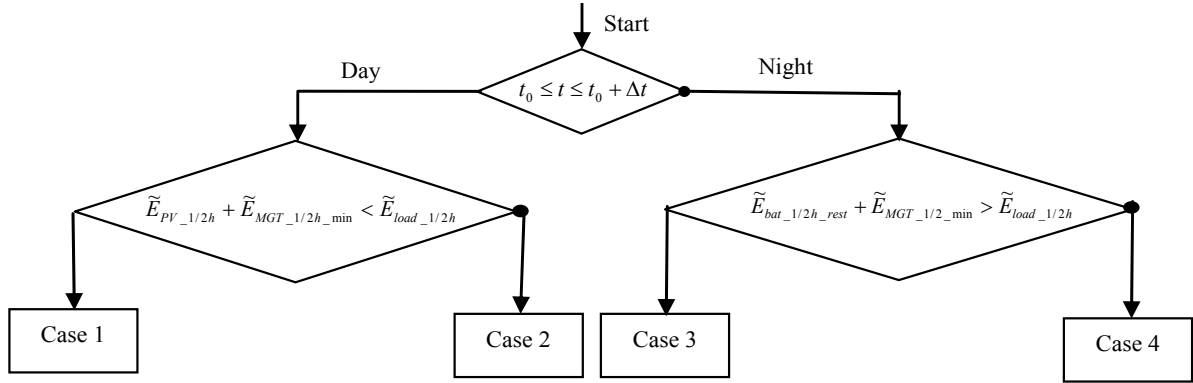


Figure IV.14 Determination of operating cases

#### IV.4.4. Practical application

In order to illustrate the theoretical results, the power planning (24h-ahead) is calculated with the load forecasting (Figure IV.12), as well as the estimated PV power (Figure IV.9) and with  $t_0=7h00$  and  $\Delta t=12h30$ .

Estimations of the required energy during the day for the loads ( $\tilde{E}_{Load\_day}$ ) and the available energy from the PV panels ( $\tilde{E}_{PV\_day}$ ) show that too much renewable energy is available (Figure IV.15).

As the gas microturbine must produce the minimum energy during the day, the surplus energy is estimated as:

$$\Delta\tilde{E} = \tilde{E}_{PV\_day} - \tilde{E}_{Load\_day} + \tilde{E}_{MGT\_day\_min} < E_{bat\_max} \quad (R. IV-16)$$

$$\tilde{E}_{MGT\_day\_min} = \int_{t_0}^{t_0+24h} P_{MGT\_min} dt \quad (R. IV-17)$$

This energy can be stored in batteries. The required energy from the gas microturbine for the night operation is then deduced (Figure IV.16):

$$\tilde{E}_{MGT\_night} = \tilde{E}_{Load\_night} - \tilde{E}_{bat\_night} \quad (R. IV-18)$$

With  $\tilde{E}_{bat\_night} = \Delta\tilde{E}$ .

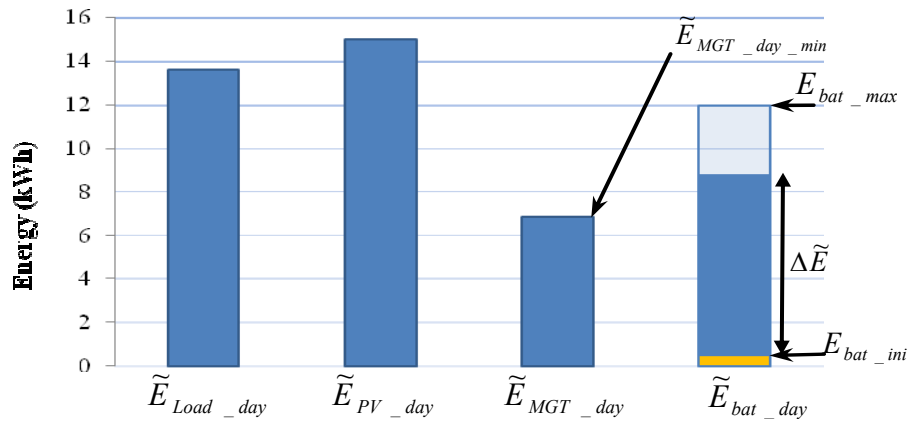


Figure IV.15 Energy analysis for the daytime

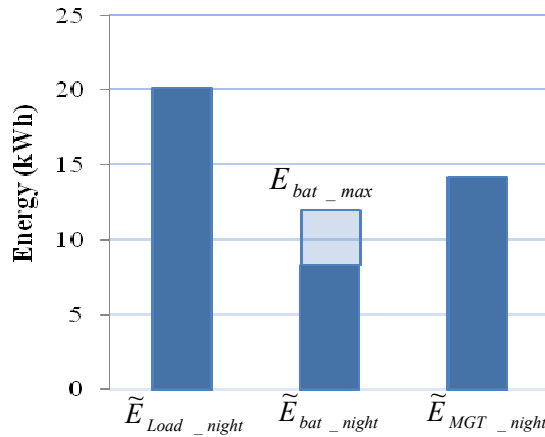


Figure IV.16 Energy analysis for the nighttime

As a communication network exists, the estimated value of the battery energy can be replaced by a sensed value, which is sent by the E-box at the beginning of the night ( $t_0 + \Delta t$ ). Calculated power references from the determinist algorithm are shown on fig. IV.17. Between 7h00 and 7h30, the PV power is not enough (Figure IV.9) then the power reference for the gas turbine is equal to the load demand (Figure IV.12). Between 9h00 and 17h00; the gas turbine power reference is controlled with a minimum power (Figure IV.17).

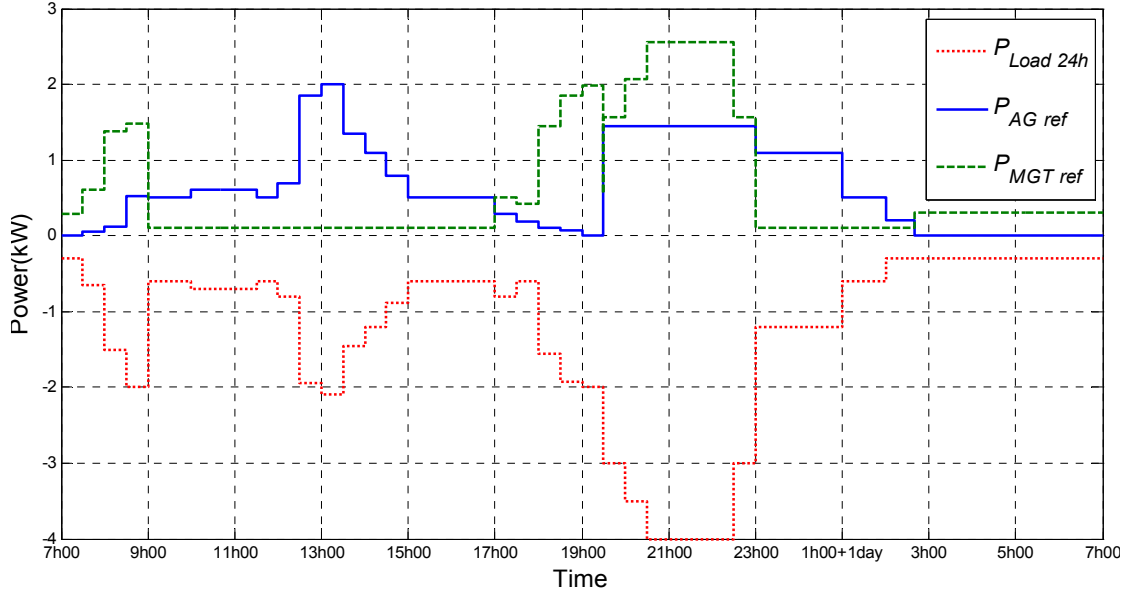


Figure IV.17 Power references from the power planning in the central energy management

## IV.5. Medium-term energy management

### IV.5.1.Reduction of the uncertainty (MGCC)

Power references from the long-term energy management are calculated by 24h ahead planning from the load and PV production forecasting. Sometimes the real situation (weather conditions, power demand by loads) are different from the forecasted conditions. In practice, If we consider the current forecasted loads ( $\tilde{P}_{Load\_1/2h}$ ) and forecasted PV production ( $\tilde{P}_{PV\_1/2h}$ ) for the next half of an hour, we get then the following deviation from the 24h-ahead forecasted data:

$$\Delta P_{PV\_1/2h} = \tilde{P}_{PV\_1/2h} - \tilde{P}_{PV\_24h} \quad (\text{R. IV-19})$$

$$\Delta P_{Load\_1/2h} = \tilde{P}_{Load\_1/2h} - \tilde{P}_{Load\_24h} \quad (\text{R. IV-20})$$

The medium-term energy management takes into account these different conditions by modifying locally power references according to the real situations. This operating is quiet similar to the secondary control in large power systems. Here the refreshment is done each half of an hour in the Micro Grid Central Controller as:

$$P_{AG\_ref1} = P_{AG\_ref0} + \Delta P_{AG1\_1/2h} \quad (\text{R. IV-21})$$

with  $P_{AG\_ref1}$ , the power reference after the medium-term energy management;

$P_{AG\_ref0}$ , the power reference after the daily power planning;

$\Delta P_{AG1\_1/2h}$ , the power modification of the medium-term energy management.

The modified reference of the medium-term energy management depends on the correction of the PV prediction and of the load forecasting:

$$\Delta P_{AG1\_1/2h} = \Delta P_{PV\_1/2h} + \Delta P_{Load\_1/2h} \quad (\text{R. IV-22})$$

In a same way, the power reference for the micro turbine is corrected:

$$P_{MGT\_ref1} = P_{MGT\_ref0} + \Delta P_{MGT\_1/2h} \quad (\text{R. IV-23})$$

with  $P_{MGT\_ref1}$ , the power reference after the medium-term energy management;

$P_{MGT\_ref0}$ , the power reference after the daily power planning;

$\Delta P_{MGT\_1/2h}$ , the power modification of the medium-term energy management.

After the correction of the power references, the Micro Grid Central Controller sends these corrected power references to the Local Controller for each generator (PV active generator and Micro Gas turbine) through the communication bus.

#### IV.5.2. Energy management of batteries (LC)

In the active generator, the critical sources, which are impacted by the medium term management, are the batteries. Deep discharging, under charging and overcharging may damage batteries and shorten their lifetime. So in order to optimize the use of the batteries, only one charging / discharging cycle in 24h has been set. Moreover, during the daytime, the battery charging power reference ( $P_{bat\_ref0}$ ) is set as a constant during each half hour according to the active generator power reference ( $P_{AG\_ref0}$ ), the local short-term PV power prediction ( $\tilde{P}_{PV\_1/2h}$ ) and the estimated state of charge of batteries ( $\tilde{SOC}(t)$ ) during this half hour. Moreover, the batteries are not set in the discharging mode during the daytime. The algorithm of the daytime charging is started as soon as the sensed PV power is higher than the load power demand.

$$\tilde{P}_{PV\_1/2h} - P_{AG\_ref1} > 0 \quad (\text{R. IV-24})$$

If the predicted PV power ( $\tilde{P}_{PV\_1/2h}$ ) is lower than the load reference during a half hour ( $P_{AG\_ref1}$ ), the batteries are not charged and are in stand-by mode (Figure IV.18). Otherwise, they are charged in this half hour but, before, the battery energy constraint should be considered.

If the batteries are fully charged, they will remain in stand-by mode; otherwise the battery power constraint should be taken into account.

If the surplus PV power (the remaining PV power after satisfying the load) is less than the rated battery power, the batteries can be charged with this maximum power, otherwise the batteries are in stand by.

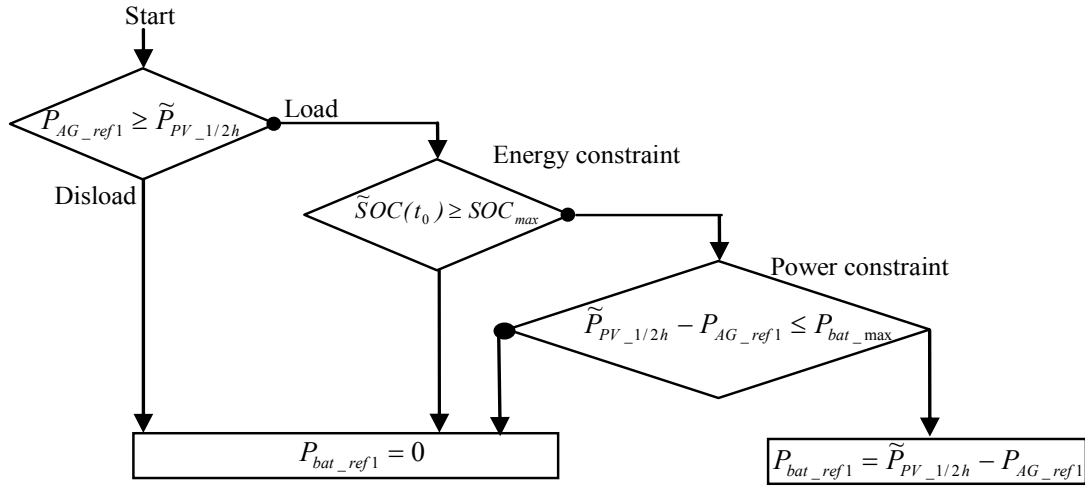


Figure IV.18 Flow diagram for the battery charging algorithm during the day

In the night, the batteries are discharged. The discharging power reference is calculated each half of an hour according to the SoC. In the same way, the energy capacity limit and the discharging power limit should also be considered (Figure IV.19).

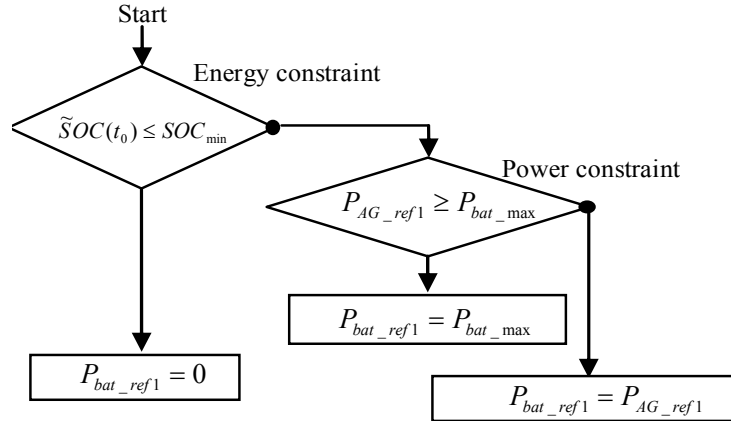


Figure IV.19 Flow diagram for the battery discharging algorithm during the night

## IV.6. Short-term power management

### IV.6.1. Primary frequency regulation

#### a. Organization

The central energy management system sends wished power references  $P_{AG\_ref1}$  and  $P_{MGT\_ref1}$  each half of an hour. These quantities are the refreshed and planned exchanged powers for this duration. As real time variations exist in the load and also in the produced PV power, a primary frequency control must be used to adjust in real time the power production of generators in order to achieve the real-time power balancing [Url 10a]. The two generators inside the micro grid can share this control function (chap. 3, paragraph III.5.5).

A primary frequency control and the local controller of a gas micro turbine have been studied in [Li 09] and are recalled in Appendix VII. A primary frequency control has been designed inside the active generator in order to ensure the short-term power balancing [Cou 08].

When the frequency deviation exceeds a pre-defined threshold value, the controller is activated to increase or decrease the power for restoring the power balance [Cou 08]. A droop constant gives the additional power that is supplied as a function of the frequency deviation (Figure IV.20).

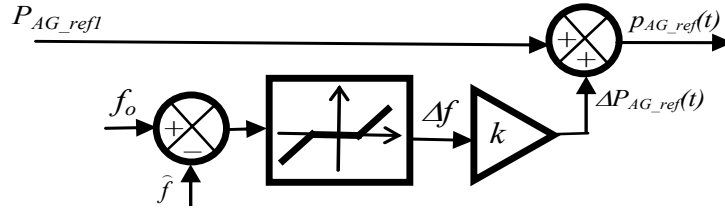


Figure IV.20 Droop controller for primary frequency control

#### IV.6.2. Power balancing strategies for the active generator

The active generator has to provide the real time power reference ( $p_{AG\_ref}(t)$ ), which is the sum of the secondary power reference ( $P_{AG\_ref1}$ ) with the real time primary power reference ( $\Delta P_{AG\_ref}(t)$ ).

For our application, the battery power will be constant during an half of an hour (Paragraph IV.5). The real-time power balancing must be implemented by a power buffer with fast dynamic capabilities. As shown in Chapter 1 (paragraph I.3.2), ultra capacitors are fast dynamic storage systems with high power exchange capabilities. So they are suitable for the optimal charging of the battery and for supplying peak power to the grid if necessary, but their energy density is low.

As batteries are now charged or discharged with a constant power reference, the power sharing level of the control system (Figure IV.21) must be adapted. One algorithm is still executed and calculates power references for the ultracapacitors, PV panels and the inverter according to a selected operating mode and the measured quantities (

Figure IV.21).

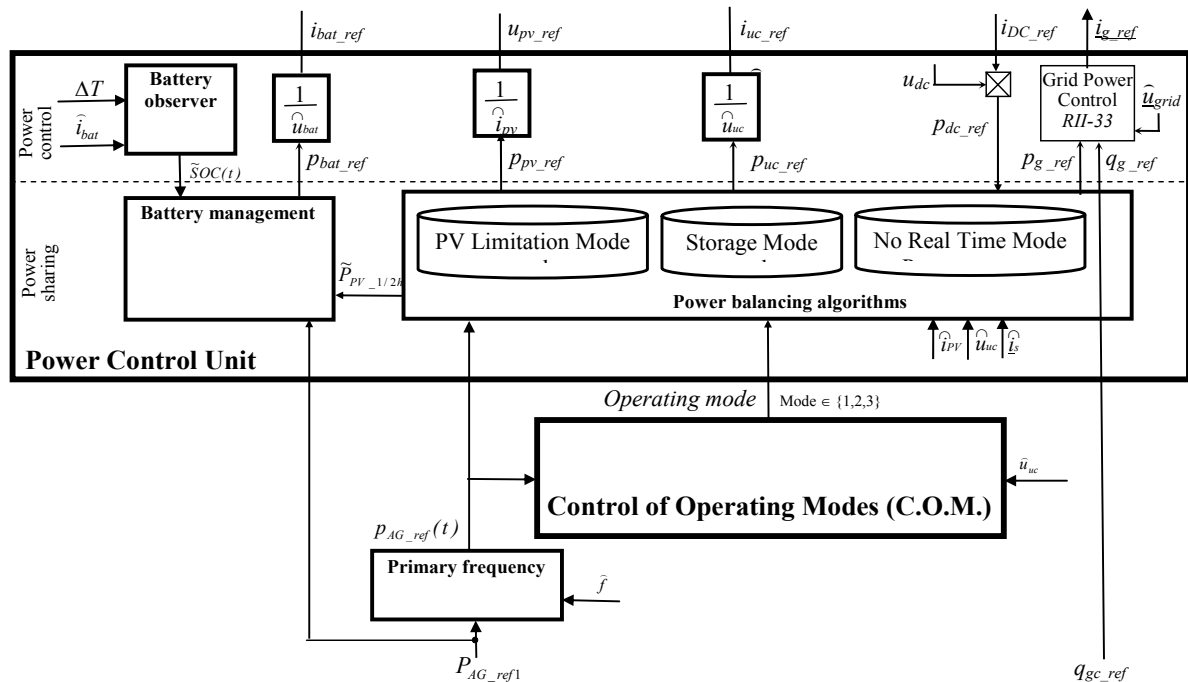


Figure IV.21 Modified control system for the application

Then these power references are transformed to current or voltage references with closed loop controls. The day case and night case are respectively detailed. In real time, the SOC is also calculated and then the loading in the last 1/2h is stopped if necessary.

**b. Control of operating modes**

Here the power reference of the batteries is different since a constant battery power reference replaces the low-pass filter used in chapter 2. In this application the SoC of batteries is managed by the MGCC in order to maximize the value of the PV power (Figure IV.21).

The PV limitation mode of the PV based active generator (paragraph II.4.3) is normally not possible if batteries are well sized. Anyway this operating mode is kept even it is (normally) not required for this application. Other modes remain unchanged as well as the selection of these operating modes (Figure II.33).

**c. Energy management of the ultracapacitors**

Now the batteries are dispatched by the MGCC and so the controllability of the active PV based generator relies on the state of charge of ultracapacitors. As batteries are now unavailable for the load/disload of ultracapacitors, energy from PV panels will be used to load them and injection to the grid will be used to disload them. The strategy is then derived from the Figure III.36 in order to modify the grid power reference in this emergency mode (fig. IV.22).



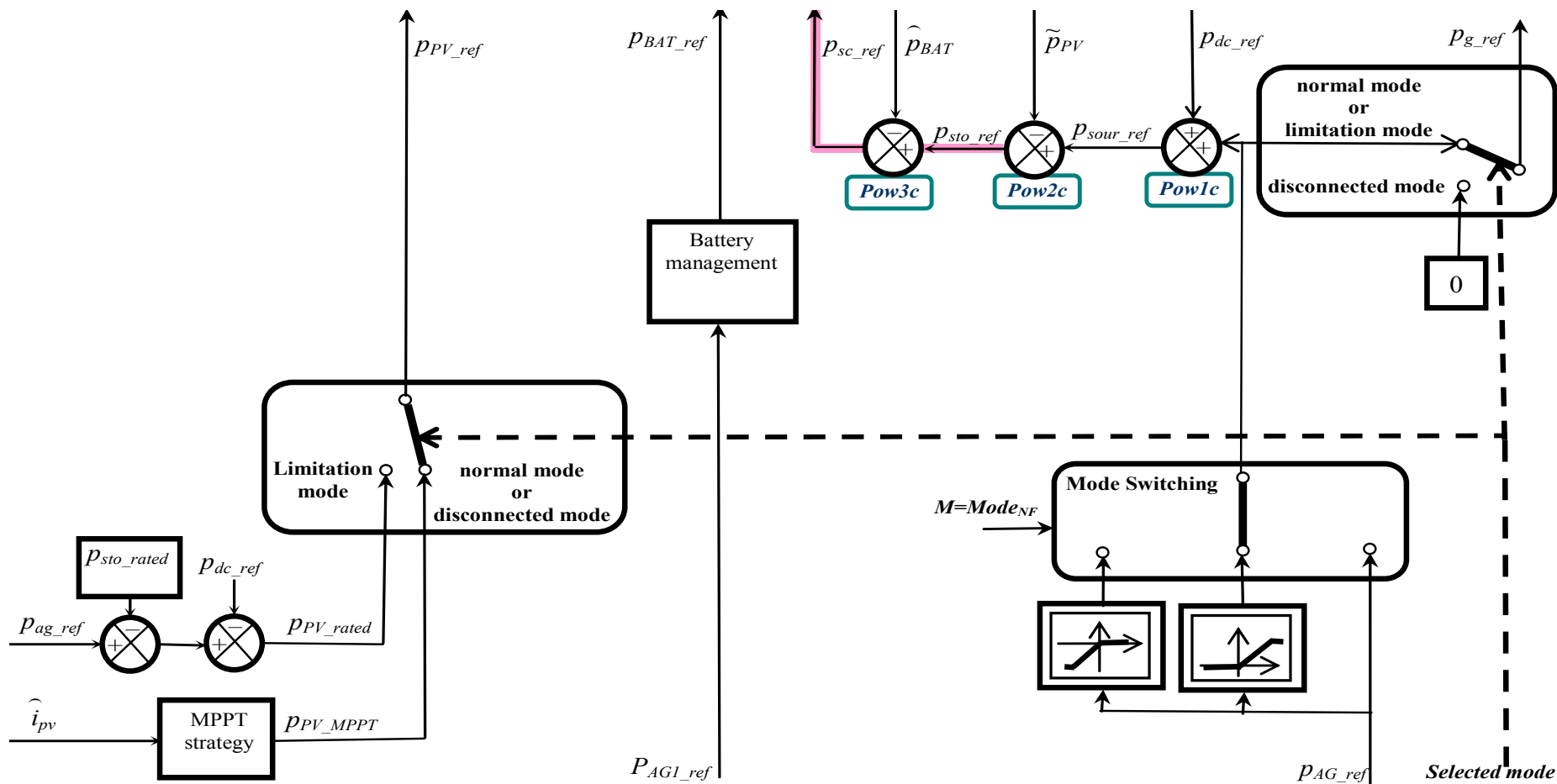


Figure IV.22: Block diagram of the power sharing level

## **IV.7.Experimental tests through Hardware in the Loop simulations**

### **IV.7.1.Description of the experimental platform**

Control algorithms of the MGCC have been tested and validated through real-time simulations under similar conditions as the residential microgrid may face in reality. These tests thus validating the pre analysis are performed through off-line simulations. Real-time analysis consists in using real parts of the electrical component under operating conditions very close to reality. However, in general it is difficult to make the testing of in situ because of the risks involved (disruption of service, etc. ), high costs involved (staff, equipment, etc.) and lack of flexibility (limited number and type of tests). Hardware In the Loop consists to simulate in real time the operating conditions and to reproduce them by using a power amplifier. Consequently, this type of analysis provides more realistic results as the simulation off-line regarding the operation of the device under study.

In order to verify above algorithms for the residential micro grid application, our energy management system has been implemented on the L2EP experimental platform: “Distributed Energy” at the “Arts & Métiers Paristech” research center and with the real time simulator: OPAL RT. A micro grid platform has been set up with a central control host (Figure IV.23)

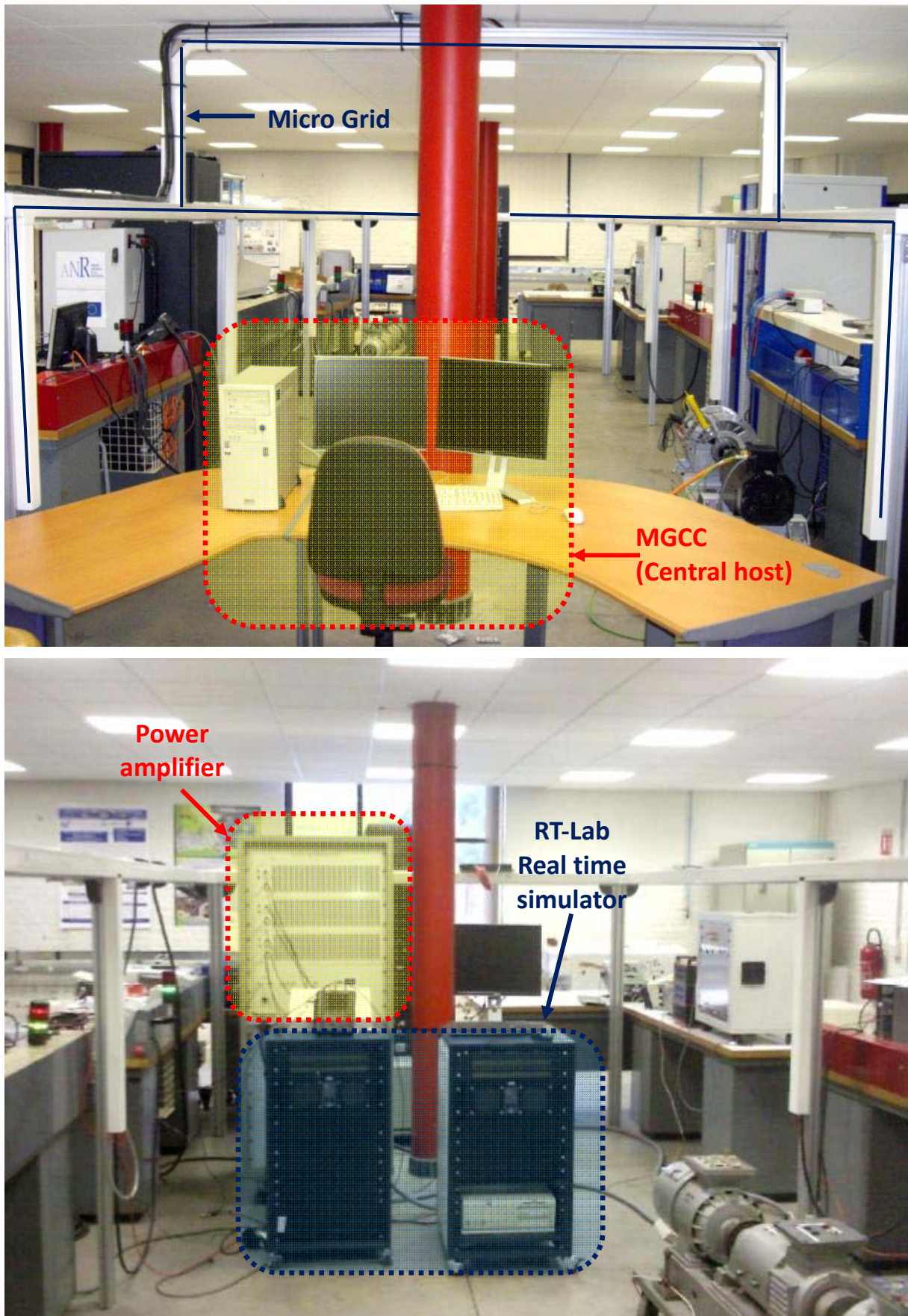


Figure IV.23 Micro Grid platform

The objective of the experimental work is to validate the MGCC by a Hardware-In-the-

Loop (HIL) test and to show the coordinated operation of different sources (PV active generator and micro gas turbine) in the microgrid. The HIL organization is presented in the Figure IV.24. Test devices are divided into two classes: the microgrid devices (the DER units, loads etc.) and the control devices (the LCs, the MGCC, etc.).

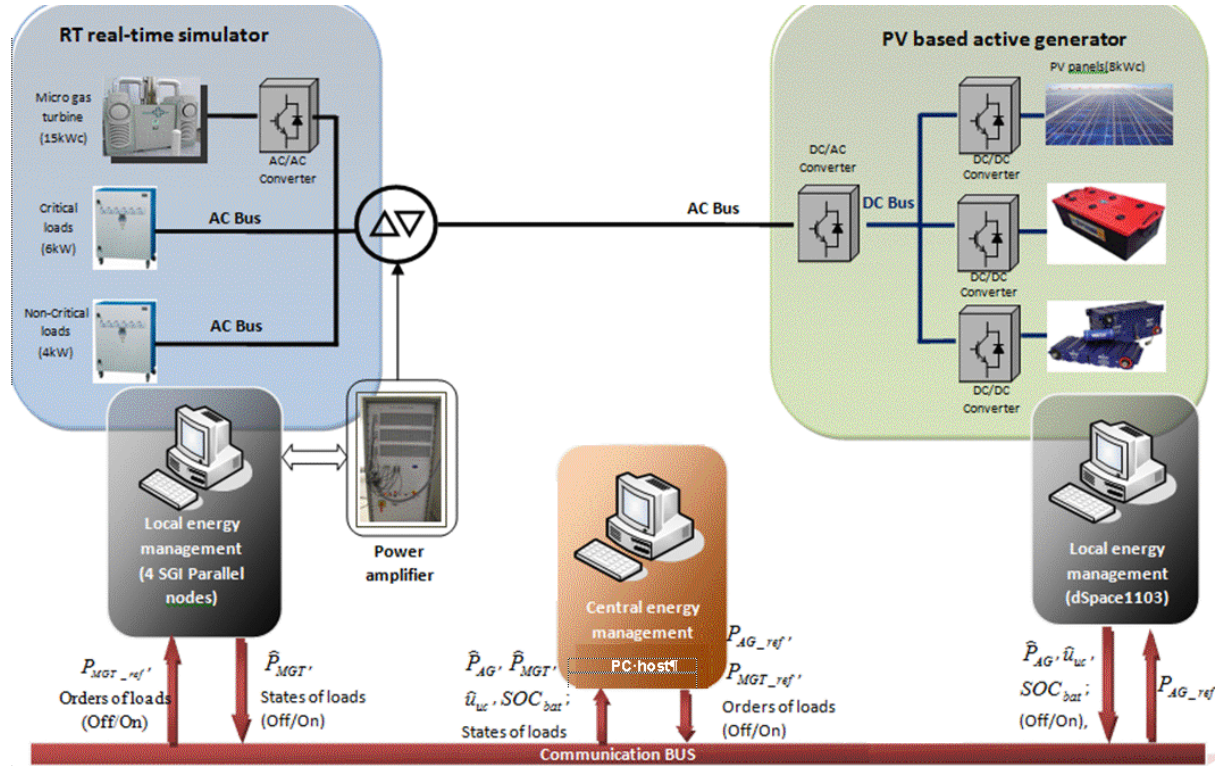


Figure IV.24 HIL test set up

Three types of devices are used:

- The real PV based active generator, which is fed by a DC current source for emulating identical PV power productions in order to compare various control algorithms in the same illumination conditions;
- Virtual devices are simulated under the real-time simulator OPAL RT-Lab in four SGI parallel cores. It includes the micro turbine generator, 4kW non-critical loads and 6kW passive loads. Passive loads represent the critical loads and must remain connected to the microgrid during the test;
- A power amplifier, which is used as an interface to create the point of coupling of the active generator; it is interfaced to the real time simulator via Analog to Digital Conversion cards and Digital to Analog Conversion cards.

The control devices are composed of four parts:

- A DSpace 1103 card is used to implement the LC of the PV based active generator;
- The MGCC is implemented in a PC with a SCADA software (PCView). It communicates with the LCs;
- The LCs of the micro turbine unit and the load controllers are integrated into the RT-lab software simulator;
- The communication bus exchanges the signals between the MGCC and LCs.

An Ethernet with a Modbus protocol for the communication is used and enables the connection of various devices, for example a system that measures currents and voltages and the communication of data to a computer. For our application exchanged data are shown on

Figure IV.25. Modbus is suited to connect a supervisory computer with a Remote Terminal Unit (RTU) in Supervisory Control And Data Acquisition (SCADA) systems.

To make comparisons, several different tests are carried out with different sizes of PV panel installation and different sizes of loads.

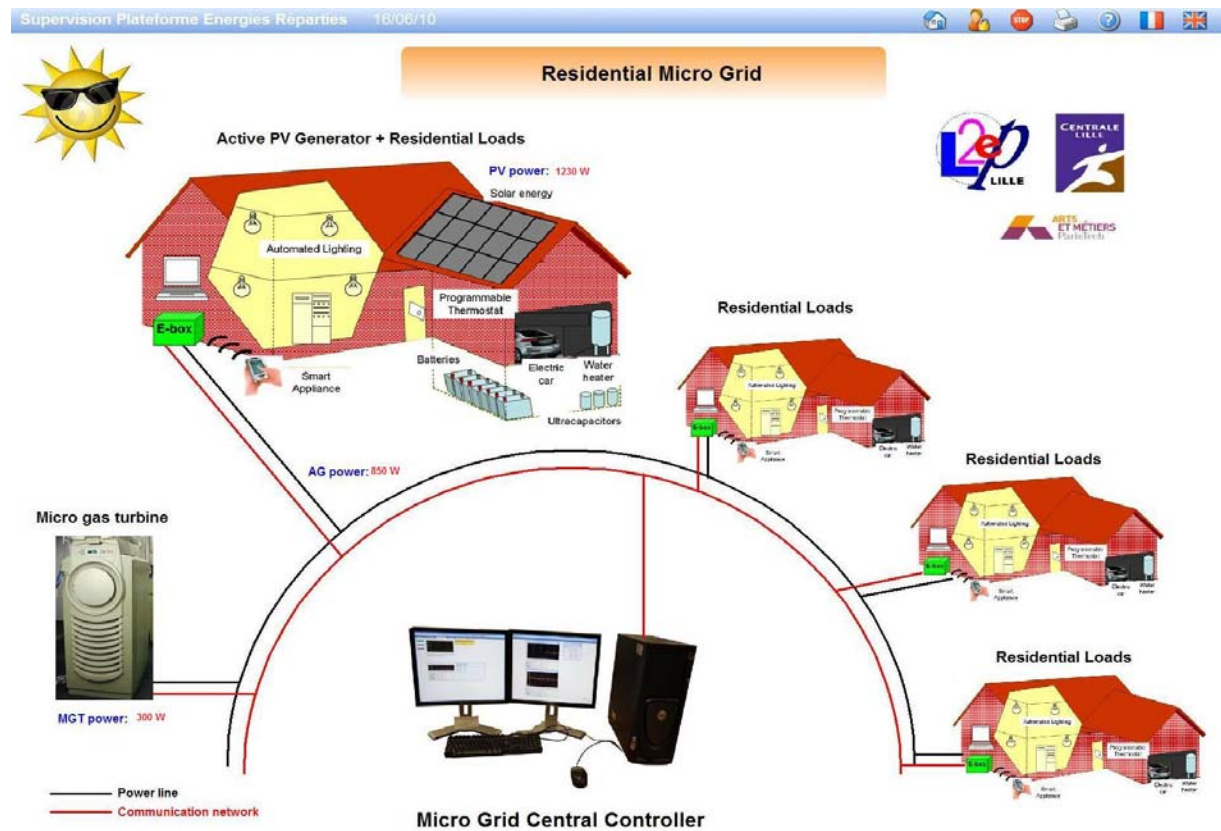


Figure IV.25 Supervisor screen of Micro Grid Central Controller (PCView)

#### IV.7.2. Analysis of the self consumption of one house

The first case is studied with a PV panels' installation of 3kW peak power and 3kW rated local loads for one house. 106Ah batteries are used with 800W maximum charging power and a 500W maximum discharging power. The 24h-ahead PV power prediction and the load forecasting for the test are given in following figures with  $t_0 = 7h00$  and  $t_0 + \Delta t = 18h00$ .

The various energies are first calculated as explained in paragraph IV 3.3 for the day-time and then for the night-time. During the day the available energy from PV panels is larger than the required one to feed the loads. The stored energy in batteries corresponds then to energy from the gas turbine, which remains switched on with a delivered minimum power. This stored energy is retrieved for the night operation.

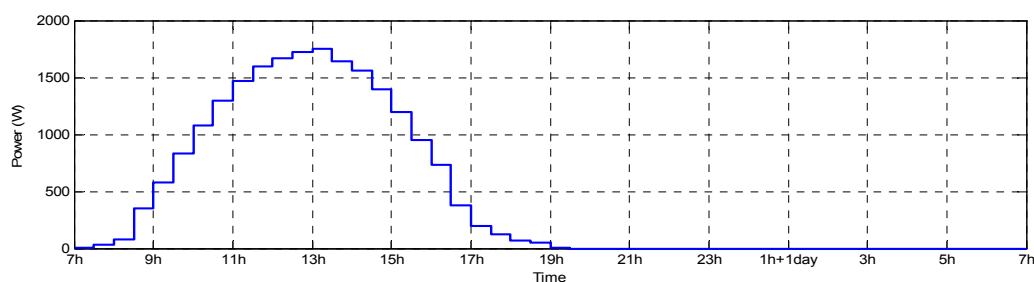


Figure IV.26 24 hour-ahead PV Power forecasting for the self consumption of one house

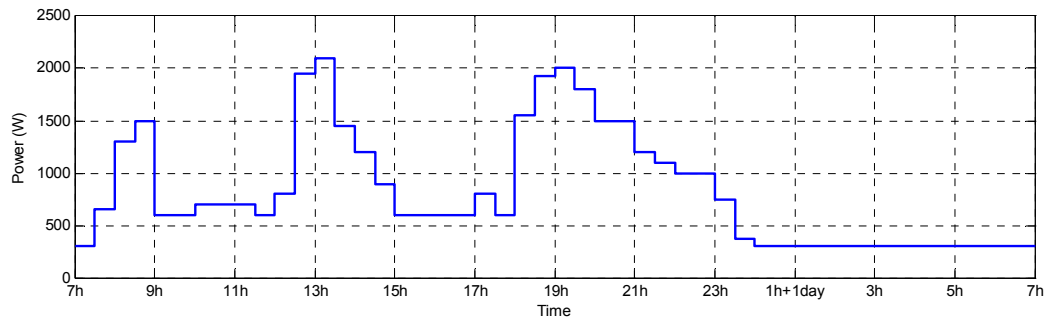


Figure IV.27 24 hour-ahead load forecasting for the self consumption of one house

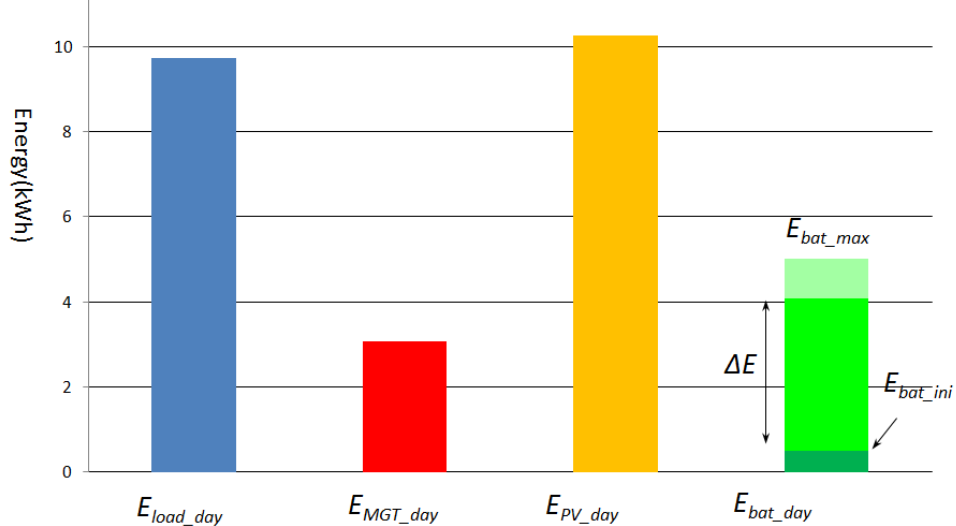


Figure IV.28 Energy analysis for the day-time of the self consumption of one house

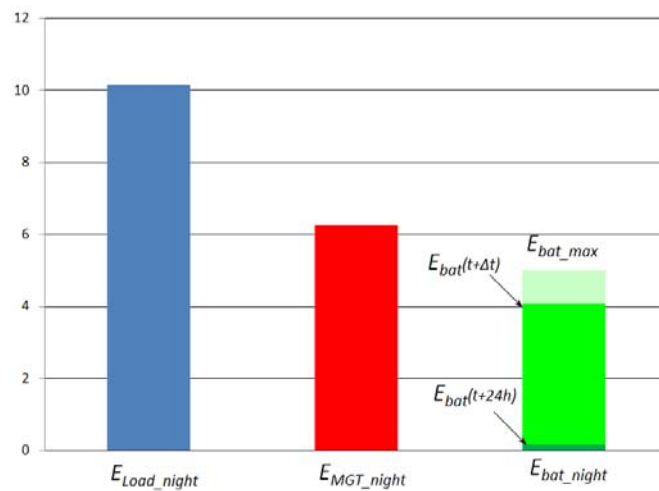


Figure IV.29 Energy analysis for the night-time the self consumption of one house

Power references (Figure IV.30 and Figure IV.31) are calculated by the Micro Grid Central Controller and are sent to Local Controllers. It is clear that between 12h30 and 13h30, PV panels are able to supply the loads but the micro turbine must not be switched off and must be driven with a minimum power (100W, case 2 during the daytime, R.IV-9 and R.IV-10). The same situation appears in the morning between 8h00 and 9h00. The obtained calculated power references show that a good use of the PV based generator during these durations (Figure IV.30) and so a reduction of the micro turbine power reference to the minimum value (Figure IV.31).

At 18h00 (start of the night-time) batteries are loaded and the power reference is then calculated (R.IV-12) to disload them with a maximum rated current until 23h30 (Figure IV.30). We recall that the rated current of batteries is less than the one from PV panels. After the load has decreased and so the power reference for batteries is modified until the end of the night-time.

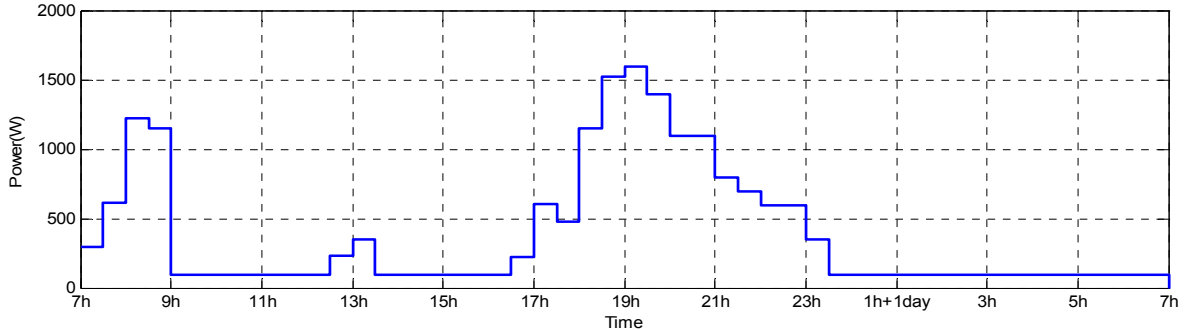


Figure IV.30 Micro gas turbine power reference setting for the self consumption of one house

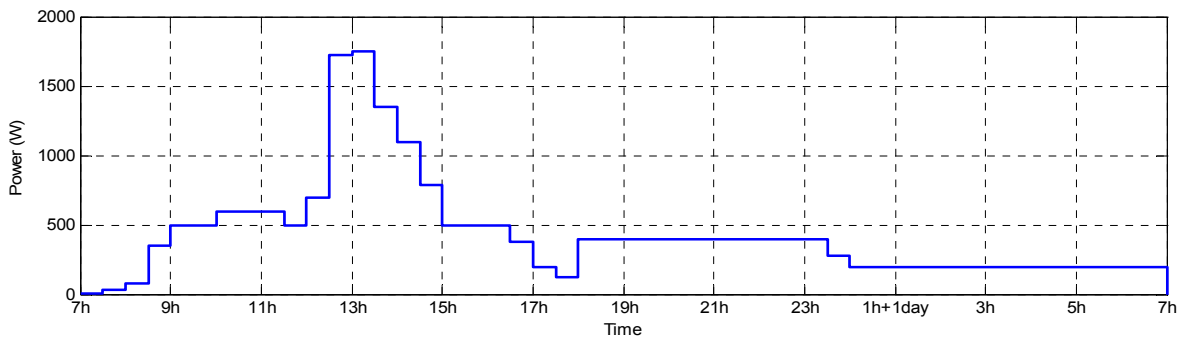


Figure IV.31 PV active generator power reference setting for the self consumption of one house

Sensed powers on the experimental platform are shown on (Figure IV.32) and are equal to power references.

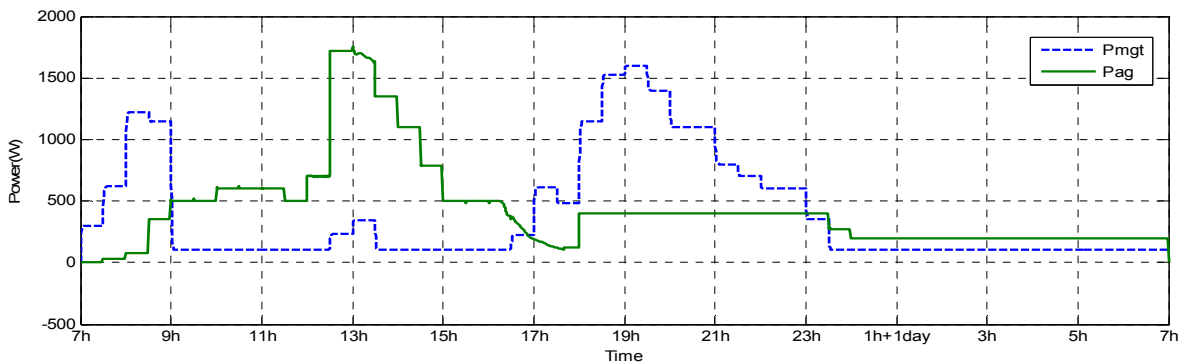


Figure IV.32 Generated powers in the micro grid for the self consumption of one house

The sensed PV power and battery power inside the active generator are shown on Figure IV.32. A part of the PV power is lost at 11h30 because the PV power is reduced. At the same time, the battery current is at the rated value in a loading mode. For this test an increase sizing of batteries may avoid this loss. During the night time the batteries delivers a nearly constant power with a rated value between 18h00 and 23h30 (the rated value un disloading mode is not the same as in the loading mode) since the load demand is high. After this battery power is decreased and the turbine power is on the minimum value after 24h00.

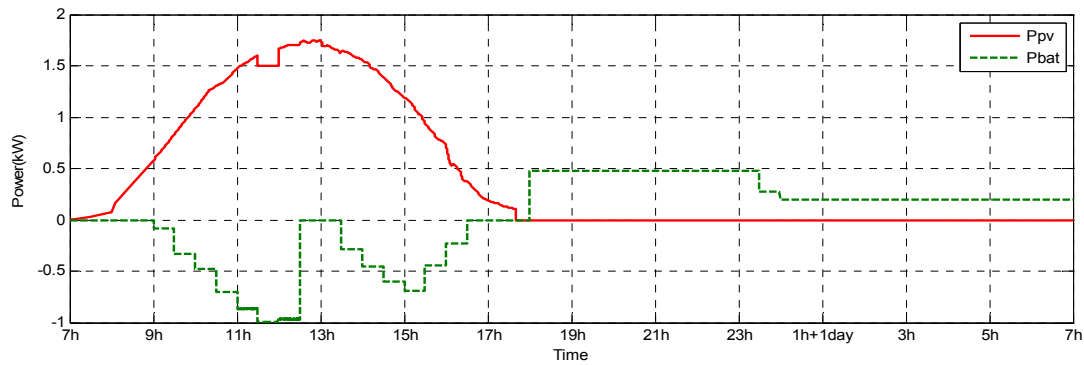


Figure IV.33 Sensed powers inside the PV active generator for the self consumption of one house

The following figure shows the evolution of the battery SOC for the self consumption of one house.

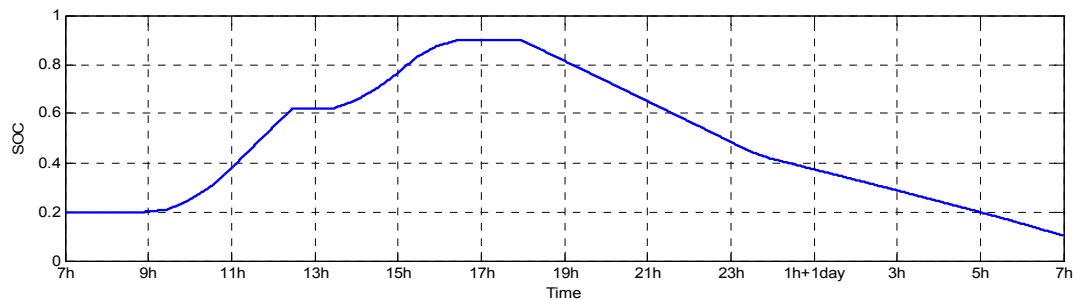


Figure IV.34 Time evolution of batteries SOC for the self consumption of one house

From the above figure, one charging and discharging cycle of the batteries during 24 hours are effectively set.

The power planning is determined for a period of half of one hour. Then deviations occur in this time base. Nevertheless, even if the obtained average value of powers is good, the instantaneous values of power can have considerable differences with the planned references.

A zoom is shown on Figure IV.35 during a constant generated PV power. When an instantaneous load increase occurs, the battery can not provide the full power compensation because of its slow dynamic characteristic. Under this condition, the ultracapacitors are used for the fast power compensation.

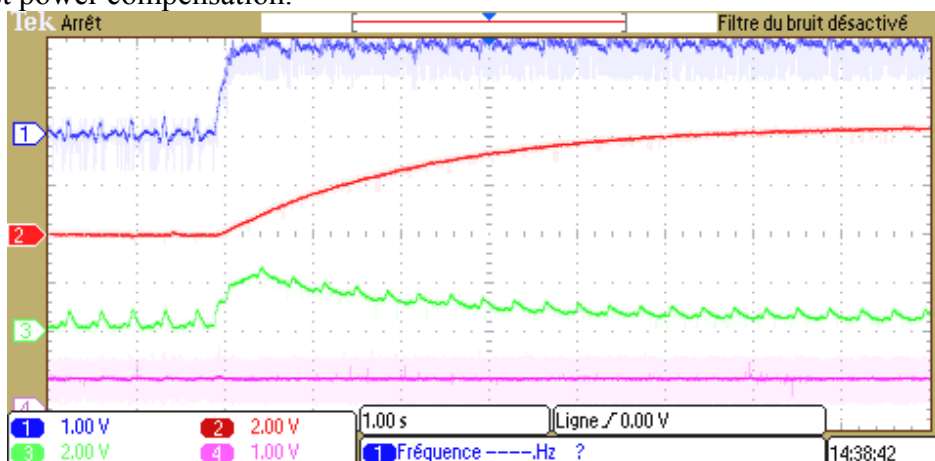


Figure IV.35 Ultracapacitors dynamic power compensation

$p_{AG\_mes}$ (Ch1): 100W/div;  $p_{bat\_mes}$ (Ch2): 100W/div ;  $p_{uc\_mes}$ (Ch3): 150W/div;  $p_{PV\_mes}$  (Ch4) 150W/div.

On Figure IV.36, the grid load remains constant. When the instantaneous generated PV power increases, the battery is charged with a constant power, but it can not absorb all the



surplus PV power. In this case, the ultracapacitors are used to achieve the real-time power balancing.

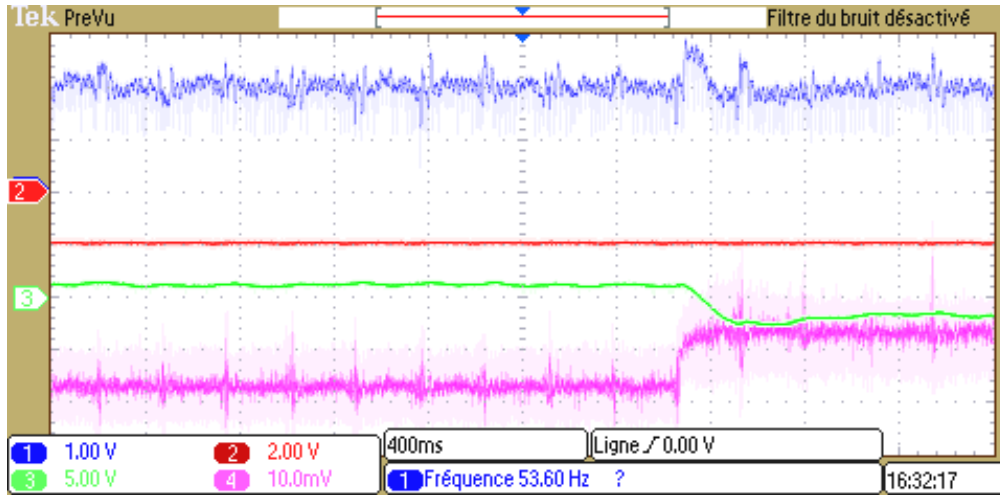


Figure IV.36 Ultracapacitors dynamic power absorption

$p_{AG\_mes}$ (Ch1): 100W/div;  $p_{bat\_mes}$ (Ch2): 100W/div ;  $p_{uc\_mes}$ (Ch3): 150W/div;  $p_{PV\_mes}$  (Ch4) 150W/div.

So for both cases the use of ultracapacitors enables the production in real time of a constant power during half of an hour.

Comments:

To get an easier verification, the primary frequency control is disabled for these tests.

According to experimental results, the consumed electrical energies of each generator in the micro grid can be deduced. So for the case 1, the PV power provides 53% of the total power supply and the MGT power covers the remaining 47% power (Figure IV.37).

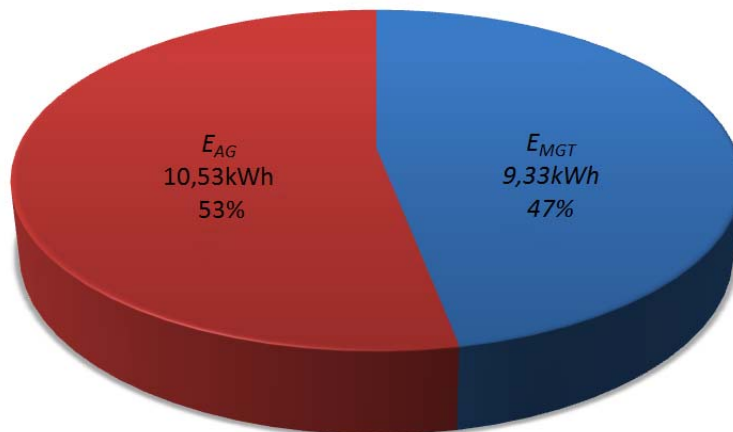


Figure IV.37 Energy consumption percentages for case1

### IV.7.3. Increasing the penetration ratio in a residential network

#### a. Impact of one producer

The previous 3kW prosumer (PV based generator) is now located in a residential network with three other consumers. A 12kW rated local loads for the four houses is considered. The PV power prediction and the load forecasting for the test are given in the following figure.

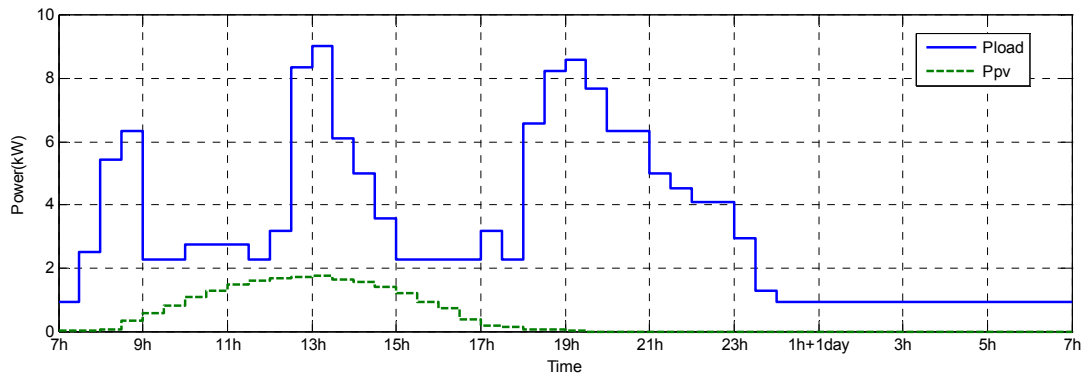


Figure IV.38 24 hour-ahead PV power and load forecasting

According to the forecasting information, the PV energy is much lower than the demanded power of the total loads. According to this day-ahead analysis, batteries will not be used.

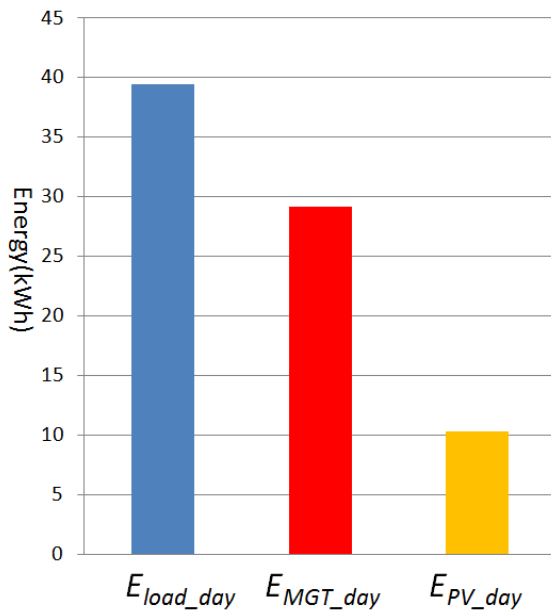


Figure IV.39 Energy analysis for the day-time

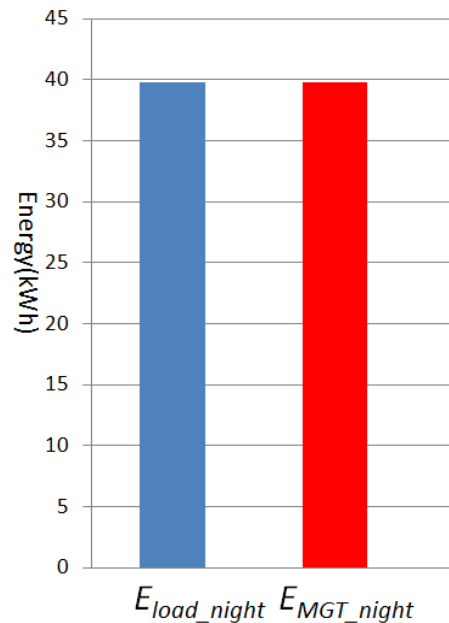


Figure IV.40 Energy analysis for the night-time

As previously sensed powers on the experimental platform are equal to power references. Reference powers from the MGCC show a full contribution of the PV generation (without power limitation) but least than the gas turbine (Figure IV.41). For this case, in local the storage devices are not used, because the required load power is always more than the PV power during the daytime. This is confirming that for a small penetration of PV production, all the production can be sent to the grid and so storage is unnecessary.

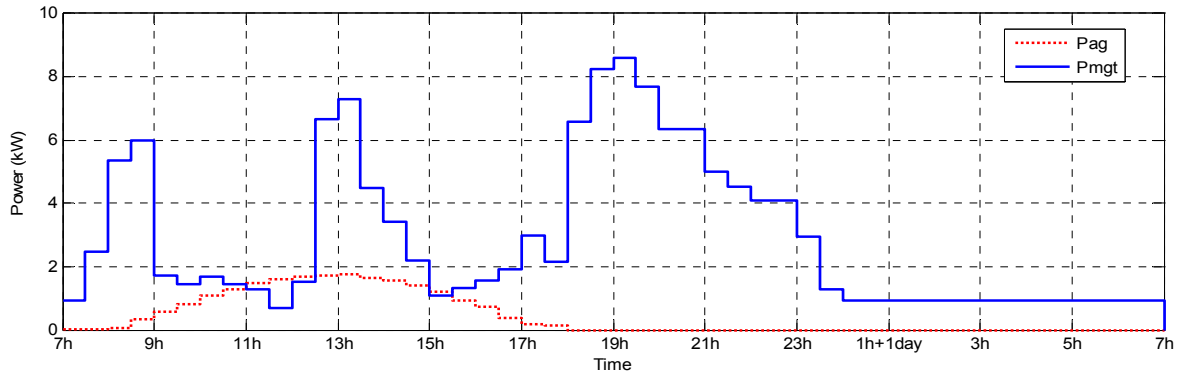


Figure IV.41 Central Micro Grid Controller Power References setting for the case of one producer

According to experimental results, the produced electrical energies of each generator can be deduced. The PV power provides 17% of the total power supply and the MGT power covers the remaining power 83% (Figure IV.42).

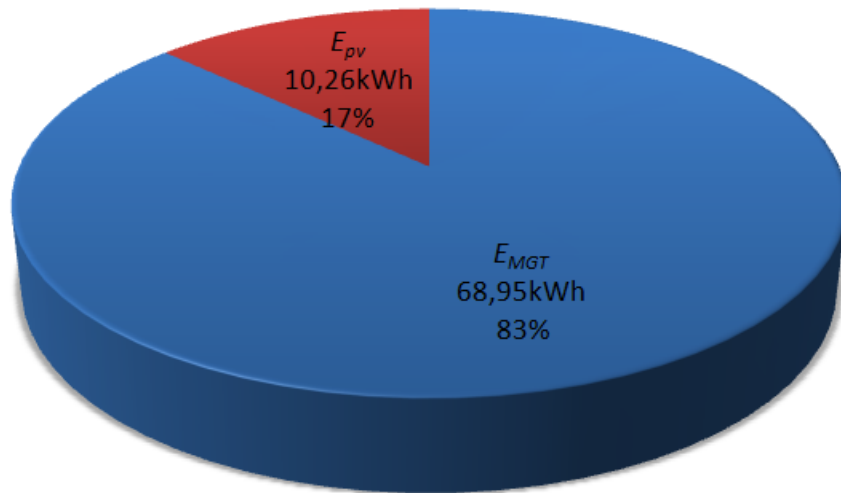


Figure IV.42 Energy consumption percentages for the case of one producer

**b. Impact of full scaled PV based producers**

In this studied case the four houses have each one 3kW peak power PV panels. The considered load profile is the same as previously. For this test, there is no storage installation in local. As houses are closed, PV productions are nearly equal and the total PV power is shown on Figure IV.43; the load forecasting remains the same.

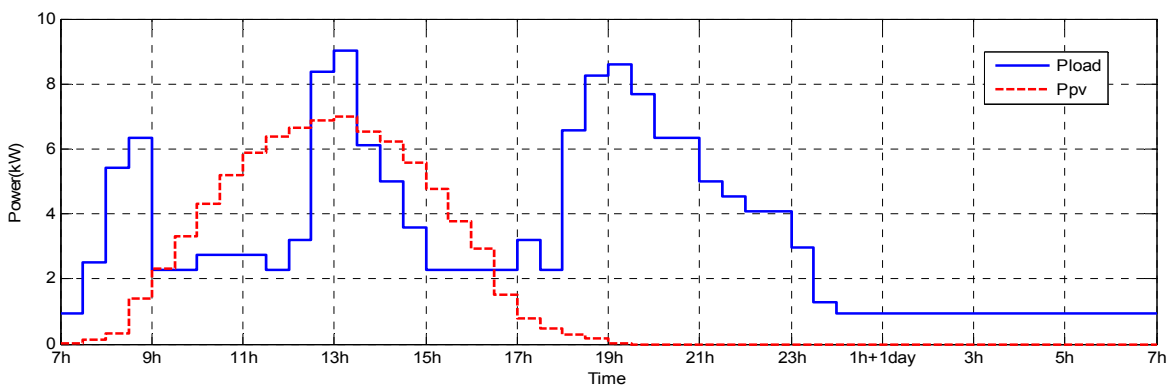


Figure IV.43 24 hour-ahead PV power and load forecasting

In order to make easier comparisons, the four power references for prosumers have been summed in Figure IV.44. Sensed PV powers are also summed in Figure IV.45. Between 9h00 and 12h30 and between 13h30 and 16h30, the PV power is limited and the gas turbine is driven with his minimum value since the loads are not enough. Hence a part of the available PV power is lost. Moreover the turbine has to provide alone the power peak at 19h00. The PV power provides 36% of the total power supply and the MGT power covers the remaining power 64% (Figure IV.46).

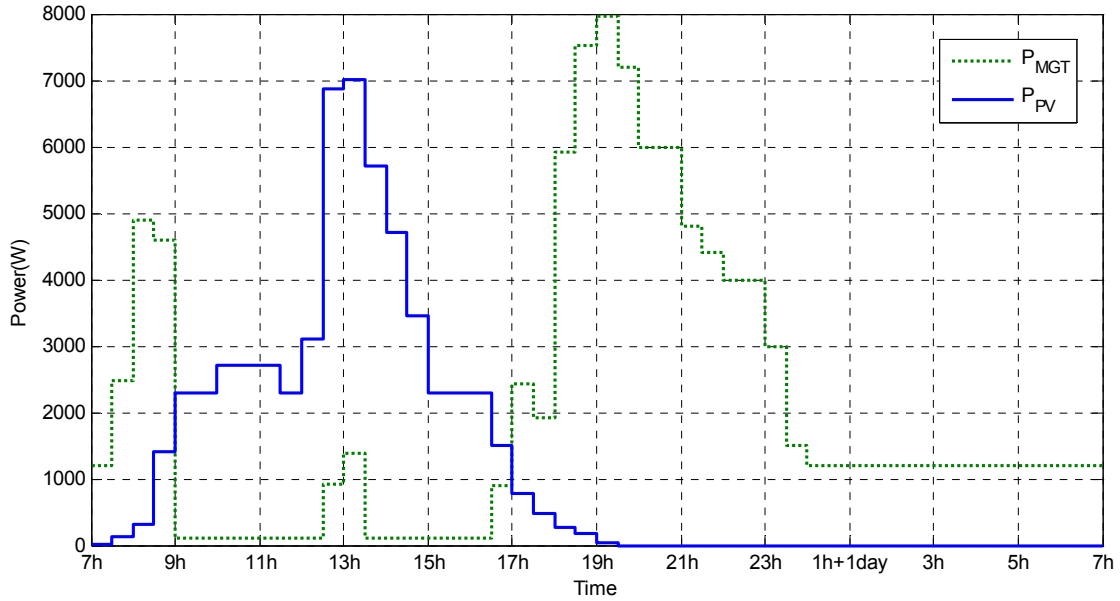


Figure IV.44 Central Micro Grid Controller power references setting

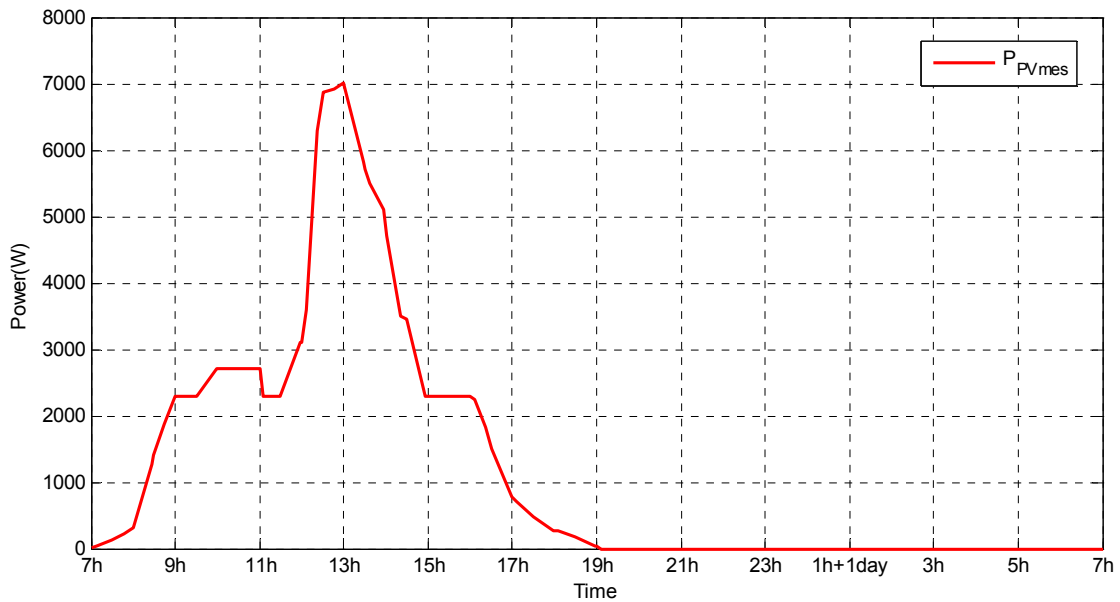


Figure IV.45 Total sensed PV power

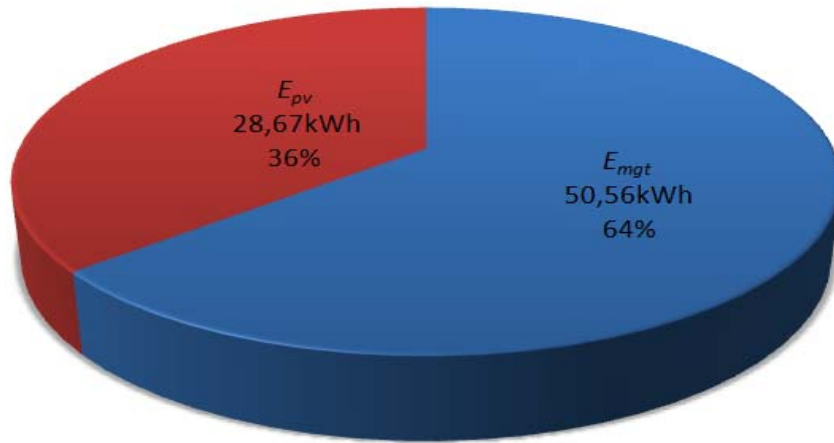


Figure IV.46 Energy consumption percentages for full scaled PV based producers without energy storage

**c. Impact of full scaled PV based prosumers with energy storages**

4 sets of 106Ah batteries are now added with a total 3200 W maximum charging power and a total 2000 W maximum discharging power. The same 24 hour-ahead PV power prediction and load forecasting are used.

The energy analysis shows that the total available PV energy is larger than the requested one from loads during the day. The available energy for battery storage is nearly equal to the energy of the gas turbine during the day. This energy is used for the night operating and so reduces the energy from the gas turbine during the night-operating.

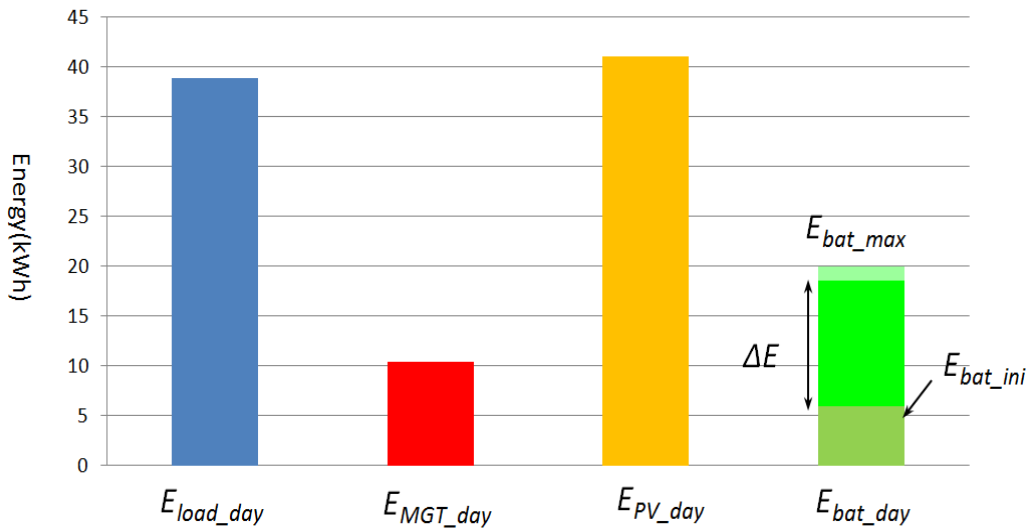


Figure IV.47 Energy analysis for the day-time for full scaled PV based producer

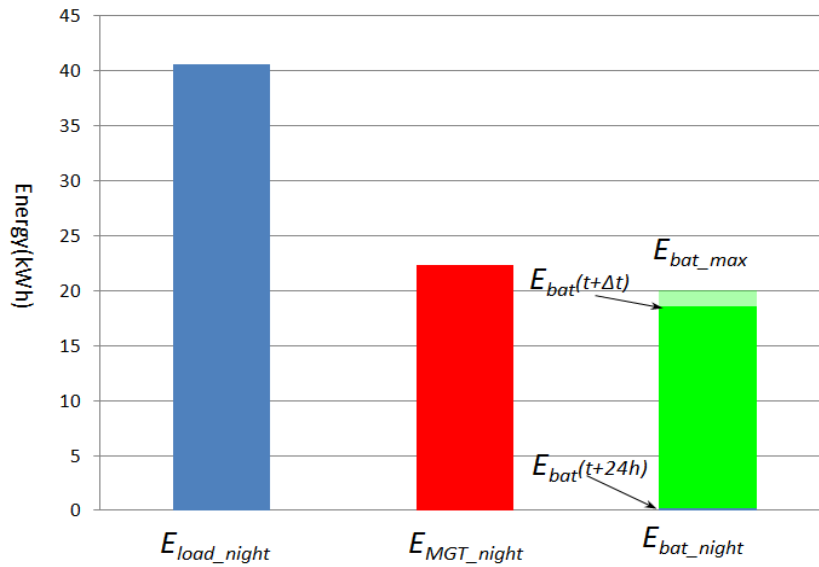


Figure IV.48 Energy analysis for the night-time for full scaled PV based producer

During the day the PV power is the same as previously. At the start of the night-time power references for prosumers are setting to disload batteries. The turbine peak power is a little bite decreased (Figure IV.49, Figure IV.50).

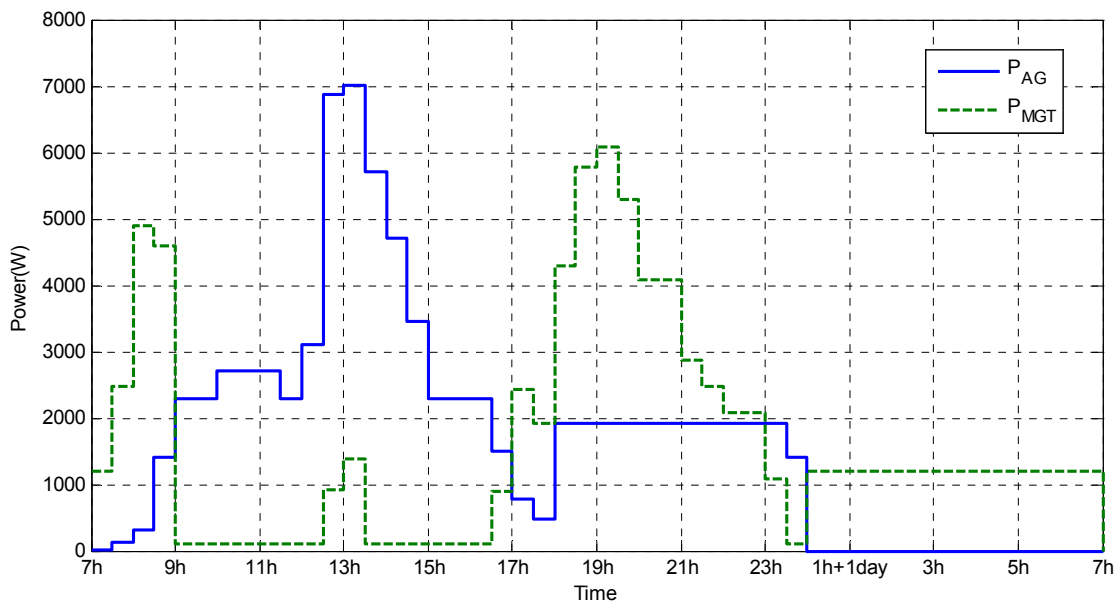


Figure IV.49 Central Micro Grid Controller power references for full scaled PV based prosumers with energy storages

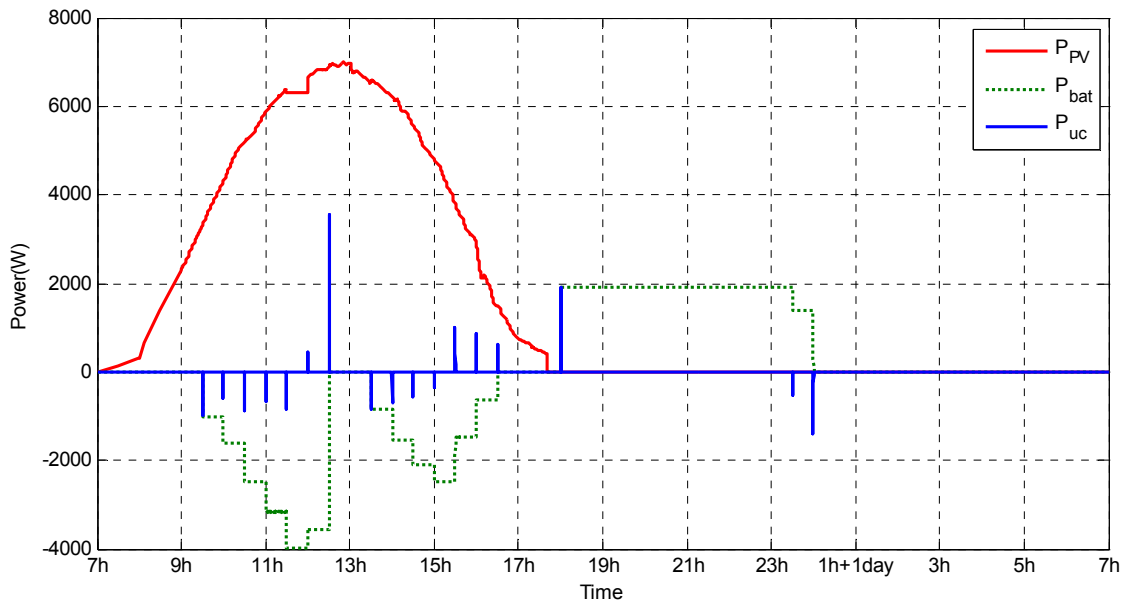


Figure IV.50 Local PV active generator controller power references setting for full scaled PV based prosumers with energy storages

Thanks to the batteries, more PV power is used and the penetration of the PV power generation is increased to 41%.

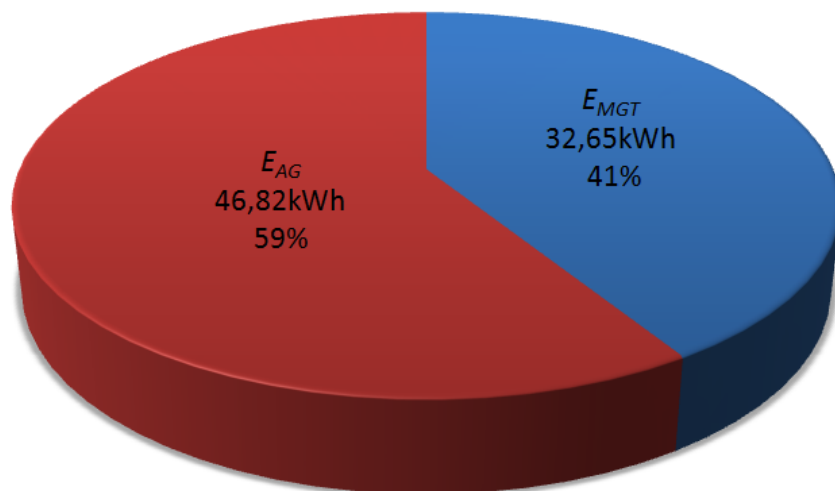


Figure IV.51 Energy consumption percentages for full scaled PV based producer

## IV.8. Conclusions

The main objective of this chapter is to describe the conceptual technical architecture developed to enable prosuming by the use an active generator and the application of microgrid concepts. A planning and an innovative energy management system concept for the smart networking of active based DGs into a residential micro grid are presented. A coordinated management of energy resources is proposed through a communication network. The energy management is organized in three parts: the long-term energy management, the medium-term energy management and the short-term power management.

The long-term energy management takes into account the PV power prediction and the load forecasting and makes a 24-hour power planning. It also determines the loading and

disloading tracking of batteries by taking into account the available PV power and the load demand. A deterministic algorithm is proposed and is based on predicted data about the load and the PV production.

Then the medium-term energy management sets the power references for each generator every half hour according to available new PV power and load forecasting. In the same time, a battery charging and discharging algorithm with a constant power is implemented.

The active generator contributes to the short-term power management of the microgrid by using a primary frequency control.

The inner power balancing is performed in real time by using ultracapacitors.

In the end of this chapter, the correct coordination of generators and the correct distribution of powers are tested on a real time simulator. One advantage is the fact that control functions are executed onto real control devices in real time. The hybrid real-time analysis enables the test of algorithms for the energy management of the residential distribution power system face to situations, which can reproduce the various static and dynamic phenomena that can occur in a real power system. As example in this chapter for an identical PV illumination and a load profile, results from various configurations have been compared and show the impact of the battery sizing on the penetration of PV power in an electrical system.





# *General conclusion*



Faced with the challenges of the energy and the environmental crisis, the development of renewable energies is encouraged. But their intermittent and fluctuant characteristics restrict the use of PV power as a main source of an electrical system. In this PhD thesis, the concept of the PV based active generator is presented and consists in coupling on a common DC bus energy storage systems by in order to smooth the PV power fluctuations and to constitute an available energy reserve.

In the first chapter, PV panels are modeled as a DC current source with the current output dependant on the terminal voltage, the temperature and the solar irradiation. According to the analysis of the different storage technologies, the batteries and the ultracapacitors are respectively chosen for the long-term energy storage unit and the fast power responding storage units. The different models of storage components are detailed. Finally, the appropriate models are applied for the whole system modeling.

In the second chapter, the whole PV active generator is modeled by the macroscopic energetic representation, which highlights the power conversion chains. Then a hierarchical structure of the control system has been proposed. The structure of this hierarchical control system includes 4 levels: switching control, automatic control, power control and mode control. Each one performs precise control tasks and is designed by applying a “multilevel formalism”..

A state of the art about micro grids is presented. The different control methods for the generator-side converter implement respectively the different operation mode of the micro grid (grid connected mode and islanded mode). The grid following strategy and the power dispatching strategy enable the transformation of distributed generators into dispatchable generators. Various functions of an energy management for an electrical system are also defined.

The last chapter presents a determinist planning and an innovative energy management system concept for the smart networking of DGs into a residential micro grid. A coordinated management of energy resources is proposed through a communication network. For the integration of PV active generators in this microgrid, an embedded local energy management is in charge of local power production and participation to the ancillary services. Then a central Energy Management System of the micro grid is implemented through the long-term power planning, the medium-term power set point adjusting and the short-term power balancing. In the end, experimental results from the tests on a laboratory microgrid platform valid the control strategies.

This thesis has developed a PV based active generator with an energy storage system in a DC-coupled structure. Several strategies for the energy management of storage units are designed to provide power references and provide ancillary services to the electrical grid

A technical conceptual architecture of an electrical system has been developed to enable active renewable production and exploit its benefits

Various microgrid concepts and control systems has been extended for managing DGs in a residential microgrid by using a communication network. A time-scale analysis method is applied for the energy management of this micro grid. The proposed management strategies allow a smarter operation by coordinating different sources by a long-term power determinist planning, half-hour set point adjusting and a real-time power balancing.

First application cases have been developed and only partially responds to the problem of energy management have been exposed. It would be interesting to further explore and study various scenarios for different load profiles and production from renewable energy. In this work, a deterministic approach has been chosen for the power operational planning

with a strong assumption to have the load forecast and production forecast of intermittent generators.

The prediction errors are compensated in real time by the primary controllers, which then no longer guarantees necessarily a maximum value for renewable energy and then the system loses much of its interest. Improvements about the reactivity to prediction errors or uncertainties could be sought.

Further works can now be oriented to the optimization of the residential microgrid system by considering the economic (initial investment cost, the operation and maintenance cost) and environmental impacts ( $\text{CO}_2$ ,  $\text{NO}_x$  emissions). A non linear optimization with multi optimization variables is required and may be studied in the future.

# *Appendix*



## Appendix I. Technical data of multisource

### A.I.1. PV panels



## BP 3160

160 Watt Photovoltaic Module

High-efficiency photovoltaic module using silicon nitride multicrystalline silicon cells

#### Performance

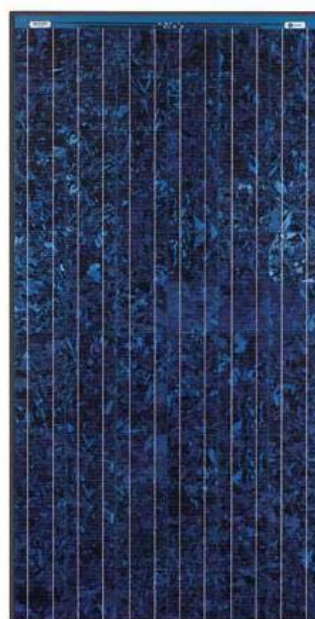
Rated power ( $P_{max}$ )	160W
Power tolerance	± 5%
Nominal voltage	24V
Limited Warranty <sup>1</sup>	25 years

#### Configuration

<b>B</b> BP 3160B	Bronze frame with output cables and polarized Multicontact (MC) connectors
<b>S</b> BP 3160S	Clear universal frame with output cables and polarized Multicontact (MC) connectors
<b>L</b> BP 3160L	Unframed laminate version of BP 3160S
<b>U</b> BP 3160U	Clear universal frame with standard junction box

#### Electrical Characteristics<sup>2</sup>

	BP 3160
Maximum power ( $P_{max}$ ) <sup>3</sup>	160W
Voltage at Pmax ( $V_{mp}$ )	35.1V
Current at Pmax ( $I_{mp}$ )	4.55A
Warranted minimum $P_{max}$	152W
Short-circuit current ( $I_{sc}$ )	4.8A
Open-circuit voltage ( $V_{oc}$ )	44.2V
Temperature coefficient of $I_{sc}$	(0.065±0.015)%/°C
Temperature coefficient of $V_{oc}$	-1160±20mV/°C
Temperature coefficient of power	-0.5±0.05)%/°C
NOCT (Air 20°C; Sun 0.8kW/m <sup>2</sup> ; wind 1m/s)	47±2°C
Maximum series fuse rating	15A (S, L); 20A (U)
Maximum system voltage	600V (U.S. NEC & IEC 61215 rating) 1000V (TUV Rheinland rating)



#### Mechanical Characteristics

Dimensions	<b>B,S,U</b>	Length: 1593mm (62.8")	Width: 790mm (31.1")	Depth: 50mm (1.97")
	<b>L</b>	Length: 1580mm (62.2")	Width: 783mm (30.8")	Depth: 19mm (0.75")
Weight	<b>B,S,U</b>	15.0 kg (33.1 pounds)		
	<b>L</b>	12.4 kg (27.3 pounds)		
Solar Cells	<b>B,S,L,U</b>	72 cells (125mm x 125mm) in a 6x12 matrix connected in series		
Output Cables	<b>B,S,L</b>	RHW AWG# 12 (4mm <sup>2</sup> ) cable with polarized weatherproof DC rated Multicontact connectors; asymmetrical lengths - 1250mm (-) and 800mm (+)		
Junction Box	<b>U</b>	Standard junction box with 6-terminal connection block; IP 54, accepts PG 13.5, M20, ½ inch conduit, or cable fittings accepting 6-12mm diameter cable. Terminals accept 2.5 to 10mm <sup>2</sup> (8 to 14 AWG) wire.		
Diodes	<b>B,S,L,U</b>	Three 9A, 45V Schottky by-pass diodes included		
Construction	<b>B,S,L,U</b>	Front: High-transmission 3mm (1/8 <sup>th</sup> inch) tempered glass; Back: Tedlar; Encapsulant: EVA		
Frame	<b>B,S,U</b>	Anodized aluminum alloy type 6063T6 Universal frame; Color: bronze (B); silver (S,U)		

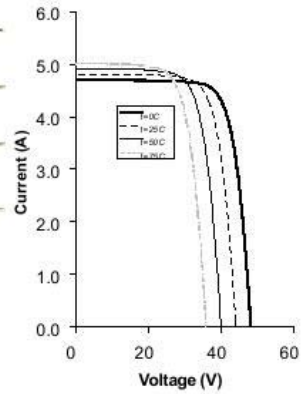
1. Warranty: Power output for 25 years. Freedom from defects in materials and workmanship for 5 years. See our website or your local representative for full terms of these warranties.
2. These data represent the performance of typical BP 3160 products, and are based on measurements made in accordance with ASTM E1036 corrected to SRC (STC.)
3. During the stabilization process that occurs during the first few months of deployment, module power may decrease by up to 3% from typical  $P_{max}$ .



**Quality and Safety**

<b>ESTI</b>	Module power measurements calibrated to World Radiometric Reference through ESTI (European Solar Test Installation at Ispra, Italy)
<b>CE</b>	Manufactured in ISO 9001-certified factories; conforms to European Community Directives 89/33/EEC, 73/23/EEC, 93/68/EEC; certified to IEC 61215
<b>TUV</b>	Framed modules certified by TÜV Rheinland as Safety Class II (IEC 60364) equipment for use in systems up to 1000 VDC
<b>UL</b>	Listed by Underwriter's Laboratories for electrical and fire safety (Class C fire rating)
<b>FM</b>	Approved by Factory Mutual Research in NEC Class 1, Division 2, Groups C & D hazardous locations (U)

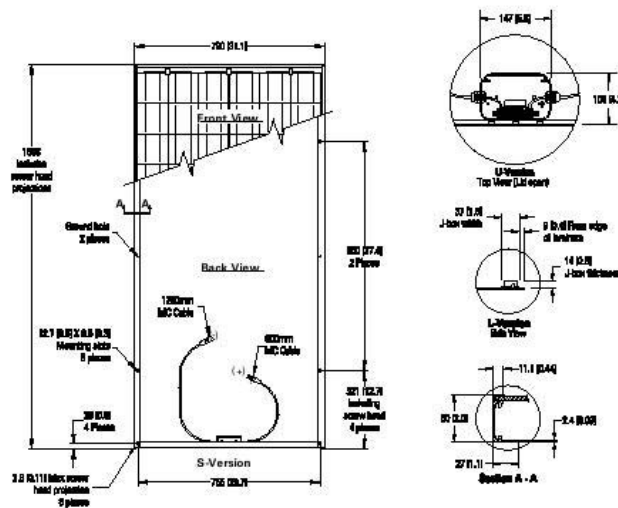
**BP 3160 I-V Curves**



**Qualification Test Parameters**

Temperature cycling range	-40°C to +85°C (-40°F to 185°F)
Humidity freeze, damp heat	85% RH
Static load front and back (e.g. wind)	50psf (2400 pascals)
Front loading (e.g. snow)	113psf (5400 pascals)
Hailstone impact	25mm (1 inch) at 23 m/s (52mph)

Dimensions in brackets are in inches. Unbracketed dimensions are in millimeters. Overall tolerances ±3mm (1/8")



**Included with each module:** self-tapping grounding screws, instruction sheet, and warranty document.

**Note:** This publication summarizes product warranty and specifications, which are subject to change without notice.



## A.I.2. Lead-acid battery



### Batteries de stockage

3



### Série STECO

#### Batteries de stockage - C100

ST 3000 / 3500 / 4000

#### DONNÉES TECHNIQUES

Note : toutes nos indications peuvent faire l'objet de changements sans préavis



	ST 3000	ST 3500	ST 4000
<b>Caractéristiques générales</b>			
Tension nominale	12 Volts	12 Volts	12 Volts
Capacité C100 (5h-20h / décharge à 20°)	186 Ah	118 Ah	148 Ah
Courant nominal	8 A	8,8 A	8,8 A
Quantité d'électrolyte par batterie III	6,600	5,420	5,210
Densité de l'électrolyte (à 20°C temp-20)	1,280	1,280	1,280
Température de service	-15°C/+40°C	-15°C/+40°C	-15°C/+40°C
Décharge profonde en % de Ch	90%	90%	90%
Tension de floatage à 20°C (référence à 110)	13,50 V	13,50 V	13,50 V
Tension de décharge profonde	10,50 V	10,50 V	10,50 V
Tension max de charge / rapide (CHG / en floatage)	14,40 / 13,50 V	14,40 / 13,50 V	14,40 / 13,50 V
Intensité max de charge	28 A	30 A	30 A
Autodécharge batterie remplie	4 %	4 %	4 %

#### Autres données

Formes pleins	Carré conical	Carré conical	Carré conical
Paléfix de manipulation	Oui	Oui	Oui

#### Poids / dimensions

Poids (sans / avec électrolyte)	18,710 / 26,490 Kg	18,220 / 26,140 Kg	27,820 / 38,560 Kg
Dimensions	345x172x249 mm	300x175x213 mm	512x180x223 mm

### Série STECO

#### Batteries de stockage C100

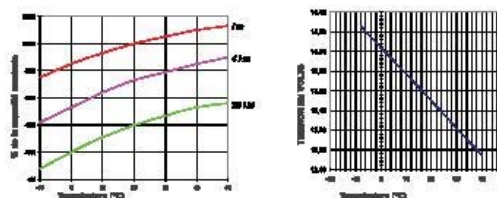
#### Certifiés CE

- Gamme en C100
- Durée de vie optimale
- Large gamme

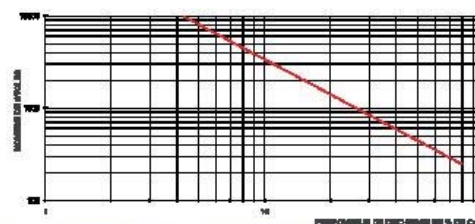
Contact :

[Infos@ecolephoto.fr](mailto:Infos@ecolephoto.fr)

> Influence de la température sur les performances d'exploitation



> Interférence au système



#### Ecole Distribution

ZI MOZINOR lot numéro 10  
2 à 20 av. du président G. Mitterrand 89100 Montmaillemont FRANCE

Capital 30 000€ RCE Bourgoy 492 871 003

### A.I.3. Ultracapacitor



#### MC BMOD Power Series 48v BOOSTCAP® Ultracapacitor Modules

<b>p</b>	<b>Series: MC BMOD Power</b> <b>48 Volt Module</b>	<ul style="list-style-type: none"> <li>» Ultra Low Internal Resistance</li> <li>» Highest Power Performance Available</li> <li>» Lowest Time Constant</li> </ul>
----------	---	--

› **Features:**

- » 48.6V Operating Voltage
- » Ultra Low internal resistance
- » Over 1M duty cycles
- » Individually balanced cells
- » Voltage and temperature sensor output included
- » Compact, rugged, fully enclosed and splash proof design

› **Applications:**

- » Transportation
- » Automotive
- » Industrial
- » UPS
- » Telecommunication



› **Overview:**

The Power-type ultracapacitor product line gives customers in the automotive and transportation sector a much wider range of choices to meet their energy storage and power delivery requirements.

The modules are specifically engineered for hybrid vehicle drive trains, automotive subsystems and other heavy duty applications that require the lowest equivalent series resistance (ESR) and highest efficiency available.

In addition to meeting or exceeding demanding automotive and transportation application requirements for both watt-hours of energy storage and watts of power delivery per kilogram, all of these products will perform reliably for more than one million discharge-recharge cycles.

The proprietary architecture and material science on which BOOSTCAP® products are based enable continued leadership in controlling costs, flexibility in product offerings and allow application specific performance tailoring. The cells used in the modules operate at 2.7 volts, enabling them to store more energy and deliver more power per unit volume than any other commercially available ultracapacitor products.

MC BMOD Power Series 48v BOOSTCAP® Ultracapacitor Modules

› BMOD Series 48v Specifications:

Item	Performance	
Operating Temperature Range	-40 °C to +65 °C	
Storage Temperature Range	-40 °C to +70 °C	
Rated Voltage	48.6 V DC	
Capacitance Tolerance	+20/-5%	
Resistance Tolerance	Max.	
Temperature Characteristics	Capacitance Change	Within ± 5% of initial measured value at 25 °C ( at -40 °C)
	Internal Resistance	Within 150% of initial measured value at 25 °C (at -40 °C)
Endurance	After 1500 hours application of rated voltage at 65 °C	
	Capacitance Change	Within 20% of initial specified value
	Internal Resistance	Within 60% of initial specified value
Shelf Life	After 1500 hours storage at 65 °C without load shall meet specification for endurance	
Life Test	After 10 years at rated voltage and 25 °C	
	Capacitance Change	Within 30% of initial specified value
	Internal Resistance	Within 150% of initial specified value
Cycle Test	Capacitors cycled between specified voltage and half rated voltage under constant current at 25 °C (1 million)	
	Capacitance Change	Within 30% of initial specified value
	Internal Resistance	Within 150% of initial specified value

› BMOD Series 48v Product Specifications:

Maxwell Part No.	Capacitance (F)	ESR, DC (mohm)	ESR, 1kHz (mohm)	Ic (mA)
BMOD0083 P048	80	12.3	9.8	3.0
BMOD0110 P048	110	9.5	7.6	4.2
BMOD0165 P048	165	7.1	5.2	5.2

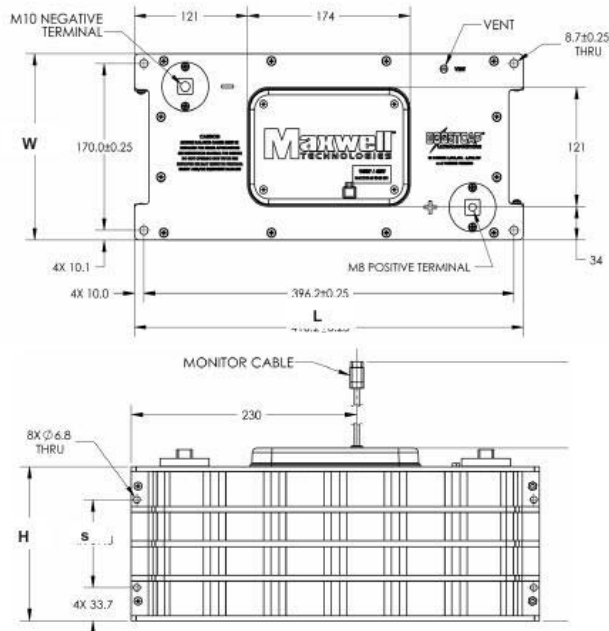
› BMOD Series 48v Product Properties:

Maxwell Part No.	Rth (C/W)	Isc (A)	E <sub>max</sub> (Wh/kg)	P <sub>max</sub> (W/kg)	Pd (W/kg)
BMOD0083 P048	0.39	3,900	2.48	5,400	2,000
BMOD0110 P048	0.33	4,300	2.91	6,200	2,400
BMOD0165 P048	0.25	4,800	3.81	7,900	3,200



**MC BMOD Power Series 48v BOOSTCAP® Ultracapacitor Modules**

› **Dimensions:**



Part Number	Vol (l)	Mass (kg)	Size (mm)			
			L (+/- 0.25)	W (+/- 0.25)	H (+/- 0.25)	s (+/- 0.5)
BMOD0083 P048	8.5	11.0	416.2	190.1	103.2	53.7
BMOD0110 P048	9.8	12.4	416.2	190.1	120.2	70.7
BMOD0165 P048	12.6	14.2	416.2	190.1	156.7	89.3

Product dimensions and specifications may change without notice. Please contact Maxwell Technologies directly for any technical specifications critical to application.

› **Markings: Modules are marked with the following information**

Rated capacitance, rated voltage, product number, name of manufacturer, positive and negative terminal, warning marking, serial #

› **Mounting Recommendations:**

Modules can be secured at 8 locations, 4 front face and/or 4 bottom face, at provided holes for M8 bolt. Follow user manual instructions for terminal, balance and output connections.

Patent Pending

Worldwide Headquarters	European Office	 <a href="http://www.maxwell.com">www.maxwell.com</a>
MAXWELL TECHNOLOGIES 9244 Balboa Avenue • San Diego, 92123 CA, USA PHONE: + (1) 858 503 3300 FAX: + (1) 858 503 3301 EMAIL: info@maxwell.com	MAXWELL TECHNOLOGIES SA CH-1728 Rossens • Switzerland PHONE: +41 (0) 26 411 85 00 FAX: +41 (0) 26 411 85 05 EMAIL: info@maxwell.com	



› **Additional Technical Information:**

Capacitance and ESR, DC measured per document 1007239

$I_c$  = Leakage current after 72 hours, 25°C       $I_{sc}$  = short circuit current (maximum peak current)

$R_{th}$  = Thermal resistance

$$E_{max} = \frac{\frac{1}{2} CV^2}{3600 \times mass} \qquad P_{max} = \frac{V^2}{4R (1kHz) \times mass} \qquad P_d = \frac{0.12V^2}{R (DC) \times mass}$$

**Disclaimer of Warranty/Limitation of Liability  
for Uses in Life Support Devices or Critical Systems**

Maxwell Technologies, Inc. and its Affiliates ("Maxwell") provide no warranties of any kind either express or implied, including (without limitation) the implied warranties of merchantability and fitness, for uses of its products as components in life support devices or critical systems.

"Life support devices" are devices or systems, which (a) are intended for surgical implant into a living body, or (b) support or sustain life, and whose failure to perform when properly used in accordance with the instructions provided in the labeling can be reasonably expected to result in bodily injury to the user. An example of a life support device includes, but is not limited to, a heart pacemaker.

A "critical system" is any system whose failure to perform can affect the safety or effectiveness of a higher level system, or cause bodily or property injury by loss of control of the higher level device or system. An example of a critical system includes, but is not limited to, aircraft avionics.

Maxwell will not be liable to you for any loss or damages, either actual or consequential, indirect, punitive, special, or incidental, arising out of or relating to these terms.

Patent Pending

Worldwide Headquarters	European Office	 <a href="http://www.maxwell.com">www.maxwell.com</a>
MAXWELL TECHNOLOGIES 9244 Balboa Avenue • San Diego, 92123 CA, USA PHONE: +1(1) 858 503 3300 FAX: +1(1) 858 503 3301 EMAIL: info@maxwell.com	MAXWELL TECHNOLOGIES SA CH-1728 Rossens • Switzerland PHONE: +41 (0) 26 411 85 00 FAX: +41 (0) 26 411 85 05 EMAIL: info@maxwell.com	

## Appendix II. Comparison of ultracapacitor model simulation and experimentation test

En imposant un échelon de courant  $i_L$ , la Figure AII-1 montre l'évolution temporelle de la tension  $v_{sc}$ .

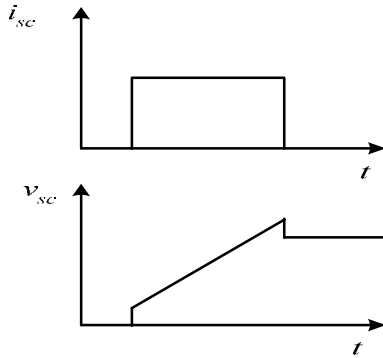


Figure AII-1. Evolution temporelle de  $v_{sc}$  en fonction de  $i_{sc}$

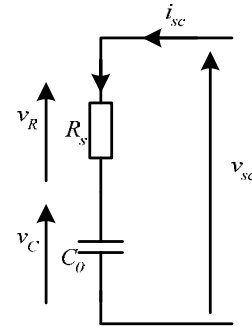


Figure AII-2. Modèle simplifié du supercondensateur

A partir du modèle simplifié obtenu (Figure AII-2), nous avons établi un modèle présenté à la Figure AII-3. Les supercondensateurs sont représentés par une source électrique ayant le courant de l'inductance du filtre en entrée  $i_{sc}$  et la tension en sortie  $v_{sc}$ .

Les équations sont présentées ci-après (AII-1), (AII-2) et (AII-3).

$$i_{sc} = C_0 \frac{dv_C}{dt} \rightarrow \frac{dv_C}{dt} = \frac{1}{C} \cdot i_{sc} \quad (\text{AII-1})$$

$$v_R = R_s i_L \quad (\text{AII-2})$$

$$v_{sc} = v_C + v_R \quad (\text{AII-3})$$

Un essai est effectué pour comparer entre la simulation et l'expérimentation. En imposant un profil de courant  $i_{sc}$  (Figure AII-3), on a tracé l'évolution temporelle de tension  $v_{sc}$  présentée à la Figure AII-4. La tension obtenue par simulation correspond bien à celle mesurée par l'expérimentation. Cette comparaison valide donc notre modélisation.

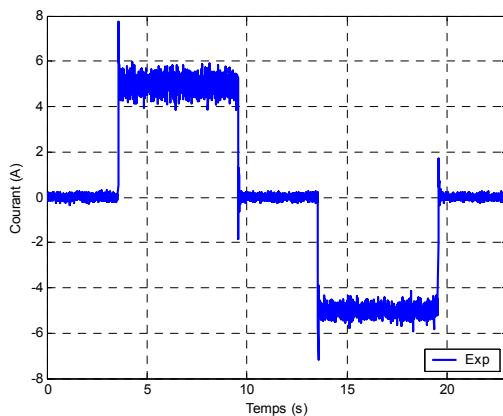


Figure AII-3. Evolution temporelle de  $i_{sc}$

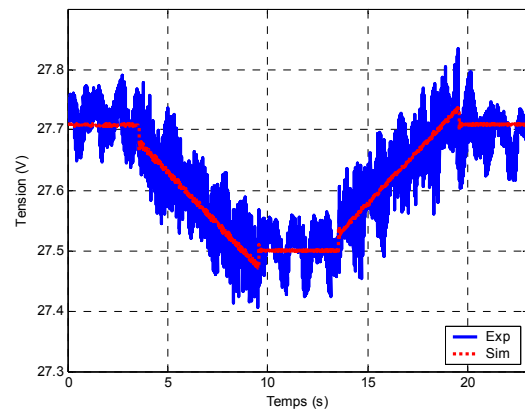


Figure AII-4. Evolution temporelle de  $v_{sc}$  en fonction de  $i_{sc}$

## Appendix III. Equivalent Continuous Modeling of Power Converters

### A.III.1. Fundamental recall

Equivalent continuous models of the power electronic converters are sufficient for our study, because we do with the power balancing and energy management strategies of a hybrid power system in order to transform it into an active generator [Rob 01][Rob 02]. In our study, three types of power converters are used: 1) the DC chopper, 2) the three-phase inverter and 3) the three-phase rectifier. They are all connected to a DC-bus capacitor. The studies with the equivalent continuous modeling of power converters are carried out under the following assumptions:

- switches are ideal;
- switchings are instantaneously;
- switches are considered as short circuits in ON state and as open circuits in OFF state.

A switching function ( $s_{ij}$ ) is defined for each power switch. It represents the ideal commutation order and takes the values 1 when the switch is closed (ON) and 0 when it is opened (OFF).

$$s_{ij} \in \{0,1\} \text{ with } \begin{cases} i \in \{1,2,3\} \text{ n}^\circ \text{ of the leg} \\ j \in \{1,2\} \text{ n}^\circ \text{ of the switch in the commutation circuit} \end{cases}$$

As ideal power switches are considered, the switches in a same commutation circuit are in complementary states:

$$s_{i1} + s_{i2} = 1 \quad \forall i \in \{1,2,3\}$$

### A.III.2. Equivalent continuous modeling

#### a. DC chopper modeling

In our power electronic structure a DC chopper is located between a current source and a voltage source. For the super-capacitor storage system, the current source is the choke  $L_{sc}$  and generates the current  $i_{sc}$ . The DC-bus capacitor is the voltage source and generates the voltage ( $u_{dc}$ ) (Figure AIII-1).

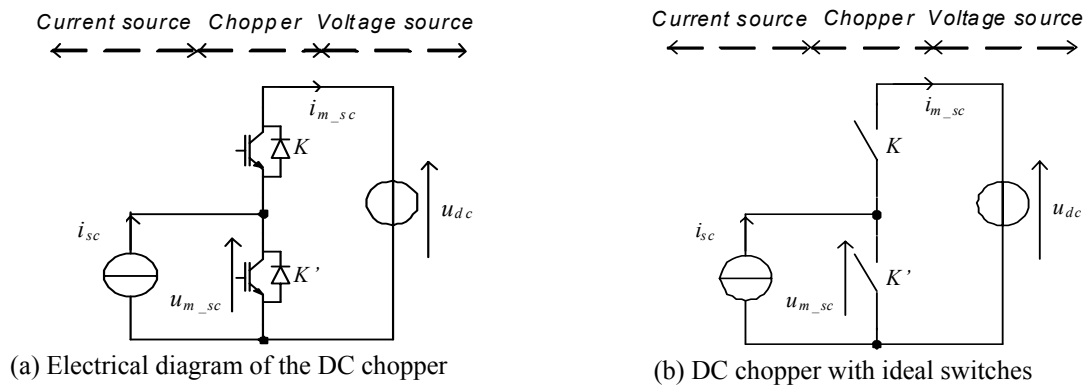


Figure AIII-1: Diagram of the DC chopper in the super-capacitor storage system



The modulation functions of the DC chopper can be expressed from the switching function ( $s_{sc1}$ ) of the first switch in the commutation circuit:

$$m_{sc} = s_{sc1}$$

Then the modulated voltage  $u_{m\_sc}$  and the modulated current  $i_{m\_sc}$  of the DC chopper are obtained as follows:

$$\begin{cases} u_{m\_sc} = m_{sc} u_{dc} \\ i_{m\_sc} = m_{sc} i_{sc} \end{cases}$$

In practice, a connection controller is used to create the two complementary switching functions ( $s_{sc1}$  and  $s_{sc2}$ ) with necessary dead times from the modulation function  $m_{sc}$ . Then the switching functions are converted into ON/OFF signal for each semi-conductor switch through some drivers and optocouplers. The modulation function  $m_{sc}$  is obtained by comparing an average modulation function  $\langle m_{sc} \rangle$  with a triangular signal  $\zeta$  (Figure AIII-2).

In theory, when the modulation frequency of the carrier signal  $\zeta$  is much higher than the frequency domain of the control signal (which is a continuous value for the DC chopper), the average modulation function can be obtained as follows:

$$\langle m_{sc} \rangle = \frac{1}{\Delta t} \int_{t_0}^{t_0+\Delta t} m_{sc}(t) dt + m_{sc}(t_0).$$

By considering that the voltage  $u_{dc}$  and the current  $i_{sc}$  are constant during the time interval  $\Delta t$ , the average values of the modulated voltage  $\langle u_{m\_sc} \rangle$  and the modulated current  $\langle i_{m\_sc} \rangle$  are expressed as follows:

$$\begin{cases} \langle u_{m\_sc} \rangle = \langle m_{sc} \rangle u_{dc} \\ \langle i_{m\_sc} \rangle = \langle m_{sc} \rangle i_{sc} \end{cases}$$

As result, the equivalent average model of the DC chopper is obtained and the electrical diagram is shown in Fig.B-3. Finally, a variable  $\langle m_{sc} \rangle$  can be used to model the DC chopper.

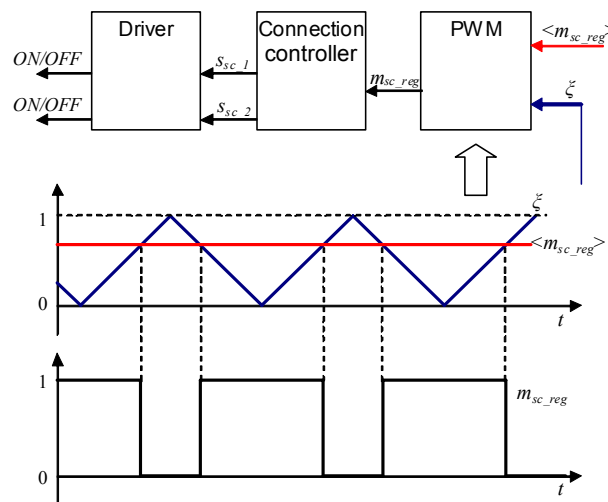


Figure AIII-2: Classical PWM method

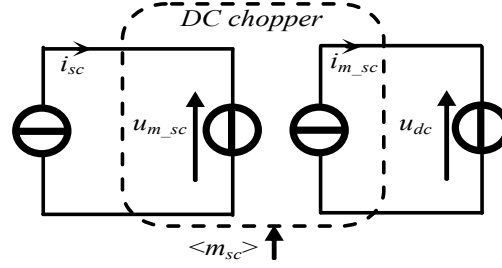


Figure AIII-3: Equivalent average electrical diagram of the DC chopper

**b. Three-phase inverter modeling**

In our study, a three-phase voltage source inverter VSI is used to connect the DC bus to the AC grid [Fra 99]. The task is to invert in real time the DC voltage into AC modulated voltages. The three-phase VSI is located between a three-phase current source and a voltage source. For the grid power conversion system, the current sources come from the choke filters and is set to generate the AC line current ( $\underline{i}_{line}=[i_{line\_1} \ i_{line\_2}]^T$ ) and the voltage source comes from the DC bus and is set to generate the DC-bus voltage ( $u_{dc}$ ) (Figure AIII-4).

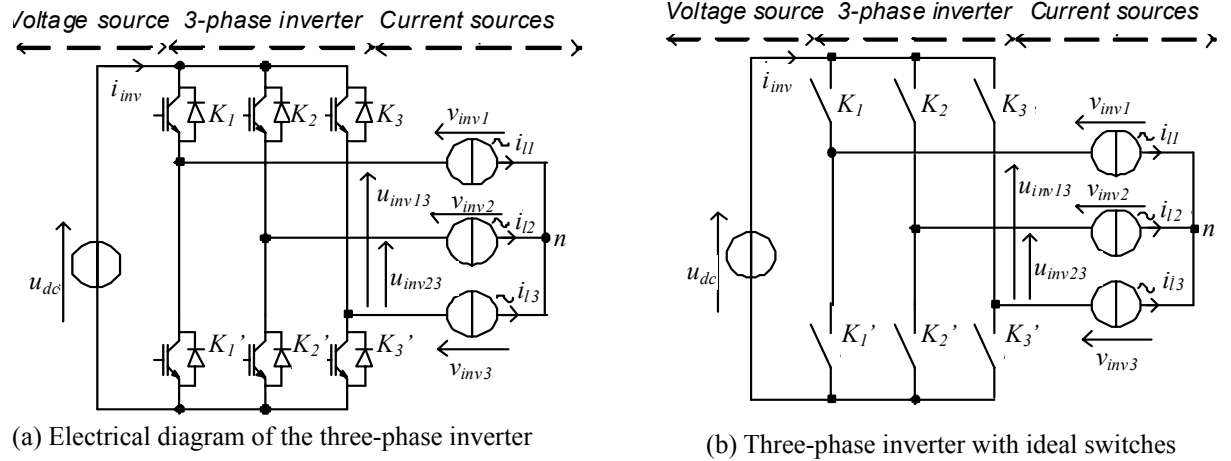


Figure AIII-4: Diagram of the three-phase inverter in the grid power conversion system

The modulation functions ( $\underline{m}_{inv}=[m_{inv13} \ m_{inv23}]$ ) of the three-phase inverter can be expressed from the switching functions ( $\underline{s}_{inv}=[s_{inv11} \ s_{inv21} \ s_{inv31}]$ ) of first switches of the three commutation circuits :

$$\underline{m}_{inv}(t) = \begin{bmatrix} m_{inv13}(t) \\ m_{inv23}(t) \end{bmatrix} = \begin{bmatrix} 1 & 0 & -1 \\ 0 & 1 & -1 \end{bmatrix} \begin{bmatrix} s_{inv11}(t) \\ s_{inv21}(t) \\ s_{inv31}(t) \end{bmatrix}.$$

Then the modulated voltage ( $\underline{u}_{inv}=[u_{inv13} \ u_{inv23}]^T$ ) and the modulated current  $i_{inv}$  of the three-phase inverter are obtained from the DC-bus voltage and the line currents ( $\underline{i}_l=[i_{l1} \ i_{l2}]$ ), which are considered constant during the time window  $\Delta t$  :

$$\begin{cases} \underline{u}_{inv}(t) = \underline{m}_{inv}(t) u_{dc} \\ \underline{i}_{inv}(t) = \underline{m}_{wg}^T(t) \underline{i}_l \end{cases}.$$

In practice, a connection controller is used to create the six switching functions  $\{s_{inv11},$

$S_{inv12}, S_{inv21}, S_{inv22}, S_{inv31}, S_{inv32}$  with necessary dead times from the modulation function  $m_{inv}$ . Then the switching functions are converted into ON/OFF state of each switch through some drivers and optocouplers. The modulation function  $m_{inv}$  can be obtained by comparing an average modulation function  $\langle m_{inv} \rangle$  with a triangular signal  $\zeta$  (Figure AIII-5).

In theory, when the modulation frequency of the carrier signal  $\zeta$  is much higher than the frequency domain of the control signals (which are sinusoidal values for the inverter) the average modulation function can be obtained as follows:

$$\langle \underline{m}_{inv} \rangle = \frac{1}{\Delta t} \int_{t_0}^{t_0+\Delta t} \underline{m}_{inv}(t) dt + \underline{m}_{inv}(t_0).$$

Then the average values  $\langle \underline{u}_{inv} \rangle$  and  $\langle i_{inv} \rangle$  of the modulated voltage and the modulated current are expressed as follows:

$$\begin{cases} \langle \underline{u}_{inv} \rangle = \langle \underline{m}_{inv} \rangle u_{dc} \\ \langle i_{inv} \rangle = \langle \underline{m}_{inv}^T \rangle i_l \end{cases}$$

The voltage  $u_{dc}$  and the currents  $i_l$  are assumed to be constant during the switching period. As result, the equivalent continuous model of the three-phase inverter is obtained and the electrical diagram is shown in Figure AIII-6. Finally, a vector  $\langle \underline{m}_{inv} \rangle$  can be used to model the three-phase inverter.

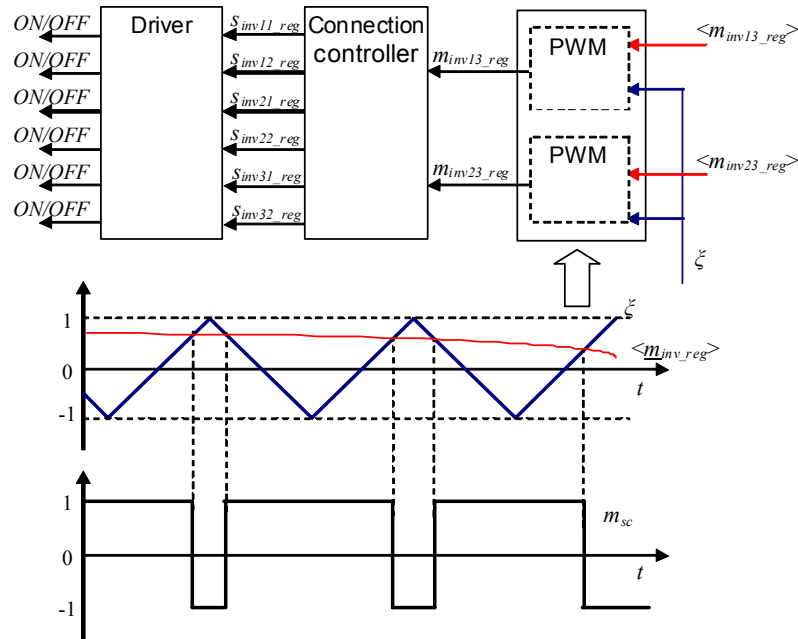


Figure AIII-5: Classical sinusoidal PWM method.

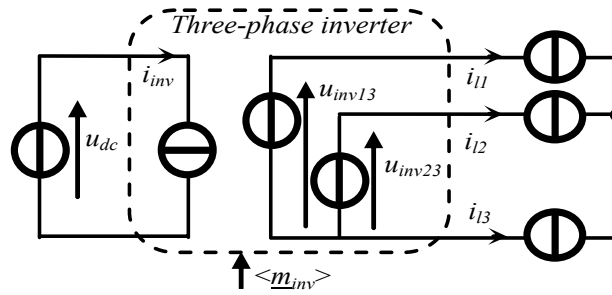


Figure AIII-6: Equivalent electrical diagram of the three-phase inverter

**c. Three-phase rectifier modeling**

A three phase rectifier is used to rectify three-phase sinusoidal currents from the machine of the wind generator. For the three-phase rectifier, similar relations are obtained for the average values of the modulated voltage ( $\langle \underline{u}_{rec} \rangle = [\langle u_{rec13} \rangle \ \langle u_{rec23} \rangle]^T$ ) and the modulated current ( $\langle i_{rec} \rangle$ ) from the DC-bus voltage  $u_{dc}$  and the currents ( $\underline{i}_{mac} = [i_{mac1} \ i_{mac2}]^T$ ) of the electrical machine, with the averaged vector ( $\langle \underline{m}_{rec} \rangle = [\langle m_{rec13} \rangle \ \langle m_{rec23} \rangle]^T$ ) of the rectifier modulation functions:

$$\begin{cases} \langle \underline{u}_{rec} \rangle = \langle \underline{m}_{rec} \rangle u_{dc} \\ \langle i_{rec} \rangle = \langle \underline{m}_{rec}^T \rangle \underline{i}_{mac} \end{cases}$$

As result, the equivalent continuous model of the three-phase inverter is obtained and the electrical diagram is shown in Figure AIII-7. Finally, a vector  $\langle \underline{m}_{rec} \rangle$  can be used to model the three-phase inverter.

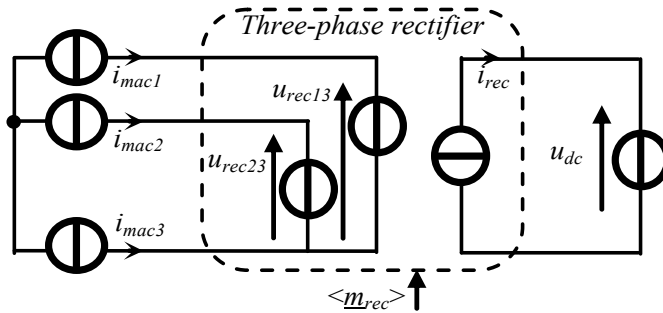


Figure AIII-7: Equivalent electrical average diagram of the three-phase rectifier

**A.III.3. Bibliography**

- [Rob 01] B. Robyns, M. Nasser, F. Berthereau, F. Labrique, “Equivalent continuous dynamic model of a variable speed wind generator” ELECTROMOTION 2001, vol.8, n°.4, pp. 202-208, dec. 2001.
- [Rob 02] B. Robyns, Y. Pankow, L. Leclercq, B. Francois, “Equivalent continuous dynamic model of renewable energy system”, ELECTRIMACS 2002, CD-ROM, 18-21 Aout 202, Montreal, Canada.
- [Mor 06] J. Moreno, M.E.Ortuzar, J.W.Dixon, “Energy-management system for a hybrid electric vehicle, using ultracapacitors and neural networks”, IEEE transactions on Industrial Electronics, vol.53, no.2, Apr. 2006, pp.614-623.

- [Fra 99] B. François, J.P. Hautier, "Pulse Position and Pulse Width Modulation of Electrical Power Conversions: Application to a Three-Phase Voltage-Fed Inverter", 3rd International Symposium on Advanced Electromechanical Motion Systems: ELECTROMOTION 1999, vol.2, pp.653-658, Patras, Greece, July 8-9,1999


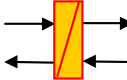
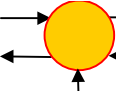
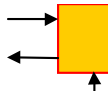
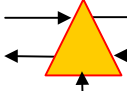
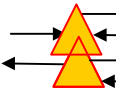


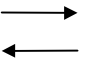
## Appendix IV. Energetic Macroscopic Representation (EMR)

EMR is based on action-reaction principle, which organises the system as interconnected subsystems according to the integral causality. Inversion of the graphical description by using specific rules leads to a Maximal Control Structure of the system. It is very suitable for research/development of complex multi-physic system [Bou 07].

### A.IV.1. Interaction principle

The system is decomposed into basic subsystems in interactions (Table AIV-1): energy sources (green ovals), accumulation elements (orange rectangles), conversion element without energy accumulation (various orange pictograms) and coupling elements for energy distribution (orange overlapped pictograms). All the elements are interconnected according to the action and reaction principle using exchange variable (arrows). The product of action and reaction variables between two elements leads to the instantaneous power exchanged.

Table AIV-1: Elements of EMR and of control

	Source of energy		Element with energy accumulation		Electromechanical converter (without energy accumulation)
	Electrical converter (without energy accumulation)		Mechanical converter (without energy accumulation)		Mechanical coupling device (energy distribution)
	Control block without controller		Control block with controller		Action and reaction variables

### A.IV.2. Causality principle

As in COG, only the integral causality is considered in EMR. This property leads to define accumulation element by a time-dependant relationship between its variables, in which its output is an integral function of its inputs. Other elements are described using relationships without time dependence. In order to respect the integral causality specific association rules are defined, but there are taught only in the expert level unit.

### A.IV.3. Inversion principle

The inversion based control theory has been initiated by COG. The control structure of a system is considered as an inversion model of the system because the control has to define the appropriated inputs to apply to the system from the desired output (Fig.A3-1). In this method, relationships without time-dependence are directly inverted (with neither control nor measurement). Because the derivative causality is forbidden, a direct inversion of time-dependence relationships is not possible. An indirect inversion is thus made using a controller and measurements. These inversion rules have been extended to EMR (blue pictograms, see Table A3-1): conversion elements are directly inverted and accumulation elements are inverted using controller. Moreover inversions of coupling element require distribution or weighted inputs. These inputs lead an organization of the energy distribution. This inversion methodology is another way to locate controllers and measurements or estimations.

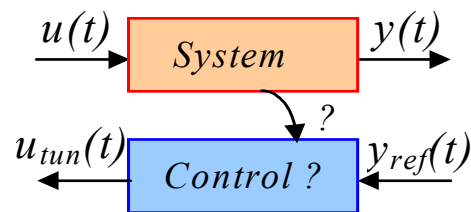


Figure AIV-1: Inversion-based control principle

### A.IV.4. Bibliography

- [Bou 07] A. Bouscayrol, A. Bruyère, P. Delarue, F. Giraud, B. Lemaire-Semail, Y. Le Menach, W. Lhomme, and F. Locment, “Teaching drive control using Energetic Macroscopic Representation – initiation level”, EPE 2007, Aalborg (Denmark), September 2007, CD-ROM.

## Appendix V. Utilisation du correcteur IP

L'annexe 5 présente l'utilisation des correcteurs IP dans la thèse. Ils sont utilisés pour concevoir la commande des éléments de stockage, comme une bobine  $L$ , une capacité  $C$ , ou une inertie  $J$ . Un correcteur IP peut être paramétré selon la structure de processus. La conception d'un correcteur IP pour deux structures de processus possibles est présentée dans cette annexe :

- Correcteur IP pour un élément de stockage seul ;
- Correcteur IP pour un élément de stockage avec un autre élément qui représente ses pertes.

### A.V.1. Calcul du correcteur IP pour un intégrateur pur

Le schéma bloc d'un correcteur IP est présenté par la figure suivante :

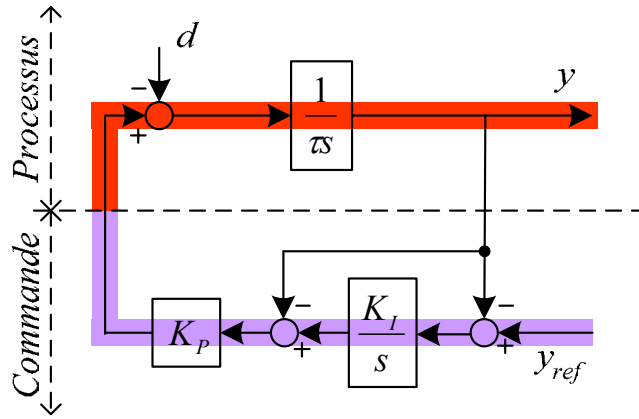


Figure AV-1. Correcteur IP pour un élément de stockage seul

La partie processus peut être une bobine  $L$  ( $\tau = L$ ), une capacité  $C$  ( $\tau = \frac{1}{C}$ ), ou une inertie  $J$  ( $\tau = J$ ). L'équation de départ est :

$$y = \frac{1}{\tau s} \left\{ K_p \left[ (y_{ref} - y) \frac{K_I}{s} - y \right] - d \right\} \quad (AV-1)$$

Suite au calcul, on obtient :

$$y = \frac{\frac{K_I K_p}{\tau}}{\frac{K_I K_p}{\tau} + \frac{K_p}{\tau} s + s^2} y_{ref} - \frac{\frac{1}{s}}{\frac{K_I K_p}{\tau} + \frac{K_p}{\tau} s + s^2} d \quad (AV-2)$$

En asservissement, on obtient donc les paramètres suivants du correcteur, en fonction de l'amortissement désiré  $\xi$  et de la fréquence désirée  $\omega_N$  :

$$K_p = 2\xi\omega_N\tau \quad (AV-3)$$



$$K_I = \frac{\omega_N^2 \tau}{K_P}$$

### A.V.2. Calcul du correcteur IP pour une fonction de transfert du 1<sup>er</sup> ordre

Le schéma bloc d'un correcteur IP est présenté par la figure suivante :

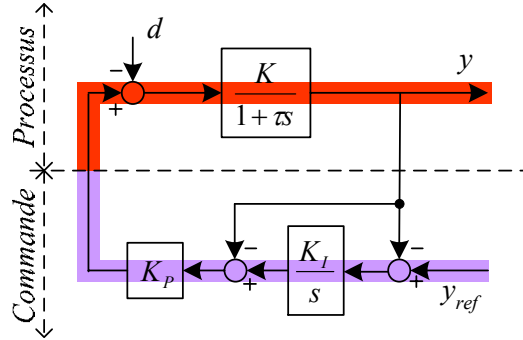


Figure AV-2. Correcteur IP pour l'élément de stockage avec les pertes

La partie processus peut être une bobine  $L$  avec une résistance  $R$  en série ( $\tau = \frac{L}{R}, K = \frac{1}{R}$ ), une capacité  $C$  avec une résistance  $R$  en parallèle ( $\tau = \frac{1}{RC}, K = R$ ), ou une inertie  $J$  avec un frottement visqueux  $f$  ( $\tau = \frac{J}{f}, K = \frac{1}{f}$ ).

L'équation de départ est :

$$y = \frac{K}{1 + \tau s} \left\{ K_P \left[ (y_{ref} - y) \frac{K_I}{s} - y \right] - d \right\} \quad (AV-4)$$

Suite au calcul, on obtient :

$$y = \frac{\frac{KK_I K_P}{\tau}}{\frac{KK_I K_P}{\tau} + \frac{1 + KK_P}{\tau} s + s^2} y_{ref} - \frac{\frac{K}{s}}{\frac{KK_I K_P}{\tau} + \frac{1 + KK_P}{\tau} s + s^2} d \quad (AV-5)$$

En asservissement, on obtient donc les paramètres suivants du correcteur, en fonction de l'amortissement désirée  $\xi$  et la fréquence désirée  $\omega_N$  :

$$K_P = \frac{2\xi\omega_N\tau - 1}{K}$$

$$K_I = \frac{\omega_N^2\tau}{KK_P} \quad (AV-6)$$

## Appendix VI. Multi-Level Representation (MLR)

The Multi-Level Representation (MLR) has been recently proposed for a synthetic and dynamic description of the electromechanical conversion systems [Li 08]. The MLR has the same advantages as the EMR. Moreover, it integrates a power calculation level and a power flow level as well as their corresponding control levels, in order to solve the most important factor of the supervision for microgrid application. Here we take the Super-Capacitor Bank (SCB) power conversion system (Fig.AVI-1) as example to explain how to make and use a Multi-Level Representation (MLR).

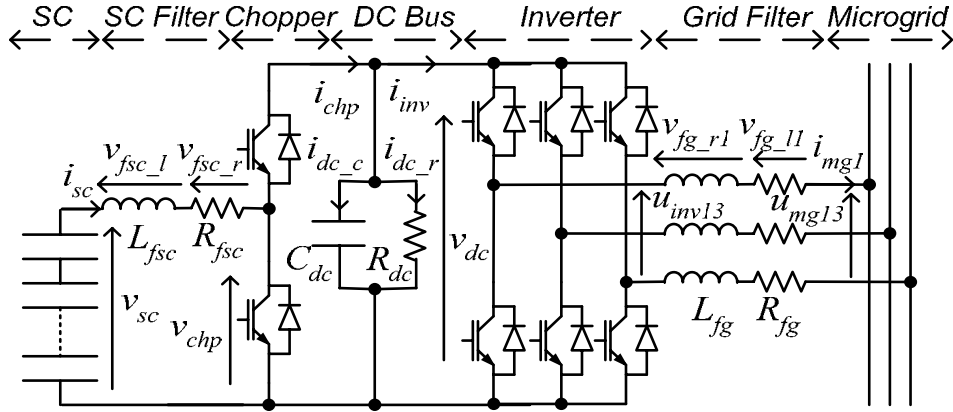


Figure AVI-1: Super-capacitor power conversion system

### Step 1: EMR level modeling

The SCB is composed of the Super Capacitor (SC), a SC filter, a chopper, a DC bus, an inverter and a three-phase grid filter (Fig.AVI-1). The first step of the SCB multi-level modeling is consists to gather dynamical equations of each element into ‘ProX’ and ‘ES’ macro blocs in order to obtain an EMR (Fig.F-3, EMR level).

#### 1) Modeling of the SC (macro bloc ‘Pro1’)

The super capacitor module is modeled as a voltage source. For the study of power system applications, the model of Zubieta and Bonert can be applied. Nevertheless, for the simplification of the study, the model with a resistor  $R_s$  and an ideal capacitor  $C_0$  in series is used.

$$\frac{dv_C}{dt} = \frac{1}{C_0} i_{sc} \quad (\text{AVI-1})$$

$$v_R = R_s i_{sc} \quad (\text{AVI-2})$$

$$v_{sc} = v_C + v_R \quad (\text{AVI-3})$$

#### 2) Modeling of the filter (‘Pro2’)

The SC filter is modeled as an inductance ( $L_{fsc}$ ) and a resistance ( $R_{fsc}$ ) in series.

$$\frac{di_{sc}}{dt} = \frac{1}{L_{fsc}} v_{fsc\_l} \quad (\text{AVI-4})$$

$$v_{fsc\_l} = v_{sc} - v_{chp} - v_{fsc\_r} \quad (\text{AVI-5})$$

$$v_{fsc\_r} = R_{fsc} i_{sc} \quad (\text{AVI-6})$$

### 3) Modeling of the chopper ('Pro3')

The chopper adapts the low voltage across the super capacitor to the desired voltage for the DC bus. An equivalent continuous model of the chopper is used by a mean value modulation function  $m_{chp}$ :

$$\begin{cases} v_{chp} = m_{chp} v_{dc} \\ i_{chp} = m_{chp} i_{sc} \end{cases}, \quad m_{chp} \in [0,1] \quad (\text{AVI-7})$$

### 4) Modeling of the grid-side DC bus ('Pro4')

The DC bus is considered as a capacitor ( $C_{dc}$ ) and a resistance ( $R_{dc}$ ) in parallel.

$$\frac{dv_{dc}}{dt} = C_{dc} i_{dc\_c} \quad (\text{AVI-8})$$

$$i_{dc\_c} = i_{chp} - i_{inv} - i_{dc\_r} \quad (\text{AVI-9})$$

$$i_{dc\_r} = \frac{1}{R_{dc}} v_{dc} \quad (\text{AVI-10})$$

### 5) Modeling of the inverter ('Pro5')

An equivalent mean modeling of the power converters is sufficient for the study. It represents fundamental phase-to-phase voltage  $\mathbf{u}_{inv} = [u_{inv13}, u_{inv23}]^T$  and line currents  $\mathbf{i}_{mg} = [i_{mg1}, i_{mg2}]^T$  components as:

$$\mathbf{u}_{inv} = \mathbf{m}_{inv} \cdot v_{dc} \quad (\text{AVI-11})$$

$$\mathbf{i}_{inv} = \mathbf{m}_{inv}^T \cdot \mathbf{i}_{mg} \quad (\text{AVI-12})$$

where  $\mathbf{m}_{inv} = [m_{inv1}, m_{inv2}]^T$  is the modulation index vector. Line voltages  $\mathbf{v}_{inv} = [v_{inv1n}, v_{inv2n}]^T$  are obtained by:

$$\mathbf{v}_{inv} = \frac{1}{3} \begin{bmatrix} 2 & -1 \\ -1 & 2 \end{bmatrix} \cdot \mathbf{u}_{inv} \quad (\text{AVI-13})$$

### 6) Modeling of the three-phase filter ('Pro6')

The line current  $\mathbf{i}_{mg}$  are deduced from the inverter voltages  $\mathbf{u}_{inv}$  and the grid voltages  $\mathbf{u}_{mg} = [u_{mg13}, u_{mg23}]^T$ .

$$\frac{d}{dt} \mathbf{i}_{mg} = \frac{1}{L_{fg}} \mathbf{v}_{fg\_l} \quad (\text{AVI-14})$$

$$\mathbf{v}_{fg\_l} = \frac{1}{3} \begin{bmatrix} 2 & -1 \\ -1 & 2 \end{bmatrix} (\mathbf{u}_{inv} - \mathbf{u}_{mg}) - \mathbf{v}_{fg\_r} \quad (\text{AVI-15})$$

$$\mathbf{v}_{fg\_r} = R_{fg} \mathbf{i}_{mg} \quad (\text{AVI-16})$$

where  $L_{fg}$  and  $R_{fg}$  are the inductance and resistance of the filter, the  $\mathbf{v}_{fg\_l} = [v_{fg\_l1}, v_{fg\_l2}]^T$  and  $\mathbf{v}_{fg\_r} = [v_{fg\_r1}, v_{fg\_r2}]^T$  are the voltages respectively across  $L_{fg}$  and  $R_{fg}$ .

7) Modeling of the microgrid ('ES')

The grid voltages  $u_{mg}$  is modeled by :

$$\underline{u}_{mg} = \begin{bmatrix} u_{mg13} \\ u_{mg23} \end{bmatrix} = \sqrt{2}A \begin{bmatrix} \sin(2\pi ft - \pi/6 + \theta_0) \\ \sin(2\pi ft - \pi/2 + \theta_0) \end{bmatrix} \quad (AVI-17)$$

where A is the rms value of the grid phase-to-phase voltage, f is the grid frequency and  $\theta_0$  is the initial angle of the grid voltage. The line currents  $i_{mg}$  are considered as disturbances for the microgrid.

**Sept 2: Power calculation level**

The second step for the multi-level modeling uses an interface, which is designed to calculate the different powers. They are classified in three terms: the intermediary powers between two elements, the exchanged powers with a storage element, and the losses (Table F-1). All equations of this level have been respectively gathered into the macro blocs named 'IntX' in the 'Power Calculation' level of the Fig.AVI-3.

**Step 3: Power flow representation level**

The third step for the multi-level modeling describes the power flow (Fig.A1-2) from the super capacitor modules to the microgrid. The macro blocs, which are named 'PowX' in the 'Power Flow' level of the Fig.A1-3, represent the modeling equations.

For the storage elements (as example the SC filter), the input power ( $P_{scf}$  from the SC) is separated into losses ( $P_{fsc\_los}$ ), the exchanged power with the storage unit ( $p_{fsc\_sto}$ ) and the output power ( $p_{fch}$ ) is expressed as:

$$Pow1: p_{fch} = P_{scf} - P_{fsc\_los} - P_{fsc\_sto} \quad (AVI-18)$$

where  $p_{fsc\_sto}$  is the total of the accumulation power ( $p_{fsc\_sto}^+$ ) and the restitution power ( $p_{fsc\_sto}^-$ ).

For the power electronic converters, the input power is equal to the output power since losses are neglected. The power flow from the SC to the microgrid is modeled by the following equations:

$$Pow2: p_{fch} = p_{chb} \quad (AVI-19)$$

$$Pow3: p_{bin} = p_{chb} - P_{dc\_los} - P_{dc\_sto} \quad (AVI-20)$$

$$Pow4: p_{bin} = p_{inf} \quad (AVI-21)$$

$$Pow5: p_{mgs} = p_{inf} - P_{fg\_los} - P_{fg\_sto} \quad (AVI-22)$$

These power equations are bidirectional. For the SCB, it is possible to perform the accumulation and the restitution of the power.

The complete multi-level modeling of the SCB is composed of three levels: EMR, Power Calculation and Power Flow (Fig.AVI-3).

**Design of the control system**

The global system has three control inputs in order to manage the system. The inverter has two independent modulation functions  $m_{inv1}$  and  $m_{inv2}$  using its switching orders. The chopper has only one modulation function  $m_{chp}$ . The control task is to reduce the power variations of the microgrid. The inverter is used to control the real and reactive power at the connection point. The control input of the chopper is used to control DC bus voltage, since the voltage of the DC bus must be constant for correct system performances. The control system is ordered by the following steps according to the rules of the multi-level representation.

The global system has three control inputs in order to manage the system. The inverter has two independent modulation functions  $m_{inv1}$  and  $m_{inv2}$  using its switching orders. The chopper has only one modulation function  $m_{chp}$ . The control task is to reduce the power variations of the microgrid. The inverter is used to control the real and reactive power at the connection point. The control input of the chopper is used to control DC bus voltage, since the voltage of the DC bus must be constant for correct system performances. The control system is ordered by the following steps according to the rules of the multi-level representation.

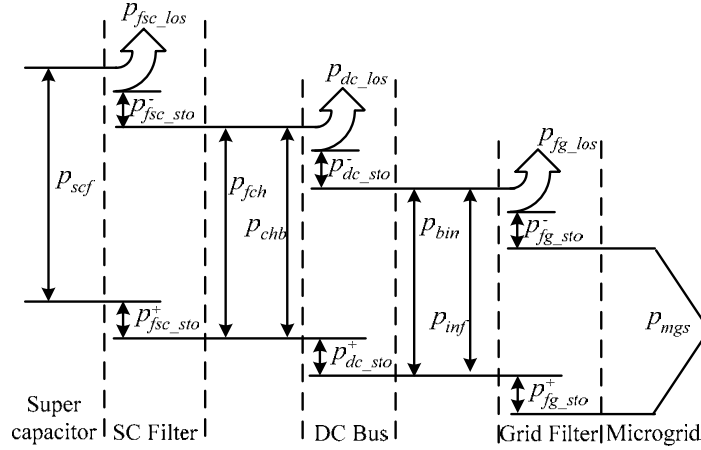


Figure AVI-2: Power flow from the SC to the microgrid

Table AVI-1: Equations of the Power calculation interface.

Intermediary powers	Storage powers	Losses
$Int1 : p_{scf} = v_{sc} i_{sc}$	$Int3 : p_{fsc\_sto} = v_{fsc\_l} i_{sc}$	$Int2 : p_{fsc\_los} = R_{fsc} i_{sc}^2$
$Int4 : p_{fch} = v_{chp} i_{sc}$	$Int7 : p_{dc\_sto} = v_{dc} i_{dc\_c}$	$Int6 : p_{dc\_los} = v_{dc}^2 / R_{dc}$
$Int5 : p_{chb} = v_{dc} i_{chp}$	$Int11 :$ $p_{fg\_sto} = (C_{23} \cdot v_{fg\_l})^T \cdot (C_{23} \cdot i_{mg})$	$Int10 :$ $p_{fg\_los} = R_{fg} (C_{23} \cdot i_{mg})^T \cdot (C_{23} \cdot i_{mg})$
$Int8 : p_{bin} = v_{dc} i_{inv}$	Where $C_{23} = \begin{bmatrix} 1 & 0 \\ 0 & 1 \\ -1 & -1 \end{bmatrix}$ is the calculation matrix from two line currents to three line currents.	
$Int9 : p_{inf} = u_{inv}^T i_{mg}$		
$Int12 : p_{mgs} = u_{mg}^T i_{mg}$		

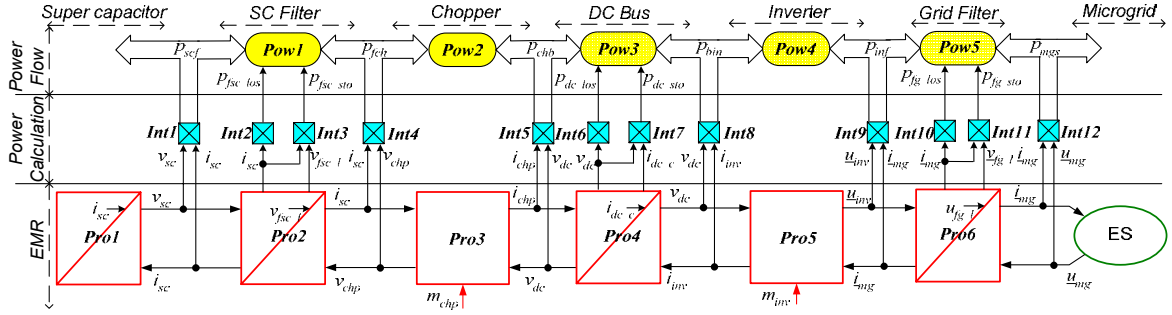


Figure AVI-3: Multi-level representation of the modeling for a Super Capacitor Bank

**Step 4: Mark the stationary quantities and the non-measurable quantities in the EMR level**

The SC terminal voltage  $v_{sc}$  changes very slowly thanks to a great quantity of stored energy. The DC bus voltage  $v_{dc}$  has also a slow dynamic, since it has to be controlled as constant in order to ensure the inverter function. At the ac side, the principal component of all quantities (voltages and currents) is 50 Hz. By modeling them into a 50 Hz rotational Park form, they become stationary. Moreover if their magnitudes are constant, they can be considered constant as  $\underline{u}_{mg}$  for the microgrid voltages. In the multi-level representation, the stationary quantities are visualized by the thick solid lines (Fig.AVI-5).

The voltages  $v_{chp}$  and  $\underline{u}_{inv}$  and the currents  $i_{chp}$  and  $i_{inv}$  are difficult to measure since they are modulated by the converters. These non-measurable quantities are visualized by the thick dashed lines (Fig.AVI-5).

**Step 5: Apply the ‘pass’ rule and the ‘block’ rule**

This step is necessary to fix the electrical chains.

When a macro bloc in the *Power Calculation* level has a stationary quantity input in the *EMR* level, it can be used to serve as a possible passage bloc between the EMR level and the Power Flow level. In this condition, this type of macro blocs is colored in the dark blue color. Such as *Int1* is colored in the dark blue for  $v_{sc}$ , *Int5*, *Int6*, *Int7* and *Int8* for  $v_{dc}$ , *Int12* for  $\underline{u}_{mg}$ .

When a non-measurable quantity in the *EMR* level is used as an input of the macro bloc for the storage element, it is impossible to design the control strategy by the inversion of another chain of this macro bloc without estimator or a corrector which rejects the disturbances. Some symbols  $\times$  are added to present the block in the control part. Such as in *Pro2*, the chain  $v_{sc} \rightarrow i_{sc}$  is blocked by the modulation quantity  $v_{chp}$ , in *Pro4*, the chain  $i_{chp} \rightarrow v_{dc}$  is blocked by the modulation quantity  $i_{inv}$ , the chain  $i_{inv} \rightarrow v_{dc}$  is blocked by the modulation quantity  $i_{chp}$ ; in *Pro6*, the chain  $\underline{u}_{mg} \rightarrow i_{mg}$  is blocked by the modulation quantity  $\underline{u}_{inv}$  (Fig.AVI-5).

**Step 6: Fix the electrical chains**

The multi-level representation helps us to find the electrical chain in the power model level in order to design the control system.

The first electrical chain is used to control the real and reactive power at the connection point to the microgrid by the modulation functions of the inverter. The path from the control input of the inverter to the powers injected to the microgrid is obvious (Fig.AVI-5):

$$m_{inv}(Pro5) \rightarrow \underline{u}_{inv}(Pro6) \rightarrow \underline{i}_{mg}(Int12) \rightarrow p_{mgs} \text{ and } q_{mgs}$$

The second electrical chain is used to control the DC bus voltage  $v_{dc}$  by the modulation function  $m_{chp}$ . Since  $v_{dc}$  is a stationary quantity which is suitable for the processes of division in the control system (AVI-28), the first step of this electrical chain is  $m_{chp}(Pro3) \rightarrow v_{chp}$  (Fig.AVI-5). Now the arrow is pointed to the left side of the chopper, but the destination  $v_{dc}$  is at its right side. The power flow level is used to establish the relation between  $v_{chp}$  and  $v_{dc}$ . At the left side of the chopper, there is only one bloc *Int1* for the passage. So the electrical chain is drawn from  $v_{chp}$  to  $i_{sc}$  in order to reach *Int1*. Since both external currents ( $i_{chp}$  and  $i_{inv}$ ) of the DC bus are modulation quantities, the end of the electrical chain in the power flow level is fixed on the DC bus storage power  $p_{dc\_sto}$ . Finally the equations *Int7* and *Pro4* are used to reach the DC bus voltage from  $p_{dc\_sto}$ . The second electrical chain is (Fig.AVI-5):

$$m_{chp}(Pro3) \rightarrow v_{chp}(Pro2) \rightarrow i_{sc}(Int1) \rightarrow p_{scf}(Pow1) \rightarrow p_{fch} \\ (Pow2) \rightarrow p_{chb}(Pow3) \rightarrow p_{dc\_sto}(Int7) \rightarrow i_{dc\_c}(Pro4) \rightarrow v_{dc}$$

### **Step 7: Control the fast dynamic quantities by the inversion of EMR**

The control system of fast dynamic quantities is obtained by using inversion rules of equations from the *EMR* modeling level (Fig.AVI-5). Hence a grid current controller (macro bloc ‘*Pro6c*’ in the Fig.AVI-5) is required to enslave grid currents to prescribed reference ( $\underline{i}_{mg\_ref}$ ). Two controllers (‘*Pro3c*’ and ‘*Pro5c*’) are used for power electronic converters. A voltage controller (‘*Pro4c*’) is used to set the DC bus voltage reference and a current controller (‘*Pro2c*’) sets the super capacitor current reference (Fig.AVI-5). The following sections give the details of each macro control bloc in the ‘*Control of Dynamic Quantities*’ level (‘*ProXc*’) in the Fig.AVI-5.

#### **1) Grid connection controller (‘*Pro6c*’)**

A Park transform is used with a synchronization with the first line voltage. In this frame, filter equations are written as:

$$\begin{cases} \frac{di_{mgd}}{dt} = \frac{1}{L_{fg}} (v_{invd} - v_{mgd} - R_{fg}i_{mgd} - L_{fg}\omega_s i_{mgq}) \\ \frac{di_{mgq}}{dt} = \frac{1}{L_{fg}} (v_{invq} - v_{mgq} - R_{fg}i_{mgq} + L_{fg}\omega_s i_{mgd}) \end{cases} \quad (AVI-23)$$

The control of these current is obtained by a compensation of grid voltages, a current decoupling and a closed loop control (Fig.AVI-4).

#### **2) Inverter controller (‘*Pro5c*’)**

Phase-to-phase voltages are obtained by inversion of the equation (AVI-13):

$$\begin{cases} u_{inv13\_ref} = v_{inv1\_ref} - v_{inv3\_ref} \\ u_{inv23\_ref} = v_{inv2\_ref} - v_{inv3\_ref} \end{cases} \quad (\text{AVI-24})$$

Modulation functions are calculated by inversion of (AVI-11):

$$m_{inv1\_ref} = \frac{u_{inv13\_ref}}{\hat{v}_{dc}}, \quad m_{inv2\_ref} = \frac{u_{inv23\_ref}}{\hat{v}_{dc}} \quad (\text{AVI-25})$$

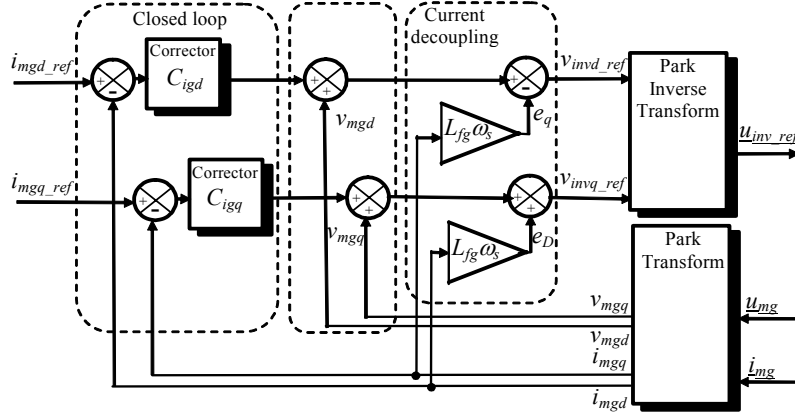


Figure AVI-4: Grid connection controller (macro bloc 'Pro6c')

A vector is defined as:  $\underline{m}_{inv\_ref} = [m_{inv1\_ref}, m_{inv2\_ref}]^T$ . Hence current references can be assumed equal to grid currents.

### 3) DC bus voltage controller ('Pro4c')

The DC bus voltage is controlled by the current  $i_{dc\_c}$  (Fig.AVI-1).

$$i_{dc\_c\_reg} = K_{dc\_p} (v_{dc\_ref} - \hat{v}_{dc}) \quad (\text{AVI-26})$$

where  $K_{dc\_p}$  is the proportional parameter of the corrector for the DC bus voltage control.

### 4) SC current controller ('Pro2c')

A control loop of the SC current generates the voltage reference of the chopper ( $v_{chp\_reg}$ ) as:

$$v_{chp\_reg} = \hat{v}_{sc} - K_{fsc\_p} (i_{sc\_reg} - \hat{i}_{sc}) \quad (\text{AVI-27})$$

where  $K_{fsc\_p}$  is the proportional parameter of the corrector for the super capacitor current control.

### 5) Chopper controller ('Pro3c')

The modulation function of the chopper  $m_{chp\_ref}$  is calculated with the DC bus voltage measurement:

$$m_{chp\_ref} = \frac{v_{chp\_reg}}{\hat{v}_{dc}} \quad (\text{AVI-28})$$

## Step 8: Power calculation control



The *Power Calculation Control* level is designed by the inversion or the estimation of the *Power Calculation* level.

$$Int1c : i_{sc\_reg} = \frac{P_{scf\_reg}}{\hat{v}_{sc}} \quad (AVI-29)$$

$$Int7e : p_{dc\_sto\_reg} = v_{dc} i_{dc\_c\_reg} \quad (AVI-30)$$

The grid current references are deduced (*Int12c*) from the equation *Int12* for the real power (Table AVI-1) and the following equation for the reactive power:

$$Q_{mgs} = \frac{1}{\sqrt{3}} ((2u_{mg23} - u_{mg13})i_{mg1} - (2u_{mg13} - u_{mg23})i_{mg2}) \quad (AVI-31)$$

$$Int12c : \begin{cases} i_{mg1\_ref} = \frac{(2u_{mg13} - u_{mg23})p_{mgs\_ref} + \sqrt{3}u_{mg23}q_{mgs\_ref}}{2u_{mg13}^2 - 2u_{mg13}u_{mg23} + 2u_{mg23}^2} \\ i_{mg2\_ref} = \frac{(2u_{mg23} - u_{mg13})p_{mgs\_ref} - \sqrt{3}u_{mg13}q_{mgs\_ref}}{2u_{mg13}^2 - 2u_{mg13}u_{mg23} + 2u_{mg23}^2} \end{cases} \quad (AVI-32)$$

### Step 9: Power flow control

The power flow control is obtained by model inversion of the *Power Flow* level with anticipation of calculated filter losses ( $\tilde{p}_{fsc\_los}$  and  $\tilde{p}_{fg\_los}$ ) (Table AVI-1). The exchanged powers with the filters ( $p_{fsc\_sto}$  and  $p_{fg\_sto}$ ) and the losses in the DC bus ( $p_{dc\_los}$ ) are slight enough to be neglected.

$$Pow1c : p_{scf\_reg} = p_{fch\_reg} + \tilde{p}_{fsc\_los} \quad (AVI-33)$$

$$Pow2c : p_{fch\_reg} = p_{chb\_reg} \quad (AVI-34)$$

$$Pow3c : p_{chb\_reg} = p_{bin\_reg} + p_{dc\_sto\_reg} \quad (AVI-35)$$

$$Pow4c : p_{bin\_reg} = p_{inf\_reg} \quad (AVI-36)$$

$$Pow5c : p_{inf\_reg} = p_{mgs\_ref} + \tilde{p}_{fg\_los} \quad (AVI-37)$$

### Storage level protection

The terminal voltage of the super capacitor represents its energy storage level. For security reasons, it should be between the maximal allowed value and 50% of this value for an efficiency reason.

In order to limit the terminal voltage of the SC, an additional control function has to be used (macro bloc 'SLP' in the *Power Supervision* level of the Fig.AVI-5).

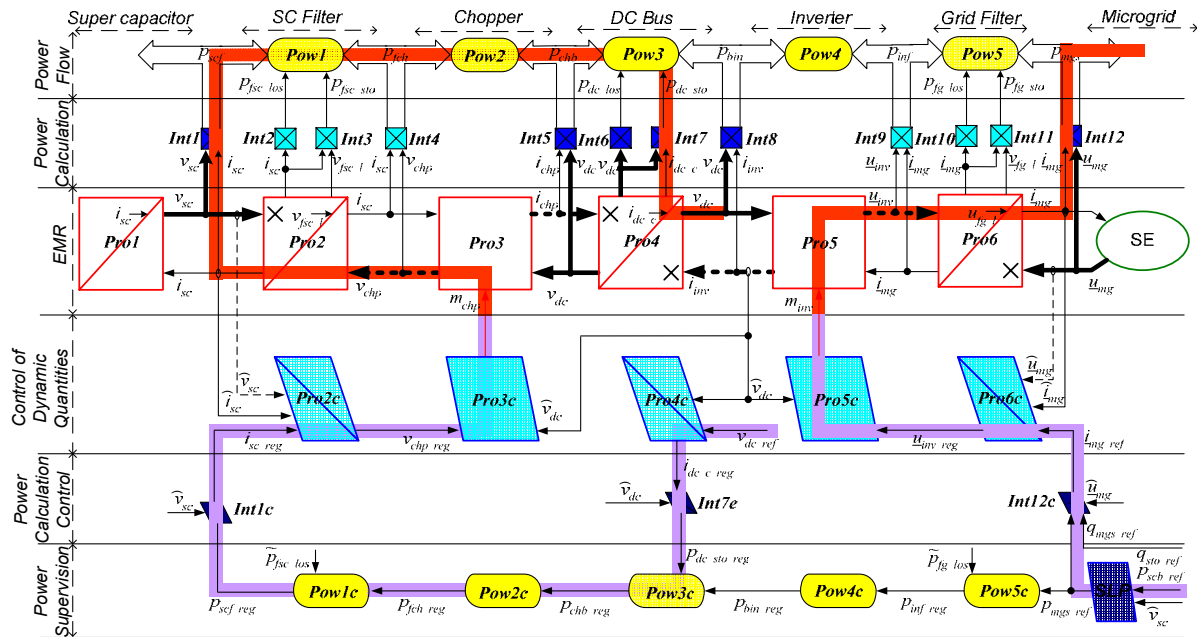


Figure AVI-5: Control system of the Super Capacitor Bank

## Appendix VII. Modeling of the gas micro turbine

### A.VII.1. Presentation

In this research work, a gas micro turbine system (Capstone M330) is studied and is represented in the following figure [LAS 01] [YIN 01] [CAP 06] [Li 09]. In this appendix a detailed modeling is presented, and then a simplified model for the local control design is presented. Finally, a simplified model is presented for the operational planning of the electrical system.

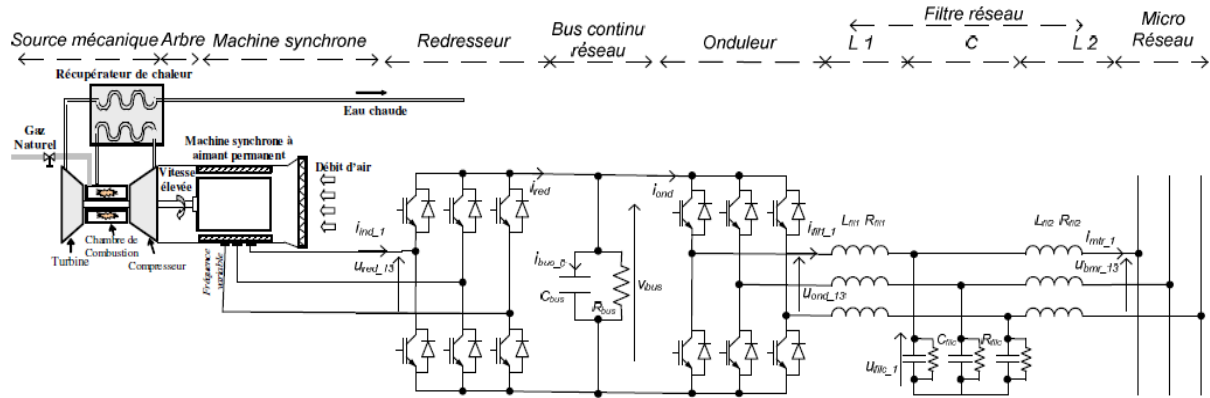


Figure AVII-1: Gas micro turbine power generation system

### A.VII.2. Conversion of primary energy

The dynamic modeling and simulation of a micro turbine have been discussed in several references [ROW 83] [HAN 93] [NER 94] [ALH 02] [FET 04]. A simplified model is used in this paragraph [NIK 02] [NIK 05].

Heat escape is used to preheat air before it enters the combustion room. This can reduce about 50 percents of the gas consumption. The combustion room mixes the heated air with the gas and the burns. The explosion of this mix air in the turbine drives the gas compressor and the generator to 96,000 rpm. The heated air is reused in the regenerator before being evacuated out of the exhaust. The mass flow of gas  $m_f(t)$  and the mass flow of air  $m_0(t)$  can be considered proportional to the gain  $k$  (62.5):

$$m_0(t) = km_f(t) \tag{AVII-1}$$

A compressor is used to pressurize the mass flow of input air, and to increase the temperature of the air entering the combustion room. The flow of air leaving the compressor is the same as the entry with a time delay:

$$m_c(t) = m_0(t - \tau_c) \tag{AVII-2}$$

The delay  $\tau_c$  (1.3 ms) depends on the gas velocity and the length of the compressor. The generated thermal power in the compressor is expressed by:

$$P_{th,c}(t) = 1.19 * 10^{-3} C_p (m_0(t) + m_c(t)) \frac{T_c - T_a}{2} \quad (\text{AVII-3})$$

where

$C_p$  is the power coefficient of thermal power (470),

$T_a$  (210 °C) and  $T_c$  (25°C) are the room temperature and the compressor outlet temperature.

The mechanical power of compressor  $P_{m,c}$  is controlled by the following equation:

$$\tau_c \frac{dP_{m,c}}{dt} = P_{th,c} - P_{m,c} \quad (\text{AVII-4})$$

The mass flow of air from the compressor and the mass flow of fuel are injected into the entrance of the combustion room. The air and gas are mixed and burned in the combustion room. The time delay associated with this process is ( $\tau_{cc}$  1.4 ms):

$$m_{cc}(t) = m_c(t - \tau_{cc}) + m_f(t - \tau_{cc}) \quad (\text{AVII-5})$$

The generated thermal power in the combustion room is not involved in the mechanical power of the micro turbine, and is expressed by:

$$P_{th,cc}(t) = 1.19 * 10^{-3} C_p m_{cc}(t) [T_{cc} - T_c] \quad (\text{AVII-6})$$

where  $T_{CC}$  is the outlet temperature of the combustion room (982°C).

The mass flow of gas at the outlet  $m_{cc}(t)$  of the combustion room is an input variable of the turbine. The time delay associated with this process is  $\tau_T$  (0.294 ms), and the mass flow of air from the turbine is given by:

$$m_T(t) = m_{cc}(t - \tau_T) \quad (\text{AVII-7})$$

The generated thermal power in this step is expressed by:

$$P_{th,T} = 1.19 * 10^{-3} C_p (m_T(t) + m_{cc}(t)) \frac{T_{cc} - T_T}{2} \quad (\text{AVII-8})$$

where  $T_T$  is the temperature of the outlet of the turbine (316°C).

The mechanical power  $P_{m,T}$  of the turbine is governed by the following differential equation:

$$\tau_T \frac{dP_{m,T}}{dt} = P_{th,T} - P_{m,T} \quad (\text{AVII-9})$$

The mechanical power output of the MGT is respectively obtained from the mechanical power of the compressor and turbine mechanical power:

$$P_{sma} = P_{m,T} - P_{m,c} \quad (\text{AVII-10})$$

Then, the torque is deduced using the speed of the turbine:

$$C_{tur} = \frac{P_{sma}}{\Omega_{arb}} \quad (\text{AVII-11})$$

### A.VII.2. Mechanical part

The simplified dynamic model of the mechanical part based on the following equations:

$$\begin{cases} \frac{d\Omega_{arb}}{dt} = \frac{1}{J} C_{arb\_s} \\ C_{arb\_s} = C_{tur} - C_{em} - C_{viscous} \\ C_{viscous} = f_{vis} \Omega_{arb} \end{cases} \quad (\text{AVII-12})$$

where

$J$  is the inertia (represents the total inertia  $0.001 \text{ kg}\cdot\text{m}^2$ ), which appears on the generator rotor;

$f_{vis}$  is the viscous friction of the mechanical transfer, modeled by a coefficient ( $1.5 \cdot 10^{-5}$ );

$C_{arb}$  is the total torque;

$C_{em}$  is the electromagnetic torque;

$C_{viscous}$  is the torque of viscous friction.

### A.VII.3. Electrical energy conversion part

The electrical diagram of the energy conversion part is presented in the following figure:

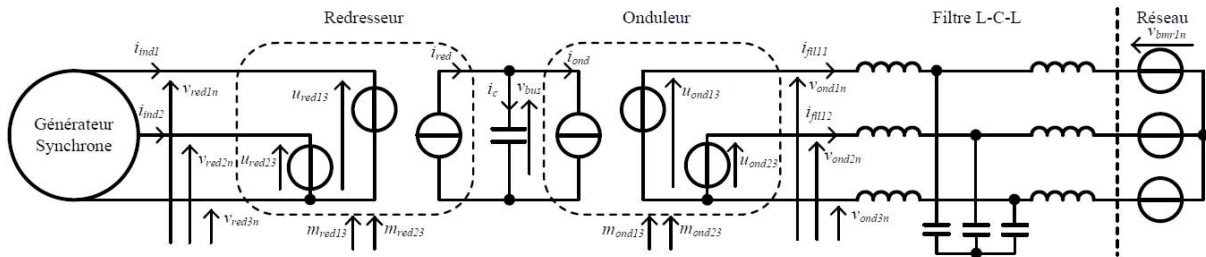


Figure AVII-2: Electrical energy conversion part diagram

The used generator is a permanent magnet synchronous machine with two smooth poles. The synchronous machine is cooled by a ventilation system mounted on the axis of the micro turbine. The voltage of the generator is alternative and the frequency and the amplitude are variable. At 1600 Hz (96,000 rpm), the output power of the machine is 30 kVA and the RMS value of its nominal voltages is 400 V.

For the rectifier, this model represents the low-frequency components of voltages and currents as:

- sources of voltage ( $u_{red13}$  and  $u_{red23}$ ) dependent on the DC bus voltage by the

conversion functions ( $m_{red13}$  and  $m_{red23}$ );

- a current source ( $i_{red}$ ) dependent alternating currents through the same conversion functions.

$$\begin{cases} \langle i_{red} \rangle = \langle m_{red}^T \rangle \cdot i_{ind} \\ \langle u_{red} \rangle = \langle m_{red} \rangle \cdot v_{bus} \end{cases} \quad (\text{AVII-13})$$

For the same modeling of the 3-phase inverter and the filters is already presented in the Chapter II.

#### **A.VII.4. Modeling for the design of the local control system**

A simplified model of a real generator with control systems of the frequency and the voltage RMS value [SAA 99] [LAW 01] [DEL 06] has been developed in [Li 09] and is recalled here. The purpose of the model is to describe mathematically the transient stability of the electrical quantities from the power generator (such as the frequency variation or the voltage variation). So the mathematic equations are established with only variation quantities ( $\Delta$ ) of physical variables. The model using an IEEE standard has been used and is composed of four parts:

- the mechanical part;
- the voltage regulation;
- the coupling between these two parts;
- additional equations between the per units and the International System of Units (SI Units).

##### **a. Mechanical part**

The mechanical part is composed of a governor, a turbine, a rotating mass including equivalent loads, a regulation system and the power angle calculation [KUN 94] [SAA 99]. The difference between the reference and the real power is transformed through the hydraulic amplifier to the steam valve position command ( $\Delta P_v$ ). Assuming a linear relationship and considering a simple time constant  $\tau_g$  (0.2s), the equation for the governor can be expressed as:

$$\Delta P_v = \frac{1}{1 + \tau_g s} (\Delta P_{ref} - \Delta P_{reg}) \quad (\text{AVII-14})$$

where :

$\Delta P_{ref}$  is the change of reference real power in per unit (0, for a constant generation set point);  $\Delta P_{reg}$  is the change of the real power in per unit.

A simple prime mover model of the non-reheat steam turbine can be approximated with a single time constant  $\tau_t$  (0.5s) :

$$\Delta P_m = \frac{1}{1 + \tau_t s} \Delta P_v \quad (\text{AVII-15})$$

where  $\Delta P_m$  is the change of mechanical power output in per unit.

Therefore, the speed-load characteristic (in p.u.) is approximated by considering the rotating mass and electrical load real power, which is approximately equivalent to the electromechanical power consumed by the generator (details can be found in [SAA 99] pp. 460-463 and pp. 529-568):

$$\Delta\omega = \frac{1}{D + 2Hs}(\Delta P_m - \Delta P_c - \Delta P_e) \quad (\text{AVII-16})$$

where :

$\Delta P_c$  is the change of load real power in per unit;

$\Delta P_e$  is the change due to the effect of voltage upon real power in per unit;

$H$  is the per unit inertial constant (5 in per unit);

$D$  is expressed as a percent change of the load divided by a percent change in frequency (0.8 in per unit). Hence the load is changed by 0.8 percent for a 1 percent change in frequency.

The small change of the power angle ( $\Delta\delta$ ) is obtained by integration of the small change of the speed:

$$\Delta\delta = \frac{1}{s}\Delta\omega \quad (\text{AVII-17})$$

The regulation system is composed of a governor speed regulation with (or without) an Automatic Generation Control (AGC), which is based on an integral controller:

$$\Delta P_{reg} = -\left(\frac{1}{R} + \frac{K_I}{s}\right)(\Delta\omega_{ref} - \Delta\omega) \quad (\text{AVII-18})$$

where:

$R$  is the speed regulation ratio (0.05);

$K_I$  is the integral controller gain for the AGC (6);

$\Delta\omega_{ref}$  is the variation reference of grid frequency (0).

If the plant has not an AGC, the regulation system is expressed as:

$$\Delta P_{reg} = \frac{1}{R}\Delta\omega \quad (\text{AVII-19})$$

### **b. Voltage regulation**

The voltage regulation of the plant is composed of an amplifier, an exciter, a fourth order generator model, the calculation of the terminal voltage and a PID controller.

The amplifier is represented by a transfer function with a gain  $K_A$  (10) and a time constant  $\tau_A$  (0.1s):

$$V_A = \frac{K_A}{1 + \tau_A s} V_C \quad (\text{AVII-20})$$

$V_A$  is the terminal voltage of the amplifier in per unit and  $V_C$  is the terminal voltage reference given by the PID controller in per unit. In the simplest form, the transfer function of a modern exciter can be modeled by:

$$V_F = \frac{K_E}{1 + \tau_E s} V_A \quad (\text{AVII-21})$$

Where:

$V_F$  is the terminal voltage of the exciter in per unit;

$K_E$  is the exciter gain (1);

$\tau_E$  is a time constant (0.4s).

A fourth order generator model is used [LAW 01] [DEL 06] to obtain a better accuracy of the generator field calculation than with a simple first order generator model [WAL-96]:

$$R2: \quad E' = \frac{(1 + T_{z1}s)(1 + T_{z2}s)(1 + T_{z3}s)(1 + T_{z4}s)}{(1 + T_{p1}s)(1 + T_{p2}s)(1 + T_{p3}s)(1 + T_{p4}s)} (V_F - K_4 \Delta\delta) \quad (\text{AVII-22})$$

Where :

$T_{p1}$  (3.9517) and  $T_{z1}$  (0.9087) are the pole-zero time constants of the first order model,

$T_{p2}$  (0.1481) and  $T_{z2}$  (0.1257) are the pole-zero time constants of the second order model,

$T_{p3}$  ( $8.38 \times 10^{-3}$ ) and  $T_{z3}$  ( $6.88 \times 10^{-3}$ ) are the pole-zero time constants of the third order model,

$T_{p4}$  ( $9.37 \times 10^{-4}$ ) and  $T_{z4}$  ( $7.75 \times 10^{-4}$ ) are the pole-zero time constants of the fourth order model,

$K_4$  is a gain.

Including the small effect of the rotor angle upon the generator terminal voltage, the generator terminal voltage can be written as [SAA 99]:

$$R3: \quad V_t = K_5 \Delta\delta + K_6 E' \quad (\text{AVII-23})$$

$K_5$  is the gain of the change in the terminal voltage for a small change in rotor angle with a constant stator emf (-0.1) and  $K_6$  is the gain of the change in the terminal voltage for a small change in the stator emf with a constant rotor angle (0.5). A PID controller is used to improve the dynamic response as well as to reduce or eliminate the steady-state error:

$$R4: \quad V_C = (K_{PC} + \frac{K_{IC}}{s} + K_{DC}s)V_t \quad (\text{AVII-24})$$

Where:

$K_{PC}$  is proportional gain (3);

$K_{IC}$  is integral gain (0.7);

$K_{DC}$  is derivative gain of the PID controller (0.2).

### c. Coupling between these two parts

Equation R5 represents the interaction between the frequency regulation and the voltage regulation. The small change in the real power due to the effect of voltage can be expressed as:

$$R5: \quad \Delta P_e = P_s \Delta\delta + K_2 E' \quad (\text{AVII-25})$$

$P_s$  is the synchronizing power coefficient in per unit (1.5) and  $K_2$  is the change in



electrical power for a small change in the stator emf (0.2).

**d. Adaptation between the per units and SI units**

The adaptation between the per units and SI units is derived by the equations *R12*, *R13* and *R14*. The change for the grid frequency is calculated as:

$$R12 : \quad \omega_{(\text{rad/s})} = 2\pi f_{\text{ref}(\text{Hz})} + \Delta\omega_{(\text{rad/s})} \quad (\text{AVII-26})$$

$$\Delta\omega_{(\text{rad/s})} = 2\pi f_{\text{ref}(\text{Hz})} \Delta\omega_{(\text{pu})} \quad (\text{AVII-27})$$

where  $f_{\text{ref}}$  is the grid frequency (50 Hz).

The change from per unit to SI unit (volt) for the voltage is given as:

$$R13 : \quad \begin{cases} u_{gd13(\text{V})} = \sqrt{3}V_{t(\text{pu})}V_{m(\text{V})} \sin(\omega t - \frac{1}{6}\pi + \theta_0) \\ u_{gd23(\text{V})} = \sqrt{3}V_{t(\text{pu})}V_{m(\text{V})} \sin(\omega t - \frac{1}{2}\pi + \theta_0) \end{cases} \quad (\text{AVII-28})$$

Where:

$\mathbf{u}_{gd} = [u_{gd13}, u_{gd23}]^T$  is the vector of phase-to-phase terminal voltages;

$V_m$  is the nominal voltage value of the plant;

$\theta_0$  is the initial angle.

The change from SI units (Watt) to per unit of load power fluctuations is expressed as:

$$R14 : \quad \Delta P_c = \frac{1}{P_{ngd}} (\mathbf{u}_{gd}^T \cdot \mathbf{i}_{bgd} - P_{ngd}) \quad (\text{AVII-29})$$

$P_{ngd}$  is the nominal generated real power by the plant (200 kW) and  $\mathbf{i}_{bgd} = [i_{bgd1}, i_{bgd2}]^T$  is the vector of generator currents.

### A.VII.5. Simplified power model for the design of the operational planning

In order to implement the energy management, a simplified model is used for the power modeling and energy management. The response time of the power output of the whole gas turbine with the control system is set as 30 seconds. So the power model of the gas turbine can be approximated with a first order model:

$$P_{MGT} = \frac{1}{1 + \tau_{MGT} \cdot s} P_{MGT\_ref} \quad (\text{AVII-30})$$

where  $P_{MGT}$  is the power output from the simplified model,

$P_{MGT\_ref}$  is the setpoint of the micro gas turbine and

$$\tau_{MGT} = 10s .$$

# *General Bibliography*



*A*

- [Awa 08] B. Awad, J. Wu, N. Jenkins, "Control of distributed generation", *Elektrotechnik & Informationstechnik*, Vol.125, No 12, pp.409-414, August 2008, Springer
- [Aya 07] M.Y. Ayad et al, "Voltage regulated hybrid DC power source using supercapacitors as energy storage device", Elsevier, *Energy Conversion and Management*, vol. 48, Jul.2007, pp. 2196-2202.

*B*

- [Bar 05] M. Barnes, A. Dimeas, A. Engler, C. Fitzer, N. Hatziargyriou, C. Jones, S. Papathanassiou, and M. Vandenberg, "MicroGrid laboratory facilities", 2005 IEEE International Conference on Future Power Systems, Wind Engineering, 16-18 Nov. 2005.
- [Bar 07] J. A. Baroudi, V. Dinavahi, A. M. Knight, "A review of power converter topologies for wind generators", *Renewable Energy*, 32 (14): 2369–2385.
- [Bef 08] Le bilan énergétique de la France, édition 2008, Ministère de l'Écologie, de l'Énergie, du Développement durable et de l'Aménagement du territoire
- [Bha 05] R.S. Bhatia, S.P. Jain, D.K. Jain, B. Singh, "Battery Energy Storage System for Power Conditioning of Renewable Energy Sources", PEDS 2005 International Conference on Power Electronics and Drives Systems, 2005 Vol. 1, pp. 501 – 506.
- [Bou 09] O. Bouhali, B. Francois, M. Berkouk, C. Saudemont, "Power sizing and control of a three-level NPC converter for grid connection of wind generators", *Electromotion journal*, vol. 16, pp. 38-48, January 2009

*C*

- [Cal 03] R. Caldon, F. Rossetto, R. Turri, "Analysis of dynamic performance of dispersed generation connected through inverter to distribution networks", 17<sup>th</sup> International Conference on Electricity Distribution, CIRED 2003, 12-15 May 2003, Barcelona, Spain.
- [Cha 05] V. A. Chaudhari, "Automatic peak power tracker for solar PV modules using dSPACE software", Thesis in Master of Technology, Maulana Azad National Institute of Technology (Deemed University), July 2005.
- [Cho 96] T.W.S. Chow, C.T. Leung, "Neural network based short-term load forecasting using weather compensation", *IEEE Transactions on Power Systems*, Nov 1996, Volume: 1,1 Issue:4, pp. 1736-1742.
- [Cob 08] S. Cobben, "Bronsbergen: The First Micro Grid in the Netherlands", *Kythnos 2008 Symposium on Micro Grids*, Greece, June 2<sup>nd</sup>
- [Cop 10] W. Copppe, L. Geurts, A. Woyte, R. Belmans, J. Neyens, J. Nijs, "Determining the value of decentralized grid-connected photovoltaic electricity in Belgium",

ULR: <http://www.kuleuven.be/ei/Public/publications/EIWP01-01.pdf>

- [Cou 08] V. Courtecuisse, "Supervision d'une centrale multisources à base d'éoliennes et de stockage d'énergie connectée au réseau électrique", thèse de doctorat, L2EP, ENSAM, 20/11/2008.

## D

- [Dav 09] A. Davigny, "Participation aux services système de fermes d'éoliennes à vitesse variable intégrant du stockage inertiel d'énergie", N° 4066, Thèse de doctorat, University of Lille, USTL, 11/12/2007
- [Deg 06] Ph. Degobert, S. Kreuawan, X. Guillaud, "Micro-grid powered by photovoltaic and micro turbine", International Conference on Renewable Energy and Power Quality (ICREPQ'06), Palma de Mallorca, Spain, April 5-7, 2006.
- [Del 06] D. Delcour, "Etude d'un réseau hybride multi sources décentralisé mettant en œuvre un système de production photovoltaïque", Mémoire C.N.A.M., 31/10/ 2006.
- [Dim 04] A. Dimeas, N. D. Hatziargyriou, "A multiagent system for MicroGrids", IEEE Power Eng Soc Gen Meet, 2004(1), 55–8.
- [Dim 05] A. Dimeas and N. D. Hatziargyriou, "Operation of a Multi-Agent System for Microgrid Control", IEEE Transactions on Power Systems, vol. 20, Issue 3, pp. 1447-1455, Aug. 2005.
- [Dim 07] A. Dimeas, N. D. Hatziargyriou, "Agent based control for microgrids", IEEE Power Engineering Society General Meeting, Tampa, USA, June 2007.

## E

- [Eeg 09] Gesetz zur Neuregelung des Rechts der Erneuerbaren Energien im Strombereich und zur Änderung damit zusammenhängender Vorschriften, Erneuerbare-Energien-Gesetz, Deutschland, EEG 2009.
- [Elh 00] M. E. El-Hawary, "Electrical Energy Systems", CRC Press, 2000
- [End 01] M. Endo, T. Takeda, Y.J. Kim, K. Koshiba and K. Ishii, "High power Electric Double Layer Capacitor (EDLC's); from operating principles to pore size control in advanced active carbon", Carbon Science, vol. 1, pp. 117-128, 2001
- [Erd 10] ERDF (Électricité Réseau Distribution France), Website, [www.erdfdistribution.fr](http://www.erdfdistribution.fr).
- [Eud 04] Eudeep Project, "Conclusions – methodologies to build market configurations suited to DER development, Trading of DER in competitive market", Keynote paper, WP3-S5, 2004.
- [Ewe 07] European Wind Energy Association, "EWEA Executive summary Analysis of Wind Energy in the EU-25", European Wind Energy Association, Retrieved 2007/03/11.

*F*

- [Fra 99] B. François, J.P. Hautier, "Pulse Position and Pulse Width Modulation of Electrical Power Conversions: Application to a Three-Phase Voltage-Fed Inverter", 3rd International Symposium on Advanced Electromechanical Motion Systems: ELECTROMOTION 1999, vol. 2, pp. 653-658, Patras, Greece, July 8-9,1999
- [Fei 08] E. A. Feinberg, D. Genethliou, "Applied Mathematics for Power Systems: Load Forecasting", chapter 12, Applied Mathematics.
- [Fig 09] E. Figueres, G. Garcera, J. Sandia, F-G Espin, J. Rubio, « Sensitivity study of the dynamics of three-phase photovoltaic inverters with an LCL grid filter", IEEE Transactions on industrial electronics, vol.56, no.3, March 2009
- [Fog 09] G. Foggia, "Pilotage Optimal de Système Multi-sources pour le Bâtiment", thèse de l'Institut Polytechnique de Grenoble, 17 juillet 2009

*G*

- [Gaz 06] H. Gaztanaga Arantzamendi, "Etude de structures d'intégration des systèmes de génération décentralisée : Application aux microréseaux", Thèse de doctorat, l'Institut Nationale Polytechnique de Grenoble, 15 décembre 2006.
- [Gei 09] R. Geipel, N. Hatziaargyriou, A. Dimeas, S. Hatzivasiliadis , "Experimental Validation of Islanding mode of operation", Report of More Microgrid, 30-12-2009
- [Ger 03] O. Gergaud, G. Robin, B. Multon, H. Ben Ahmed, "Energy modelling of a lead-acid battery within hybrid wind/ photovoltaic systems", SATIE-Brittany Branch, EPE 2003, Toulouse, 2003, CD-ROM.
- [Gre 06] M. A. Green, "Consolidation of Thin-film Photovoltaic Technology: The Coming Decade of Opportunity," Progress in Photovoltaics: Research and Applications, vol. 14, pp. 383-392, August 2006.
- [Gua 03] D. Guasch, S. Silvestre, "Dynamic battery model for photovoltaic applications", Revue: Progress in photovoltaics: Research and applications, Volume 11 Issue 3, pp. 193 - 206, 2003.
- [Gup 09] N. Gupta, G. F. Alapatt, R. Podila, R. Singh, K.F. Poole, "Prospects of Nanostructure-Based Solar Cells for Manufacturing Future Generations of Photovoltaic Modules", International Journal of Photoenergy 2009.

*H*

- [Haj 07] A. Hajizadeh, M.A. Golkar, "Intelligent power management strategy of hybrid distributed generation system", Elsevier, Electrical Power and Energy System, 2007, pp.783-795.

- [Hat 05] N. Hatziargyriou, A. Dimeas, A.G. Tsikalakis, et al, "Management of MicroGrids in market environment", International Conference Future Power System, 2005, pp. 1–7.
- [Hat 07] N. Hatziargyriou, H. Asano, R. Iravani and C. Marnay, "Microgrids- an overview of ongoing research, development and demonstration Projects", IEEE power & energy magazine, pp.78-94, July/August 2007
- [Her 06] H. G. Guillermo, I. Reza, "Current injection for active islanding detection of electronically-interfaced distributed resources", IEEE Trans Power Deliv 2006, 21(3), pp. 1698–705.
- [Hua 08] J. Y. Huang, C.W. Jiang, R. Xu, "A review on distributed energy resources and MicroGrid", Renewable and sustainable Energy reviews, 12/2008, pp. 2472-2483.

## *I*

- [Iea 00] IEA (International energy agency), "World Energy Outlook 2000", 2000.
- [Iea 03] International energy agency (IEA), "Renewable energy into the mainstream", IEA Renewable Energy Working Party, 2003.
- [Ise 09] Fraunhofer ISE (Institute Solar Energiesysteme), "World Record: 41.1% efficiency reached for multi-junction solar cells at Fraunhofer ISE", January 14<sup>th</sup>, 2009, Freiburg.

## *J*

- [Jay 05] N. Jayawarna, N. Jenkins, M. Barnes, et al, "Safety analysis of a MicroGrid", Int Conf Future Power Syst, 2005, pp.1–7.

## *K*

- [Kai 06] R. Kaiser, "Optimized battery-management system to improve storage lifetime in renewable energy systems", Journal of Power Sources Volume 168, Issue 1, 25 May 2007, pp. 58-65.
- [Kat 06] F. Katiraei, M.R. Iravani, "Power management strategies for a microgrid with multiple distributed generation units", IEEE Trans. on Power Systems, vol. 21, No. 4, pp. 1821-1831, November 2006.
- [Kat 08] F. Katiraei, M.R. Iravani, N. Hatziargyriou, A. Dimeas, "Microgrids Management", IEEE Power and Energy Magazine, vol. 6, pp. 54-65, May/June 2008.
- [Kim 08] S. Kim, J. Jeon, C. Cho, J. Ahn, S. Kwon, "Dynamic modeling and control of a grid-connected hybrid generation system with versatile power transfer", IEEE Transactions on industrial electronics, vol. 55, no. 4, April 2008
- [Kle 08] J. Kleissl, "Solar Power Forecasting at UC San Diego", Internet technical report, Dept of Mechanical & Aerospace Engineering, UCSD, url: <http://maeresearch.ucsd.edu/kleissl/SolarPowerForecasting.pdf>
- [Kok 05] J.K. Kok, C.J. Warner and I.G. Kamphuis, "Powermatcher: Multiagent control in the electricity infrastructure", Proceedings of Autonomous Agents and

Multi-Agent Systems, Utrecht, Netherlands, 25-29 July 2005.

- [Kro 08] B. Kroposki, R.Lasseter, T.Ise, S. Morozumi, S. Papathanasiou, N. Hatziargyriou, "Making microgrids work", IEEE Power&Energy magazine, may/june 2008
- [KUN 94] P. Kundur, "Power system stability and control", McGraw-Hill, pp. 389-417, 1994.
- [Kyo 09] "Kyoto Protocol: Status of Ratification", United Nations Framework Convention on Climate Change, 2009-01-14, Retrieved 2009-05-06.

## L

- [Laf 08] M. Lafoz, L. Garcia-Tabarés, M. Blanco, "Energy management in solar photovoltaic plants based on ESS", Power Electronics and Motion Control Conference, EPE-PEMC 2008, 13<sup>th</sup>, Poznan, 1-3 Sept. 2008, CD-ROM
- [Las 02] R. Lasseter, A. Akhil, C. Marnay, J. Stephens, J. Dagle, R.Guttromson, and al., "Integration of distributed energy resources – The MicroGrid concept", CERTS MicroGrid Review, April 2002.
- [Las 03] R. Lasseter, A. Abbas, "Integration of distributed energy resources: The CERTS MicroGrid concept", Consortium for Electric Reliability Technology Solutions, California Energy Commission, 2003: P50003–089F.
- [Las 04] R. Lasseter, P. Paigi, "MicroGrid: a conceptual solution", IEEE Annual Power Electronic Specialists Conference, 6, 2004(1):4285–90.
- [Law 01] B.E. Law, "Simulation of the transient response of synchronous machines", Honours Thesis for the degree of Bachelor, University of Queensland, 2001.
- [Lho 05] W. Lhomme, P. Delarue, P. Barrade, A. Bouscayrol, A. Rufer, "Design and Control of a Supercapacitor Storage System for Traction Applications", IEEE-IAS'05, Hong Kong (China), Vol. 3, pp. 2013-2020, 10-2005.
- [Li 08a] P. Li, P. Degobert, B. Robyns, B. Francois, "Implementation of interactivity across a resilient microgrid for power supply and exchange with an active distribution network", CIRED Seminar 2008: SmartGrids for Distribution, Frankfurt, June 2008, CD-ROM.
- [Li 08b] P. Li, B. Francois, Ph. Degobert, B. Robyns, "Multi-level representation for control design of a super capacitor storage system for a microgrid connected application ", ICREPQ'08, Santander, 12-14 mars 2008.
- [Li 08c] C.H. Li, X.J. Zhu, G. Y. Cao, S. Sui, M. R. Hu, "Dynamic modelling and sizing optimization of stand-alone photovoltaic power systems using hybrid energy storage technology", Renewable Energy, Vol. 34, N° 3, March 2009, pp. 815-826.
- [Li 09] P. Li, "Formalisme pour la Supervision des Systèmes Hybrides Multi-Sources de Générateurs d'Energie Répartie : Application à la Gestion d'un Micro Réseau", PhD thesis report, June 2009, Ecole Centrale de Lille
- [Lu 08] D. Lu, T. Zhou, H. Fakham, B. Francois, "Design of a power management



system for a PV station including various storage technologies", 13<sup>th</sup> International Power Electronics and Motion Control Conference, EPE-PEMC 2008, Poznan, 1-3 septembre 2008, 9-2008, CD-ROM

- [Lu 09a] D. Lu, T. Zhou, H. Fakham, B. François, "Application of Petri nets for the energy management of a photovoltaic based power station including storage units", *Renewable energy*, Elsevier, Vol. 35, Issue 6, pp. 1117-1124
- [Lu 09b] D. Lu, B. Francois, "Strategic framework of an energy management of a microgrid with photovoltaic-based active generator", *Electromotion 2009*, Lille, 1-3 July 2009, CD-ROM

## M

- [Mar 05] J.N. Marie-Francoise, H. Gualous, R. Outbib, A. Berthon, "42V power net with supercapacitor and battery for automotive applications", Elsevier, *Journal of Power Sources*, vol.143, 2005, pp.275-283.
- [Mar 07] C. Marnay and R. Firestone, "Microgrids: An emerging paradigm for meeting building electricity and heat requirements efficiently and with appropriate energy quality", the European Council for an Energy Efficient Economy 2007 Summer Study, La Colle sur Loup, France, 4-9 June 2007.
- [Mcm 98] J.S. Mcmenamin, and F.A. Monforte, "Short term energy forecasting with neural networks", *Energy Journal*, 19(4), pp.43-61, 1998.
- [Met 10] Site internet, <http://www.recepteur-meteo.com/>
- [Mil 09] A.Milo, H. Gaztanaga, I. Etxeberria-Otadui, E. Bilbao, P. Rodriguez, "Optimization of an experimental hybrid microgrid operation: Reliability and economic issues", *PowerTech*, 2009 IEEE Bucharest.
- [Mis 08] S. Mishra, "Short Term Load Forecasting Using Computational Intelligence methods", Masters thesis, National Institute of Technology Rourkela, 2008.
- [Mor 06] J. Moreno, M.E. Ortuzar, J.W. Dixon, "Energy-management system for a hybrid electric vehicle, using ultracapacitors and neural networks", *IEEE transactions on Industrial Electronics*, vol. 53, no. 2, Apr. 2006, pp. 614-623.

## P

- [Par 09] U. Parinyacupt, "Data monitoring on Kythnos", in EC-project "More Microgrids". WPF: October 2009
- [Pay 07] A. Payman, S. Perfederici, F. Meibody-Tabar, "Implementation of a flatness based control for a fuel cell-ultracapacitor hybrid system", *Power Electronics Specialists Conference, IEEE-PESC'07*, June 2007.
- [Pea 08] A.D. Peacock, D. Jenkins, M. Ahadzi, A. Berry and S. Turan, "Micro wind turbines in the UK domestic sector", *Journal "Energy and buildings"*, 2008, Vol. 40, N°7, pp.1324-1333.
- [Ped 08] M.A. PEDRASA, "Overview of microgrid management and control", Internetdocument, [www.ceem.unsw.edu.au/content/userDocs/OverviewofMicrogrid-ManagementandControl.pdf](http://www.ceem.unsw.edu.au/content/userDocs/OverviewofMicrogrid-ManagementandControl.pdf), September, 2008.

- [Pee 09] Eefje Peeters, Régine Belhomme, Carlos Battle, François Bouffard, Seppo Karkkainen, Daan Six, Maarten Hommelberg, "ADDRESS: Scenarios and architecture for active demand development in the smart grids of the future", C I R E D 20th International Conference on Electricity Distribution Prague, 8-11 June 2009
- [Pen 07] Daniel Pendicka, "Storing energy from the wind in compressed-air reservoirs", Journal: The New Scientist, Vol. 195, Issue 2623, 29 September 2007, pp. 44-47.
- [Pil 02] P. A. Pilavachi, "Mini- and micro-gas turbines for combined heat and power", Applied Thermal Engineering, Vol. 22, Issue 18, December 2002, pp. 2003-2014

## R

- [Rau 80] H. S. Rauschenbach, "Solar Cell Array Design Handbook", Van Nostrand-Reinhold, NY, 1980.
- [Ren 09] REN21 (Renewable energy policy network for the 21st century), "Renewables Global Status Report 2009 Update"(PDF), p.8.
- [Rif 09] Y. RIFFONNEAU, "Gestion des flux energetiques dans un systeme photovoltaïque avec stockag e connecté au réseau", thèse de l'Institut Polytechnique de Grenoble, 23 octobre 2009
- [Rob 01] B. Robyns, M. Nasser, F. Berthereau, F. Labrique, "Equivalent continuous dynamic model of a variable speed wind generator" ELECTROMOTION 2001, vol.8, n°4, pp. 202-208, dec. 2001.
- [Rob 02] B. Robyns, Y. Pankow, L. Leclercq, B. Francois, "Equivalent continuous dynamic model of renewable energy system", ELECTRIMACS 2002, CD-ROM, 18-21 Aout 202, Montreal, Canada.

## S

- [SAA 99] H. SAADAT, "Power system analysis", McGraw-Hill International Editions, pp. 527-569, 1999.
- [Sha 04] F. Shawn, "A method for predicting PV module and array performance at other than standard reporting conditions", North Carolina Solar Center, 2004.
- [Spy 00] R. Spyker, R. M. Nelms, "Analysis of Double Layer Capacitors Supplying Constant Power Loads," IEEE Transactions on Aerospace and Electronic Systems, Vol. 36, No. 4, Oct. 2000.

## T

- [Thi 10] Y. Thiaux, "Optimisation des profils de consommation pour minimiser les coûts économique et énergétique sur cycle de vie des systèmes photovoltaïques autonomes et hybrides : Évaluation du potentiel de la technologie Li-ion ", PhD report, Ecole Normale Supérieure de Cachan, 2010.

- [Tho 09] P. Thounthong, S. Rael, B. Davat, "Energy management of fuel cell/battery/supercapacitor hybrid power source for vehicle applications", Elsevier, Journal of Power Source, pp. 376-381, 01/08/2009.
- [Tra07] T. Tran-Quoc, M. Braun et al. "Using control capabilities of DER to participate in distribution system operation", PowerTech, 2007, Switzerland, pp. 561–566.

## U

- [URL 06a] "Offshore stations experience mean wind speeds at 80 m that are 90% greater than over land on average.", Evaluation of global wind power, (URL accessed January 30<sup>th</sup>, 2006).  
[http://www.stanford.edu/group/efmh/winds/global\\_winds.html](http://www.stanford.edu/group/efmh/winds/global_winds.html)
- [URL 06b] "Renewable energy", Wikipedia (URL accessed January 30, 2006), [http://en.wikipedia.org/wiki/Renewable\\_energy](http://en.wikipedia.org/wiki/Renewable_energy)
- [URL 06c] G. Strbac, A. Shakoor, M. Black, D. Pudjianto and T. Boppc, "Impact of wind generation on the operation and development of the UK electricity systems", Journal "electric power systems research", Vol. 77, No.9, pp. 1214-1272, Elseviers
- [URL 09a] C. Pinto Bastos, "Contributions of solar and wind energy to the world electrical energy demand", (URL accessed October 15, 2009), [http://www.sefidvash.net/fbnr/pdfs/Solar\\_and\\_Wind\\_Energy.pdf](http://www.sefidvash.net/fbnr/pdfs/Solar_and_Wind_Energy.pdf)
- [URL 09b] "Solar power. How to use its energy", Accessed on 12 Dec 2009 (URL: <http://www.petervaldivia.com/technology/energy/solar-power.php>).
- [URL 09c] "Solar energy", Accessed on 12 Dec 2009(URL: <http://www.howardhallfarm.com/solarenergy.html>).
- [URL 09d] Wikipedia, "Lead-acid battery", Accessed on 12 Dec 2009 (URL: [http://en.wikipedia.org/wiki/Lead-acid\\_battery](http://en.wikipedia.org/wiki/Lead-acid_battery)).
- [URL 09e] "Lead-acid battery", Accessed on 12 Dec 2009 (URL: <http://www.reuk.co.uk/Lead-Acid-Batteries.htm>).
- [URL 09f] Advanced capacitor technologies, Accessed on 12 Dec 2009, (URL:<http://www.act.jp/eng/index.htm>).
- [URL 09g] "Thermal energy storage", Wikipedia, URL:  
[http://en.wikipedia.org/wiki/Thermal\\_energy\\_storage](http://en.wikipedia.org/wiki/Thermal_energy_storage)
- [Url 10a] "US Invests in Smart Grid Training", (URL accessed Juin.15,2010) <http://www.consumerenergyreport.com/2010/04/12/us-invests-in-smart-grid-training/>
- [Url 10b] Site of CERTS, (URL accessed Feb.15,2010), <http://certs.lbl.gov>
- [Url 10c] GridNet + Sprint for US Smart Grid,  
<http://www.dailywireless.org/2010/09/14/gridnet-sprint-for-us-smart-grid/>
- [Url 10d] RTE (Réseau de Transports d'Electricité) de France, "consommation française d'électricité caractéristiques et méthode de prévision", web site <http://www.rte->

france.com/

[Url 10e] “Battery and Energy Technologies”, <http://www.mpoweruk.com/chargers.htm>

[Url 10f] U.S. department of energy, The SMART GRID: an introduction. Report, <http://www.oe.energy.gov/smartgrid.htm>

V

[Van 08] M. Vandenberg, Report “Data monitoring on Kythnos” for Task TF3, 2008-12-09

X

[Xia 04] W. Xiao, W.G. Dunford, A. Capel, “A novel modeling method for photovoltaic cells”, IEEE Power electronics specialists conference, Aachen, Allemagne, 2004, CD-ROM.

Y

[Yu 04] X. Yu, K. Strunz, “Combined long-term and short-term access storage for sustainable energy system”, 2004 IEEE Power Engineering Society General Meeting, vol. 2 pp. 1946-1951, 10 June 2004.

Z

[Zho 09a] T. Zhou, P. Li, B. Francois, “Power Management Strategies of a DC-Coupled Hybrid Power System for Microgrid Operations”, the 13<sup>th</sup> International European Power Electronics Conference and Exhibition (EPE2009), CD-ROM, Barcelona, Spain.

[Zho 09b] T. Zhou, B. Francois, “Modeling and control design of hydrogen production process for an active hydrogen/wind hybrid power system”, International Journal of Hydrogen Energy, vol.34, iss.1, Jan.2009, pp. 21-30

[Zho 09c] T. Zhou, B. Francois, “Real-Time Emulation of a Hydrogen Production Process for assessment of an Active Wind Energy Conversion System”, IEEE Transactions on Industrial Electronics, vol. 56, iss. 3, March 2009, pp. 737–746.

[Zho 09d] T Zhou, "Supervision de la répartition de puissances au sein d'une centrale multi source pour la génération d'électricité à base d'énergie renouvelable", Thèse de doctorat de l'Ecole Centrale de Lille, 29/06/2009

[Zho 09e] T. Zhou, B. Francois, "Electrical Energy Systems"Energy Management and Power Control of an Hybrid Active Wind Generator for Distributed Power Generation and Grid Integration", accepted to IEEE Transactions on Industrial Electronics, 2009

[Zub 00] L. Zubieta, R. Bonert, “Characterization of double-layer capacitors for power electronics applications”, IEEE Transactions on Industry Applications, Jan-Feb 2000, vol. 36, issu. 1, pp. 199-200.

### Résumé

L'intégration de panneaux PhotoVoltaïques (PV) dans un système électrique réduit la consommation des sources fossiles et apporte des avantages environnementaux. Toutefois, l'intermittence et les fluctuations de puissance détériorent la qualité d'alimentation électrique. La solution ici proposée est d'ajouter des éléments de stockage, coordonnés par un contrôleur local qui gère les flux de puissance entre toutes les sources et la disponibilité énergétique. Ce générateur actif PV peut générer des références de puissance et fournir des services « système » au réseau électrique. Puis, les concepts liés au micro réseau sont transposés pour concevoir un système central de gestion de l'énergie d'un réseau électrique résidentiel, qui est alimenté par des générateurs actifs PV et une micro turbine à gaz. Un réseau de communication est utilisé pour échanger des données et des références de puissance. Un système de gestion de l'énergie est développé avec différentes fonctions de contrôle sur des échelles de temps différentes afin de maximiser l'utilisation de l'énergie PV. Une planification opérationnelle quotidienne est conçue par un algorithme déterministe, qui utilise la prédiction d'énergie PV et de la charge. Ces références de puissance sont actualisées chaque demi-heure en tenant compte de la disponibilité de l'énergie PV et l'état des unités de stockage. Les erreurs de prévision et les incertitudes sont compensées par le réglage primaire de fréquence. Les résultats de simulation et les tests valident la conception de la commande du générateur actif photovoltaïque ainsi que le système central de gestion de l'énergie du réseau résidentiel étudié.

**Mots-clés:** micro réseau, réseau intelligent, supervision énergétique, énergie renouvelable, panneau photovoltaïque, stockage énergétique, batterie, supercondensateur

### Abstract

The integration of PV power generation in a power system reduces fuel consumption and brings environmental benefits. However, the PV power intermittency and fluctuations deteriorate the power supply quality. A solution is proposed by adding energy storages, which are coordinated by a local controller that controls the power flow among all sources and implements an inner energy management. This PV based active generator can generate power references and can provide ancillary services in an electric network. Then micro grid concepts are derived to design a central energy management system of a residential network, which is powered by PV based active generators and a gas micro turbine. A communication network is used to exchange data and power references. An energy management system is developed with different time-scale functions to maximize the use of PV power. An operational daily planning is designed by a determinist algorithm, which uses 24 hour-ahead PV power prediction and load forecasting. Then power references are refreshed each half of an hour by considering the PV power availability and the states of energy storage units. Prediction errors and uncertainties are compensated by primary frequency controllers. Simulation and testing results validate the design of the PV active generator local controller and the central energy management system of the studied residential network.

**Keywords:** smart grid, micro grid, energy management, renewable energy, photovoltaic panel, electrical energy storage, battery, ultracapacitor